Universidad Pública de Navarra

Departamento de Agronomía, Biotecnología y Alimentación

Mecanismos de regulación de la respuesta de las plantas a compuestos volátiles de origen microbiano

Tesis Doctoral en modalidad de compendio de artículos
para optar al título de Doctor, presentada por:

Samuel Gámez Arcas

Director: Dr. Javier Pozueta Romero

Codirector: Dr. Francisco José Muñoz Pérez

Tutora: Inmaculada Farrán Blanch

Pamplona, 2022

https://doi.org/10.48035/Tesis/2454/44657

El Dr. **Javier Pozueta Romero**, Profesor de Investigación del Consejo Superior de Investigaciones Científicas y el Dr. **Francisco José Muñoz Pérez**, Científico Titular del Consejo Superior de Investigaciones Científicas,

CERTIFICAN:

Que el trabajo titulado "Mecanismos de regulación de la respuesta de las plantas a compuestos volátiles de origen microbiano" recogido en la presente memoria, ha sido realizado por Samuel Gámez Arcas en el Instituto de Agrobiotecnología (CSIC/ Gobierno de Navarra) bajo su supervisión y que cumple las condiciones exigidas por la legislación vigente para optar al grado de Doctor. Samuel Gámez Arcas ha disfrutado de una beca predoctoral de la Universidad Pública de Navarra. Este trabajo ha sido financiado por el Ministerio de Ciencia e Innovación (MICINN) and Agencia Estatal de Investigación (AEI) / 10.13039/501100011033/ (proyectos BIO2016-78747-P y PID2019-104685GB-100)

Y para que así conste, firman la presente en Pamplona, a 19 de Octubre de 2022.

POZUETA ROMERO FRANCISCO JAVIER - DNI 13760579R

Firmado digitalmente por POZUETA ROMERO FRANCISCO JAVIER - DNI 13760579R
Fecha: 2022.10.18 13:18:12 +02'00'

Fdo. Javier Pozueta Romero

MUÑOZ PEREZ FRANCISCO JOSE - DNI 07868528K

Firmado digitalmente por MUÑOZ PEREZ FRANCISCO JOSE - DNI 07868528K
Fecha: 2022.10.18 13:33:17 +02'00'

Fdo. Francisco José Muñoz Pérez

La tesis Doctoral comprendida en este volumen es un compendio de trabajos previamente publicados y está organizada según el modelo sugerido por la Comisión Académica del Programa de Doctorado en Biotecnología de la Universidad Pública de Navarra. De esta manera, los resultados obtenidos durante la realización de la misma se agrupan en 2 capítulos. Cada capítulo contiene una introducción específica, presenta los resultados, describe los materiales y métodos utilizados y concluye con una discusión. Por lo tanto, cada capítulo agrupa la información necesaria relacionada con el tema que en él se desarrolla permitiendo su lectura de manera independiente. Además, este documento incluye un resumen, una introducción general y los objetivos planteados.

Publicaciones incluidas en la tesis:

Gámez-Arcas S, Baroja-Fernández E, García-Gómez P, Muñoz FJ, Almagro G, Bahaji A, Sánchez-López ÁM, Pozueta-Romero J (2022a) Action mechanisms of small microbial volatile compounds in plants. J. Exp. Bot. 73: 498-510.
Journal Impact Factor: 7.298
Position in the area: 15/239
Thematic area: Plant Science

Gámez-Arcas S, Muñoz FJ, Ricarte-Bermejo A, Sánchez-López ÁM, Baslam M, Baroja-Fernández E, Bahaji A, Almagro G, De Diego N, Dolezal K, Novák O, Leal-López J, Morcillo RJL, Castillo AG, Pozueta-Romero J (2022b) Glucose-6-P/phosphate translocator2 mediates the phosphoglucose-isomerase-1 independent response to microbial volatiles. Plant Physiol. doi: 10.1093/plphys/kiac433.
Journal Impact Factor: 8.005
Position in the area: 12/239
Thematic area: Plant Science

A mi abuela, mi ángel de la guarda.

AGRADECIMIENTOS

Aún recuerdo esa cálida mañana de verano en la que, junto con mi compañera de vida y mi incansable familia, pusimos rumbo a la fría pero acogedora Pamplona. Todos estos años han supuesto un gran aprendizaje para mí, tanto a nivel personal como a nivel profesional. Y no quería dejar pasar la ocasión de dar las gracias a todas esas personas que de alguna manera u otra han formado parte de esta etapa.

Quiero dar las gracias a Paco, también conocido como Lamberhuerta en redes sociales. Mi director, el que me enseñó todo lo que sé. Desde usar diferentes colores en el cuaderno de laboratorio hasta diseñar un primer. Y además de enseñarme a ser científico, me alimentó con sus maravillosos tomates de la huerta. Si hoy en día puedo dedicarme a ser investigador es en gran medida por su culpa. Muchas gracias, Paco.

Agradecer sin duda también la labor de mi otro director Javier. La persona que me brindó la oportunidad de formar parte de este proyecto. Me enseñó a tener un pensamiento crítico, a no ser conformista y, sobre todo, me enseñó a cuestionar cualquier dogma establecido. ¡Ah!, se me olvidaba, me enseñó que una PCR negativa no es un resultado. Muchas gracias, Javier.

En estas líneas tampoco me quiero olvidar de todos mis compañeros del Instituto de Agrobiotecnología. Todos ellos, sin excepción, han aportado algo a esta aventura que es la tesis doctoral. Edurne, fuiste un pilar fundamental de esta experiencia, sin ser mi directora, lo fuiste. Ángela, la doctora de referencia, la figura indispensable que tiene que estar entre el director y el doctorando. Nunca olvidaré el día que me dejaste tu coche automático y casi nos matamos porque confundí el freno con el embrague que no existe en este tipo de coches. Abdel, la persona con la que más me he reído en Pamplona. Me mostró que la delicadeza y la paciencia son fundamentales en la investigación y también me enseñó en qué zona de Pamplona podía pelarme y comprar dátiles de calidad. Goi, la chica del HPLC, me enseñó a ser profesional y que un mac siempre será mejor que un windows. Kinia y Pablo, mis compis, los doctorandos que ya son doctores, el hombro donde llorar (y criticar a los jefes). Muchas gracias a todo este maravilloso equipo humano sin el que no hubiera sido posible llevar a cabo esta tesis.

Quiero dar las gracias a un parque, el parque de la Vuelta del Castillo. Este era mi sitio de refugio. El parque donde iba a correr todos los días, donde mejoré como atleta, donde conocí al gran Antonio Etxeberria y a mi binomio Pedro "el caleta". Con ellos, y muchos más, compartí miles de kilómetros corriendo. Hubo días de frio, días de lluvia y viento, pero siempre había un compañero con el que compartir zancadas y hablar de cómo nos había ido el día o de qué musculo nos dolía. Muchas gracias parque, no sabes lo importante que fuiste para mí.

Y como dicen que es de bien nacidos ser agradecidos, me gustaría dar las gracias a mis padres. Los pilares que sujetan mi vida y que literalmente hicieron posible todo esto. Una vez leí una pregunta que decía ¿Tú de mayor querías ser tú? La respuesta no la sé, pero de lo que estoy seguro es que quiero ser, al menos, un tenue reflejo de lo que ellos son. Ella no lo sabe, pero las llamadas con mi madre en el camino del laboratorio a casa eran para mi uno de los mejores momentos de mi día. Él no lo sabe, pero, aunque no habláramos a diario, sé que estaba al tanto de todos mis progresos. Muchas gracias papá y mamá, ojalá el tiempo nos regale la oportunidad de compartir muchos más momentos de esta vida y pueda devolveros de alguna manera todo lo que habéis hecho por mí y por mis hermanos.

Y por último y no menos importante, me quiero acordar de mi compañera de vida. La persona que sin dudarlo se lanzó a la piscina y se vino a Pamplona conmigo. Los dos junto aprendimos que somos invencibles y que nada podrá con nosotros. También aprendimos a ser padres de un bicho peludo llamado Sushi, aprendimos a poner una lavadora y aprendimos que no hay nada más difícil que darle la vuelta a una tortilla. Bella, quiero darte las gracias por apoyarme en los momentos difíciles y por enseñarme que con trabajo y perseverancia todo es posible, te amo y te admiro.

Abuela, allá donde estés seguro que estarás orgullosa de tu nieto. Tu nieto ahora es doctor. Pero no de esos que te recetaba hacerte los "analises", es algo un poco diferente y difícil de explicar. Gracias abuela, porque fuiste mi amiga y me enseñaste a superar cualquier obstáculo que se presentara en el camino.

ÍNDICE

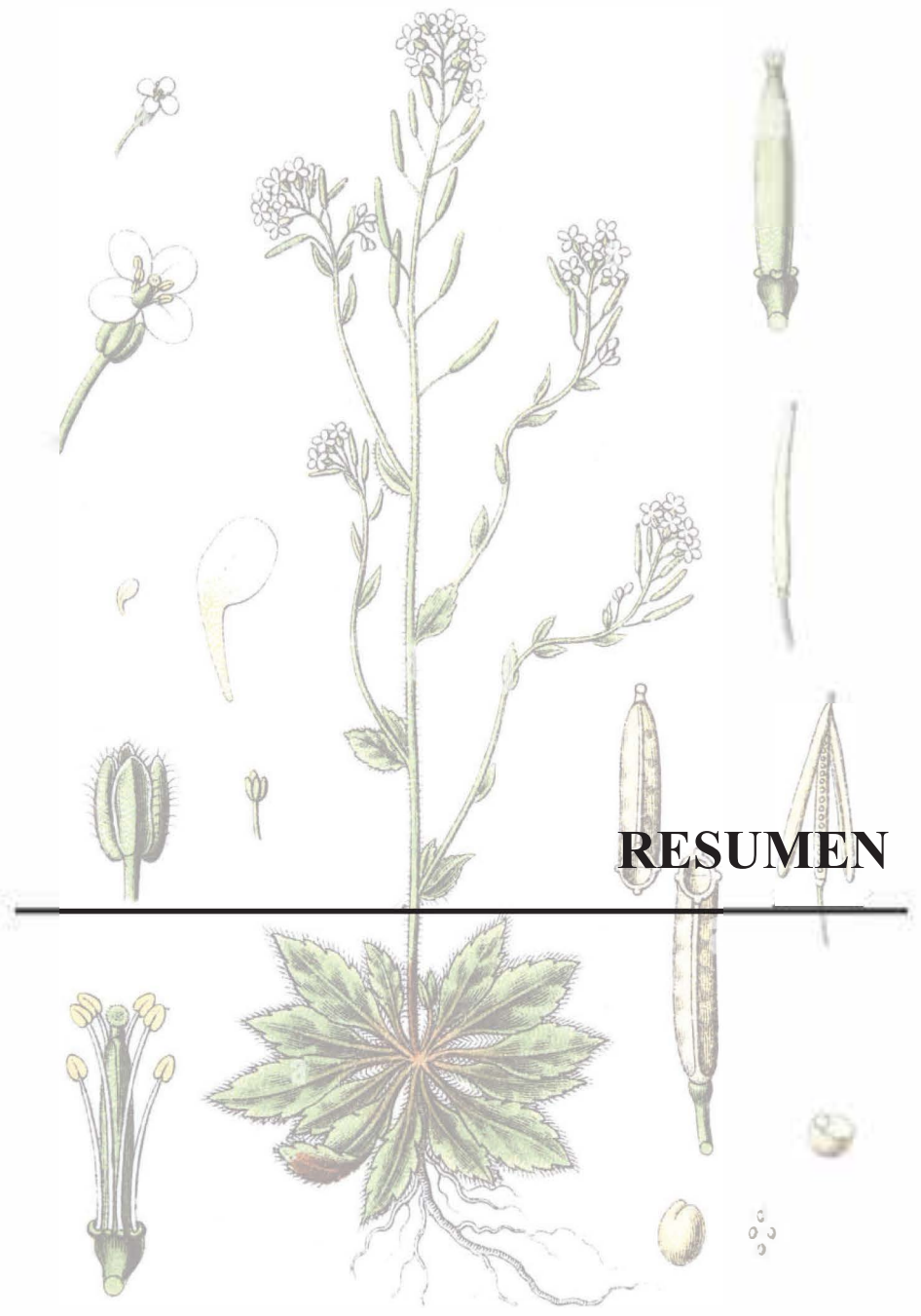

RESUMEN

Las plantas son metaorganismos que regulan su desarrollo y metabolismo en respuesta a diferentes estímulos externos. Conviven con microorganismos emisores de compuestos que difunden a través del suelo tales como azúcares, proteínas, exopolisacáridos, sideróforos, ácidos grasos, ácidos orgánicos, aminoácidos y hormonas que modifican la fotosíntesis, el metabolismo y el crecimiento de las plantas (Philippot et al., 2013; De-la-Peña and Loyola-Vargas, 2014; Backer et al., 2018). Los microorganismos beneficiosos también emiten compuestos volátiles (VCs) que fomentan el crecimiento, la captación de nutrientes y la fotosíntesis, modulan la arquitectura de la raíz, activan la respuesta de defensa de la planta e incrementan su resistencia al estrés salino y la sequía (Ryu et al., 2003; Zhang et al., 2008; Splivallo et al., 2009; Zhang et al., 2009; Gutiérrez-Luna et al., 2010; Kanchiswamy et al., 2015; Park et al., 2015; Ledger et al., 2016). Estudios llevados a cabo por el grupo de investigación en el que he realizado mi tesis doctoral demostraron que las bacterias y los hongos fitopatógenos también emiten VCs con propiedades bioestimulantes (Sánchez-López et al., 2016b). Cambios en el crecimiento, la fotosíntesis, el desarrollo y el metabolismo de la planta inducidos por VCs microbianos están asociados a grandes variaciones en el transcriptoma, el proteoma y el redox-proteoma de la planta (Sánchez-López et al., 2016b; Ameztoy et al., 2019, 2021). Tales variaciones sugieren que la respuesta de la planta a los VCs microbianos está regulada tanto a nivel transcripcional como no-transcripcional. Con el fin de profundizar en los mecanismos que median la relación entre la planta y los microorganismos, en este trabajo investigué el papel que juega el transportador de hexosas fosfato plastidial (GPT2) inducible por VCs en la respuesta de la planta modelo de laboratorio *Arabidopsis thaliana* a VCs emitidos por el hongo fitopatógeno *Altenaria alternata*. Además, investigué el papel que juega en dicha respuesta el residuo de cisteína 95 de la fructosa bifosfatasa plastidial (cFBP1), un enzima del ciclo de Calvin-Benson cuya actividad está sujeta a cambios en el estado redox inducibles por la luz.

En el capítulo 1 de esta tesis presento los resultados de mi investigación sobre el papel que juega GPT2 en la respuesta de las plantas a VCs microbianos. Para realizar esta investigación, analicé y comparé el crecimiento, la fotosíntesis y el proteoma de plantas *wild type* (WT), mutantes carentes GPT2 (*gpt2-1*), mutantes carentes PGI1 (*pgi1-2*) y doble mutante *pgi1-2gpt2-1* cultivadas en presencia o ausencia de VCs fúngicos. Además, caractericé la respuesta a estos compuestos de plantas *pgi1-2/gpt2-*

1 que expresan GPT2 bajo el control de un promotor específico de haces vasculares. Finalmente, caractericé el patrón de expresión de *GPT2* en plantas que expresan el gen reportero *GUS* bajo la acción de la secuencia promotora de *GPT2*. Los resultados obtenidos mostraron que, de manera similar a lo que ocurre en plantas WT, los VCs fomentan el crecimiento, la fotosíntesis y la acumulación de citoquininas activas y almidón en plantas *pgi1-2* y *gpt2-1*. Tal respuesta fue reducida en plantas *pgi1-2gpt2-1* y se revirtió a WT al expresar GPT2 en haces vasculares. Estudios comparativos de los proteomas de plantas *pgi1-2* y *pgi1-2gpt2-1* mostraron que GPT2 regula la expresión de proteínas relacionadas con la fotosíntesis. Es más, los estudios de expresión mostraron que *GPT2* se expresa en haces vasculares y está sujeto a complejos mecanismos de regulación. Globalmente, los resultados presentados en este capítulo indican que en condiciones en las cuales la actividad de PGI está reducida, la respuesta de la planta a VCs microbianos conlleva una regulación de la expresión de proteínas relacionadas con la fotosíntesis a través de mecanismos en los que *GPT2* juega un papel importante en la provisión de sustrato necesario para la producción de citoquininas en haces vasculares.

Trabajos llevados a cabo en el grupo de investigación en el que he realizado este mi tesis mostraron que la exposición a VCs microbianos conlleva cambios globales en el redox-proteoma de las plantas (Ameztoy et al., 2019). Tales cambios incluían la reducción de residuos de cisteína altamente conservados a lo largo de la evolución de enzimas del ciclo de Calvin-Benson. En el capítulo 2 presento los resultados de mi investigación sobre el papel que juega el residuo de cisteína 95 de la cFBP1 en su actividad, en la fotosíntesis y en la respuesta de las plantas a VCs microbianos. Para realizar esta investigación, comparé las propiedades electroforéticas y cinéticas de cFBP1 WT y una forma mutada en la que el residuo de cisteína 95 fue sustituido por un residuo de serina (C95S). Además, comparé la fotosíntesis y el crecimiento de plantas de Arabidopsis *cfbp1* carentes de cFBP1 endógena que expresan ectópicamente formas WT o C95S de cFBP1. Los resultados mostraron que el residuo de cisteína 95 juega un papel importante en la actividad de cFBP1 y en la fotosíntesis, pero no en el crecimiento de Arabidopsis.

INTRODUCTION

Plants are metaorganisms that host a complex and dynamic microbial consortium of bacteria, fungi, archaea and protists which communicate with plants by exchanging chemical signals throughout the phytosphere (Philippot et al., 2013; Delgado-Baquerizo et al., 2016; Huang et al., 2019). Such interactions are important for plant productivity and fitness (De-la-Peña and Loyola-Vargas, 2014). In the precolonization phase, before direct contact with plants occurs, beneficial and phytopathogenic bacteria and fungi emit complex mixtures of volatile compounds (VCs). Depending on microbial culture conditions, these compounds promote plant growth and photosynthesis as well as drastic transcriptomic, proteomic and metabolic changes mediated by activation of phytohormone signaling (Ryu et al., 2003; Zhang et al., 2007, 2009; Ezquer et al., 2010; Kwon et al., 2010; Zhang et al., 2010; Bitas et al., 2015; Kanchiswamy et al., 2015; Sánchez-López et al., 2016a,b; Cordovez et al., 2017; Piechulla et al., 2017; Li et al., 2018b; Tyagi et al., 2018; Ameztoy et al., 2021). These volatiles also induce systemic drought tolerance, improve nutrient acquisition, and modulate root system architecture (RSA) (Cho et al., 2008; Splivallo et al., 2009; Gutiérrez-Luna et al., 2010; Ditengou et al., 2015; Garnica-Vergara et al., 2016; Camarena-Pozos et al., 2019; García-Gómez et al., 2020).

Growth and developmental changes promoted by microbial VCs have frequently been associated with volatile organic compounds (VOCs) with molecular masses ranging between ~45 Da and 300 Da, which belong to different chemical classes including alkenes, alcohols, ketones, benzenoids, pyrazines, sulfides, terpenes, etc. (reviewed in Kanchiswamy et al., 2015; Fincheira and Quiroz, 2018; Tyagi et al., 2018). At present, more than 2000 microbial VOCs emitted by more than 1000 microorganisms are registered in the microbial VOC database (Lemfack et al., 2018; http://bioinformatics.charite.de/mvoc). However, microorganisms also release a limited number of VCs with molecular masses of less than ~45 Da (hereafter designated as "small VCs") such as inorganic VCs (e.g. hydrogen sulfide [H_2S], molecular hydrogen, nitric oxide [NO], nitrogen dioxide [NO_2], nitrous oxide, carbon monoxide [CO], carbon dioxide [CO_2], hydrogen cyanide [HCN] and ammonia) (Engel et al., 1972; Wharton and Weintraub, 1980; Siegel and Siegel, 1987; Nandi and Sengupta, 1998; Conrath et al., 2004; Blom et al., 2011; Shatalin et al., 2011; Schreiber et al., 2012; Weise et al., 2013) and VOCs (e.g. ethylene, ethane, formaldehyde, methanol and acetylene) (Schink and Zeikus, 1980; Donnelly and Dagley, 1980; Splivallo et al., 2009; Lemfack

et al., 2018; Ballester and González-Candelas, 2020). Some of these small VCs are very reactive with proteins and/or act as signaling molecules that promote photosynthesis, growth and developmental changes, and enhance tolerance to abiotic stresses when exogenously applied in a discrete form and/or in low concentrations (Nonomura and Benson, 1992; Dong et al., 2003; He et al., 2004; Ramírez et al., 2006; Cao et al., 2007; Xie et al., 2008; Guo et al., 2009; Jin et al., 2009, 2013; Splivallo et al., 2009; Chen et al., 2011; Takahashi et al., 2011; Xie et al., 2012; Dooley et al., 2013; Lisjak et al., 2013; Han et al., 2014; Lin et al., 2014; Takahashi et al., 2014; Wang and Liao, 2016; Yang et al., 2016; Zhu et al., 2016; Gautam et al., 2021) (**Table 1**). Although emissions of some of these compounds by microbes are important determinants in plant-microbe interactions (Weingart et al., 2001; Johnson et al., 2008; Molina-Favero et al., 2008; Splivallo et al., 2009; van Bockhaven et al., 2015), their mechanisms of action from perception to the processes that induce growth are still poorly understood.

In many cases, exposure of plants to VOCs with molecular masses ranging between ~45 Da and 300 Da either failed to reproduce or only partially reproduced the effects induced by the microbial volatile emissions (Groenhagen et al., 2013; Naznin, et al., 2013; Cordovez et al., 2017). This indicates that VOCs with molecular masses ranging between ~45 Da and 300 Da may be only partly responsible for the growth-promoting effects of microbial VCs. Recently, using a "box-in-box" *in vitro* co-cultivation system in which plants are grown in the vicinity of microbial cultures covered with charcoal filters that adsorb VOCs of molecular masses higher than ~45 Da, evidence has been provided that small VCs are important determinants of plant responses to microbial volatile emissions (García-Gómez et al., 2019, 2020; Ameztoy et al., 2019, 2021).

1.The necessity of developing a co-cultivation system to study plant responses to VCs and circumvent microbial respiratory CO_2 effects

A number of studies on plant´s responses to microbial VCs under controlled laboratory conditions have been conducted using sealed split Petri dish-based co-cultivation systems in which plants are exposed to complex mixtures of VCs released by nearby microbial cultures. All known microorganisms that produce plant growth-promoting volatiles are heterotrophic and thus emit respiratory CO_2 when grown under aerobic conditions. In sealed co-cultivation systems, microbial respiratory CO_2 can accumulate

Table 1: Small microbial VCs and their actions on plants

Volatile compound	Molecular weight (Da)	Microbial production (references)	Action on plants (references)
Inorganic compounds			
Molecular hydrogen (H_2)	2.01	Nandi and Sengupta, 1998	Promotion of growth and formation of adventitious roots. Enhancement of salt tolerance (Dong et al., 2003; Xie et al., 2012; Jin et al., 2013; Lin et al., 2014; Zhu et al., 2016)
Hydrogen sulfide (H_2S)	36.1	Shatalin et al., 2011	Enhancement of growth, photosynthesis, germination success and fruit yield. Reduction of time for germination (Chen et al., 2011; Dooley et al., 2013)
Nitric oxide (NO)	30.00	Wharton and Weintraub, 1980; Conrath et al., 2004; Johnson et al., 2008; Molina-Favero et al., 2008; Schreiber et al., 2012; García-Gómez et al., 2019	Promotion of growth and photosynthesis. Enhancement of photosynthetic nitrogen and sulfur use efficiencies. Repression of floral transition (He et al., 2004; Johnson et al.,2008; Jin et al., 2009; Molina-Favero et al., 2008; Gautman et al., 2021)
Nitrogen dioxide (NO_2)	46.00	Wharton and Weintraub, 1980	Promotion of growth and flowering. Enhancement of fruit yield (Takahashi et al., 2011; Takahashi et al., 2014)
Carbon monoxide (CO)	28.01	Engel et al.,1982; Siegel and Siegel, 1987; Garcia-Gómez et al., 2019	Promotion of lateral root formation and root hair development. Enhancement of tolerance to salt and nutrient deficiency stresses (Cao et al., 2007; Guo et al., 2008; Xie et al., 2008; Guo et al,. 2009; Han et al., 2014; Wang and Liao, 2016; Yang et al., 2016)
Carbon dioxide (CO_2)	44.01		Promotion of growth, flowering, starch accumulation and changes in root architecture (Makino and Mae 1999; Ainsworth and Rogers, 2007; Song et al., 2009; Niu et al., 2011)
Organic compounds			
Ethylene (C_2H_4)	28.05	Splivallo et al., 2009; Lemfack et al., 2018; Ballester and González-Candelas, 2020	Induction of lateral root shortening and root hair elongation (Weingart et al., 2001; Splivallo et al., 2009)
Methanol (CH_3OH)	32.04	Schink and Zeikus, 1980; Donnelly and Dagley, 1980; Lemfack et al., 2018)	Enhanced growth and fruit yield (Nonomura and Benson, 1992; Ramírez et al., 2006)

to high levels in the headspace (Kai and Piechulla, 2009; Venneman et al., 2020). Similar to complex mixtures of microbial VCs, elevated CO_2 enhances photosynthesis, and promotes plant growth, flowering, starch accumulation and changes in root architecture (Makino and Mae, 1999; Ainsworth and Rogers, 2007; Song et al., 2009; Niu et al., 2011). Several authors have therefore argued that the responses of plants grown in the vicinity of microbial cultures in enclosed dual-culture systems, or other experimental setups that inhibit unhindered gas exchange, could be due largely to accumulation of elevated levels of microbial respiratory CO_2 (Casarrubia et al., 2016; Piechulla and Schnitzler, 2016; Zhang et al., 2021). To circumvent respiratory CO_2 effects, evaluate its contribution in VC-based microbe-plant interactions and identify potentially bioactive VCs, a simple "box-in-box" co-cultivation system was developed in which the plant and microbial cultures are placed in a container sealed with a 9 Micron thickness plasticized polyvinyl chloride (PVC) wrap (Cell Ofix SLU, Valencia, Spain) (**Figure 1A**). Due to its flexibility and gas permeation properties, this type of film is normally used in food packaging. The headspace VC concentration in the sealed container is the result of balances between fungal and plant VC emission rates, fungal metabolization of VCs emitted by plants, plant metabolization of VCs emitted by fungi, and the VC permeation rates through the PVC film, which in turn depends upon the differential pressures between the gases of the headspace and outside ambient atmosphere. Features and benefits of the "box-in-box" co-cultivation system for studying plant responses to microbial volatile emissions are described in García-Gómez et al. (2019). Among others, the system enables the filtration of microbial VCs according to their molecular masses and thus makes it possible to investigate the responses of plants to VCs of defined molecular masses. In addition, the system permits easy online monitoring of VCs in the headspace of the sealed container (**Figure 1B**). Due to relatively high permeability of plasticized PVC to CO_2 and water vapor, the system minimizes increases in microbial respiratory CO_2 in the growth container´s headspace, and prevents condensation of the respiratory water emitted by the fungal cultures.

2. Small VCs other than CO_2 are important determinants of plant responses to microbial volatile emissions

Using plants grown in the vicinity of different fungal cultures covered with charcoal

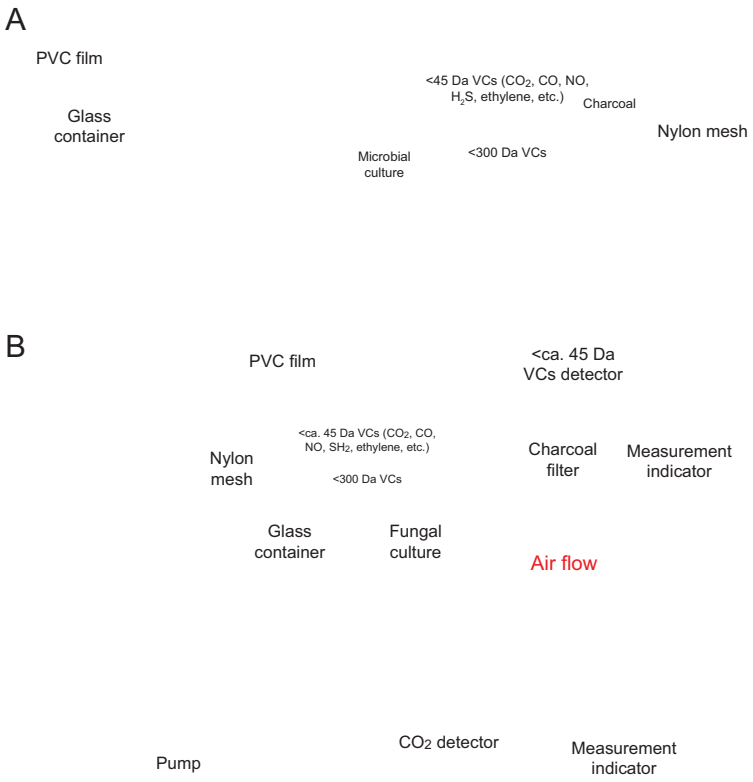

Figure 1: Plasticized PVC wrap- and charcoal filter-based "box-in-box" co-cultivation system. (A) Illustration of the system used to characterize the response of plants to small microbial VCs. (B) Illustration of the system used to online monitor levels of VCs emitted by microbial and/or plant cultures in the headspace of the growth chamber. The indicated small VCs (e.g. CO, NO, H_2S, ethylene, etc.) are putative biologically active compounds emitted by a fungal culture that is included in the PVC-sealed container.

filters capturing VCs of molecular masses higher than ~45 Da, García-Gómez et al. (2019) investigated the contribution of small VCs to plant responses to microbial volatiles. The study showed that morphological, biochemical and transcriptomic changes in plants in response to charcoal-filtered VCs emitted by nearby microbial cultures were identical to those of plants exposed to microbial VCs without charcoal filtration. This strongly indicated that, in the plasticized PVC wrap- and charcoal filter-based "box-in-box" co-cultivation system, small bioactive VCs are important determinants of the plants´ responses to microbial volatile emissions. The study also revealed that, in this system, respiratory CO_2 accumulating in the headspace of the growth chamber plays only a minor role, if any, in plant growth, developmental and

biochemical responses to VCs emitted by adjacent microbial cultures (García-Gómez et al., 2019).

Cultures of two fungal species increased CO and NO concentrations in the headspace of the growth chambers (García-Gómez et al., 2019). Similar to the application of small VCs emitted by diverse microorganisms, exogenous application of low concentrations of NO and CO promotes growth, lateral root (LR) formation and chlorophyll accumulation (He et al., 2004; Guo et al., 2008, 2009; Xuan et al., 2008). Furthermore, as with the application of small VCs emitted by some fungal species, application of ethylene induces LR shortening and root hair (RH) elongation (Negi et al., 2008; Lewis et al., 2011; García-Gómez et al., 2020). The response of plants exposed to small microbial VCs may therefore be at least partly due to plant perception of microbial CO, NO and/or ethylene.

3. Many of the transcriptional changes occurring in leaves exposed to small microbial VCs are due to enhanced photosynthetic signaling.

Exposure to small VCs emitted by the fungal phytopathogen *Alternaria alternata* promotes the accumulation of photosynthetic pigments, stimulates photosynthetic electron transport (PET) and improves the light use efficiency (Sánchez-López et al., 2016a,b). Consistently, small fungal VCs enhance net rates of CO_2 assimilation and the accumulation of primary photosynthates such as starch and soluble sugars in leaves of exposed plants (Sánchez-López et al., 2016a,b). An increase in PET promoted by small VCs creates conditions for the production of reactive oxygen species (ROS), which may result in photoinhibition and subsequent photooxidation. To prevent this damage, photosynthesis is subject to feedback inhibition by elevated sugar levels through mechanism(s) that require enhanced ABA and/or reduced cytokinin (CK) signaling (Moore et al., 2003; Rolland et al., 2006; Kushwah and Laxmi, 2014). It is noteworthy that exposure to small fungal VCs reduces ABA levels and enhances those of plastid-localized 2-C-methyl-D-erythritol 4-phosphate (MEP) pathway-derived CKs in leaves (Sánchez-López et al., 2016a,b; Ameztoy et al., 2019, 2021; García-Gómez et al., 2019). It thus appears that the sustained high levels of photosynthetic activity and the lack of photosynthetic inhibition by high sugar content in leaves of plants exposed to small fungal VCs is due, at least partly, to enhanced CK and reduced ABA production and signaling.

Plants response to small VCs emitted by *A. alternata* is associated with drastic changes in the leaf transcriptome, particularly in the expression of ABA- and CK-responsive genes involved in multiple processes including light harvesting, ROS scavenging, cell wall biosynthesis and metabolism of starch, carotenoids, glucosinolates, anthocyanins and carotenoids (Sánchez-López et al., 2016b; Ameztoy et al., 2019; García-Gómez et al., 2019). Mutants with reduced CK content or sensitivity respond poorly to small fungal VCs (Sánchez-López et al., 2016b). Plant responses to these compounds must therefore involve, at least in part, ABA- and CK-mediated transcriptional regulation. A striking alteration in the leaf transcriptome of small fungal VC-treated plants is the strong up-regulation of the gene that codes for the class 1 non-symbiotic haemoglobin (Sánchez-López et al., 2006b). Non-symbiotic haemoglobins are involved in NO scavenging and fixation, protection against nitrosative stress and modulation of signal transduction pathways of hormones including CK and ABA (Hebelstrup and Jensen, 2008; Hebelstrup et al., 2012; Hill, 2012; Kuruthkulangarakoola et al., 2017). High expression of these proteins promotes early flowering and growth (Hunt et al., 2002; Hebelstrup and Jensen, 2008). Accordingly, enhanced growth and developmental changes promoted by small fungal VCs can be ascribed, at least in part, to enhanced expression of non-symbiotic haemoglobins. Another striking alteration in the leaf transcriptome of plants that is promoted by small fungal VCs involves the up-regulation of the CPN20 gene which encodes a platidial co-chaperonin that functions negatively in ABA signaling (Zhang et al., 2013). Small fungal VCs also up-regulate the expression of the CK-induced *GPT2* gene which encodes a plastidic glucose-6-P (G6P)/Pi transporter (Kunz et al., 2010). This would suggest that GPT2-mediated incorporation of cytosolic G6P into the chloroplast and subsequent conversion into starch is involved in the starch over-accumulation process promoted by small VCs. In line with this presumption, Sánchez-López et al. (2016a) reported that VCs emitted by *A. alternata* promote the accumulation of exceptionally high levels of starch in mesophyll cells of starch-deficient pgi1 plants impaired in the conversion of fructose-6-P from the Calvin-Benson cycle (CBC) into G6P, likely as a consequence of the activation of plastidial phosphoglucose isomerase1 (PGI1)-independent, non-canonical starch biosynthetic pathway(s) that involve GPT2.

Changes in the transcriptomes of leaves of plants exposed to VCs emitted by phylogenetically distant microbial species are quite similar (Sánchez-López et

al., 2016b), indicating that transcriptome resetting in response to small VCs involves highly conserved regulatory mechanisms. These changes are similar to those seen in leaves of plants briefly exposed to elevated CO_2 or increased irradiance (García-Gómez et al., 2019). All of these treatments promote photosynthetic CO_2 fixation. It is therefore conceivable that many transcriptomic changes in the leaves of plants exposed to small microbial VCs result from signaling of enhanced photosynthetic CO_2 fixation (see below).

4. Regulation of plant responses to small microbial VCs is primarily non-transcriptional

Small microbial VCs emitted by different microorganisms promote distinct developmental changes in roots and leaves of exposed plants, despite inducing similar transcriptional changes (Sánchez-López et al., 2016b; García-Gómez et al., 2019). These observations suggest that the regulation of some plant responses to microbial VCs is primarily non-transcriptional (García-Gómez et al., 2019). This hypothesis is supported by findings showing that treatment with small VCs emitted by *A. alternata* (i) do not alter the levels of transcripts encoding most proteins that are differentially expressed following plant exposure to VCs (Sánchez-López et al., 2016b; García-Gómez et al., 2020; Ameztoy et al., 2021), (ii) promote global changes in the thiol redox proteome in leaves (Ameztoy et al., 2019), (iii) only weakly alter growth and metabolism in plants with impaired redox regulation of photosynthesis (Ameztoy et al. 2019, 2021) and (iv) alter the expression of proteins involved in the protein quality control (PQC) system (Ameztoy et al., 2021).

4.1 Leaf responses to small microbial VCs involve global changes in the thiol redox proteome that affect photosynthesis

Thioredoxins (Trxs) are important components of plants´ thiol redox regulation machinery which modulate activities of target proteins. Plastids contain an NADPH-dependent Trx reductase, called NTRC, which has been suggested to play important roles in the avoidance of toxic levels of ROS through reduction of H_2O_2-detoxifying 2-Cys peroxiredoxins (Prxs) (Pérez-Ruiz, 2006; Kirchsteiger et al., 2009; Pulido et al., 2010; Puerto-Galán et al., 2015) and in control of PET (Naranjo et al., 2016). NTRC also participates in the regulation of the redox status of stromal target

proteins, including diverse Trxs that control the redox status of CBC enzymes, via its functional relationship with 2-Cys Prxs (Yoshida and Hisabori, 2016; Nikkanen et al., 2016; Ojeda et al., 2017; Pérez-Ruiz et al., 2017) and chlorophyll biosynthetic enzymes (Tsuzuki et al., 2011; Du et al., 2012; Richter et al., 2013; Pérez-Ruiz et al., 2014; Da et al., 2017). VCs emitted by *A. alternata* exert weak stimulatory effects on growth, photosynthesis, leaf and root development and metabolism in NTRC knockout (ntrc) plants (Li et al., 2011; Ameztoy et al., 2019). This indicates that (i) NTRC is an important mediator of plant responses to small fungal VCs, probably due to its regulatory action on photosynthesis-related mechanisms and/or the overall redox status of the plant (Ameztoy et al., 2019), and (ii) redox activation of photosynthetic CO_2 fixation is an important determinant of plant responses to small microbial VCs. In support of the latter hypothesis, Ameztoy et al. (2021) have shown that, unlike in WT plants, *A. alternata* small VCs do not stimulate growth and do not promote metabolic and proteomic changes in *cfbp1* plants impaired in the redox-sensitive fructose-1,6-bisphosphatase isoform 1 (cFBP1) of the CBC. Small fungal VCs poorly alter the expression of ABA- and CK-responsive genes in leaves of *ntrc* plants (Ameztoy et al., 2019), which suggests that NTRC participates indirectly in small VC signaling through as yet to be identified mechanisms of regulation of the redox status and activity of proteins involved in hormone signaling.

OxiTRAQ-based quantitative and site-specific redox-proteomic analyses have revealed that small VCs emitted by *A. alternata* induce global reduction of the thiol redox proteome of leaves of WT plants, and highlighted the possible involvement of redox switching mechanisms in VC signaling (Ameztoy et al., 2019). Fungal VC treatment promotes reduction of cysteine residues of photosynthesis-related proteins such as CBC enzymes (e.g. cFBP1, sedoheptulose-1,7-bisphosphatase and phosphoribulokinase), and proteins involved in photochemical reactions (e.g. PSAN and FNRL). Small fungal VCs also promote the reduction of cysteine residues in PrxQ, which is involved in H_2O_2 breakdown in the thylakoids. Although highly conserved throughout land plants and algae, cysteine residues that are reduced by small VCs are not located in the regulatory Trx redox domains of their respective proteins (Ameztoy et al., 2019). Thus, it was suggested that these cysteine residues could play roles in the response to small microbial VCs by controlling the stability of the proteins and/or formation of complexes with other proteins that influence photosynthesis (Ameztoy et

al., 2019).

Unlike in WT plants, small fungal VCs promote global oxidation of the redox-proteome of leaves of ntrc plants. These compounds promote oxidation of highly conserved cysteine residues of PSAN and PrxQ in ntrc plants, which indicates that these proteins are subject to redox regulation in VC-exposed plants through mechanisms directly involving NTRC. In addition, small fungal VCs promote oxidation of highly conserved cysteine residues in proteins involved in water oxidation and formation of molecular oxygen (e.g. PSBO-1) (Murakami et al., 2005). Small VCs also promote oxidation of highly conserved cysteine residues of FNR1 that are essential for FNR1 enzymatic activity (Aliverti et al., 1993). FNR1 is implicated in cyclic electron transfer around PSI to produce ATP (Johnson, 2005), and in the generation of NADPH required for stromal redox regulation, reduction of NTRC and its target proteins, including CBC enzymes (Ceccarelli et al., 2004). It therefore seems that the weak response of ntrc plants to small fungal VCs is at least partly due to reduced photosynthesis as a consequence of PSAN, PSBO-1 and FNR1 oxidation and/or H_2O_2 overaccumulation as a result of PrxQ oxidation.

4.2 Leaf responses to small microbial VCs involve proteostatic regulation of the MEP and shikimate pathways by enhanced photosynthesis signaling

The CBC is an essential source of substrates for the synthesis of secondary metabolites important for growth and development such as phenylpropanoids and isoprenoids via the plastid-localized shikimate and the MEP pathways, respectively. Modulation of the metabolic flux towards both pathways involves the regulation of the provision of CBC intermediates (Henkes et al., 2001; Ghirardo et al., 2010; Pokhilko et al., 2015). Fine-tuning of the shikimate pathway involves the redox- and Clp protease complex-mediated proteostatic regulation of the pathway's first enzyme, phospho-2-dehydro-3-deoxyheptonate aldolase (Entus et al., 2002; Tzin et al., 2012; Nishimura et al., 2013). Moreover, modulation of the MEP pathway involves the transcriptional regulation of the expression of MEP pathway genes (Carretero-Paulet et al., 2002; Córdoba et al., 2009), the allosteric inhibition of the pathway's first enzyme, 1-deoxy-D-xylulose-5-phosphate synthase (DXS) by MEP pathway products (Banerjee et al., 2013; Ghirardo et al., 2014), and the proteostatic regulation of DXS by components of the plastidial PQC system such as chaperones and the Clp protease complex (Pulido et

al., 2013; Llamas et al., 2017; Rodriguez-Concepcion et al., 2019).

Highly sensitive label-free high-throughput differential proteomic studies revealed that small VCs emitted by *A. alternata* reduce the levels of proteins of the Clp protease system in leaves, and concomitantly augment those of proteins that accumulate to higher levels in Clp-defective mutants than in WT plants (Ameztoy et al., 2021). Proteins in this group include enzymes of the MEP and shikimate pathways, chaperones involved in folding and assembly of newly imported plastid proteins, and thioredoxins that participate in the redox regulation of CBC enzymes and enzymes involved in the synthesis of photosynthetic pigments (Ameztoy et al., 2021). In addition, small fungal VCs down-regulate the levels of enzymes involved in the carotenoid-to-ABA conversion process. These changes in the leaf proteome could explain, at least in part, the enhancement of photosynthetic CO_2 fixation, reduced ABA content, and enhanced contents of starch, MEP-pathway derived compounds (e.g. chlorophyll and carotenoids), and shikimate-pathway derived compounds (e.g. shikimate, flavonols and anthocyanins) that are present in leaves of plants exposed to small VCs. Small VCs also down-regulate the levels of transcripts that code for proteins of the Clp protease system, and up-regulate those coding for plastidial chaperones (Ameztoy et al., 2021). No transcriptional, proteomic or metabolic changes occur in leaves of *cfbp1* mutants impaired in redox-activated cFBP1 plants upon exposure to small fungal VCs (Ameztoy et al., 2021). The overall data indicate that adaptation of the plastid proteome and metabolome to small fungal VCs in leaves involves redox-regulated, photosynthesis-driven chloroplast-to-nucleus retrograde signaling mechanisms wherein transcriptional up-regulation of plastidial chaperones and down-regulation of the Clp protease system play important roles.

4.3 Small VCs modify root metabolism and architecture, and improve nutrient and water use efficiencies in leaves through proteome resetting mechanisms

In response to environmental changes, roots adjust their metabolism and architecture through mechanisms involving long-distance communication with the aerial part of the plant (Gansel et al., 2001; Lejay et al., 2008; Kiba et al., 2019), and shifts in phytohormone and ROS signaling (Tsukagoshi et al., 2010; Lan et al., 2012; Žd'árská et al., 2013; Bouguyon et al., 2016; Mangano et al., 2017). García-Gómez et al. (2020) have shown that small VCs emitted by the fungal phytopathogen *Penicillium*

aurantiogriseum promote major RSA changes (e.g. inhibition of primary root (PR) and LR growth, stimulation de novo of LR formation and promotion of extensive proliferation and elongation of RHs), alter root metabolism, and enhance intrinsic water use efficiency and tolerance to drought. These responses can be accounted for by transcriptionally and non-transcriptionally regulated changes in the expression of proteins involved in hormone metabolism, water and nutrient transport, sucrose breakdown, redox metabolism and signaling, and HCN scavenging (García-Gómez et al., 2020).

The fungal VC treatment augments the levels of CK and ethylene biosynthetic enzymes, and also enhances the production and/or signaling of CK, ethylene and auxin in roots (García-Gómez et al., 2020). This treatment elicits only weak root developmental responses in mutants impaired in signaling by auxin, ethylene and CK, which strongly indicates that RSA changes promoted by small VCs involve the action of these hormones. Small VCs emitted by *P. aurantiogriseum* down-regulate the expression of the CK-repressed iron carrier IRT1 and auxin-repressed aquaporins at both transcript and protein levels (García-Gómez et al., 2020), which may reflect transcriptionally regulated adjustments to reduced water and Fe demands in the leaves caused by VC-promoted enhanced photosynthetic water and Fe use efficiencies. Small fungal VCs also down-regulate the expression of auxin-repressed vacuolar invertases, which together with aquaporins, control turgor pressure as a driving force for root elongation (Sergeeva et al., 2006). This indicates that root shortening in response to small VCs is at least partly due to reduced osmotic water uptake caused by auxin-mediated down-regulation of the expression of aquaporins and vacuolar invertases.

O_2^- and H_2O_2 accumulation in the apoplast plays important roles in root and RH growth and development (Foreman et al., 2003; Passardi et al., 2006). Small fungal VCs enhance levels of these compounds in roots and RHs of exposed plants (García-Gómez et al., 2020). In addition, this treatment down-regulates the expression of major determinants of apoplastic O_2^- and H_2O_2 accumulation and RH formation and development, including plasma membrane aquaporins, apoplastic peroxidases and plasma membrane calcium pumps (García-Gómez et al., 2020). This indicates that apoplastic oxidative bursts in RHs caused by root proteome resetting are important determinants of the root and RH response to small fungal VCs. In support of this hypothesis, the *rhd2* mutant, which is impaired in apoplastic O_2^- and H_2O_2 production

in RHs is unresponsive in terms of O_2^- accumulation in RHs, stimulation of RH growth, and PR and LR shortening promoted by small fungal VCs (García-Gómez et al., 2020).

In roots of WT plants, small VCs emitted by *P. aurantiogriseum* enhance the expression of CAS-C1, which converts the cysteine and HCN produced in the last step of the ethylene biosynthetic pathway into H_2S and β-cyanoalanine (García-Gómez et al., 2020). CAS-C1 has been implicated in preventing accumulation of toxic levels of HCN that would otherwise prevent RH elongation (García et al., 2010; Arenas-Alfonseca et al., 2018). Roots of plants exposed to *P. aurantiogriseum* VCs accumulate high HCN levels (García-Gómez et al., 2020). In addition, exposure to small fungal VCs does not promote RH elongation and root shortening in *cas-c1* plants (García-Gómez et al., 2020). This strongly indicates that CAS-C1 operates in the RSA changes promoted by fungal VCs through mechanisms other than by maintaining low levels of HCN. Unlike WT plants, *cas-c1* plants do not accumulate high levels of O_2^- in RHs. One possible explanation for the weak response of roots and non-responsiveness of RHs to small fungal VCs in *cas-c1* plants is therefore that root shortening and RH formation and elongation promoted by fungal VCs involves enhanced O_2^- production by as yet to be identified CAS-C1 dependent mechanisms. Because H_2S is an important modulator of RSA (Mei et al., 2017; Zhang et al., 2017; Li et al., 2018a), another explanation for the weak response of *cas-c1* roots and RHs to small fungal VCs is that this response is mediated by H_2S produced by CAS-C1.

5. Conclusions and future considerations

Microorganisms emit small VCs other than CO_2 with molecular masses of less than ~45 Da that promote plant growth and developmental as well as metabolic changes. Enough information has been compiled to propose that the response of the aerial part of the plant to small VCs involves transcriptional and non-transcriptional regulatory mechanisms that depend heavily on signaling of rapid redox-activated photosynthesis and subsequent plastidial PQC system-mediated proteostatic up-regulation of plastidial thioredoxins and enzymes of the MEP and shikimate pathways. According to this view, rapid thiol redox activation of photosynthesis-related proteins promoted by highly reactive small microbial VCs enhances PET and augments the photosynthetic production of CBC metabolic intermediates to fuel the production of compounds derived from the MEP and shikimate pathways. These compounds initiate a cascade

of reactions leading to changes in the expression of nuclear genes, notably those encoding proteins of the plastidial PQC system (**Figure 2**). The resulting reduced protease activity and enhanced expression of chaperones in the chloroplast increase the stability and activity of target proteins including thioredoxins that redox-activate photosynthesis-related proteins, and enzymes of the MEP and shikimate pathways. This situation enables high metabolic flux from the CBC towards the MEP and shikimate pathways, and guarantees a sustained high rate of photosynthesis and accelerated growth. Enough information has also been obtained to propose that small VCs emitted by some fungal phytopathogens modify root metabolism and architecture, and adjust Fe and water uptake to reduced photosynthetic water and Fe demands in the leaves by means of transcriptionally and non-transcriptionally regulated proteome resetting mechanisms that involve HCN scavenging, hormone and apoplastic H_2O_2 production and signaling and reduced expression of water and Fe transporters (**Figure 2**).

To our knowledge, transcriptome and proteome resetting promoted by small fungal VCs is the first example of an environmentally triggered modulation of the expression of genes encoding Clp protease system proteins as a way of changing the levels of MEP and shikimate pathway enzymes and hence regulating chloroplast metabolism. Also, small fungal VC-promoted accumulation of exceptionally high levels of starch in mesophyll cells of PGI1-lacking plants constitutes the first clear example of starch production through non-canonical starch biosynthetic pathway(s) in mature leaves of plants cultured under autotrophic conditions. Investigating plant responses to small microbial VCs is therefore an excellent way not only to understand plant-microbe interactions, but also to unveil fundamental mechanisms involved in metabolic regulation in plants. Some of the mechanisms involved in the response of plants to small VCs emitted by fungal phytopathogens differ from those involved in the response to those emitted by beneficial microorganisms (García-Gómez et al., 2020), which adds further interest in carrying out research on the mechanism(s) of action of these compounds, and raises questions regarding the evolution of the mechanisms involved in modulation of the response of plants to microbes and their ecological significance.

Small VCs from different microorganisms promote distinct responses in exposed plants (García-Gómez et al., 2019). This indicates that microorganisms have less that ~45 Da volatilomes with different action potentials. A big challenge

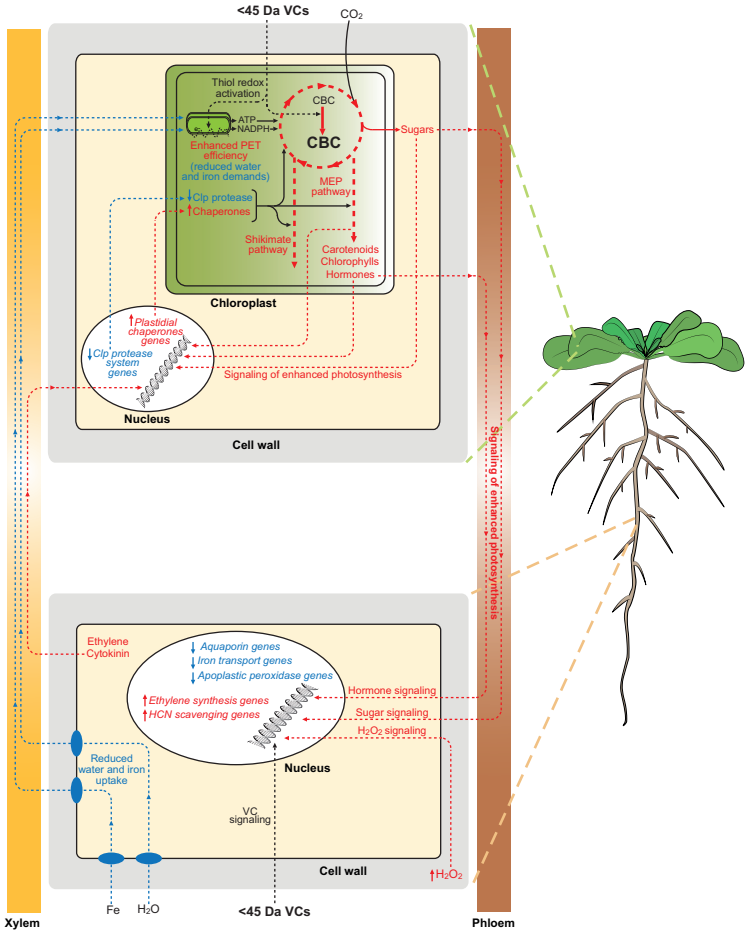

Figure 2: Suggested model of regulation of the plant response to small fungal VCs. According to this model, rapid thiol redox activation of photosynthesis-related proteins promoted by small microbial VCs enhances PET, photosynthetic CO_2 fixation and the metabolic flux towards the MEP and shikimate pathways. The resulting enhanced production of compounds from these pathways initiates cascades of reactions leading to reduced Clp protease activity and enhanced expression of chaperones in the chloroplast, which increases the stability and activity of photosynthesis-related proteins, and enzymes of the MEP and shikimate pathways. This situation guarantees high metabolic flux from the CBC towards the MEP and shikimate pathways, and a sustained high rate of photosynthesis and accelerated growth. Small microbial VCs modify root architecture and metabolism to adapt Fe and water uptake to reduced water and Fe demands in the aerial part of the plant by means of transcriptionally and non-transcriptionally regulated proteome resetting mechanisms that involve HCN scavenging, hormone and apoplastic H_2O_2 production and signaling and reduced expression of water and Fe transporters. Metabolic and signaling pathways and genes up-regulated by small fungal VCs are highlighted in red, while functions down-regulated by fungal VCs are highlighted in blue. Multistep metabolic pathways and signaling cascades are indicated by dashed arrows. Illustration from Bouché, Frédéric (2018): 2018_Arabidopsis_flowering_plant. figshare. Figure. https://doi.org/10.6084/m9.figshare.7159937.v1.

in understanding how microorganisms interact with plants is identification of the small bioactive microbial VCs that promote growth and developmental changes, and investigating their biochemical and molecular mechanism(s) of action when exogenously applied in discrete or combined forms in different parts of the plant and at concentrations resembling those in natural environments. Good candidates are NO, NO_2, CO, H_2S, ethylene and methanol. Several areas requiring further work in order to understand the mechanisms of action of small VCs have been highlighted in the text. Perhaps the greatest interest in the future may be focused on the role of GPT2 in the response of plants to small microbial VCs. GPT2 could provide G6P not only for starch biosynthesis in leaves, but also to fuel the MEP and shikimate pathways in roots. In addition, it could provide G6P for the oxidative pentose phosphate pathway in roots, which has been shown to be important in generating signals involved in the photosynthetic regulation of nutrient acquisition (Lejay et al., 2008). Investigation of the role of GPT2 in the response of plants to small microbial VCs would require the use of *gpt2* and *pgi1gpt2* mutants. This topic has been treated in the first chapter of my thesis work entitled "Glucose-6-P/phosphate translocator2 mediates the phosphoglucose-isomerase-1 independent response to microbial volatiles". Another big challenge is to determine the role in the response to small VCs of the cysteine residues of photosynthesis-related proteins whose redox status is altered upon short-term exposure to small VCs. This would require the production of genetically engineered plants expressing photosynthesis-related enzymes mutated at the redox-sensitive cysteine residues and the characterization of their responses to small VCs. This has been treated in the second chapter of my thesis work entitled "The microbial volatile-responsive redox-sensitive Cys95 residue is an important structural and functional determinant of the Calvin-Benson fructose-1,6-bisphosphatase in Arabidopsis".

Additional research is needed to understand how signals generated in the chloroplast upon brief VC exposure are transduced to the nucleus and to obtain a holistic view of the molecular mechanisms involved in the plant response to these compounds. Known signals involved in chloroplast-to-nucleus retrograde signaling include ROS generated by photosynthesis, tetrapyrroles, the sulfur metabolism by-product 3´-phosphoadenosine 5´-phosphate (PAP), the MEP pathway intermediate 2-C-methyl-D-erythritol-2,4-cyclopyrophosphate (MEcPP), isoprenes, and the CBC intermediate dihydroxyacetone phosphate (Estavillo et al., 2011; Xiao et al., 2012;

Vogel et al., 2014; Chan et al., 2016). Small fungal VCs do not promote changes in ROS levels in leaves (Ameztoy et al., 2019), suggesting that these compounds are not involved in retrograde signaling of redox-activation of photosynthesis promoted by small VCs. Microbial VCs up-regulate the expression of MEP pathway enzymes and PAP biosynthetic enzymes (Ameztoy et al., 2021). It is therefore likely that chloroplast-to-nucleus retrograde signaling of enhanced photosynthesis triggered by small VCs involves PAP and/or the MEP pathway intermediate MEcPP.

The lack of correlation between transcriptome and proteome changes occurring in plants exposed to small fungal VCs strongly indicates that the regulation of plant responses to these compounds is primarily non-transcriptional. Further studies using mutants of the PQC system will be necessary to learn the extent to which PQC-mediated proteostastic regulation of gene expression is involved in the plant response to small VCs. Many studies during the last decade based on next-generation sequencing and ribosome footprint profiling technologies have demonstrated the relevance of translational regulation to plant growth and environmental responses (Merchante et al., 2017). This type of study will be required in order to investigate the contribution of translational regulation to the response to VCs and close the gap between transcriptomic and proteomic data from small VC-exposed plants.

OBJETIVOS

El objetivo general de esta tesis es profundizar en el conocimiento de los mecanismos que regulan la respuesta de las plantas a los VCs microbianos. Para ello me planteé los siguientes objetivos específicos:

Objetivo #1: estudiar el papel que juega GPT2 en la regulación de la respuesta a VCs fúngicos de plantas de Arabidopsis impedidas en PGI1.

Objetivo #2: estudiar el papel que juega el residuo Cys95 en la estructura y función de cFBP1.

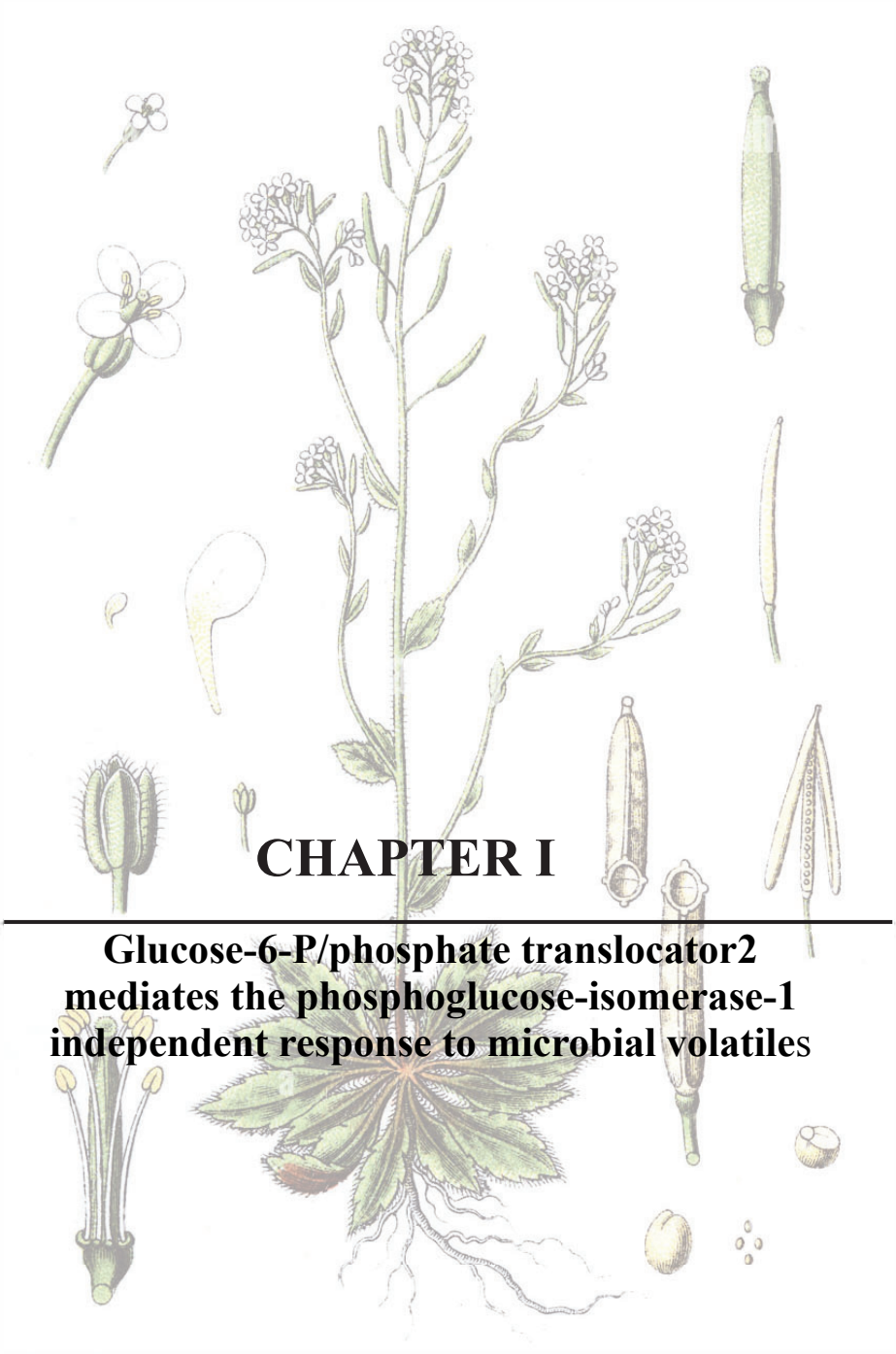

CHAPTER I

Glucose-6-P/phosphate translocator2 mediates the phosphoglucose-isomerase-1 independent response to microbial volatiles

INTRODUCTION

Phosphoglucose isomerase (PGI) catalyzes the reversible isomerization of glucose-6-P (G6P) and fructose-6-P. This enzyme participates in the early steps of glycolysis and in the regeneration of G6P pools in the pentose phosphate pathway (PPP). In mammals, in addition to its role as a glycolytic and PPP enzyme, PGI plays moonlighting roles as a cytokine and growth factor (Chaput et al., 1988; Watanabe et al., 1996; Jeffery et al., 2000). Arabidopsis has one PGI isozyme in the plastid, i.e., PGI1, which plays a key role in transitory starch production in mesophyll cells of leaves, connecting the Calvin-Benson cycle (CBC) with the canonical starch biosynthetic pathway (Yu et al., 2000; Fünfgeld et al., 2022). Its activity is modulated by glycolytic and PPP metabolic intermediates (Dietz, 1985; Backhausen et al., 1997) and by its redox status (Heuer et al., 1982). PGI1 interacts with some plastid-localized members of the 14-3-3 family of proteins (McWhite et al., 2020; https://thebiogrid.org/13853/summary/*arabidopsis-thaliana*/*pgi1*.html), which regulate multiple biological processes by phosphorylation-dependent protein-protein interactions (Denison et al., 2011). Some phosphorylation sites of PGI1 are flanked by redox-sensitive cysteine residues that respond to environmental changes (Reiland et al., 2009; Wang et al., 2013; Liu et al., 2014; Yin et al., 2017; https://phosphat.uni-hohenheim.de/). It thus appears that PGI1 is subject to complex regulatory mechanisms.

PGI1-lacking *pgi1-2* plants display reduced photosynthetic capacity and slow growth phenotypes, and accumulate low levels of starch and fatty acids in leaves and seeds, respectively (Bahaji et al., 2015; Bahaji et al., 2018). Moreover, these plants accumulate low levels of isoprenoid hormones derived from the plastid-localized 2-C-methyl-D-erythritol 4-P (MEP) pathway that are important for growth, development and photosynthesis including active forms of gibberellins (GAs) and trans-zeatin (tZ) type cytokinins (CKs) (Bahaji et al., 2015; Bahaji et al., 2018). PGI1 is mainly expressed in root tips and vascular tissues of cotyledons, mature leaves and roots (Bahaji et al., 2018), where genes involved in the synthesis of MEP pathway-derived isoprenoid hormones are strongly expressed (Silverstone et al., 1997; Miyawaki et al., 2004; Mitchum et al., 2006; Behnam et al., 2013; Yang et al., 2020). Thus, we have proposed that PGI1 is an important determinant of photosynthesis, metabolism, growth, reproductive development and seed yield, probably due to its involvement in the synthesis of storage reserves in the embryo and PPP/glycolytic

metabolic intermediates necessary for the synthesis of MEP pathway-derived isoprenoid hormones in vascular tissues (Bahaji et al., 2015; Bahaji et al., 2018).

Microorganisms emit a plethora of volatile compounds (VCs) that promote plant growth and photosynthesis as well as strong developmental and metabolic changes (Zhang et al., 2008; Sánchez-López et al., 2016b; Martínez-Medina et al., 2017; Camarena-Pozos et al., 2019; Baroja-Fernández et al., 2021; Sharifi et al., 2022; Vlot and Rosenkranz, 2022). Recently, using a "box-in-box" *in vitro* co-cultivation system in which plants were grown in the vicinity of microbial cultures covered with charcoal filters, we showed that VCs of molecular masses of less than ca. 45 Da (hereinafter designated as "small VCs") are important determinants of plant responses to microbial volatile emissions (Ameztoy et al., 2019; García-Gómez et al., 2019; García-Gómez et al., 2020; Ameztoy et al., 2021; Gámez-Arcas et al., 2022a). Regulation of these responses is primarily non-transcriptional and involves global changes in the proteome (Ameztoy et al., 2021) and thiol redox proteome, particularly in photosynthesis- and starch biosynthesis-related proteins (Li et al., 2011; Ameztoy et al., 2019). Responses to small VCs also involve CK-mediated mechanisms wherein long-distance communication between roots and the aerial part of the plant play important roles (García-Gómez et al., 2019; García-Gómez et al., 2020; Gámez-Arcas et al., 2022a). Like in wild-type (WT) plants, small VCs promote growth, photosynthesis and tZ accumulation in *pgi1-2* plants (Sánchez-López et al., 2016a). These compounds also promote the accumulation of exceptionally high levels of starch in *pgi1-2* leaves (Sánchez-López et al., 2016a). Therefore, the response of plants to small VCs involves PGI1-independent mechanisms, including the activation of an as-yet unidentified non-canonical starch biosynthetic pathway(s) in mesophyll cells of leaves (Bahaji et al., 2011; Baroja-Fernández et al., 2012; Sánchez-López et al., 2016a).

A striking alteration in the transcriptome of leaves of small fungal VC-treated plants involves strong up-regulation of levels of transcripts of *GPT2* (At1g61800) (Sánchez-López et al., 2016b), a gene that codes for a plastidial G6P/Pi transporter (Kammerer et al., 1998). *GPT2* is implicated in dynamic photosynthetic acclimation to environmental changes, such as increased irradiance through mechanisms involving signalling of G6P partitioning between chloroplasts and the cytosol, and resetting of the photosynthesis-related proteome (Athanasiou et al., 2010; Dyson et al., 2015; Miller et al., 2017; Karim, 2021). Dyson et al. (2014) have suggested that *GPT2* plays an

important role in sugar sensing or signaling during germination and the transition from heterotrophic to autotrophic growth in developing seedlings. At the transcript level, *GPT2* has low, almost undetectable expression in WT leaves (Athanasiou et al., 2010; Weise et al., 2019; https://bar.utoronto.ca/eplant), but is induced in starch deficient mutants (Kunz et al., 2010). In leaves, different abiotic stress treatments promote the accumulation of *GPT2* transcripts in vascular and epidermal cells, but not in the mesophyll (Berkowitz et al., 2021). Elevated photosynthesis, phosphate starvation or exogenous sugar supply up-regulate *GPT2* transcript levels (Hammond et al., 2003; Gonzali et al., 2006; Athanasiou et al., 2010; van Dingenen et al., 2016; García-Gómez et al., 2019; Weise et al., 2019) and promote starch accumulation (Makino et al., 1999; Athanasiou et al., 2010; Lei et al., 2011). In addition, 35S promoter-driven *GPT2* expression restores to WT the low starch content phenotype of *pgi1-2* leaves (Niewiadomski et al., 2005). It is thus conceivable that accumulation of high levels of starch in leaves of WT and *pgi1-2* plants promoted by small microbial VCs is due, at least partly, to enhanced GPT2-mediated incorporation of cytosolic G6P into the chloroplasts and subsequent conversion into starch, thus bypassing the PGI1 reaction (Sánchez-López et al., 2016b). Furthermore, because PGI1 is strongly expressed in vascular tissues and root tip cells (Bahaji et al., 2018), it is likely that changes promoted by small VCs in leaves are due to enhanced GPT2-mediated incorporation of cytosolic G6P into non-photosynthetic plastids of vascular tissues and root tip cells and subsequent PGI1-mediated metabolization into growth and photosynthesis determinants including isoprenoid hormones. To test these hypotheses and clarify the mechanisms involved in plant responses to small microbial VCs, we compared the growth, photosynthetic, starch and tZ contents as well as proteomic responses of WT, *GPT2*-null *gpt2-1*, *PGI1*-null *pgi1-2* and *pgi1-2gpt2-1* plants to small VCs emitted by the fungal phytopathogen Alternaria alternata. We also characterized the response of *pgi1-2gpt2-1* plants ectopically expressing *GPT2* under the control of the vascular tissue-specific Athspr promoter (Zhang et al., 2014) to small VCs. Moreover, using plants transformed with constructs carrying the *GPT2* promoter fused to the GUS reporter, we examined the *GPT2* expression pattern. Results presented in this work provide strong evidence that, under conditions in which PGI1 activity is reduced, long-distance action of GPT2 plays an important role in the response of plants to small VCs through mechanisms involving resetting of the photosynthesis-related proteome in

leaves. Evidence is provided that *GPT2* is subject to complex regulatory mechanisms that impede its expression in mesophyll cells of leaves.

RESULTS

The response of *pgi1-2gpt2-1* plants to small fungal VCs is weaker than that of WT and *pgi1-2* plants

We compared growth, starch accumulation and photosynthesis responses of WT, *gpt2-1*, *pgi1-2* and *pgi1-2gpt2-1* plants (**Table 1**) to VCs of molecular masses of less than ca. 45 Da emitted by adjacent *A. alternata* cultures. As shown in **Figure 1**, in the absence of small fungal VCs, the sizes and weights of rosettes of these plants were comparable to each other. Small fungal VCs strongly promoted rosette growth in WT, *pgi1-2* and, to a lesser extent, *pgi1-2gpt2-1* plants (**Figure 1**). The relatively weak promotion of growth of *pgi1-2gpt2-1* plants by small fungal VCs could be rescued by the ectopic expression of *PGI1* or *GPT2* under the control of the *35S* promoter (**Figure 1**).

Table 1: Plants used in this work.

Designation	Description	Source
Wasilewskija-2 (Ws-2)	Wild type	N1601
pgi1-2	*PGI1* knockout mutant	Kunz et al. (2010)
gpt2-1	*GPT2* knockout mutant	GABI_454H06
pgi1-2gpt2-1	*pgi1-2* and *gpt2-1* double mutant	Bahaji et al. (2015)
pgi1-2gpt2-1 35S:PGI1	*pgi1-2gpt2-1* mutant expressing *PGI1* under the control of the cauliflower mosaic virus *35S* promoter	This work
pgi1-2gpt2-1 35S:GPT2	*pgi1-2gpt2-1* mutant expressing *GPT2* under the control of the cauliflower mosaic virus *35S* promoter	This work
pgi1-2gpt2-1 promAthspr:GPT2	*pgi1-2gpt2-1* mutant expressing *PGI1* under the control of the vascular tissue- and root tip-specific *Athspr* promoter	This work
promAthspr:GUS	WT plants expressing *GUS* under the control of the vascular tissue- and root tip-specific *Athspr* promoter	This work
promGPT2:GUS	WT plants expressing *GUS* under the control of the *GPT2* promoter	This work
promGPT2:GPT2-GUS	WT plants expressing translationally fused GPT2-GUS under the control of the *GPT2* promoter	This work
35S:GPT2-GUS	WT plants expressing translationally fused GPT2-GUS under the control of the cauliflower mosaic virus *35S* promoter	This work

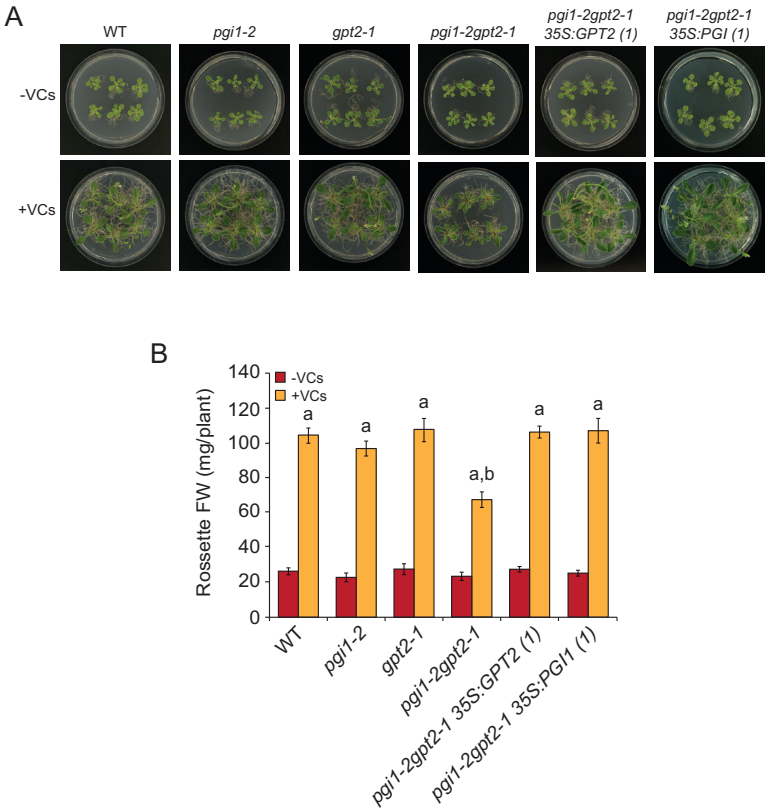

Figure 1: The growth response of *pgi1-2gpt2-1* plants to small fungal VCs is weaker than that of WT and *pgi1-2* plants. (A) External phenotypes and (B) rosette FW of WT, *pgi1-2*, *gpt2-1* and *pgi1-2gpt2-1* plants, and plants from one representative line each of *pgi1-2gpt2-1* transformed with *35S:GPT2* or *35S:PGI1* (*pgi1-2gpt2-1 35S:GPT2(1)* and *pgi1-2gpt2-1 35S:PGI1(1),* respectively) cultured in the absence or continuous presence of small fungal VCs for one week. Values in panel (B) are means ± SE for three biological replicates (each a pool of 12 plants) obtained from four independent experiments. Lowercase letters indicate significant differences, according to Student´s *t*-test ($P<0.05$) between: "a" VC-treated and non-treated plants, and "b" VC-treated WT and mutant plants. .

In the absence of small fungal VCs, the starch content in mature leaves of *gpt2-1* plants was comparable to that of WT plants, as revealed by starch iodine staining (**Figure 2A**) and quantitative starch content measurement (**Figure 2B**) analyses. In keeping with Bahaji et al. (2015), the starch content in *pgi1-2* and *pgi1-2gpt2-1* mature leaves was ca. 15% of that of WT leaves (**Figure 2**). The "low starch content" phenotype of *pgi1-2gpt2-1* plants could be rescued by the ectopic expression of *PGI1* under the control of the *35S* promoter but not by that of *GPT2*. Small fungal VCs

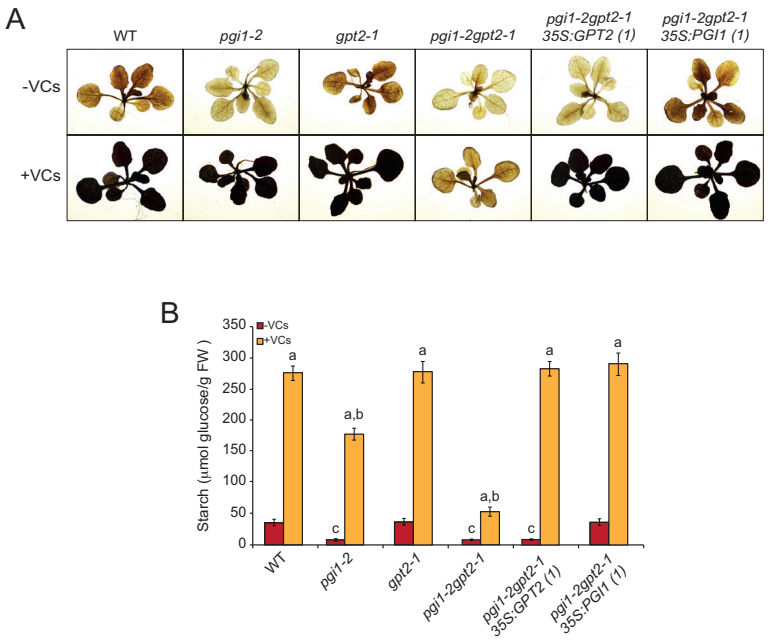

Figure 2: The starch accumulation response of *pgi1-2gpt2-1* plants to small fungal VCs is weaker than that of WT and *pgi1-2* plants. (A) Starch content and (B) iodine staining of leaves of WT, *pgi1-2*, *gpt2-1* and *pgi1-2gpt2-1* plants and plants from one representative line each of *pgi1-2gpt2-1* transformed with *35S:GPT2* or *35S:PGI1* (*pgi1-2gpt2-1 35S:GPT2(1)* and *pgi1-2gpt2-1 35S:PGI1(1)*, respectively) cultured in the absence or continuous presence of small VCs for one week. Values in panel (A) are means ± SE for three biological replicates (each a pool of 12 plants) obtained from four independent experiments. Lowercase letters indicate significant differences, according to Student´s *t*-test (P<0.05) between: "a" VC-treated and non-treated plants, "b" VC-treated WT plants and mutants, and "c" VC non-treated WT and mutant plants.

promoted the accumulation of exceptionally high levels of starch in leaves of exposed WT and *gpt2-1* plants (**Figure 2**). In keeping with Sánchez-López et al. (2016b), these compounds also induced strong accumulation of starch in leaves of *pgi1-2* plants, although to a lesser extent than in leaves of WT plants (**Figure 2**). Small VCs increased the starch content in leaves of *pgi1-2gpt2-1* plants to levels much lower than those of VC-exposed *pgi1-2* leaves and comparable to those of WT leaves not exposed to small VCs (**Figure 2**). The weak promotion of starch accumulation by small VCs in leaves of *pgi1-2gpt2-1* plants could be rescued to WT levels by the ectopic expression of either *PGI1* or *GPT2* under the control of the *35S* promoter (**Figure 2**).

In the absence of small VCs, values of the net rates of CO_2 assimilation (A_n) at all intracellular CO_2 concentration (C_i) levels, the maximum rate of carboxylation

by Rubisco (V_{cmax}) and the maximum electron transport demand for RuBP regeneration (J_{max}) in *gpt2-1* plants were comparable to those of WT plants (**Figure 3A, D, E**). In *pgi1-2* plants, these values were lower than those in WT plants (**Figure 3B, D, E**), consistent with Bahaji et al. (2015), and similar to those of *pgi1-2gpt2-1* plants (**Figure 3C, D, E)**. As expected, small VCs enhanced A_n values at all C_i levels as well as Vcmax and Jmax values in WT plants (**Figure 3A, D, E**). Values of these photosynthetic parameters in small VC-treated *gpt2-1* plants were comparable to those of VC-treated WT plants (**Figure 3A, D, E**). In *pgi1-2* plants, small VCs enhanced values of A_n at all C_i levels as well as V_{cmax} and J_{max} to those of VC-non-treated WT plants (**Figure 3B, D, E**). Small fungal VCs induced a small, statistically non-significant increase of A_n, V_{cmax} and J_{max} values in *pgi1-2gpt2-1* plants (**Figure 3C, D, E**). In both presence and absence of small fungal VCs, the "low photosynthetic capacity" phenotype of *pgi1-2gpt2-1* plants could be restored to almost WT levels by ectopic expression of *PGI1* or *GPT2* under the control of the *35S* promoter (**Supplemental Figure S1**).

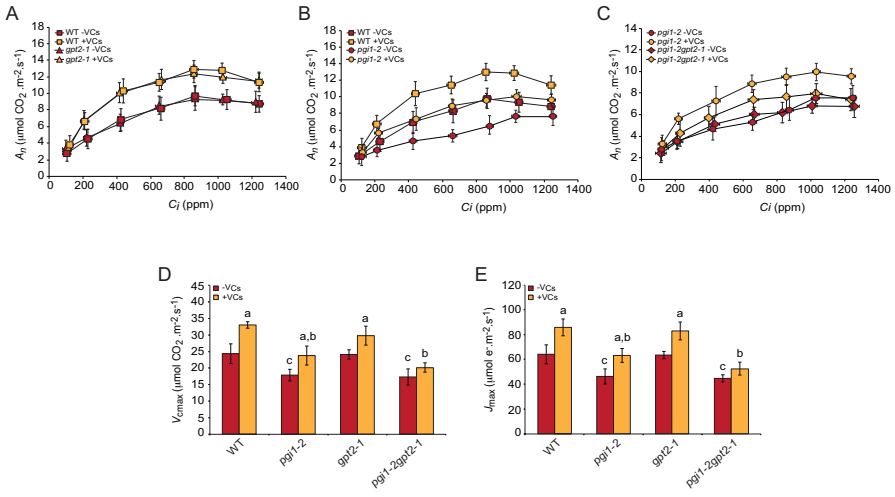

Figure 3: The photosynthetic response of *pgi1-2gpt2-1* plants to small fungal VCs is weaker than that of WT and *pgi1-2* plants. Curves of net CO_2 assimilation rate (A_n) versus intercellular CO_2 concentration (Ci) in leaves of (A) WT and *gpt2-1* plants, (B) WT and *pgi1-2* plants, and (C) *pgi1-2* and *pgi1-2gpt2-1* plants cultured in the absence or continuous presence of small VCs released by adjacent *A. alternata* cultures for 3 days. (D) V_{cmax} and (E) J_{max} values calculated from the A_n/C_i curves. Treatment started 28 days after sowing plants. In (A), (B) and (C), values are means ± SE for four plants. In (D) and (E), values are means ± SE for four biological replicates (each a pool of four plants) obtained from four independent experiments. Lowercase letters indicate significant differences, according to Student´s *t*-test ($P<0.05$), between: "a" VC-treated and non-treated plants, "b" VC-treated WT and mutants, and "c" VC non-treated WT and mutant plants.

Knocking out *GPT2* decreases the content of tZ in *pgi1-2* plants

Having established *GPT2*'s involvement in the *pgi1-2* growth, photosynthetic and starch accumulation responses to small fungal VCs, we compared the effects of these compounds on the tZ contents in *pgi1-2* and *pgi1-2gpt2-1* plants. For this, we measured the tZ contents in mature leaves of *pgi1-2* and *pgi1-2gpt2-1* plants cultured in the absence or continuous presence of small fungal VCs. We also measured the tZ contents in leaves of WT plants. Under both experimental conditions, the tZ content in *pgi1-2gpt2-1* leaves (0.71 ± 0.10 and 1.87 ± 0.18 pmol g^{-1} DW in plants cultured in the absence and presence of VCs, respectively) was significantly lower than in *pgi1-2* plants (1.59 ± 0.11 and 2.34 ± 0.27 pmol g^{-1} DW in plants cultured in the absence and presence of VCs, respectively), which in turn accumulated lower levels of tZ than WT leaves (2.54 ± 0.52 and 3.60 ± 0.05 pmol g^{-1} DW in plants cultured in the absence and presence of VCs, respectively).

Vascular tissue- and root tip-specific expression of *GPT2* is sufficient to revert to WT the poor response of *pgi1-2gpt2-1* plants to small VCs

PGI1 is strongly expressed in root tips and vascular tissues of roots, cotyledons, hypocotyls and fully expanded mature leaves (Bahaji et al., 2018). It is thus likely that vascular expression of *GPT2* plays an important role in the response of *pgi1-2* plants to small VCs. To test this hypothesis, we characterized *pgi1-2gpt2-1* plants transformed with *promAthspr:GPT2*, which express *GPT2* under the control of the vascular tissue-specific *Athspr* promoter (Zhang et al., 2014) (**Table 1**). As shown in **Figure 4A**, preliminary histochemical analyses of *promAthspr:GUS* plants transformed with *promAthspr* fused to the *GUS* reporter showed vascular tissue and root tip specificity of *promAthspr*, both in the absence and presence of small VCs. Data obtained from 3 independent lines of *pgi1-2gpt2-1* plants transformed with *promAthspr:GPT2* revealed that, in the absence of small fungal VCs, vascular and root tip-specific GPT2 expression almost completely restored to WT the photosynthetic capacity of *pgi1-2gpt2-1* plants (**Figure 4B**) but did not restore the "low starch content" phenotype of these plants (**Figure 4C**). In the presence of small fungal VCs, vascular- and root tip-specific GPT2 expression completely restored to WT the weight of VC-exposed *pgi1-2gpt2-1* plants (**Figure 4D**) and almost completely restored to WT the photosynthetic capacity and starch content of these plants (**Figure 4B, C**).

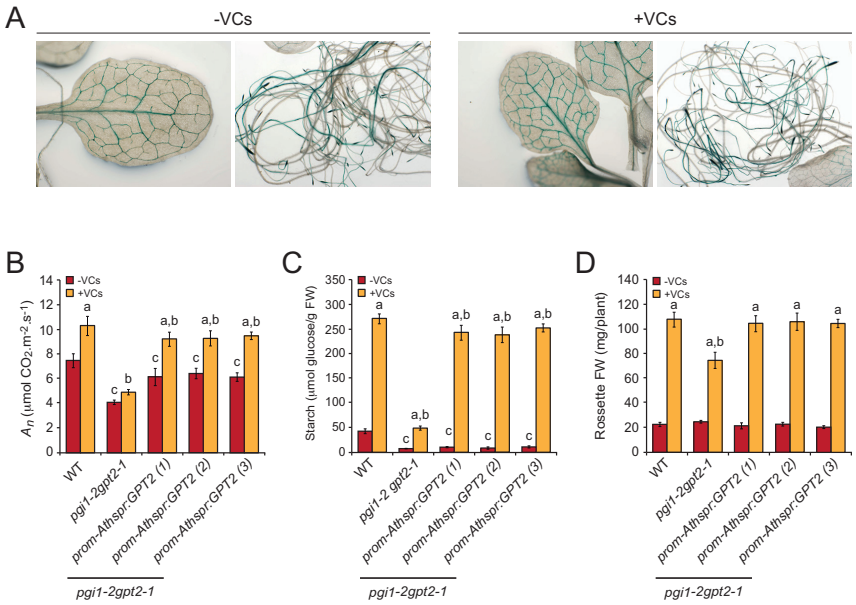

Figure 4: Vascular tissue- and root tip-specific expression of GPT2 is sufficient to revert to WT the poor response of *pgi1-2gpt2-1* plants to small VCs. (A) Expression pattern of the *Athspr* promoter in transgenic *promAthspr:GUS* plants cultured in the absence or presence of small fungal VCs for one week, as manifested by GUS histochemical staining of leaves and roots, (B) A_n at 400 ppm CO_2, (C) starch content and (D) rosette FW of WT, *pgi1-2gpt2-1* and three independent lines of *pgi1-2gpt2-1* transformed with *promAthspr:GPT2* cultured in the absence or continuous presence of small VCs for one week. In (B), values are means ± SE for four plants. Values in panels (C) and (D) are means ± SE for three biological replicates (each a pool of 12 plants) obtained from four independent experiments. In (B), (C) and (D), lowercase letters indicate significant differences, according to Student´s t-test ($P<0.05$), between: "a" VC-treated and non-treated plants, "b" VC-treated WT and mutants, and "c" VC non-treated WT and mutant plants.

Knocking out *PGI1* and *GPT2* decreases the expression of photosynthesis-related proteins

To obtain insights into the PGI1- and GPT2- mediated molecular mechanisms involved in the responses of plants to small VCs, we carried out high-throughput differential proteomic analyses between leaves of (i) WT plants cultured in the absence or presence of small VCs, (ii) VC-exposed *gpt2-1* and VC-exposed WT plants, (iii) VC-exposed *pgi1-2* and VC-exposed WT plants, and (iv) VC-exposed *pgi1-2gpt2-1* and VC-exposed WT plants. As a preliminary step to establish the VC exposure time for harvesting leaf samples, we carried out a time-course qRT-PCR analysis of *GPT2* transcript levels in leaves of WT plants cultured in the absence or presence of small VCs. We found that the pattern of *GPT2* transcript content in VC-exposed leaves was

similar to that previously reported in leaves of plants exposed to increased irradiance (Athanasiou et al., 2010). During the first 16 h of VC exposure, *GPT2* transcript levels increased rapidly, and then fell to reach a steady-state significantly greater than that of the controls after 3 days of VC exposure **(Supplemental Figure S2**). Based on these observations, we decided to conduct proteomic analyses using leaves of plants exposed to small VCs for 2 days, which still exhibited high *GPT2* transcript levels. These analyses revealed that small fungal VCs promoted widespread proteome resetting in all genotypes analyzed. The results obtained can be summarized as follows:

(i) 425 out of the 4188 proteins identified in the comparative study between leaves of WT plants cultured in the absence or presence of small VCs were differentially expressed (**Supplemental Table S1**). Using the broad characterizations outlined by the MapMan tool (https://mapman.gabipd.org/) (Thimm et al., 2004), the proteins differentially expressed by small VCs were assembled into 29 functional groups (**Supplemental Figure S3A**). Predicted locations of these proteins using the SUBA4 Arabidopsis protein subcellular localization database (Hooper et al., 2017) included almost all cellular compartments, but the locations associated with the greatest number of proteins were the cytosol and plastid (**Supplemental Table S1; Supplemental Figure S3B**). Nearly 70% of these proteins were identified as differentially expressed by small VCs in a previous differential proteomic study using a Col-O background (Ameztoy et al., 2021) (**Supplemental Table S1**). No statistically significant changes in the levels of GPT2 protein were observed upon small fungal VC treatment (**Supplemental Table S1**).

(ii) Only 6 out of the 4187 proteins identified in the comparative study between small VC-exposed *gpt2-1* leaves and VC-exposed WT leaves were differentially expressed (**Supplemental Table S2**). No statistically significant differences in GPT2 levels were observed between leaves of small VC-exposed *gpt2-1* and VC-exposed WT plants.

(iii) 64 out of the 4186 proteins identified in the comparative study between VC-exposed *pgi1-2* leaves and VC-exposed WT leaves showed statistically different expression levels (**Supplemental Table S3, Figure 5A**). Nearly 35% of these differentially expressed proteins (DEPs) were predicted to have a plastidial location and 10 of them were photosynthesis-related proteins (**Supplemental Table S3, Figure 5C**).

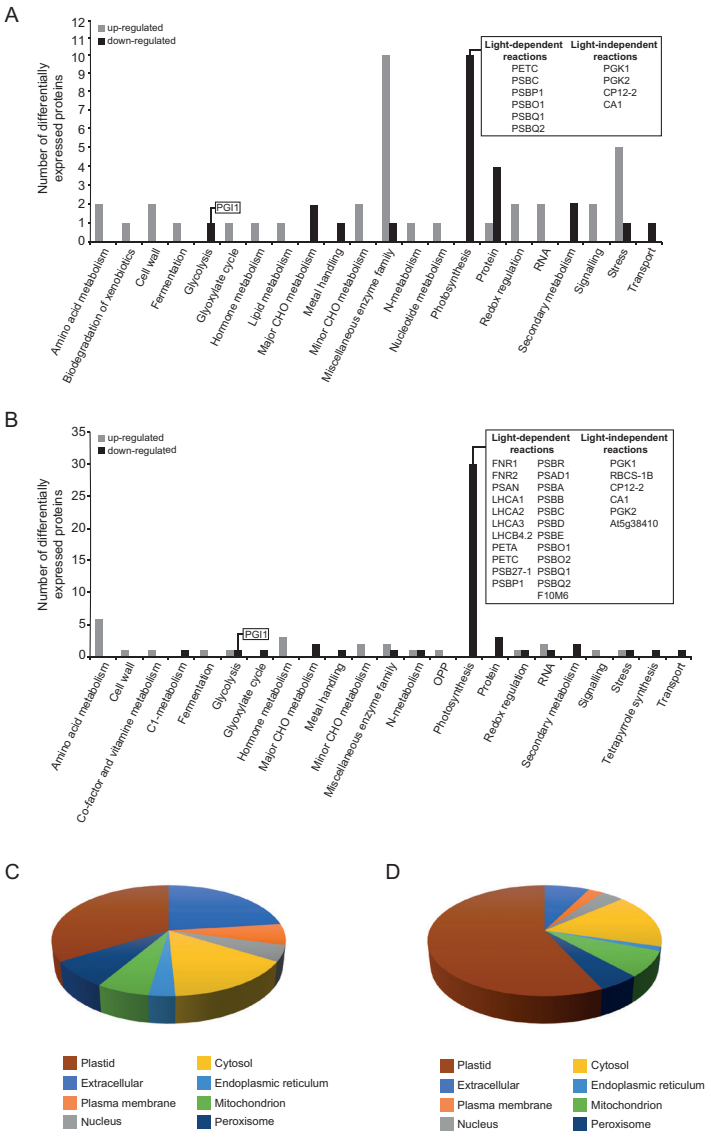

Figure 5: Knocking out *PGI1* and *GPT2* decreases the expression of photosynthesis-related proteins in small VC-exposed plants. The graphics represent the functional categorization and localitation of differentially expressed proteins (DEPs) in the comparative study between leaves of *pgi1-2* and WT plants (A and C) and *pgi1-2gpt2-1* and WT plants (B and D) cultured in the presence of small VCs for two days. In A and B, proteins that were significantly down- or up-regulated in mutants are arranged according to the putative functional category assigned by MapMan software. The numbers of up- and down-regulated proteins in each categorical group are indicated by gray and black bars, respectively. In C and D, DEPs are classified according to their subcellular localization. DEPs discussed here are shown in the boxes. The data were obtained from Supplemental Table S4 and Supplemental Table S6**.**

(iv) 81 out of the 4148 proteins identified in the comparative study between VC-exposed *pgi1-2gpt2-1* leaves and VC-exposed WT leaves showed statistically significant different expression levels (**Supplemental Table S4, Figure 5B**). Nearly 70% of these DEPs were predicted to have a plastidial location, and 29 of them were photosynthesis-related proteins (**Supplemental Table S4, Figure 5D**).

We next considered whether differences in the proteomes of VC-exposed *pgi1-2gpt2-1* leaves and VC-exposed WT leaves were due to differential perception and/or signalling of small VC or to knocking out of both *PGI1* and *GPT2*. We thus conducted differential proteomic analyses between leaves of *pgi1-2gpt2-1* and WT plants cultured in the absence of small fungal VCs. As shown in **Supplemental Table S5 and Supplemental Figure S4**, the majority of the proteins differentially expressed between leaves of *pgi1-2gpt2-1* and WT plants not exposed to VCs were also differentially expressed between leaves of small VC-exposed *pgi1-2gpt2-1* and WT plants (cf. **Supplemental Table S4, Figure 5B**). Therefore, we concluded that the reduced levels of photosynthesis-related proteins in VC-exposed *pgi1-2gpt2-1* plants were due to the lack of PGI1 and GPT2 rather than to differences in perception and/or signalling of small VC in the two genotypes.

***GPT2* expression regulation**

Proteomic data showing that small VCs did not enhance the GPT2 protein content in exposed leaves strongly indicated that *GPT2* expression is subjected to complex regulation. To test this hypothesis, we conducted qRT-PCR analyses of *GUS* transcript levels and GUS histochemical staining analyses in WT plants transformed with *promGPT2:GUS*, which expressed *GUS* under the control of the 1.1 kb *promGPT2* region immediately upstream the translation start codon of GPT2 (**Table 1**). We also characterized plants transformed with *promGPT2:GPT2-GUS* and *35S:GPT2-GUS*, which expressed translationally fused GPT2-GUS under the control of *promGPT2* and the *35S* promoter, respectively (**Table 1**).

As shown in **Figure 6A**, *GUS* transcript levels in leaves of *promGPT2:GUS* plants not exposed to small VCs were ca. 2-fold lower than in *35S:GPT2-GUS* leaves, indicating that the *promGPT2* sequence has strong promoter activity. However, *GUS* transcript levels in *promGPT2:GPT2-GUS* leaves were extremely lower than in *promGPT2:GUS* leaves, both in the absence and presence of small VCs. Exposure to

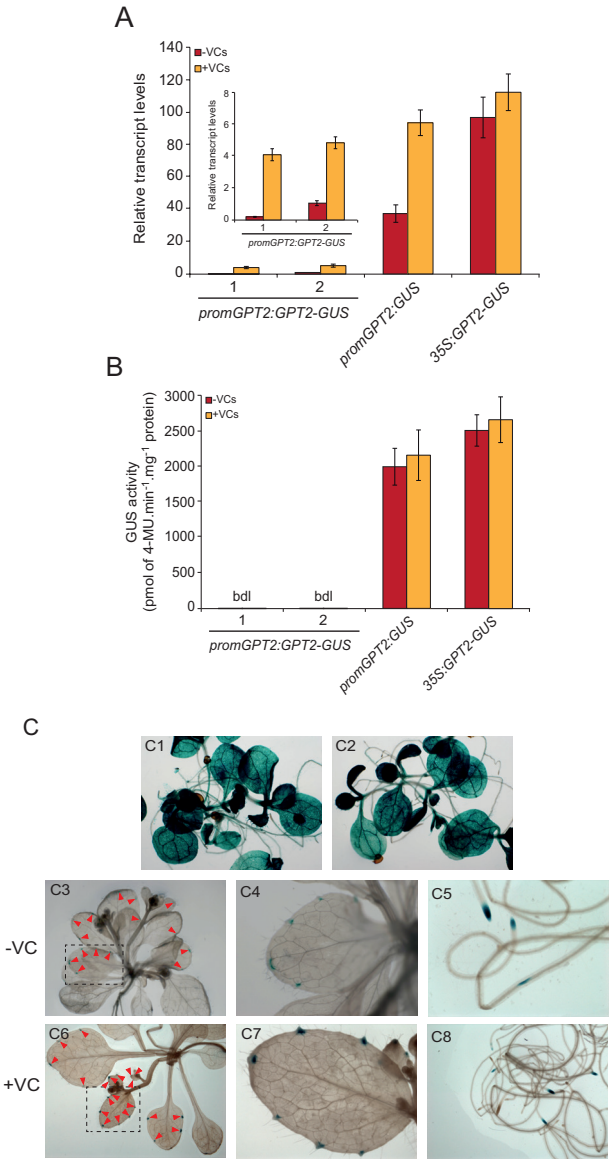

Figure 6: *GPT2* expression is subjected to complex regulation. (A) Relative *GUS* transcript levels and (B) GUS activity in leaves of *promGPT2:GPT2-GUS*, *promGPT2:GUS* and *35S:GPT2-GUS* plants cultured in the absence or presence of small VCs for two days. (C) Histochemical localization of GUS activity in *promGPT2:GUS* (C1) and *35S:GPT2-GUS* (C2) plants cultured in the absence of small VCs, and *promGPT2:GPT2-GUS* plants cultured in the absence (C3-C5) or presence (C6-C8) of small VCs for two days. In "A", the inset shows the relative GUS transcript levels in leaves of two independent representative lines of *promGPT2:GPT2-GUS* plants. Values in panels (A) and (B) are means ± SE for three biological replicates (each a pool of 12 plants) obtained from four independent experiments. bdl: below detection limit, which was established at 2 pmol of 4-MU.min^{-1} mg^{-1} protein.

small VCs enhanced *GUS* transcript levels in *promGPT2:GUS* and *promGPT2:GPT2-GUS* leaves, but not in *35S:GPT2-GUS* leaves (**Figure 6A**), indicating that *promGPT2* has the regulatory elements necessary for driving downstream gene expression in response to small VCs. Histochemical GUS activity analyses revealed that *promGPT2:GUS* and *35S:GPT2-GUS* plants exhibited strong GUS activity in all tissues and cell types of leaves and roots (**Figure 6C**). Regardless of the presence of small fungal VCs, different independent lines of *promGPT2:GPT2-GUS* plants showed detectable GUS activity mainly in root tips and vascular tissues around hydathodes, but not in other tissues such as the mesophyll of leaves (**Figure 6C**). Consistently, GUS activities in leaves of *promGPT2:GPT2-GUS* plants cultured in the absence or presence of VCs were negligible (**Figure 6B**). These results strongly indicated that *GPT2* expression is subject to complex regulatory mechanisms wherein *GPT2* coding sequences play important roles.

DISCUSSION

GPT2 is an important determinant of the response of *pgi1-2* plants but not of WT plants to small VCs

Plants adjust their photosynthetic processes to fluctuating environmental conditions to avoid photoinhibition and maximize yield through changes in the structure and composition of the photosynthetic apparatus (Gjindali et al., 2021). Such changes, referred to as dynamic photosynthetic acclimation, alter metabolism and endow plants with the necessary plasticity to withstand changes in their environment. Previous studies using *gpt2* plants have shown that exposure of leaves to increased irradiance enhances photosynthesis through a *GPT2*-mediated dynamic photosynthetic acclimation process, involving transient accumulation of *GPT2* transcripts and widespread reengineering of the leaf proteome (Athanasiou et al., 2010; Dyson et al., 2015; Miller et al., 2017). Here, we showed that enhancement of photosynthesis, growth and leaf starch content, and changes in the leaf proteome in *gpt2-1* plants promoted by small VCs are similar to those of WT plants (**Figures 1-3, Supplemental Table S2**). This strongly indicates that the molecular mechanisms involved in acclimation to increased irradiance and response to microbial VC exposure are different. We also showed that the response of *pgi1-2gpt2-1* plants to small VCs was weaker than that of *pgi1-2* plants (**Figure 1-3**). Moreover, leaves of VC-exposed *pgi1-2gpt2-1* plants accumulated lower levels

of a large number of photosynthesis-related proteins than VC-exposed *pgi1-2* leaves, which in turn accumulated lower levels of some of these proteins than VC-exposed WT leaves (**Supplemental Tables S3, S4, Figure 5**). The overall data indicate that (i) unlike in WT plants, *GPT2* plays an important role in the regulation of dynamic photosynthetic acclimation, growth, metabolism and expression of photosynthesis-related proteins in response to small fungal VCs in *pgi1-2* plants, and (ii) the weak photosynthetic, growth and starch accumulation responses of *pgi1-2gpt2-1* plants to small VCs relative to WT and *pgi1-2* plants can be ascribed, at least partly, to reduced expression of photosynthesis-related proteins.

The response of *pgi1-2* plants to small VCs involves *GPT2* but not enhanced levels of GPT2 protein in leaves

Small VCs promoted transitory accumulation of *GPT2* transcripts in leaves (**Supplemental Figure S2**), which may represent a case of activation of gene expression upon stress and subsequent decay during acclimation and restoration of homeostasis to a prestress state (Crisp et al., 2017; Garcia-Molina et al., 2020). Although transcript abundance on its own cannot be used to infer changes in the proteome and fluxes in central metabolism (Nakaminami et al., 2014; Schwender et al., 2014) this indicated that enhanced incorporation of cytosolic G6P into chloroplasts caused by increased GPT2 expression in leaves could be involved in the plant´s response to small VCs. However, our differential proteomic analyses did not detect any statistically significant accumulation of GPT2 protein in leaves promoted by small VCs (**Supplemental Table S1**) (Sánchez-López et al., 2016b; Ameztoy et al., 2021). These analyses also did not detect statistically significant higher levels of GPT2 protein in WT leaves than in *gpt2-1* and *pgi1-2gpt2-1* leaves (**Supplemental Tables S2, S4**). Moreover, histochemical GUS activity analyses of leaves of plants transformed with *promGPT2:GPT2-GUS* did not detect any enhancement of GUS activity promoted by small fungal VCs (**Figure 6B, C**). Thus, the overall data indicated that (i) in keeping with the protein abundance database (https://pax-db.org/protein/612928), GPT2 protein levels in Arabidopsis leaves are marginally low; and (ii) in contrast to our initial hypothesis (Sánchez-López et al., 2016b), the response of *pgi1-2* plants to small VCs does not involve enhanced incorporation of cytosolic G6P into the chloroplast of leaf mesophyll cells caused by increased GPT2 expression.

Vascular and root tip *GPT2* expression plays an important role in the PGI1-independent response to small VCs

MEP pathway derived tZ-type CKs are mainly synthesized in the root tips and the vascular tissues and then transported to shoots, where they regulate growth and processes including the expression of photosynthesis-related proteins and the photosynthetic acclimation to environmental changes (Miyawaki et al., 2004; Aloni et al., 2005; Boonman et al., 2007; Žd'árská et al., 2013; Kieber and Schaller, 2014; Ko et al., 2014; Cortleven and Schmülling, 2015). Root tips, vascular tissues and hydathodes express *PGI1* and genes involved in rate-limiting steps of plastidic CK biosynthesis, translocation and signaling (Bürkle et al., 2003; Miyawaki et al., 2004; Ferreira and Kieber, 2005; Bahaji et al., 2018). Here, we showed that tZ levels in VC-exposed *pgi1-2gpt2-1* leaves were lower than in VC-exposed *pgi1-2* leaves, which in turn accumulated lower levels of tZ than VC-exposed WT leaves. In addition, we found that *GPT2* is expressed in root tips and leaf vascular tissues around hydathodes, which are considered as transfer stations of CKs between xylem and phloem (Bürkle et al., 2003; Aloni et al., 2005; Nagawa et al., 2006). Furthermore, we found that vascular- and root tip-specific GPT2 expression is sufficient to almost completely restore to WT levels the poor growth, photosynthetic and starch accumulation responses of *pgi1-2gpt2-1* plants to small VCs (**Figure 4**). Therefore, the overall data indicated that the expression of PGI1 and GPT2 in root tips and vascular cells plays key roles in the response of plants to small VCs through mechanisms that harmonize the carbon status of the plant with growth, photosynthesis and metabolism. One such mechanisms could involve the provision of plastids of vascular and root tip cells with G6P derived from the metabolization of sucrose coming from leaves to fuel glycolysis or the PPP and provide precursors for the synthesis of MEP pathway-derived tZ, which once transported to leaves, initiate a cascade of signaling reactions, leading to changes in the expression of photosynthesis- and growth-related proteins (**Figure 7**). According to this view, *GPT2* expression could play an important role in the response of plants to small VCs under conditions in which G6P-metabolizing PGI1 activity is low. Yeasts, plants and animal cells possess transporter-like proteins, designated as transceptors, that act as receptors involved in nutrient sensing (Ho et al., 2009; Lima et al., 2010; Yang et al., 2012; Zhang et al., 2014; Volpe et al., 2016; Steyfkens et al., 2018). So far, no sugar transceptor has been identified in plants. We speculate that GPT2 could act

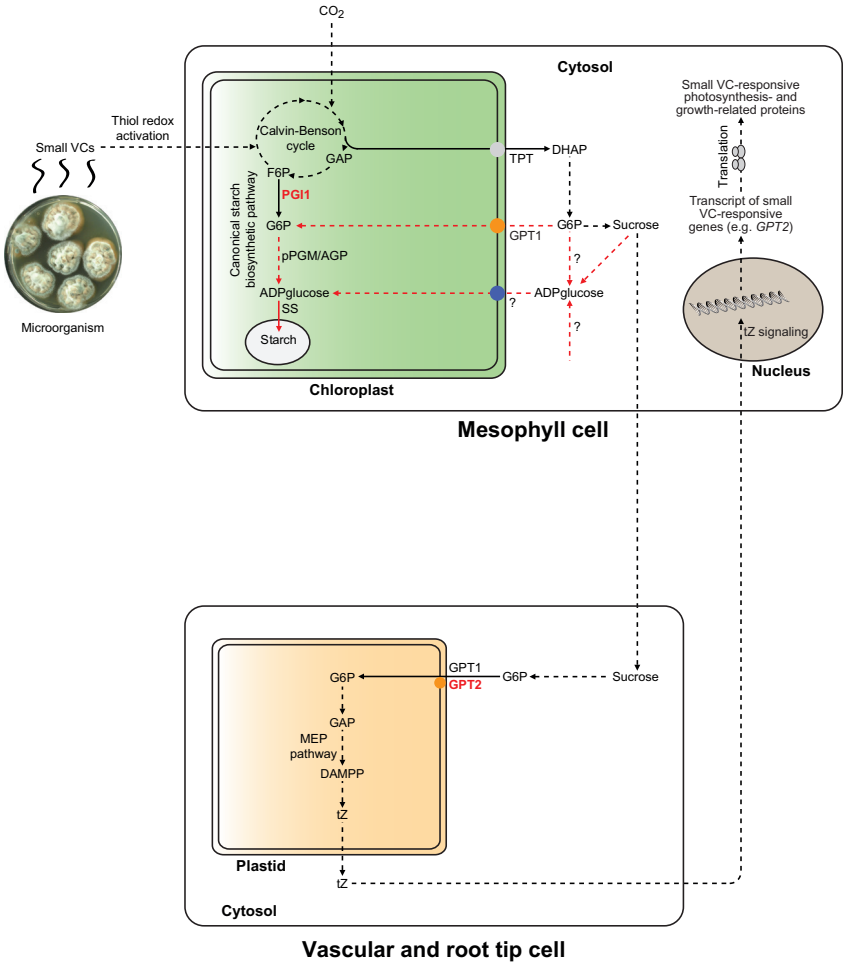

Figure 7: Suggested hypothetical model of regulation of the plant response to small fungal VCs by vascular and root tip GPT2 and PGI1 expression. According to this model, the response of plants to small fungal VCs involves mechanisms wherein signalling of both rapid thiol redox activation of photosynthesis in mesophyll cells of leaves (Ameztoy et al., 2019; 2021) and enhanced glycolytic or PPP activity in vascular tissues of roots play important roles. Thiol redox activation of photosynthesis promoted by small VCs increases the production of photosynthates (mainly sucrose), which are transported to vascular tissues and root tip cells and metabolized to G6P in the cytosol. This compound enters the plastid through the GPT transporters to fuel the plastid-localized glycolysis or PPP, where PGI1 participates in the metabolization of G6P. GAP produced by the PPP or glycolysis enters the MEP pathway to fuel the production of tZ, which is transported to mesophyll cells, where it initiates a cascade of reactions, leading to changes in the expression of photosynthesis-related proteins. This process guarantees a sustained high rate of photosynthesis and accelerated growth. According to this hypothetical model, VC-promoted starch overaccumulation in both WT and *pgi1-2* leaves could be a consequence of the stimulation of metabolic flux through non-canonical starch biosynthetic pathway(s) (highlighted in dashed red lines) that bypass PGI1 through the transport of cytosolic hexoses (e.g., G6P and/or ADPglucose) into the chloroplasts. pPGM: plastidial phosphoglucomutase; AGP: ADPglucose pyrophosphorylase; SS: starch synthase; TPT: triose-P transporter.

as a G6P receptor for long-distance signaling of the carbon status of the plant under changing environmental conditions. However, further work is necessary to test this hypothesis.

Unlike in *pgi1-2gpt2-1* plants, small VCs promoted the accumulation of exceptionally high levels of starch in the mesophyll of *pgi1-2* leaves (**Figure 2**). This, and the fact that small VCs enhanced GPT2 transcript levels, may in principle indicate that these compounds activate a non-canonical starch biosynthetic pathway(s) involving GPT2-mediated incorporation of cytosolic G6P, which once in the chloroplast of mesophyll cells of *pgi1-2* leaves is converted to starch. However, this idea conflicts with the facts that (i) leaves accumulate negligible levels of GPT2 protein both in the presence and absence of small VCs (**Supplemental Tables S1, S2, Figure 6C**), and (ii) vascular- and root tip-specific *GPT2* expression strongly enhanced the starch content in leaves of small VC-exposed *pgi1-2gpt2-1* plants (**Figure 4**). It is thus conceivable that the accumulation of high levels of starch in leaves of small VC-exposed *pgi1-2* plants and *pgi1-2gpt2-1* plants specifically expressing *GPT2* in vascular tissues is due to both uptake of cytosolic hexoses into the chloroplast through non-GPT2 transporter system(s) and enhanced photosynthesis promoted by proteome resetting mechanisms, wherein vascular and root tip *GPT2* expression plays an important role (**Figure 7**). Regarding the mechanism(s) of uptake of cytosolic hexoses into the chloroplasts that can act as precursors for the synthesis of starch in leaves of small VC-exposed plants, it should be noted that plastids from Arabidopsis have two functional G6P/Pi translocators: GPT1 and GPT2 (Kammerer et al., 1998). GPT1 plays an important role in starch biosynthesis in floral tissues and guard cells (Flütsch et al., 2022). Histochemical analyses of *GUS* activity in plants expressing *GUS* under the control of the *GPT1* promoter showed GUS activity in mesophyll cells of leaves, indicating that *GPT1* is expressed in the mesophyll (Niewiadomski et al., 2005). However, like GPT2, *GPT1* transcript and protein levels are extremely low in mesophyll cells, as visualized using the Plant eFP browser (https://bar.utoronto.ca/eplant) and the PAXdb: Protein Abundance Database (https://pax-db.org/protein/633665) and GPT1 immunoblot analyses of leaves (cf. Figure 7 in Baune et al., 2020). Furthermore, small microbial VCs did not enhance *GPT1* transcript levels and GPT1 protein content in leaves (Sánchez-López et al., 2016b) (**Supplemental Table S1, S3**). Further work is necessary to test the possible involvement of GPT1 in the accumulation of exceptionally high

levels of starch in microbial VC-exposed WT and pgi1-2 leaves. Chloroplasts also have a glucose transporter (pGlcT) (Weber et al., 2000) and hexokinase (Giese et al., 2005), potentially enabling the incorporation of cytosolic glucose and subsequent conversion into G6P. However, *pglct* mutants accumulate WT levels of starch during the day (Cho et al., 2011), and GlcT has been shown to act in the export to the cytosol of glucose derived from the starch breakdown during the night rather than in the import of cytosolic glucose to the chloroplasts during illumination (Weber et al., 2000; Cho et al., 2011). Chloroplasts also possess a yet to be identified transporter of the starch precursor molecule, the ADPglucose (Pozueta-Romero et al., 1991; Bahaji et al., 2014). Microbial volatiles promote the accumulation of ADPglucose and starch in leaves of plants lacking plastidial enzymes of the canonical starch biosynthetic pathway involved in the synthesis of this compound (Bahaji et al., 2011), which would indicate that small microbial VCs stimulate cytosolic ADPglucose production. One possible source of cytosolic ADPglucose in leaves is SUS (Baroja-Fernández et al., 2012). However, recent studies have shown that leaves of SUS-lacking plants accumulate WT levels of ADPglucose (Füngfeld et al., 2022). It is thus likely that starch biosynthesis in leaves of small VC-exposed *pgi1-2* plants and *pgi1-2gpt2-1* plants specifically expressing *GPT2* in vascular tissues involves, at least partly, the production of cytosolic ADPglucose through SUS-independent mechanisms and subsequent transport of this hexose into the chloroplast (**Figure 7**). However, further work is necessary to test these hypotheses.

***GPT2* expression is subjected to complex regulation**

Results presented in this work provide strong evidence that *GPT2* expression is subject to complex regulatory mechanisms. In the absence of small VCs, GUS transcript levels in *promGPT2:GUS* leaves were relatively high and comparable to those of *35S:GPT2-GUS* leaves (**Figure 6A**). This was rather surprising, as leaves not exposed to small VCs accumulate negligible levels of *GPT2* transcripts (**Supplemental Figure S2**) (Weise et al., 2019). Noteworthy, GUS transcript levels in *promGPT2:GPT2-GUS* leaves were extremely lower than in *promGPT2:GUS* leaves (**Figure 6A**). Overall, the data indicate that *GPT2* expression is subject to mechanisms mediated by cooperatively acting regulatory elements located at both sides of the translation start ATG codon of the *GPT2* gene and/or at both sides of the translation start AUG codon

of *GPT2* transcripts that impede accumulation of high *GPT2* transcript levels in leaves. The fact that small VCs enhanced *GPT2* transcript levels in leaves (**Supplemental Figure S2**) and GUS transcript levels in *promGPT2:GPT2-GUS* leaves (**Figure 6A**) would indicate that such mechanisms are partially inhibited by small VCs. Unlike *35S:GPT2-GUS* and *promGPT2:GUS* leaves showing strong GUS activity in all tissues (**Figure 6C**), GUS activity in *promGPT2:GPT2-GUS* leaves not exposed to small VCs was detectable only in vascular tissues around hydathodes, but not in other tissues such as the mesophyll (**Figure 6C**), which is consistent with the negligible accumulation of *GPT2* transcripts and GPT2 protein in the whole leaf. Small VCs did not promote accumulation of GPT2 protein in WT leaves (**Supplemental Table S1**) or GUS activity (**Figure 6B**) in *promGPT2:GPT2-GUS* leaves despite promoting accumulation of *GPT2* and *GPT2-GUS* transcripts, respectively (**Supplemental Figure S2, Figure 6A**). Overall, the data indicate that elements located around the translation start AUG codon of *GPT2* transcripts cooperatively act to impede GPT2 translation in VC-exposed mesophyll cells.

Epigenetic factors of control of gene transcription, such as small RNAs and DNA methylation, are relevant modulators of plants´ responses to the environment and their biotic interactions (Lämke and Bäurle, 2017; Alonso et al., 2019). On the other hand, mechanisms of posttranscriptional control of gene expression, such as N6-methylation of adenosine (m^6A), are important in controlling the stability and translatability of mRNAs (Arribas-Hernández and Brodersen, 2020). These mechanisms are affected by environmental factors, and strongly determine growth, development and stress adaptation (Arribas-Hernández and Brodersen, 2020). Unlike WT plants, met1 and mta mutants deficient in CG maintenance DNA methylation and m^6A transcript modulation, respectively, accumulate high levels of *GPT2* transcripts (Lister et al., 2008; Bodi et al., 2012). Therefore, it is highly conceivable that both regulation of GPT2 expression and the *GPT2*-mediated PGI1-independent response of plants to small VCs involves mechanisms wherein regulation of genomic *GPT2* DNA methylation and/or m^6A transcript modulation play important roles. However, further work is necessary to evaluate these hypotheses.

Additional remarks: enhanced photosynthesis is not the sole important determinant of enhanced growth and starch accumulation promoted by small fungal VCs

CKs are major determinants of photosynthesis and growth (Cortleven and Valcke, 2012; Kieber and Schaller, 2014). *pgi1-2* and *pgi1-2gpt2-1* plants exposed to small VCs were bigger and accumulated more starch than WT plants not exposed to small VCs, despite having comparable photosynthetic capacities (**Figures 1-3**). In addition, VC-promoted relative tZ content increase in *pgi1-2gpt2*-1 leaves (2.6-fold) was higher than in *pgi1-2* and WT leaves (1.7- and 1.4-fold, respectively). This indicates that (i) factors other than relative increase of tZ content are important for enhancement of photosynthesis by microbial VCs, and (ii) photosynthesis is not the sole important determinant of growth and metabolic changes promoted by small VCs. This agrees with current ideas arguing against photosynthesis being the main rate-controlling factor for plant growth (Körner, 2015). Starch biosynthesis is subjected to redox regulation (Hendriks et al., 2003), and small fungal VCs redox-activate starch biosynthetic enzymes (Li et al., 2011; Ameztoy et al., 2019; García-Gómez et al., 2019), which could partly explain why small VC-exposed *pgi1-2* leaves, and to a lesser extent *pgi1-2gpt2-1* leaves, accumulated more starch than leaves of WT plants not exposed to VCs (**Figure 2**). In addition, VC-exposed WT, *pgi1-2* and *pgi1-2gpt2-1* plants accumulated more ROS scavengers, enzymes of the MEP, shikimate and cytosolic glycolytic pathways, proteins involved in the synthesis of photosynthetic pigments, ribosomal proteins and chaperones than leaves of WT plants not exposed to small VCs (**Supplemental Figure S3, Figure 5**). This could explain, at least in part, the higher growth of VC-treated WT, *pgi1-2* and *pgi1-2gpt2-1* plants relative to that of non-VC-treated WT plants.

MATERIAL AND METHODS

Plants, growth conditions and sampling

The work was carried out using *Arabidopsis thaliana* L. (Heynh) wild-type plants (ecotype Wasilewskija-2, Ws-2), *pgi1-2* knock-out mutants (Kunz et al., 2010), *gpt2-1* knock-out mutants (GABI_454H06) and *pgi1-2gpt2-1* plants (Bahaji et al., 2015) (**Table 1**). We also used plants from three independent lines each of *pgi1-2gpt2-1* plants expressing *PGI1* or *GPT2* under the control of the cauliflower mosaic virus 35S promoter (*pgi1-2gpt2-1 35S:PGI1* and *pgi1-2gpt2-1 35S:GPT2*, respectively)

(**Table 1**). In addition, we used plants from ten independent lines each of WT plants expressing GUS under the control of the vascular tissue-specific *Athspr* promoter, which comprises the 1.67 kb region immediately upstream the translation start site of *Athspr* (Zhang et al., 2014) (*promAthspr:GUS*) and *pgi1-2gpt2-1* plants expressing GPT2 under the control of promAthspr (*pgi1-2gpt2-1 promAthspr:GPT2*) (**Table 1**). Moreover, we used plants from ten independent lines each of WT plants expressing GUS under the control of the 1.1 kb region immediately upstream the translation start codon of GPT2 (*promGPT2:GUS*) (**Table 1**). Furthermore, we used plants expressing *GPT2-GUS* under the control of *promGPT2* and the *35S* promoter (*promGPT2:GPT2-GUS* and *35S:GPT2-GUS*, respectively) (**Table 1**). The *35S:PGI1*, *35S:GPT2*, *promAthspr:GUS*, *promAthspr:GPT2*, *promGPT2:GUS*, *promGPT2:GPT2-GUS* and *35S:GPT2-GUS* plasmid constructs were produced using Gateway technology as illustrated in **Supplemental Figure S5** and confirmed by sequencing. Primers used for PCR amplification of *PGI1* and *GPT2* cDNA, *GUS* and the *Athspr* and *GPT2* promoters are listed in **Supplemental Table S6.** The plasmid constructs were transferred to *Agrobacterium tumefaciens* EHA105 cells by electroporation and utilized to transform Arabidopsis plants as described by Clough and Bent (1998).

Seeds were sown and plants cultured in Petri dishes (92 x 16 mm, Sarstedt, Ref. 82.1472.001) containing half-strength agar solidified Murashige and Skoog (MS) (Phytotechlab M519) medium in growth chambers providing 'long day' 16 h light (90 µmol photons sec^{-1} m^{-2}), 22 ºC /8 h dark, 18 ºC cycles. *A. alternata* was cultured in Petri dishes containing agar solidified MS medium supplemented with 90 mM sucrose. Effects of small fungal VCs on plants were investigated using the "plasticized PVC wrap and charcoal filter-based box-in-box" co-cultivation system described in García-Gómez et al. (2019) and Gámez-Arcas et al. (2022a). In this method, plants are grown in the vicinity of fungal cultures covered with charcoal filters that adsorb VCs of molecular masses higher than ca. 45 Da. VC treatment started at 14 days after sowing growth stage of plants. At the indicated incubation periods, leaves were harvested, immediately freeze-clamped and ground to a fine powder in liquid nitrogen with a pestle and mortar.

qRT-PCR analyses

Total RNA was extracted from frozen Arabidopsis leaves of *in vitro* cultured plants

using the Trizol method following treatment with RNAase-free DNAase. RNA (1.5 µg) was reverse-transcribed using polyT primers and an Expand Reverse Transcriptase kit (Roche). RT-PCR amplification of *GPT2* and *GUS* genes was performed using primers listed in **Supplemental Table S7**, and their specificity was checked by separating the obtained products on 1.8% agarose gels. The specificity of the PCR amplifications was checked by measuring heat dissociation curves (from 60 to 95 °C). Comparative threshold values were normalized to an EF-1 alfa internal control.

Determination of gas exchange rates and photosynthetic parameters

Gas exchange rates were determined as described by Sánchez-López et al. (2016b) using a LI-COR 6400 gas exchange portable photosynthesis system (LI-COR, Lincoln, NE, USA). An was calculated as described by von Caemmerer and Farquhar (1981). V_{cmax} and J_{max} values were calculated from A_n/C_i curves according to Long and Bernacchi (2003).

***GUS* expression analysis**

Expression of the *GUS* reporter gene was monitored using the histochemical staining and fluorometric assays described by Jefferson et al. (1987).

Iodine staining

Iodine staining of leaves was carried out as described by Bahaji et al. (2015). Briefly, leaves harvested at the end of the light period were fixed by immersion into 3.7% formaldehyde in phosphate buffer. Leaf pigments were then removed in 96% ethanol. Re-hydrated samples were stained in iodine solution (KI_2% (w/v) I_2 1% (w/v)) for 30 min, rinsed in deionized water and photographed.

Analytical procedures

Levels of tZ were determined according to Novák et al. (2008). Recovery experiments were conducted by adding known amounts of metabolite standards to the frozen slurry immediately after the addition of extraction solutions. The difference between the measurements from samples with and without added standards was used as an estimate of the percentage recovery. All presented concentrations of these metabolites were corrected for losses during extraction. The total photosynthetic pigments content

was quantified according to Lichtenthaler (1987). Starch was measured with an amyloglucosidase-based test kit (Boehringer Mannheim).

Proteomic analysis

High-throughput, isobaric labeling-based differential proteomic analyses were conducted essentially as described in Sánchez-López et al. (2016a), but with the following modifications. The tryptic peptides were labelled using a TMT6plex Isobaric Mass Tagging kit (Thermo Fischer Scientific). Search engines were configured to match potential peptide candidates with a mass error tolerance of 25 ppm and fragment ion tolerance of 0.02Da, allowing for up to two missed tryptic cleavage sites, and a maximum isotope error (^{13}C) of 1, fixed MMTS modification of cysteine, variable oxidation of methionine, production of pyroglutamic acid from glutamine or glutamic acid at the peptide N-terminus, acetylation of the protein N-terminus and modification of lysine and peptide N-terminus with TMT6plex reagents. Statistical significance was measured using *q*-values (FDR). The cut-off for identifying DEPs was established at FDR $\leq$ 0.05% and log2 ratios (+VC treatment vs. –VC treatment) of $>$ 0.3 (for proteins whose expression was up-regulated by fungal VCs) or $<$ -0.3 (for proteins whose expression was down-regulated by VCs).

Statistical analysis

Unless otherwise indicated, presented data are means (± SE) obtained from 3-4 independent experiments, with 3 replicates for each experiment. The significance of differences between plants VCs was statistically evaluated with Student´s *t*-test using SPSS software. Differences were considered significant if $P<0.05$.

SUPPLEMENTAL MATERIAL

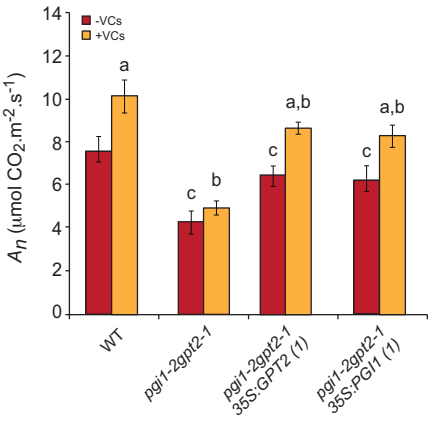

Supplemental Figure S1: Net CO_2 assimilation rate *(A_n)* at 400 ppm CO_2 of WT and *pgi1-2gpt2-1* plants and plants from one representative line each of *pgi1-2gpt2-1* transformed with *35S:PGI1* or *35S:GPT2* (*pgi1-2gpt2-1 35S:PGI1(1)* and *pgi1-2gpt2-1 35S:GPT2(1)*, respectively). Values are means ± SE for three biological replicates (each a pool of 12 plants) obtained from four independent experiments. Lowercase letters indicate significant differences, according to Student´s *t*-test (P<0.05), between: "a" VC-treated and non-treated plants, "b" VC-treated WT and mutants, and "c" VC-non-treated WT plants and mutants.

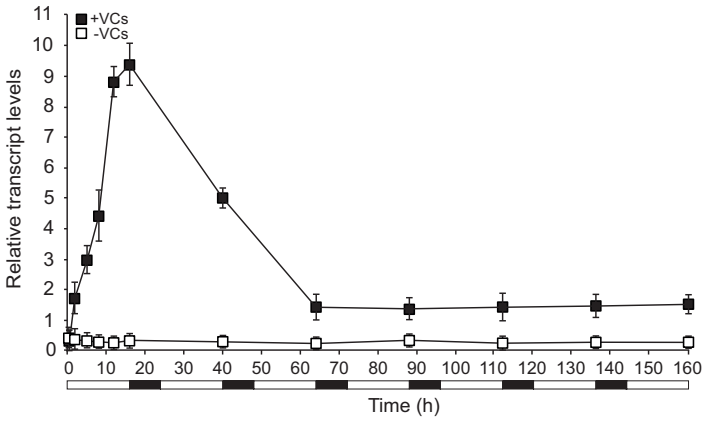

Supplemental Figure S2: Time-course of *GPT2* transcript levels in leaves of WT plants cultured in the absence or continuous presence of small VCs emitted by adjacent *A. alternata* cultures for 160 hours. Values are means ± SE for three independent experiments..

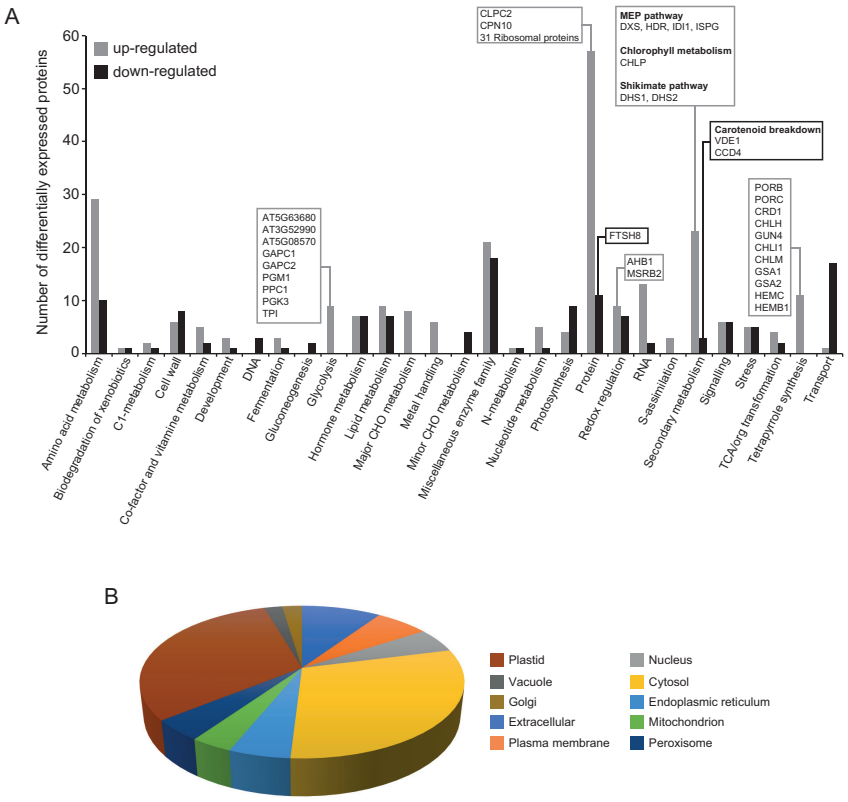

Supplemental Figure S3: Small VCs promote changes in the leaf proteome of WT plants. (A) Functional categorization of differentially expressed proteins (DEPs) in leaves of WT plants cultured in the presence of small VCs emitted by adjacent *A. alternata* cultures for 2 days. Proteins that were significantly down- or up-regulated following VC exposure are arranged according to the putative functional category assigned by MapMan software. The numbers of up- and down-regulated proteins in each categorical group are indicated by gray and black bars, respectively. DEPs discussed here are shown in the boxes.

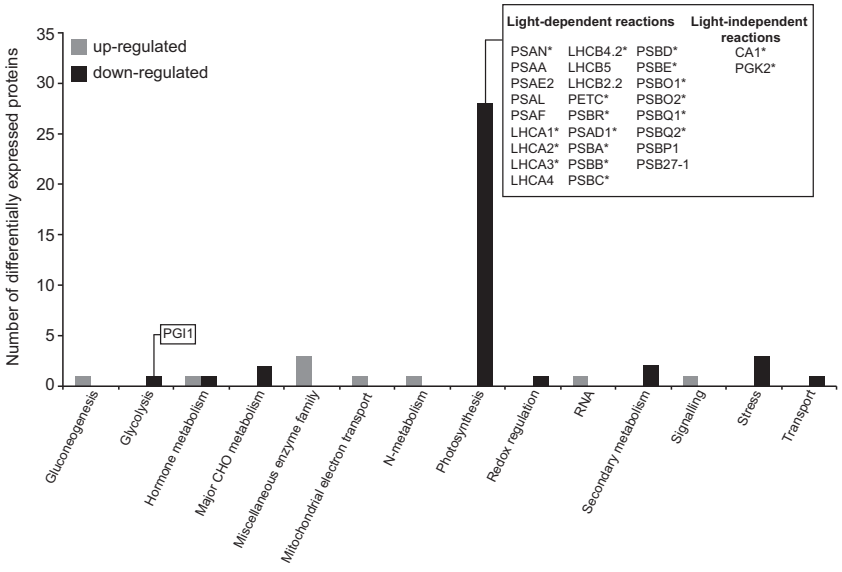

Supplemental Figure S4: Knocking out *GPT2* and *PGI1* decreased the expression of photosynthesis-related proteins in leaves of plants not exposed to small VCs. The graphic represents the functional categorization of differentially expressed proteins (DEPs) in the comparative study between leaves of WT and *pgi1-2gpt2-1* plants cultured in the absence of small VCs emitted by adjacent *A. alternata* cultures for 2 days. Proteins that were significantly down- or up-regulated in *pgi1-2gpt2-1* plants are arranged according to the putative functional category assigned by MapMan software. The numbers of up- and down-regulated proteins in each categorical group are indicated by gray and black bars, respectively. The data were obtained from **Supplemental Table S5**. DEPs discussed here are shown in the boxes, and asterisks indicate DEPs identified in the comparative proteomic study between leaves of WT and *pgi1-2gpt2-1* plants cultured in the presence of small VCs (cf. **Figure 5B**).

Supplemental Figure S5: Stages in the construction of the *35S:PGI1*, *35S:GPT2*, *35S:GPT2-GUS*, *promGPT2:GPT2-GUS*, *promGPT2:GUS*, *promAthspr:GPT2* and *promAthspr:GUS* plasmids. Plasmid constructs were produced using Gateway technology and confirmed by sequencing. Primers used for PCR amplification of complete *PGI1* and *GPT2* cDNAs obtained from the RIKEN Arabidopsis cDNA collection (Seki et al., 1998; Seki et al., 2002), the *Athspr* and *GPT2* promoters from genomic Arabidopsis DNA and *GUS* are listed in **Supplemental Table S6**.

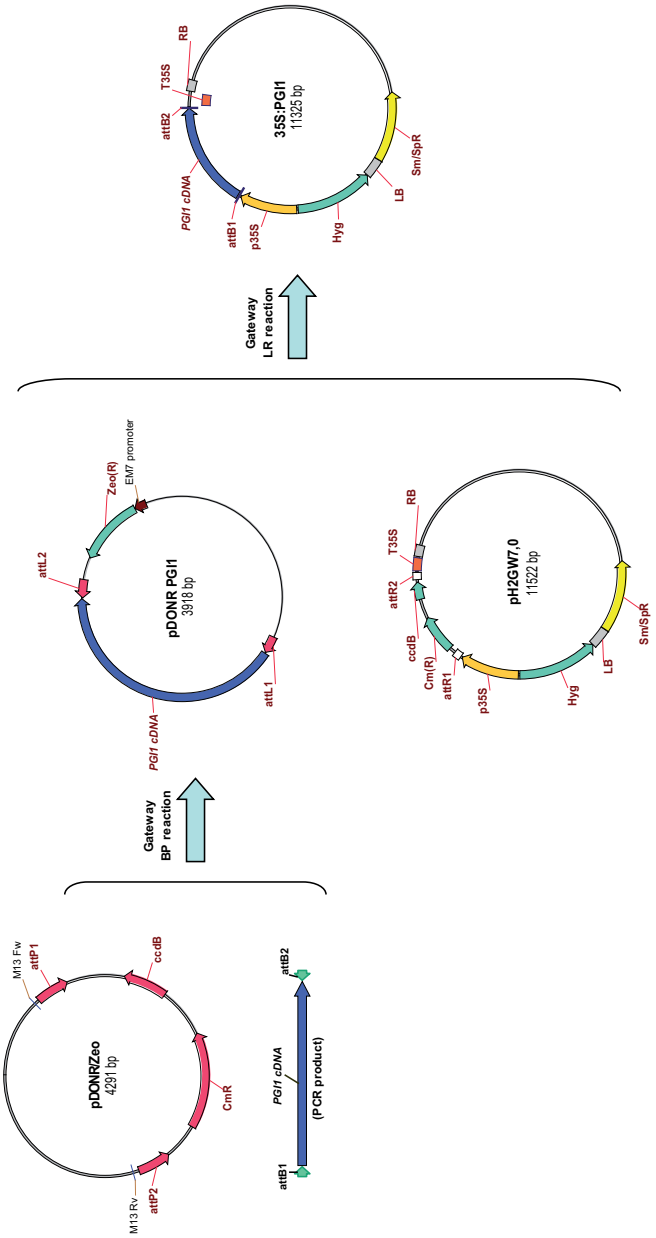

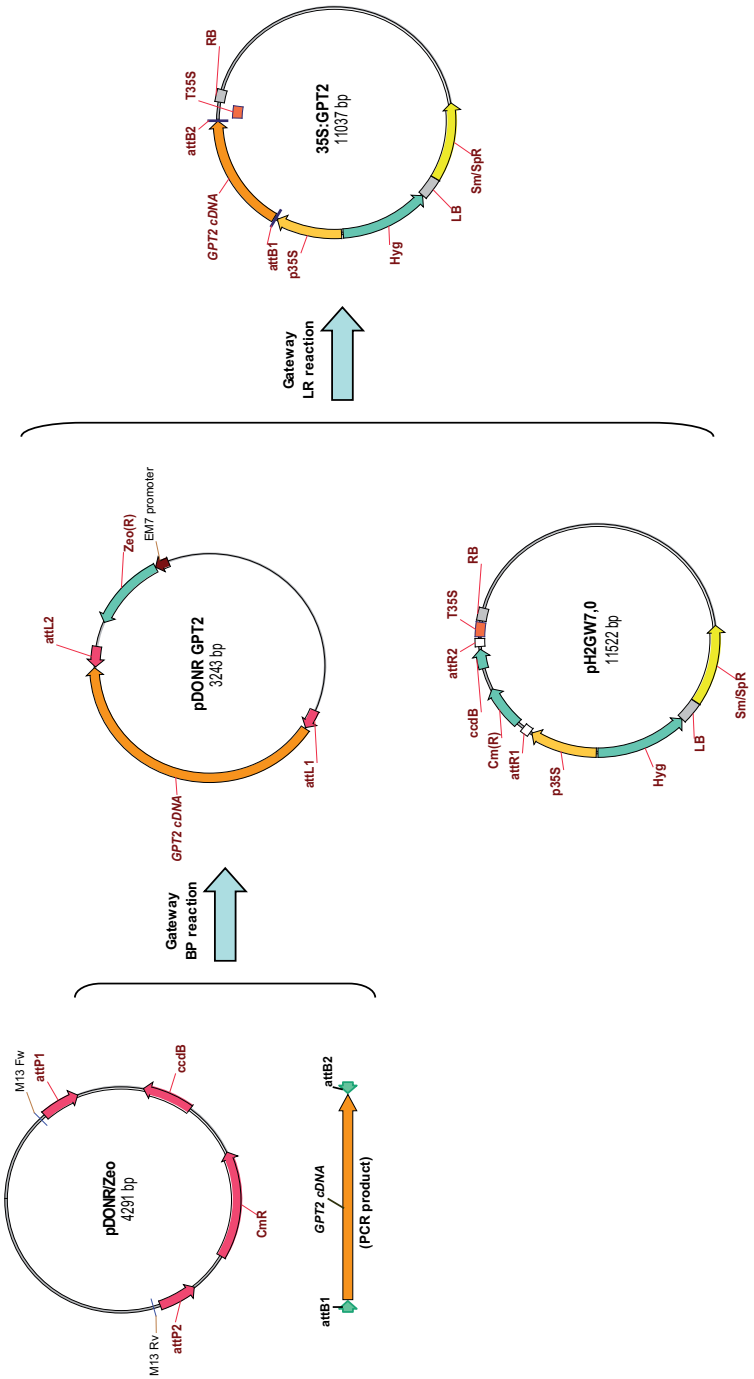

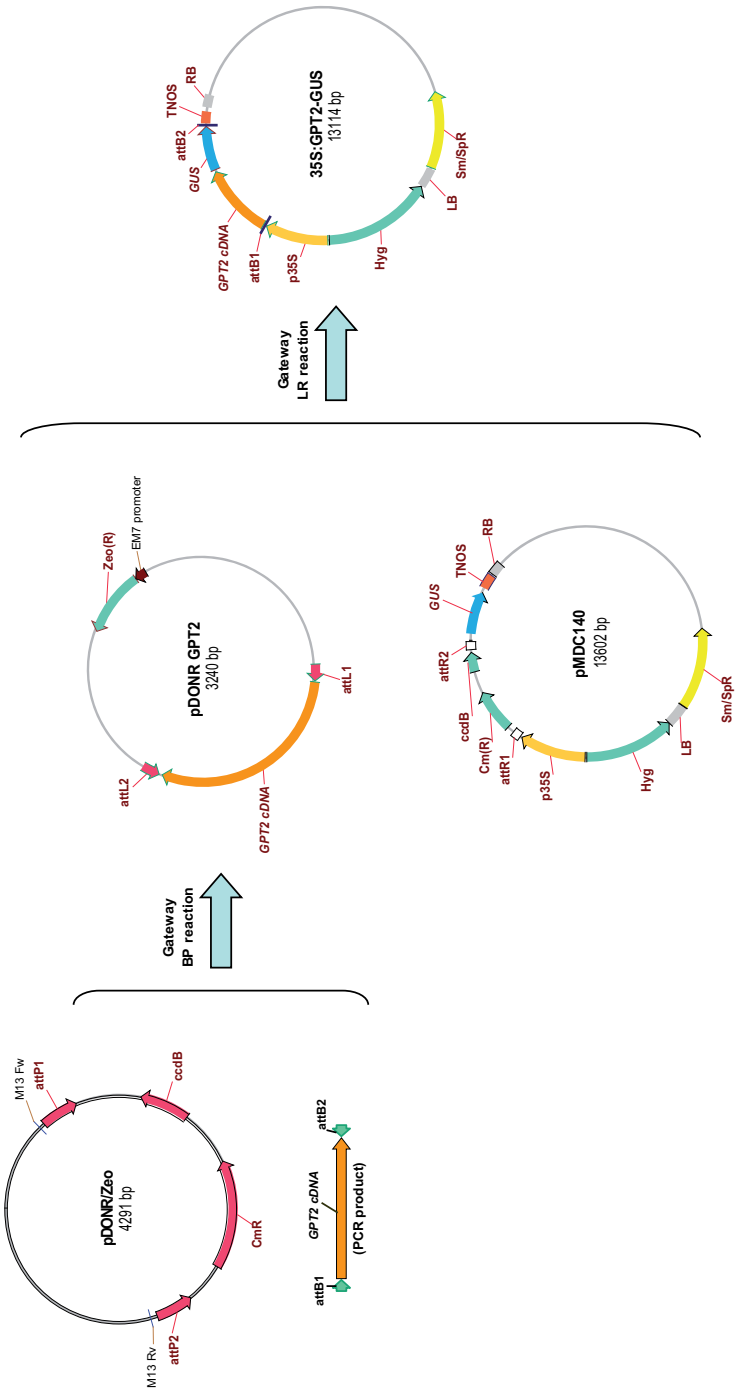

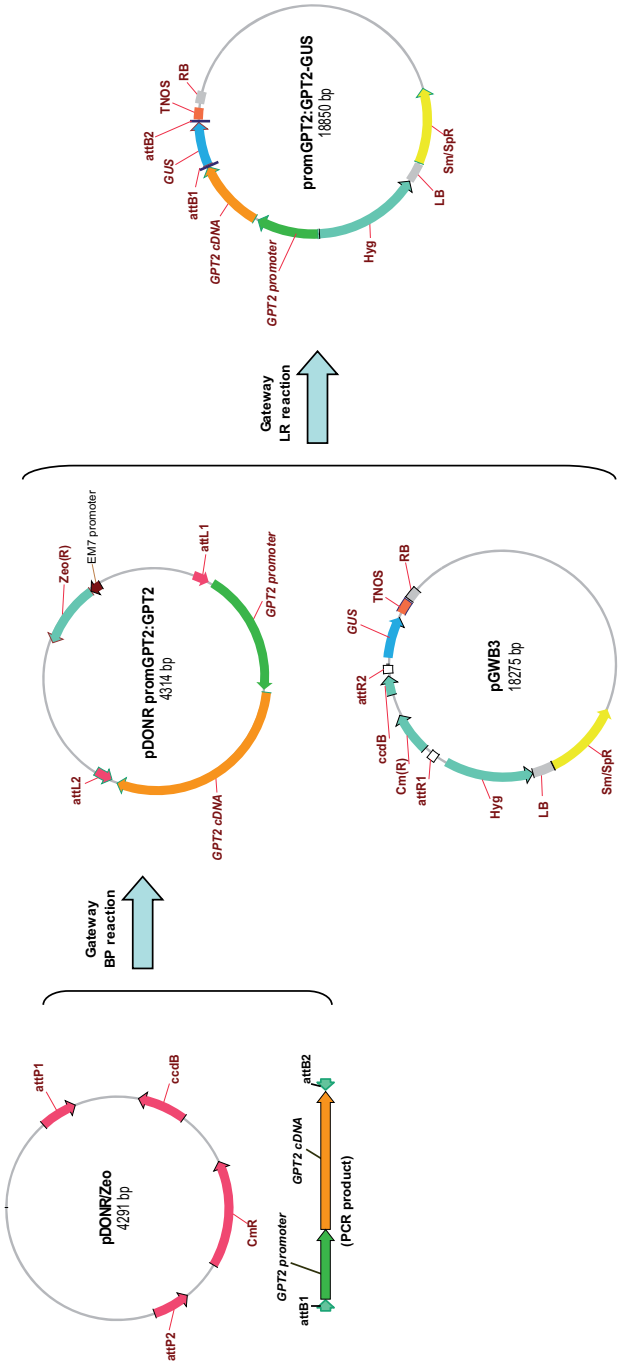

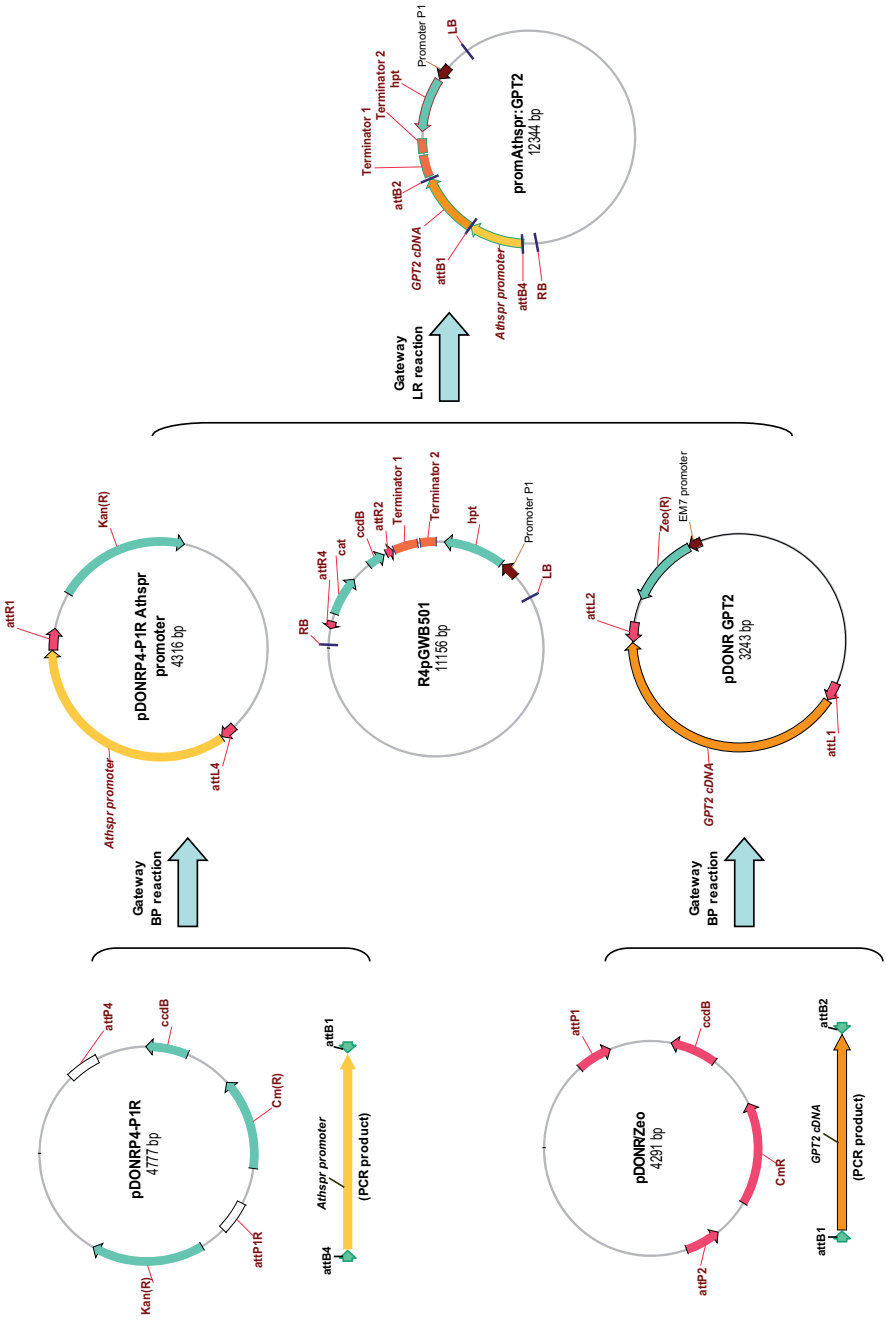

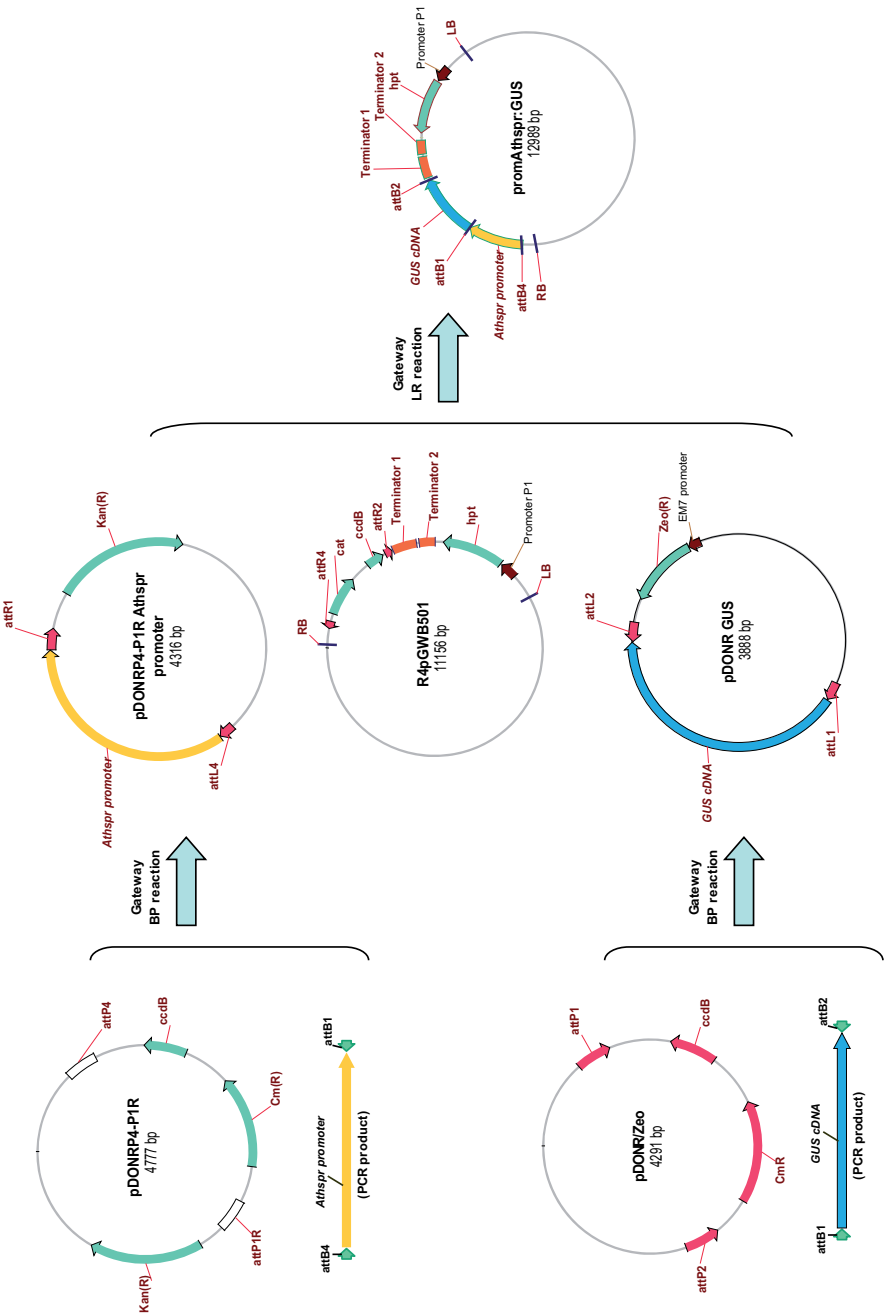

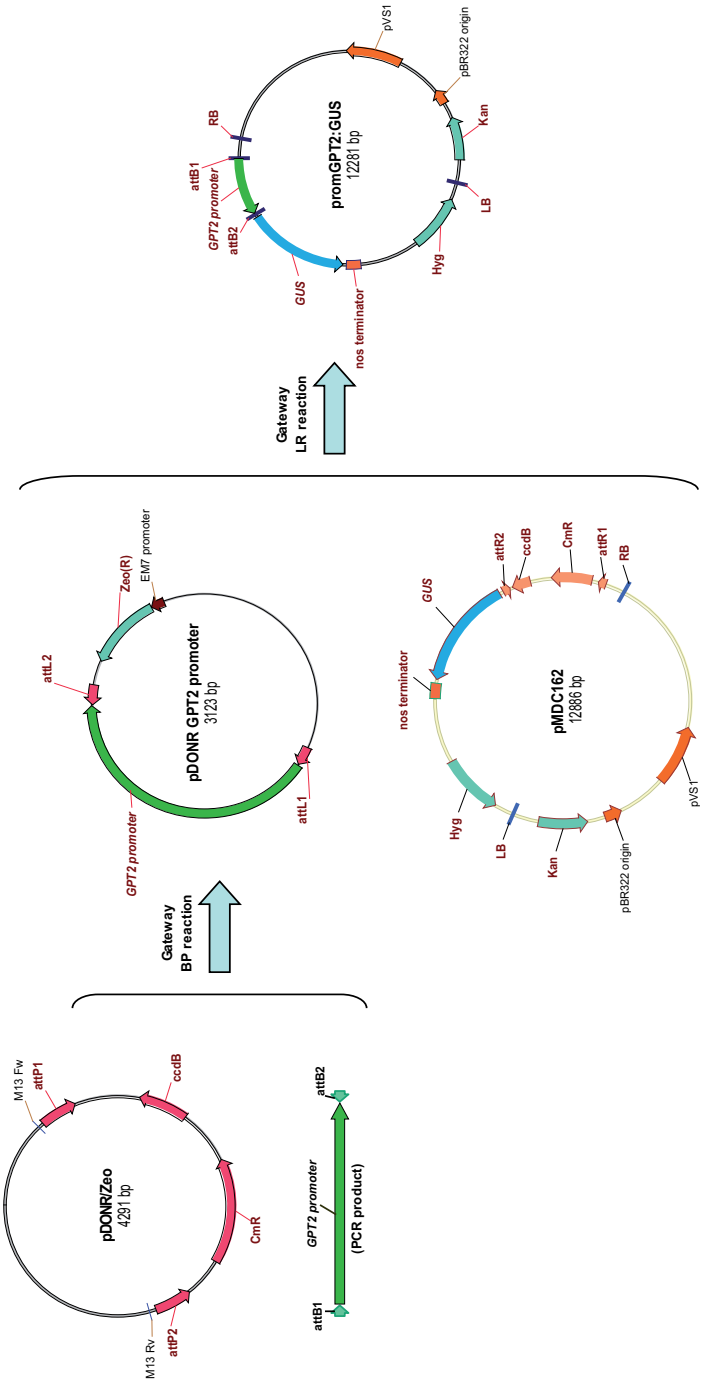

Table S1: List of proteins that are differentially expressed by small fungal VCs in leaves of WT (Ws-2) plants with a "confident" statistical significance level (small fungal VC-treated vs. non-treated plants). DEPs are classified according to their functions. DEPs that are discussed in the main text are highlighted in orange. DEPs identified in the proteomic study of leaves of Col-O plants exposed to small fungal VCs for 3 days (Ameztoy et al., 2021) are highlighted in yellow.

Accession number	Protein ID	Fold change (log2)	Subcellular location	qvalue (FDR)	Description
Amino acid metabolism					
AT5G14200	Q9FMT1	1,179	plastid	0,002	3-isopropylmalate dehydrogenase 3, chloroplastic OS=Arabidopsis thaliana GN=IMDH3 PE=1 SV=1
AT3G19710	Q9LE06	1,036	cytosol	0,015	Methionine aminotransferase BCAT4 OS=Arabidopsis thaliana GN=BCAT4 PE=1 SV=1
AT1G02500	P23686;Q9LUT2	0,965	cytosol	0,027	S-adenosylmethionine synthase 1 OS=Arabidopsis thaliana GN=SAM1 PE=1 SV=2
AT1G17745	O04130	0,856	plastid	0,002	D-3-phosphoglycerate dehydrogenase 2, chloroplastic OS=Arabidopsis thaliana GN=PGDH2 PE=1 SV=2
AT1G65960	Q42472;Q9LSH2	0,772	cytosol	0,006	Glutamate decarboxylase 2 OS=Arabidopsis thaliana GN=GAD2 PE=1 SV=1
AT4G19710	O81852;Q9SA18	0,685	plastid	0,001	Bifunctional aspartokinase/homoserine dehydrogenase 2, chloroplastic OS=Arabidopsis thaliana GN=AKHSDH2 PE=1 SV=1
AT3G03780	Q9SRV5	0,68	cytosol	0,001	5-methyltetrahydropteroyltriglutamate--homocysteine methyltransferase 2 OS=Arabidopsis thaliana GN=MS2 PE=1 SV=1
AT2G45440	Q9FVC8	0,633	plastid	0,031	4-hydroxy-tetrahydrodipicolinate synthase 2, chloroplastic OS=Arabidopsis thaliana GN=DHDPS2 PE=1 SV=2
AT1G31230	Q9SA18	0,631	plastid	0,001	Bifunctional aspartokinase/homoserine dehydrogenase 1, chloroplastic OS=Arabidopsis thaliana GN=AKHSDH1 PE=1 SV=1
AT3G13110	Q39218	0,629	mitochondrion	0,027	Serine acetyltransferase 3, mitochondrial OS=Arabidopsis thaliana GN=SAT3 PE=1 SV=3
AT3G49680	Q9M401	0,613	plastid	0,001	Branched-chain-amino-acid aminotransferase 3, chloroplastic OS=Arabidopsis thaliana GN=BCAT3 PE=1 SV=1
AT5G19550	P46645	0,6	cytosol	0,001	Aspartate aminotransferase, cytoplasmic isozyme 1 OS=Arabidopsis thaliana GN=ASP2 PE=1 SV=2
AT2G36880	Q9SJL8	0,599	cytosol	0,001	S-adenosylmethionine synthase 3 OS=Arabidopsis thaliana GN=METK3 PE=1 SV=1
AT2G20610	Q9SIV0	0,596	cytosol	0,001	S-alkyl-thiohydroximate lyase SUR1 OS=Arabidopsis thaliana GN=SUR1 PE=1 SV=1
AT4G01850	P17562;P23686;Q9LUT2	0,595	cytosol,nucleus	0,004	S-adenosylmethionine synthase 2 OS=Arabidopsis thaliana GN=SAM2 PE=1 SV=1
AT5G17920	O50008;Q0WNZ5;Q9SRV5	0,558	cytosol	0,003	5-methyltetrahydropteroyltriglutamate--homocysteine methyltransferase 1 OS=Arabidopsis thaliana GN=MS1 PE=1 SV=1
AT1G74040	Q9C550;Q9LPR4	0,504	plastid	0,003	2-isopropylmalate synthase 2, chloroplastic OS=Arabidopsis thaliana GN=IPMS2 PE=1 SV=1
AT1G80560	P93832;Q9FMT1;Q9SA14	0,475	plastid	0,013	3-isopropylmalate dehydrogenase 2, chloroplastic OS=Arabidopsis thaliana GN=IMDH2 PE=1 SV=1
AT1G22410	Q9SK84	0,462	plastid	0,038	Phospho-2-dehydro-3-deoxyheptonate aldolase OS=Arabidopsis thaliana GN=F12K8.24 PE=3 SV=1
AT3G61440	Q9S757	0,433	mitochondrion	0,004	Bifunctional L-3-cyanoalanine synthase/cysteine synthase C1, mitochondrial OS=Arabidopsis thaliana GN=CYSC1 PE=1 SV=1
AT5G11520	P46644;P46645	0,432	peroxisome	0,019	Aspartate aminotransferase 3, chloroplastic OS=Arabidopsis thaliana GN=ASP3 PE=1 SV=1
AT3G48560	P17597	0,429	plastid	0,027	Acetolactate synthase, chloroplastic OS=Arabidopsis thaliana GN=ALS PE=1 SV=1
AT5G65780	Q9FYA6;Q9M401	0,406	plastid	0,034	Branched-chain-amino-acid aminotransferase 5, chloroplastic OS=Arabidopsis thaliana GN=BCAT5 PE=1 SV=1
AT5G04740	Q9LZ23	0,382	plastid	0,028	ACT domain-containing protein ACR12 OS=Arabidopsis thaliana GN=ACR12 PE=2 SV=1
AT5G11880	Q94A94	0,376	plastid	0,049	Diaminopimelate decarboxylase 2, chloroplastic OS=Arabidopsis thaliana GN=LYSA2 PE=1 SV=1
AT4G23600	Q9SUR6	0,345	peroxisome	0,028	Cystine lyase CORI3 OS=Arabidopsis thaliana GN=CORI3 PE=1 SV=1
AT1G23310	Q9LR30	-0,308	peroxisome	0,048	Glutamate--glyoxylate aminotransferase 1 OS=Arabidopsis thaliana GN=GGAT1 PE=1 SV=1
AT2G33150	Q56WD9	-0,342	peroxisome	0,028	3-ketoacyl-CoA thiolase 2, peroxisomal OS=Arabidopsis thaliana GN=PED1 PE=1 SV=2
AT4G34030	Q9LDD8	-0,458	mitochondrion	0,034	Methylcrotonoyl-CoA carboxylase beta chain, mitochondrial OS=Arabidopsis thaliana GN=MCCB PE=2 SV=1
AT1G68010	Q9C9W5	-0,515	peroxisome	0,001	Glycerate dehydrogenase HPR, peroxisomal OS=Arabidopsis thaliana GN=HPR PE=1 SV=1
AT3G47340	P49078	-0,543	cytosol	0,014	Asparagine synthetase [glutamine-hydrolyzing] 1 OS=Arabidopsis thaliana GN=ASN1 PE=2 SV=2
AT2G13360	Q56YA5	-0,575	peroxisome	0,001	Serine--glyoxylate aminotransferase OS=Arabidopsis thaliana GN=AGT1 PE=1 SV=2
AT1G03090	Q42523	-0,661	mitochondrion	0,005	Methylcrotonoyl-CoA carboxylase subunit alpha, mitochondrial OS=Arabidopsis thaliana GN=MCCA PE=1 SV=2
AT4G33150	Q9SMZ4	-0,903	cytosol	0,001	Alpha-aminoadipic semialdehyde synthase OS=Arabidopsis thaliana GN=LKR/SDH PE=1 SV=1
AT3G45300	Q9SWG0	-1,057	mitochondrion	0	Isovaleryl-CoA dehydrogenase, mitochondrial OS=Arabidopsis thaliana GN=IVD PE=1 SV=2

Accession number	Protein ID	Fold change (log2)	Subcellular location	qvalue (FDR)	Description
AT1G11840	F4IAH9	0,337	peroxisome	0,039	Lactoylglutathione lyase OS=Arabidopsis thaliana GN=GLX1 PE=1 SV=1
AT1G53580	Q9C8L4	-0,549	mitochondrion	0,003	Persulfide dioxygenase ETHE1 homolog, mitochondrial OS=Arabidopsis thaliana GN=GLY3 PE=1 SV=3
C1-metabolism					
AT1G50480	Q9SPK5	0,354	cytosol	0,026	Formate--tetrahydrofolate ligase OS=Arabidopsis thaliana GN=THFS PE=2 SV=1
AT3G59970	Q9SE60	0,335	cytosol	0,032	Methylenetetrahydrofolate reductase 1 OS=Arabidopsis thaliana GN=MTHFR1 PE=1 SV=1
AT5G14780	Q9S7E4	-0,316	mitochondrion	0,036	Formate dehydrogenase, chloroplastic/mitochondrial OS=Arabidopsis thaliana GN=FDH1 PE=1 SV=1
Cell wall					
AT4G32410	O48946	0,873	golgi,plasma mem	0,036	Cellulose synthase A catalytic subunit 1 [UDP-forming] OS=Arabidopsis thaliana GN=CESA1 PE=1 SV=1
AT1G63000	Q9LQ04;Q9SYM5	0,571	cytosol	0,035	Bifunctional dTDP-4-dehydrorhamnose 3,5-epimerase/dTDP-4-dehydrorhamnose reductase OS=Arabidopsis thaliana GN=NRS/ER PE=1
AT4G37800	Q8LER3	0,545	extracellular	0,003	Probable xyloglucan endotransglucosylase/hydrolase protein 7 OS=Arabidopsis thaliana GN=XTH7 PE=2 SV=2
AT5G39320	Q9FM01;Q9LIA8	0,488	extracellular	0,014	UDP-glucose 6-dehydrogenase 4 OS=Arabidopsis thaliana GN=UGD4 PE=1 SV=1
AT3G29360	Q9LIA8	0,441	extracellular	0,022	UDP-glucose 6-dehydrogenase 2 OS=Arabidopsis thaliana GN=UGD2 PE=1 SV=1
AT5G15650	Q9LFW1	0,409	golgi	0,05	UDP-arabinopyranose mutase 2 OS=Arabidopsis thaliana GN=RGP2 PE=1 SV=1
AT3G10740	Q9SG80	-0,412	extracellular	0,033	Alpha-L-arabinofuranosidase 1 OS=Arabidopsis thaliana GN=ASD1 PE=1 SV=1
AT3G60900	Q9LZX4	-0,556	plasma membrane	0,031	Fasciclin-like arabinogalactan protein 10 OS=Arabidopsis thaliana GN=FLA10 PE=1 SV=1
AT2G45470	O22126	-0,588	plasma membrane	0,001	Fasciclin-like arabinogalactan protein 8 OS=Arabidopsis thaliana GN=FLA8 PE=1 SV=1
AT5G06860	Q9M5J9	-0,819	extracellular	0,002	Polygalacturonase inhibitor 1 OS=Arabidopsis thaliana GN=PGIP1 PE=1 SV=1
AT1G65310	O80803;P24806	-0,909	extracellular	0,007	Probable xyloglucan endotransglucosylase/hydrolase protein 17 OS=Arabidopsis thaliana GN=XTH17 PE=1 SV=1
AT5G06870	Q9M5J8	-0,952	extracellular	0,003	Polygalacturonase inhibitor 2 OS=Arabidopsis thaliana GN=PGIP2 PE=2 SV=2
AT5G49360	Q9FGY1	-1,041	extracellular	0	Beta-D-xylosidase 1 OS=Arabidopsis thaliana GN=BXL1 PE=1 SV=1
AT4G30270	P24806;Q38857	-1,214	extracellular	0,001	Xyloglucan endotransglucosylase/hydrolase protein 24 OS=Arabidopsis thaliana GN=XTH24 PE=1 SV=2
Co-factor and vitamine metabolism					
AT5G50210	Q9FGS4	0,6	plastid	0,026	Quinolinate synthase, chloroplastic OS=Arabidopsis thaliana GN=QS PE=1 SV=1
AT5G54770	Q38814	0,539	plastid	0,001	Thiamine thiazole synthase, chloroplastic OS=Arabidopsis thaliana GN=THI1 PE=1 SV=1
AT5G66120	Q8VYV7	0,324	peroxisome	0,048	3-dehydroquinate synthase, chloroplastic OS=Arabidopsis thaliana GN=DHQS PE=1 SV=1
AT3G14990	Q9FPF0	-0,457	golgi	0,004	Protein DJ-1 homolog A OS=Arabidopsis thaliana GN=DJ1A PE=1 SV=1
AT2G38230	O80448	-0,589	cytosol	0	Pyridoxal 5'-phosphate synthase subunit PDX1.1 OS=Arabidopsis thaliana GN=PDX11 PE=1 SV=1
Development					
AT1G18080	O24456;Q9C4Z6;Q9LV28	0,523	cytosol	0,031	Receptor for activated C kinase 1A OS=Arabidopsis thaliana GN=RACK1A PE=1 SV=2
AT4G21150	Q93Z16	0,364	endoplasmic retic	0,024	Dolichyl-diphosphooligosaccharide--protein glycosyltransferase subunit 2 OS=Arabidopsis thaliana GN=RPN2 PE=1 SV=1
AT2G44060	O80576	0,309	cytosol	0,05	At2g44060 OS=Arabidopsis thaliana GN=At2g44060 PE=2 SV=1
AT4G12420	Q9SU40	-0,413	plasma membrane	0,019	Monocopper oxidase-like protein SKU5 OS=Arabidopsis thaliana GN=SKU5 PE=1 SV=1
DNA					
AT3G54560	O23628	-0,413	nucleus	0,045	Histone H2A variant 1 OS=Arabidopsis thaliana GN=H2AV PE=1 SV=1
AT3G45980	O23629	-0,564	nucleus	0,012	Histone H2B.6 OS=Arabidopsis thaliana GN=H2B PE=1 SV=3
AT4G31210	F4JRX3	-1,097	plastid	0,022	DNA topoisomerase, type IA, core OS=Arabidopsis thaliana GN=At4g31210 PE=3 SV=1

Accession number	Protein ID	Fold change (log2)	Subcellular location	qvalue (FDR)	Description
Fermentation					
AT1G77120	P06525	1,881	cytosol	0,001	Alcohol dehydrogenase class-P OS=Arabidopsis thaliana GN=ADH1 PE=1 SV=2
AT4G36250	Q70E96	0,472	cytosol	0,009	Aldehyde dehydrogenase family 3 member F1 OS=Arabidopsis thaliana GN=ALDH3F1 PE=2 SV=2
AT5G54960	Q9FFT4	0,455	cytosol	0,031	Pyruvate decarboxylase 2 OS=Arabidopsis thaliana GN=PDC2 PE=2 SV=1
AT1G54100	Q9SYG7	-0,83	cytosol	0	Aldehyde dehydrogenase family 7 member B4 OS=Arabidopsis thaliana GN=ALDH7B4 PE=2 SV=3
Gluconeogenesis					
AT4G15530	O23404	-0,441	plastid	0,004	Pyruvate, phosphate dikinase 1, chloroplastic OS=Arabidopsis thaliana GN=PPDK PE=1 SV=2
AT5G09660	Q9ZP05	-0,568	peroxisome	0,006	Malate dehydrogenase 2, peroxisomal OS=Arabidopsis thaliana GN=PMDH2 PE=2 SV=1
Glycolysis					
AT5G63680	Q9FFP6;Q9FNN1	0,685	cytosol	0,026	Pyruvate kinase OS=Arabidopsis thaliana GN=At5g63680 PE=3 SV=1
AT3G52990	Q94KE3	0,541	cytosol	0,003	Pyruvate kinase OS=Arabidopsis thaliana GN=At3g52990 PE=2 SV=1
AT1G13440	Q9FX54	0,481	cytosol,nucleus	0,022	Glyceraldehyde-3-phosphate dehydrogenase GAPC2, cytosolic OS=Arabidopsis thaliana GN=GAPC2 PE=1 SV=1
AT5G08570	Q9FNN1	0,463	cytosol	0,015	Pyruvate kinase OS=Arabidopsis thaliana GN=At5g08570 PE=2 SV=1
AT3G04120	P25858;Q9FX54	0,431	cytosol,nucleus	0,004	Glyceraldehyde-3-phosphate dehydrogenase GAPC1, cytosolic OS=Arabidopsis thaliana GN=GAPC1 PE=1 SV=2
AT1G09780	O04499	0,425	cytosol	0,011	2,3-bisphosphoglycerate-independent phosphoglycerate mutase 1 OS=Arabidopsis thaliana GN=PGM1 PE=2 SV=3
AT1G53310	Q9MAH0	0,404	cytosol	0,011	Phosphoenolpyruvate carboxylase 1 OS=Arabidopsis thaliana GN=PPC1 PE=1 SV=1
AT1G79550	Q9SAJ4	0,352	cytosol	0,02	Phosphoglycerate kinase 3, cytosolic OS=Arabidopsis thaliana GN=PGK3 PE=1 SV=1
AT3G55440	P48491	0,318	cytosol	0,036	Triosephosphate isomerase, cytosolic OS=Arabidopsis thaliana GN=TPI PE=1 SV=2
Hormone metabolism					
AT1G12010	O65378	0,856	peroxisome	0,011	1-aminocyclopropane-1-carboxylate oxidase 3 OS=Arabidopsis thaliana GN=At1g12010 PE=2 SV=1
AT1G62380	Q41931	0,602	golgi	0,001	1-aminocyclopropane-1-carboxylate oxidase 2 OS=Arabidopsis thaliana GN=ACO2 PE=2 SV=2
AT2G23600	O80476	0,543	cytosol	0,014	Methylesterase 2 OS=Arabidopsis thaliana GN=MES2 PE=1 SV=1
AT3G44310	P32961	0,524	cytosol	0,001	Nitrilase 1 OS=Arabidopsis thaliana GN=NIT1 PE=1 SV=2
AT1G24100	O48676	0,472	plasma membrane	0,035	UDP-glycosyltransferase 74B1 OS=Arabidopsis thaliana GN=UGT74B1 PE=1 SV=1
AT3G25770	Q9LS02	0,399	plastid	0,049	Allene oxide cyclase 2, chloroplastic OS=Arabidopsis thaliana GN=AOC2 PE=1 SV=1
AT3G45140	P38418	0,316	plastid	0,035	Lipoxygenase 2, chloroplastic OS=Arabidopsis thaliana GN=LOX2 PE=1 SV=1
AT3G07390	Q94BT2	-0,364	plasma membrane	0,045	Auxin-induced in root cultures protein 12 OS=Arabidopsis thaliana GN=AIR12 PE=1 SV=3
AT1G05560	Q9LR44	-0,483	plastid	0,028	UDP-glycosyltransferase 75B1 OS=Arabidopsis thaliana GN=UGT75B1 PE=1 SV=1
AT5G48180	Q93XW5	-0,596	cytosol	0,006	Nitrile-specifier protein 5 OS=Arabidopsis thaliana GN=NSP5 PE=2 SV=1
AT3G44300	P32962	-0,612	cytosol	0,005	Nitrilase 2 OS=Arabidopsis thaliana GN=NIT2 PE=1 SV=1
AT2G33830	P93017	-0,613	peroxisome	0,013	Dormancy-associated protein homolog 1 OS=Arabidopsis thaliana GN=DRMH1 PE=1 SV=1
AT4G19170	O49675	-1,252	plastid	0,001	Probable carotenoid cleavage dioxygenase 4, chloroplastic OS=Arabidopsis thaliana GN=CCD4/NCED4 PE=1 SV=1
AT3G02480	Q9M892	-1,918	cytosol	0,001	AT3g02480/F16B3_11 OS=Arabidopsis thaliana GN=At3g02480 PE=2 SV=1

Accession number	Protein ID	Fold change (log2)	Subcellular location	qvalue (FDR)	Description
Lipid metabolism					
AT2G20900	Q9C5E5	1,401	cytosol	0,002	Diacylglycerol kinase 5 OS=Arabidopsis thaliana GN=DGK5 PE=2 SV=1
AT4G30950	P46312	0,763	plastid	0,001	Omega-6 fatty acid desaturase, chloroplastic OS=Arabidopsis thaliana GN=FAD6 PE=1 SV=2
AT2G33470	O22797	0,593	golgi	0,038	Glycolipid transfer protein 1 OS=Arabidopsis thaliana GN=GLTP1 PE=2 SV=1
AT3G08770	Q9LD84	0,552	extracellular	0,032	Non-specific lipid-transfer protein 6 OS=Arabidopsis thaliana GN=LTP6 PE=2 SV=1
AT4G33030	O48917	0,545	plastid	0,003	UDP-sulfoquinovose synthase, chloroplastic OS=Arabidopsis thaliana GN=SQD1 PE=1 SV=1
AT1G54580	P25701	0,512	plastid	0,047	Acyl carrier protein 2, chloroplastic OS=Arabidopsis thaliana GN=ACP2 PE=1 SV=2
AT2G43710	O22832	0,492	plastid	0,006	Stearoyl-[acyl-carrier-protein] 9-desaturase 7, chloroplastic OS=Arabidopsis thaliana GN=FAB2 PE=1 SV=1
AT1G73600	Q9C6B9	0,491	cytosol	0,01	Phosphoethanolamine N-methyltransferase 3 OS=Arabidopsis thaliana GN=NMT3 PE=2 SV=2
AT1G48600	Q944H0	0,446	cytosol	0,007	Phosphomethylethanolamine N-methyltransferase OS=Arabidopsis thaliana GN=NMT2 PE=2 SV=2
AT2G05990	Q9SLA8	-0,42	plastid	0,006	Enoyl-[acyl-carrier-protein] reductase [NADH], chloroplastic OS=Arabidopsis thaliana GN=MOD1 PE=1 SV=1
AT5G10160	Q9LX13	-0,422	plastid	0,028	(3R)-hydroxymyristoyl-[acyl carrier protein] dehydratase-like protein OS=Arabidopsis thaliana GN=T31P16_150 PE=2 SV=1
AT4G26690	Q9SZ11	-0,424	plasma membrane	0,018	Glycerophosphodiester phosphodiesterase GDPD13 OS=Arabidopsis thaliana GN=GDPD13 PE=1 SV=3
AT5G54500	Q9LSQ5	-0,427	plasma membrane	0,012	NAD(P)H dehydrogenase (quinone) FQR1 OS=Arabidopsis thaliana GN=FQR1 PE=1 SV=1
AT4G16760	O65202	-0,436	peroxisome	0,01	Peroxisomal acyl-coenzyme A oxidase 1 OS=Arabidopsis thaliana GN=ACX1 PE=1 SV=1
AT3G51840	Q96329	-0,624	peroxisome	0,002	Acyl-coenzyme A oxidase 4, peroxisomal OS=Arabidopsis thaliana GN=ACX4 PE=1 SV=1
AT4G27780	Q9STP8	-0,897	endoplasmic retici	0,035	Acyl-CoA-binding domain-containing protein 2 OS=Arabidopsis thaliana GN=ACBP2 PE=1 SV=1
Major CHO metabolism					
AT1G32900	Q9MAQ0	0,88	plastid	0	Granule-bound starch synthase 1, chloroplastic/amyloplastic OS=Arabidopsis thaliana GN=GBSS1 PE=1 SV=1
AT1G69830	Q94A41	0,81	plastid	0,002	Alpha-amylase 3, chloroplastic OS=Arabidopsis thaliana GN=AMY3 PE=2 SV=1
AT3G52180	Q9FEB5	0,749	plastid	0	Phosphoglucan phosphatase DSP4, chloroplastic OS=Arabidopsis thaliana GN=SEX4 PE=1 SV=1
AT3G46970	Q9SD76	0,509	cytosol	0,001	Alpha-glucan phosphorylase 2, cytosolic OS=Arabidopsis thaliana GN=PHS2 PE=1 SV=1
AT1G10760	Q9SAC6	0,443	plastid	0,002	Alpha-glucan water dikinase 1, chloroplastic OS=Arabidopsis thaliana GN=GWD1 PE=1 SV=2
AT2G31390	Q9SID0	0,42	cytosol	0,025	Probable fructokinase-1 OS=Arabidopsis thaliana GN=At2g31390 PE=2 SV=1
AT5G26570	Q6ZY51	0,389	plastid	0,024	Phosphoglucan, water dikinase, chloroplastic OS=Arabidopsis thaliana GN=GWD3 PE=1 SV=1
AT3G29320	Q9LU82	0,38	plastid	0,013	Alpha-glucan phosphorylase 1 OS=Arabidopsis thaliana GN=PHS1 PE=1 SV=1
Metal handling					
AT3G56090	Q9LYN2;Q9S756	1,603	plastid	0,004	Ferritin-3, chloroplastic OS=Arabidopsis thaliana GN=FER3 PE=2 SV=1
AT5G01600	Q39101	0,982	plastid	0,001	Ferritin-1, chloroplastic OS=Arabidopsis thaliana GN=FER1 PE=2 SV=1
AT3G17390	Q9LUT2;Q9SJL8	0,964	nucleus	0,004	S-adenosylmethionine synthase 4 OS=Arabidopsis thaliana GN=METK4 PE=1 SV=1
AT4G14710	Q8W108	0,458	cytosol	0,033	1,2-dihydroxy-3-keto-5-methylthiopentene dioxygenase 3 OS=Arabidopsis thaliana GN=ARD3 PE=2 SV=1
Minor CHO metabolism					
AT3G47800	Q9STT3	-0,543	extracellular	0,007	Aldose 1-epimerase OS=Arabidopsis thaliana GN=T23J7.130 PE=2 SV=1
AT5G57655	Q9FKK7	-0,823	endoplasmic retici	0,001	Xylose isomerase OS=Arabidopsis thaliana GN=XYLA PE=2 SV=2
AT2G21370	Q8L794	-0,935	plastid	0,01	Putative xylulose kinase OS=Arabidopsis thaliana GN=XK-1 PE=1 SV=1
AT5G20250	Q8RX87	-0,942	plastid	0,002	Probable galactinol--sucrose galactosyltransferase 6 OS=Arabidopsis thaliana GN=RFS6 PE=2 SV=2

Accession number	Protein ID	Fold change (log2)	Subcellular location	qvalue (FDR)	Description
Miscellaneous enzyme family					
AT1G78370	Q8L7C9	1,227	peroxisome	0	Glutathione S-transferase U20 OS=Arabidopsis thaliana GN=GSTU20 PE=1 SV=1
AT1G16410	Q949U1	1,186	endoplasmic retici	0,001	Dihomomethionine N-hydroxylase OS=Arabidopsis thaliana GN=CYP79F1 PE=1 SV=1
AT5G47990	Q9FI39	1,059	endoplasmic retici	0,022	Cytochrome P450 705A5 OS=Arabidopsis thaliana GN=CYP705A5 PE=2 SV=1
AT1G48750	Q94AQ3	0,93	extracellular	0,012	Bifunctional inhibitor/lipid-transfer protein/seed storage 2S albumin-like protein OS=Arabidopsis thaliana GN=At1g48750 PE=2 SV=1
AT2G30860	O80852	0,878	cytosol	0,001	Glutathione S-transferase F9 OS=Arabidopsis thaliana GN=GSTF9 PE=1 SV=1
AT3G14210	Q9LIG3	0,854	vacuole	0,002	GDSL esterase/lipase ESM1 OS=Arabidopsis thaliana GN=ESM1 PE=1 SV=1
AT4G13770	P48421	0,82	endoplasmic retici	0,003	Cytochrome P450 83A1 OS=Arabidopsis thaliana GN=CYP83A1 PE=1 SV=2
AT5G17050	Q9LFJ8	0,776	plastid	0,003	UDP-glycosyltransferase 78D2 OS=Arabidopsis thaliana GN=UGT78D2 PE=2 SV=1
AT4G22690	F4JLY4	0,766	endoplasmic retici	0,002	Cytochrome P450, family 706, subfamily A, polypeptide 1 OS=Arabidopsis thaliana GN=CYP706A1 PE=3 SV=1
AT4G12880	Q9STZ8	0,729	extracellular	0,021	At4g12880 OS=Arabidopsis thaliana GN=T20K18.230 PE=2 SV=1
AT1G74090	Q9C9C9	0,709	cytosol	0,001	Cytosolic sulfotransferase 18 OS=Arabidopsis thaliana GN=SOT18 PE=1 SV=1
AT2G30870	P42761	0,678	cytosol	0,003	Glutathione S-transferase F10 OS=Arabidopsis thaliana GN=GSTF10 PE=1 SV=3
AT1G02930	P42760;P46422;Q9SRY5	0,656	cytosol	0,013	Glutathione S-transferase F6 OS=Arabidopsis thaliana GN=GSTF6 PE=2 SV=2
AT2G31790	Q9SKC1	0,64	mitochondrion	0,001	UDP-glycosyltransferase 74C1 OS=Arabidopsis thaliana GN=UGT74C1 PE=2 SV=1
AT3G16420	O04314	0,638	cytosol	0	PYK10-binding protein 1 OS=Arabidopsis thaliana GN=PBP1 PE=1 SV=1
AT1G62560	Q9SXE1	0,626	endoplasmic retici	0,004	Flavin-containing monooxygenase FMO GS-OX3 OS=Arabidopsis thaliana GN=FMOGS-OX3 PE=2 SV=1
AT4G02520	P46422	0,614	cytosol	0,001	Glutathione S-transferase F2 OS=Arabidopsis thaliana GN=GSTF2 PE=1 SV=3
AT1G33811	Q8LSZ1	0,518	extracellular	0,01	GDSL esterase/lipase At1g33811 OS=Arabidopsis thaliana GN=At1g33811 PE=2 SV=1
AT2G23610	O80477	0,466	cytosol	0,038	Methylesterase 3 OS=Arabidopsis thaliana GN=MES3 PE=2 SV=1
AT3G15356	Q9LJR2	0,44	extracellular	0,01	Lectin-like protein LEC OS=Arabidopsis thaliana GN=LEC PE=1 SV=1
AT1G02920	Q9SRY5	0,387	cytosol	0,045	Glutathione S-transferase F7 OS=Arabidopsis thaliana GN=GSTF7 PE=2 SV=3
AT4G27520	Q9T076	-0,372	plasma membrane	0,022	Early nodulin-like protein 2 OS=Arabidopsis thaliana GN=At4g27520 PE=1 SV=1
AT2G29450	P46421	-0,376	cytosol	0,021	Glutathione S-transferase U5 OS=Arabidopsis thaliana GN=GSTU5 PE=2 SV=1
AT3G09260	Q9SR37	-0,438	endoplasmic retici	0,007	Beta-glucosidase 23 OS=Arabidopsis thaliana GN=BGLU23 PE=1 SV=1
AT1G30720	Q9SA87	-0,461	extracellular	0,033	Berberine bridge enzyme-like 10 OS=Arabidopsis thaliana GN=At1g30720 PE=2 SV=1
AT5G63800	Q9FFN4	-0,518	extracellular	0,004	Beta-galactosidase 6 OS=Arabidopsis thaliana GN=BGAL6 PE=2 SV=1
AT4G20860	Q9SUC6	-0,61	extracellular	0,039	Berberine bridge enzyme-like 22 OS=Arabidopsis thaliana GN=FAD-OXR PE=2 SV=1
AT3G48460	Q9STM6	-0,635	extracellular	0,034	GDSL esterase/lipase At3g48460 OS=Arabidopsis thaliana GN=At3g48460 PE=2 SV=1
AT2G29420	Q92W24	-0,648	cytosol	0,005	Glutathione S-transferase U7 OS=Arabidopsis thaliana GN=GSTU7 PE=2 SV=1
AT2G43820	O22822	-0,683	plasma membrane	0,01	UDP-glycosyltransferase 74F2 OS=Arabidopsis thaliana GN=UGT74F2 PE=1 SV=1
AT5G16970	Q39172	-0,692	cytosol	0,001	NADP-dependent alkenal double bond reductase P1 OS=Arabidopsis thaliana GN=P1 PE=1 SV=1
AT3G13750	Q9SCW1	-0,699	extracellular	0,001	Beta-galactosidase 1 OS=Arabidopsis thaliana GN=BGAL1 PE=2 SV=1
AT4G22485	A8MRQ5	-0,708	extracellular	0,021	Protease inhibitor/seed storage/LTP family protein OS=Arabidopsis thaliana GN=At4g22485 PE=4 SV=2
AT4G34138	Q8VZE9	-0,709	plasma membrane	0,008	UDP-glycosyltransferase 73B1 OS=Arabidopsis thaliana GN=UGT73B1 PE=2 SV=1
AT5G64250	Q9FMG0	-0,722	cytosol	0,001	2-nitropropane dioxygenase-like protein OS=Arabidopsis thaliana GN=At5g64250 PE=1 SV=1
AT2G44790	O80517	-0,855	plasma membrane	0,013	Uclacyanin-2 OS=Arabidopsis thaliana GN=At2g44790 PE=1 SV=1
AT4G16690	O23512	-0,876	cytosol	0,011	Probable pheophorbidase OS=Arabidopsis thaliana GN=PPD PE=1 SV=1
AT5G63810	Q9FN08;Q9LFA6;Q9SCV8	-1,067	extracellular	0,02	Beta-galactosidase 10 OS=Arabidopsis thaliana GN=BGAL10 PE=2 SV=1
AT5G56870	Q9SCV8	-1,147	extracellular	0	Beta-galactosidase 4 OS=Arabidopsis thaliana GN=BGAL4 PE=1 SV=1

Accession number	Protein ID	Fold change (log2)	Subcellular location	qvalue (FDR)	Description
N-metabolism					
AT5G53460	Q9LV03	0,592	plastid	0,001	Glutamate synthase 1 [NADH], chloroplastic OS=Arabidopsis thaliana GN=GLT1 PE=1 SV=2
AT5G07440	Q38946	-0,485	mitochondrion	0,003	Glutamate dehydrogenase 2 OS=Arabidopsis thaliana GN=GDH2 PE=1 SV=1
Nucleotide metabolism					
AT4G30530	Q9M0A7	0,676	cytosol	0,001	Gamma-glutamyl peptidase 1 OS=Arabidopsis thaliana GN=GGP1 PE=1 SV=1
AT5G03300	Q9LZG0;Q9SF85	0,44	cytosol	0,006	Adenosine kinase 2 OS=Arabidopsis thaliana GN=ADK2 PE=1 SV=1
AT4G09320	P39207	0,422	cytosol	0,007	Nucleoside diphosphate kinase 1 OS=Arabidopsis thaliana GN=NDK1 PE=1 SV=1
AT4G22930	O04904	0,419	plastid	0,035	Dihydroorotase, mitochondrial OS=Arabidopsis thaliana GN=PYR4 PE=1 SV=1
AT1G27450	P31166	0,372	cytosol	0,031	Adenine phosphoribosyltransferase 1, chloroplastic OS=Arabidopsis thaliana GN=APT1 PE=1 SV=2
AT1G14240	Q9XI62	-1,35	endoplasmic retic	0	Probable apyrase 3 OS=Arabidopsis thaliana GN=APY3 PE=2 SV=1
Photosynthesis					
AT3G21055	Q39195	0,713	plastid	0,002	Photosystem II 5 kDa protein, chloroplastic OS=Arabidopsis thaliana GN=PSBT PE=3 SV=2
AT3G62410	Q9LZP9	0,582	plastid	0,049	Calvin cycle protein CP12-2, chloroplastic OS=Arabidopsis thaliana GN=CP12-2 PE=1 SV=1
AT2G47400	Q22914	0,554	plastid	0,006	Calvin cycle protein CP12-1, chloroplastic OS=Arabidopsis thaliana GN=CP12-1 PE=1 SV=1
AT4G05180	Q41932	0,4	plastid	0,01	Oxygen-evolving enhancer protein 3-2, chloroplastic OS=Arabidopsis thaliana GN=PSBQ2 PE=1 SV=2
AT4G21280	Q9XFT3-2	-0,324	plastid	0,035	Isoform 2 of Oxygen-evolving enhancer protein 3-1, chloroplastic OS=Arabidopsis thaliana GN=PSBQ1
AT3G14420	Q9LR89	-0,392	peroxisome	0,012	Peroxisomal (S)-2-hydroxy-acid oxidase GLO1 OS=Arabidopsis thaliana GN=GLO1 PE=1 SV=1
AT5G64380	Q9FMF1	-0,498	plastid	0,017	AT5g64380/MSJ1_22 OS=Arabidopsis thaliana GN=At5g64380 PE=2 SV=1
AT3G55330	P82538	-0,536	plastid	0,001	PsbP-like protein 1, chloroplastic OS=Arabidopsis thaliana GN=PPL1 PE=1 SV=1
AT2G05070	Q9S717;Q9XF87	-0,668	plastid	0,001	Chlorophyll a-b binding protein 2.2, chloroplastic OS=Arabidopsis thaliana GN=LHCB2.2 PE=1 SV=1
AT1G20340	P42699	-0,885	plastid	0,003	Plastocyanin major isoform, chloroplastic OS=Arabidopsis thaliana GN=DRT112 PE=1 SV=2
Protein					
AT5G37680	Q8W4C8	2,034	plasma membrane	0,007	ADP-ribosylation factor-like protein 8c OS=Arabidopsis thaliana GN=ARL8C PE=2 SV=1
AT5G43010	Q9SEI3	1,21	cytosol,nucleus	0,002	26S protease regulatory subunit 10B homolog A OS=Arabidopsis thaliana GN=RPT4A PE=1 SV=1
AT2G45070	P38389	1,172	endoplasmic retic	0,013	Protein transport protein Sec61 subunit beta OS=Arabidopsis thaliana GN=At2g45070 PE=1 SV=1
AT1G01680	Q9LQ92	1,152	nucleus	0,018	U-box domain-containing protein 54 OS=Arabidopsis thaliana GN=PUB54 PE=2 SV=1
AT1G78680	O65355	0,778	vacuole	0,005	Gamma-glutamyl hydrolase 2 OS=Arabidopsis thaliana GN=GGH2 PE=1 SV=2
AT4G19006	Q8GYA6;Q8RWF0	0,693	cytosol,nucleus	0,022	26S proteasome non-ATPase regulatory subunit 13 homolog B OS=Arabidopsis thaliana GN=RPN9B PE=1 SV=1
AT3G48870	Q9SXJ7	0,666	plastid	0,001	Chaperone protein ClpC2, chloroplastic OS=Arabidopsis thaliana GN=CLPC2 PE=1 SV=1
AT3G60210	Q9M1C2	0,627	plastid	0,05	10 kDa chaperonin 1, chloroplastic OS=Arabidopsis thaliana GN=CPN10-1 PE=2 SV=1
AT4G10480	Q9SZY1	0,608	cytosol	0,001	Nascent polypeptide-associated complex subunit alpha-like protein 4 OS=Arabidopsis thaliana GN=At4g10480 PE=1 SV=1
AT5G11900	Q8VZK2	0,556	cytosol	0,024	Translation machinery-associated protein 22 OS=Arabidopsis thaliana GN=At5g11900 PE=2 SV=1
AT3G23390	O23290	0,542	cytosol	0,012	60S ribosomal protein L36a OS=Arabidopsis thaliana GN=RPL36AA PE=2 SV=3
AT5G12140	Q945Q1	0,539	endoplasmic retic	0,031	Cysteine proteinase inhibitor 1 OS=Arabidopsis thaliana GN=CYS1 PE=1 SV=2
AT5G19510	Q9SCX3	0,533	cytosol	0,001	Elongation factor 1-beta 2 OS=Arabidopsis thaliana GN=At5g19510 PE=1 SV=1
AT5G61170	Q9FNP8	0,532	cytosol	0,009	40S ribosomal protein S19-3 OS=Arabidopsis thaliana GN=RPS19C PE=2 SV=1
AT5G27700	Q3E902;Q9M337	0,522	cytosol	0,05	40S ribosomal protein S21-2 OS=Arabidopsis thaliana GN=RPS21C PE=1 SV=2
AT5G18380	Q42340	0,516	cytosol	0,045	40S ribosomal protein S16-3 OS=Arabidopsis thaliana GN=RPS16C PE=2 SV=1
AT1G15930	Q9SIP1	0,511	cytosol	0,019	40S ribosomal protein S12-1 OS=Arabidopsis thaliana GN=RPS12A PE=2 SV=1
AT3G11250	P57691;Q42112	0,497	cytosol	0,002	60S acidic ribosomal protein P0-3 OS=Arabidopsis thaliana GN=RPP0C PE=1 SV=1
AT3G53870	Q9M339;Q9SIP7	0,473	cytosol	0,048	40S ribosomal protein S3-2 OS=Arabidopsis thaliana GN=RPS3B PE=1 SV=1
AT2G44120	P60039	0,467	cytosol	0,007	60S ribosomal protein L7-3 OS=Arabidopsis thaliana GN=RPL7C PE=2 SV=1
AT5G52650	Q9LTF2	0,463	cytosol	0,013	40S ribosomal protein S10-3 OS=Arabidopsis thaliana GN=RPS10C PE=2 SV=2

Accession number	Protein ID	Fold change (log2)	Subcellular location	qvalue (FDR)	Description
AT1G30230	P48006;Q9SJ20	0,452	cytosol	0,03	Elongation factor 1-delta 1 OS=Arabidopsis thaliana GN=At1g30230 PE=1 SV=2
AT5G02240	Q94EG6	0,45	cytosol	0,008	Uncharacterized protein At5g02240 OS=Arabidopsis thaliana GN=At5g02240 PE=1 SV=1
AT3G10670	Q9CAF5	0,449	plastid	0,011	ABC transporter I family member 6, chloroplastic OS=Arabidopsis thaliana GN=ABCI6 PE=1 SV=1
AT5G35620	O04663	0,444	cytosol	0,05	Eukaryotic translation initiation factor isoform 4E OS=Arabidopsis thaliana GN=EIF(ISO)4E PE=1 SV=2
AT2G27720	P51407;Q9SLF7	0,441	cytosol	0,028	60S acidic ribosomal protein P2-1 OS=Arabidopsis thaliana GN=RPP2A PE=2 SV=2
AT2G41840	P49688	0,439	cytosol	0,006	40S ribosomal protein S2-3 OS=Arabidopsis thaliana GN=RPS2C PE=1 SV=2
AT3G45030	P49200	0,43	cytosol	0,035	40S ribosomal protein S20-1 OS=Arabidopsis thaliana GN=RPS20A PE=2 SV=2
AT2G34250	O80774	0,424	endoplasmic reticu	0,028	AT2G34250 protein OS=Arabidopsis thaliana GN=At2g34250 PE=2 SV=1
AT1G08360	Q8VZB9	0,422	cytosol	0,04	60S ribosomal protein L10a-1 OS=Arabidopsis thaliana GN=RPL10AA PE=1 SV=1
AT2G18020	P46286	0,42	cytosol	0,031	60S ribosomal protein L8-1 OS=Arabidopsis thaliana GN=RPL8A PE=1 SV=2
AT5G35530	Q9FJA6;Q9M339;Q9SIP7	0,417	cytosol	0,008	40S ribosomal protein S3-3 OS=Arabidopsis thaliana GN=RPS3C PE=1 SV=1
AT1G07940	P0DH99	0,415	cytosol	0,004	Elongation factor 1-alpha 1 OS=Arabidopsis thaliana GN=A1 PE=1 SV=1
AT1G01100	Q8LCW9	0,413	cytosol	0,032	60S acidic ribosomal protein P1-1 OS=Arabidopsis thaliana GN=RPP1A PE=2 SV=2
AT1G33120	P49209	0,408	cytosol	0,007	60S ribosomal protein L9-1 OS=Arabidopsis thaliana GN=RPL9B PE=1 SV=3
AT3G09200	Q42112	0,407	cytosol	0,031	60S acidic ribosomal protein P0-2 OS=Arabidopsis thaliana GN=RPP0B PE=1 SV=2
AT5G35680	F4K1D3	0,402	cytosol	0,043	Nucleic acid-binding, OB-fold-like protein OS=Arabidopsis thaliana GN=At5g35680 PE=3 SV=1
AT5G27770	Q9FE58;Q9M9W1	0,4	cytosol	0,035	60S ribosomal protein L22-3 OS=Arabidopsis thaliana GN=RPL22C PE=2 SV=1
AT5G02610	Q9LZ41;Q9SF53	0,4	cytosol	0,05	60S ribosomal protein L35-4 OS=Arabidopsis thaliana GN=RPL35D PE=2 SV=1
AT2G01250	P60040	0,399	cytosol	0,024	60S ribosomal protein L7-2 OS=Arabidopsis thaliana GN=RPL7B PE=1 SV=1
AT2G24200	P30184	0,397	cytosol	0,011	Leucine aminopeptidase 1 OS=Arabidopsis thaliana GN=LAP1 PE=1 SV=1
AT2G39460	Q8LD46	0,394	cytosol	0,019	60S ribosomal protein L23a-1 OS=Arabidopsis thaliana GN=RPL23AA PE=2 SV=2
AT1G72370	Q08682	0,389	cytosol	0,013	40S ribosomal protein Sa-1 OS=Arabidopsis thaliana GN=RPSaA PE=1 SV=3
AT3G12915	F4JB05;Q9ASR1	0,388	cytosol	0,012	Ribosomal protein S5/Elongation factor G/III/V family protein OS=Arabidopsis thaliana GN=MGH6.2 PE=4 SV=1
AT4G34670	Q42262;Q9CAV0	0,386	cytosol	0,022	40S ribosomal protein S3a-2 OS=Arabidopsis thaliana GN=RPS3AB PE=2 SV=3
AT2G27710	Q95LF7	0,386	cytosol	0,048	60S acidic ribosomal protein P2-2 OS=Arabidopsis thaliana GN=RPP2B PE=1 SV=1
AT1G57720	Q9FVT2	0,375	cytosol	0,022	Probable elongation factor 1-gamma 2 OS=Arabidopsis thaliana GN=At1g57720 PE=1 SV=1
AT5G20290	Q93VG5	0,374	cytosol	0,023	40S ribosomal protein S8-1 OS=Arabidopsis thaliana GN=RPS8A PE=1 SV=1
AT3G51800	Q96327	0,36	cytosol	0,028	ERB8-3 BINDING PROTEIN 1 OS=Arabidopsis thaliana GN=EBP1 PE=1 SV=1
AT2G39990	O04202	0,36	nucleus	0,038	Eukaryotic translation initiation factor 3 subunit F OS=Arabidopsis thaliana GN=TIF3F1 PE=1 SV=1
AT5G02870	P49691	0,357	cytosol	0,041	60S ribosomal protein L4-2 OS=Arabidopsis thaliana GN=RPL4D PE=1 SV=2
AT1G09640	O04487;Q9FVT2	0,356	cytosol	0,027	Probable elongation factor 1-gamma 1 OS=Arabidopsis thaliana GN=At1g09640 PE=1 SV=1
AT3G25520	Q8LBI1	0,349	cytosol	0,031	60S ribosomal protein L5-1 OS=Arabidopsis thaliana GN=ATL5 PE=1 SV=2
AT5G55220	Q859L5	0,348	cytosol	0,023	Trigger factor-like protein TIG, Chloroplastic OS=Arabidopsis thaliana GN=TIG PE=1 SV=1
AT5G15200	Q9LXG1	0,348	plastid	0,035	40S ribosomal protein S9-1 OS=Arabidopsis thaliana GN=RPS9B PE=1 SV=1
AT5G07090	P49204	0,33	cytosol	0,033	40S ribosomal protein S4-2 OS=Arabidopsis thaliana GN=RPS4B PE=2 SV=4
AT1G56070	Q9ASR1	0,322	cytosol	0,031	Elongation factor 2 OS=Arabidopsis thaliana GN=LOS1 PE=1 SV=1
AT2G20890	Q9SKT0	-0,34	plastid	0,04	Protein THYLAKOID FORMATION 1, chloroplastic OS=Arabidopsis thaliana GN=THF1 PE=1 SV=1
AT3G01480	Q9SSA5	-0,356	plastid	0,02	Peptidyl-prolyl cis-trans isomerase CYP38, chloroplastic OS=Arabidopsis thaliana GN=CYP38 PE=1 SV=1

Accession number	Protein ID	Fold change (log2)	Subcellular location	qvalue (FDR)	Description
AT5G23120	Q82660	-0,451	plastid	0,002	Photosystem II stability/assembly factor HCF136, chloroplastic OS=Arabidopsis thaliana GN=HCF136 PE=1 SV=1
AT1G06430	Q8W585	-0,487	plastid	0,003	ATP-dependent zinc metalloprotease FTSH 8, chloroplastic OS=Arabidopsis thaliana GN=FTSH8 PE=1 SV=1
AT2G45740	O80845;Q9LQ73	-0,599	peroxisome	0,033	Peroxisomal membrane protein 11D OS=Arabidopsis thaliana GN=PEX11D PE=1 SV=2
AT1G03230	Q9ZVS5	-0,6	extracellular	0,001	Aspartyl protease-like protein OS=Arabidopsis thaliana GN=F15K9.16 PE=2 SV=1
AT1G47128	P43297	-0,637	extracellular	0,001	Cysteine proteinase RD21A OS=Arabidopsis thaliana GN=RD21A PE=1 SV=1
AT5G24490	Q94K97	-0,64	plastid	0,001	Putative 30S ribosomal protein OS=Arabidopsis thaliana GN=At5g24490 PE=1 SV=1
AT1G03220	Q9ZVS4;Q9ZVS5	-0,737	extracellular	0	Aspartyl protease-like protein OS=Arabidopsis thaliana GN=F15K9.17 PE=2 SV=1
AT4G02930	Q9ZT91	-1,065	mitochondrion	0,003	Elongation factor Tu, mitochondrial OS=Arabidopsis thaliana GN=TUFA PE=1 SV=1
AT3G10060	Q9SR70	-1,186	plastid	0,001	Peptidyl-prolyl cis-trans isomerase FKBP16-4, chloroplastic OS=Arabidopsis thaliana GN=FKBP16-4 PE=1 SV=1
Redox regulation					
AT2G16060	O24520	1,757	cytosol	0,001	Non-symbiotic hemoglobin 1 OS=Arabidopsis thaliana GN=AHB1 PE=1 SV=1
AT1G35620	Q94F09	1,115	endoplasmic retici	0,028	Protein disulfide-isomerase 5-2 OS=Arabidopsis thaliana GN=PDIL5-2 PE=1 SV=1
AT4G21860	Q9C5C8-2	0,878	plastid	0,03	Isoform 2 of Peptide methionine sulfoxide reductase B2, chloroplastic OS=Arabidopsis thaliana GN=MSRB2
AT4G25100	P21276	0,714	plastid	0	Superoxide dismutase [Fe] 1, chloroplastic OS=Arabidopsis thaliana GN=FSD1 PE=1 SV=4
AT1G77510	Q9SRG3	0,496	endoplasmic retici	0,003	Protein disulfide isomerase-like 1-2 OS=Arabidopsis thaliana GN=PDIL1-2 PE=2 SV=1
AT1G20620	Q42547	0,487	peroxisome	0,001	Catalase-3 OS=Arabidopsis thaliana GN=CAT3 PE=1 SV=3
AT2G32920	O48773	0,472	endoplasmic retici	0,014	Protein disulfide-isomerase 2-3 OS=Arabidopsis thaliana GN=PDIL2-3 PE=2 SV=1
AT3G02730	Q9XFH8	0,459	plastid	0,017	Thioredoxin F1, chloroplastic OS=Arabidopsis thaliana GN=TRXF1 PE=1 SV=2
AT5G20080	P83291	0,404	mitochondrion	0,023	NADH-cytochrome b5 reductase-like protein OS=Arabidopsis thaliana GN=CBR2 PE=1 SV=2
AT5G60640	Q9FF55	0,341	endoplasmic retici	0,049	Protein disulfide isomerase-like 1-4 OS=Arabidopsis thaliana GN=PDIL1-4 PE=1 SV=1
AT3G52960	Q949U7	-0,315	plastid	0,046	Peroxiredoxin-2E, chloroplastic OS=Arabidopsis thaliana GN=PRXIIE PE=1 SV=2
AT3G26060	Q9LU86	-0,315	plastid	0,048	Peroxiredoxin Q, chloroplastic OS=Arabidopsis thaliana GN=PRXQ PE=1 SV=1
AT1G77490	Q42593	-0,365	plastid	0,03	L-ascorbate peroxidase T, chloroplastic OS=Arabidopsis thaliana GN=APXT PE=2 SV=2
AT4G09010	P82281	-0,414	plastid	0,007	Thylakoid lumenal 29 kDa protein, chloroplastic OS=Arabidopsis thaliana GN=TL29 PE=1 SV=2
AT2G31570	Q04922;P52032;Q9SZ54	-0,461	cytosol	0,028	Probable glutathione peroxidase 2 OS=Arabidopsis thaliana GN=GPX2 PE=1 SV=1
AT2G25080	P52032	-0,715	plastid	0	Phospholipid hydroperoxide glutathione peroxidase 1, chloroplastic OS=Arabidopsis thaliana GN=GPX1 PE=2 SV=2
AT4G35090	P25819	-1,169	peroxisome	0,001	Catalase-2 OS=Arabidopsis thaliana GN=CAT2 PE=2 SV=3
RNA					
AT3G53460	Q43349	0,886	plastid	0	29 kDa ribonucleoprotein, chloroplastic OS=Arabidopsis thaliana GN=CP29A PE=2 SV=2
AT2G21660	Q03250;Q03251	0,76	nucleus	0,002	Glycine-rich RNA-binding protein 7 OS=Arabidopsis thaliana GN=RBG7 PE=1 SV=1
AT4G17520	O23593;Q9LVT8	0,612	nucleus	0,003	RGG repeats nuclear RNA binding protein B OS=Arabidopsis thaliana GN=RGGB PE=1 SV=1
AT5G47210	Q9LVT8	0,571	nucleus	0,001	RGG repeats nuclear RNA binding protein C OS=Arabidopsis thaliana GN=RGGC PE=1 SV=1
AT1G73230	Q9CAT7	0,45	nucleus	0,015	Nascent polypeptide-associated complex subunit beta OS=Arabidopsis thaliana GN=At1g73230 PE=2 SV=1
AT5G52470	Q9FEF8	0,437	nucleus	0,011	Probable mediator of RNA polymerase II transcription subunit 36b OS=Arabidopsis thaliana GN=MED36B PE=1 SV=1
AT4G16830	O23523;Q9LVT8	0,419	cytosol	0,043	RGG repeats nuclear RNA binding protein A OS=Arabidopsis thaliana GN=RGGA PE=1 SV=1
AT5G07350	Q8VZG7;Q9FLT0	0,402	nucleus	0,018	Ribonuclease TUDOR 1 OS=Arabidopsis thaliana GN=TSN1 PE=1 SV=1
AT1G56110	Q9SGT7	0,398	nucleus	0,038	At1g56110/T6H22_9 OS=Arabidopsis thaliana GN=T6H22.10 PE=2 SV=1
AT4G39260	Q03251	0,37	nucleus	0,03	Glycine-rich RNA-binding protein 8 OS=Arabidopsis thaliana GN=RBG8 PE=1 SV=1
AT5G26742	Q8L758	0,328	plastid	0,038	DEAD-box ATP-dependent RNA helicase 3, chloroplastic OS=Arabidopsis thaliana GN=RH3 PE=1 SV=2
AT3G61260	Q9M2D8	-0,748	plasma membrane	0,001	Uncharacterized protein At3g61260 OS=Arabidopsis thaliana GN=At3g61260 PE=1 SV=1
AT3G55340	Q9M3B8	-0,935	nucleus	0,034	PHIP1 OS=Arabidopsis thaliana GN=T26I12.220 PE=4 SV=1

Accession number	Protein ID	Fold change (log2)	Subcellular location	qvalue (FDR)	Description
S-assimilation					
AT4G14680	O23324;Q9LIK9	0,774	plastid	0,001	ATP-sulfurylase 3, chloroplastic OS=Arabidopsis thaliana GN=APS3 PE=1 SV=1
AT3G22890	Q9LIK9	0,609	plastid	0,001	ATP sulfurylase 1, chloroplastic OS=Arabidopsis thaliana GN=APS1 PE=1 SV=1
AT5G04590	Q9LZ66	0,432	plastid	0,004	Assimilatory sulfite reductase (ferredoxin), chloroplastic OS=Arabidopsis thaliana GN=SIR PE=1 SV=1
Secondary metabolism					
AT5G23020	Q9FN52	1,181	plastid	0,01	Methylthioalkylmalate synthase 3, chloroplastic OS=Arabidopsis thaliana GN=MAM3 PE=1 SV=1
AT2G43100	Q9ZW84	1,163	plastid	0,001	3-isopropylmalate dehydratase small subunit 1 OS=Arabidopsis thaliana GN=IPMI2 PE=1 SV=1
AT4G39980	P29976;Q00218	0,944	plastid	0,009	Phospho-2-dehydro-3-deoxyheptonate aldolase 1, chloroplastic OS=Arabidopsis thaliana GN=DHS1 PE=2 SV=2
AT4G13430	Q94AR8	0,79	plastid	0	3-isopropylmalate dehydratase large subunit, chloroplastic OS=Arabidopsis thaliana GN=IIL1 PE=1 SV=1
AT3G58990	Q9LY77	0,701	plastid	0,005	3-isopropylmalate dehydratase small subunit 2 OS=Arabidopsis thaliana GN=IPMI1 PE=1 SV=1
AT4G33510	Q00218	0,584	plastid	0,001	Phospho-2-dehydro-3-deoxyheptonate aldolase 2, chloroplastic OS=Arabidopsis thaliana GN=DHS2 PE=2 SV=2
AT4G34350	Q94B35	0,54	plastid	0,001	4-hydroxy-3-methylbut-2-enyl diphosphate reductase, chloroplastic OS=Arabidopsis thaliana GN=ISPH/ISSPE/HDR PE=2 SV=1
AT5G54160	Q9FK25	0,53	cytosol	0,006	Flavone 3'-O-methyltransferase 1 OS=Arabidopsis thaliana GN=OMT1 PE=1 SV=1
AT5G60600	F4KDE8	0,447	plastid	0,002	4-hydroxy-3-methylbut-2-en-1-yl diphosphate synthase (ferredoxin), chloroplastic OS=Arabidopsis thaliana GN=ISPG/HDS PE=1 SV=1
AT1G74470	Q9CA67	0,412	plastid	0,007	Geranylgeranyl diphosphate reductase, chloroplastic OS=Arabidopsis thaliana GN=CHLP PE=1 SV=1
AT4G15560	Q38854	0,386	plastid	0,049	1-deoxy-D-xylulose-5-phosphate synthase, chloroplastic OS=Arabidopsis thaliana GN=DXS PE=1 SV=2
AT5G16440	Q38929;Q42553	0,376	plastid	0,039	Isopentenyl-diphosphate Delta-isomerase I, chloroplastic OS=Arabidopsis thaliana GN=IPP1/IDI1 PE=2 SV=3
AT1G08550	Q39249	-0,431	plastid	0,023	Violaxanthin de-epoxidase, chloroplastic OS=Arabidopsis thaliana GN=VDE1 PE=1 SV=1
Signalling					
AT2G41090	P30187	3,153	cytosol	0,001	Calmodulin-like protein 10 OS=Arabidopsis thaliana GN=CML10 PE=2 SV=1
AT1G48630	Q9C4Z6;Q9LV28	0,756	cytosol	0,001	Receptor for activated C kinase 1B OS=Arabidopsis thaliana GN=RACK1B PE=1 SV=1
AT2G30060	Q8RWG8	0,545	nucleus	0,035	Ran-binding protein 1 homolog b OS=Arabidopsis thaliana GN=RANBP1B PE=1 SV=2
AT5G61790	P29402	0,436	endoplasmic reticu	0,01	Calnexin homolog 1 OS=Arabidopsis thaliana GN=CNX1 PE=1 SV=1
AT1G56340	O04151;Q38858	0,42	endoplasmic reticu	0,015	Calreticulin-1 OS=Arabidopsis thaliana GN=CRT1 PE=1 SV=1
AT5G38480	P42644	0,408	cytosol	0,011	14-3-3-like protein GF14 psi OS=Arabidopsis thaliana GN=GRF3 PE=1 SV=2
AT3G16570	Q9LUS7	-0,477	extracellular	0,024	Rapid alkalinization factor 23 OS=Arabidopsis thaliana GN=RALF23 PE=1 SV=1
AT3G22060	Q9LRJ9	-0,799	extracellular	0,001	Cysteine-rich repeat secretory protein 38 OS=Arabidopsis thaliana GN=CRRSP38 PE=2 SV=1
AT4G20260	Q96262	-0,835	plasma membrane	0,001	Plasma membrane-associated cation-binding protein 1 OS=Arabidopsis thaliana GN=PCAP1 PE=1 SV=1
AT5G64260	Q9FE06;Q9FY71	-1,117	extracellular	0	Protein EXORDIUM-like 2 OS=Arabidopsis thaliana GN=EXL2 PE=2 SV=1
AT5G09440	Q9FY71	-1,406	extracellular	0,004	Protein EXORDIUM-like 4 OS=Arabidopsis thaliana GN=EXL4 PE=2 SV=1
AT2G33380	O22788	-1,409	cytosol	0,004	Probable peroxygenase 3 OS=Arabidopsis thaliana GN=PXG3 PE=1 SV=1
Stress					
AT1G70850	Q9SSK7	0,988	cytosol	0,031	MLP-like protein 34 OS=Arabidopsis thaliana GN=MLP34 PE=2 SV=1
AT2G14610	P33154	0,975	extracellular	0,008	Pathogenesis-related protein 1 OS=Arabidopsis thaliana GN=At2g14610 PE=1 SV=1
AT1G24020	Q93VR4	0,777	golgi	0	MLP-like protein 423 OS=Arabidopsis thaliana GN=MLP423 PE=2 SV=1
AT3G28930	P54121	0,558	cytosol	0,009	Protein AIG2 A OS=Arabidopsis thaliana GN=AIG2A PE=2 SV=1
AT5G42020	Q39043;Q9LKR3	0,379	endoplasmic reticu	0,013	Mediator of RNA polymerase II transcription subunit 37f OS=Arabidopsis thaliana GN=MED37F PE=1 SV=2
AT1G30360	Q9C8G5	-0,395	plasma membrane	0,012	CSC1-like protein ERD4 OS=Arabidopsis thaliana GN=ERD4 PE=2 SV=1
AT1G20440	P31168	-0,563	nucleus	0,004	Dehydrin COR47 OS=Arabidopsis thaliana GN=COR47 PE=1 SV=2
AT5G25610	Q08298	-0,636	extracellular	0,002	BURP domain protein RD22 OS=Arabidopsis thaliana GN=RD22 PE=2 SV=1
AT1G17860	Q9LMU2	-0,788	extracellular	0,004	Kunitz trypsin inhibitor 2 OS=Arabidopsis thaliana GN=KTI2 PE=2 SV=1
AT4G25200	Q96331	-1,077	mitochondrion	0,024	23.6 kDa heat shock protein, mitochondrial OS=Arabidopsis thaliana GN=HSP23.6 PE=2 SV=1

Accession number	Protein ID	Fold change (log2)	Subcellular location	qvalue (FDR)	Description
TCA					
AT1G10670	Q9SGY2	0,577	cytosol	0,02	ATP-citrate synthase alpha chain protein 1 OS=Arabidopsis thaliana GN=ACLA-1 PE=1 SV=1
AT5G11670	Q9LYG3	0,541	cytosol	0	NADP-dependent malic enzyme 2 OS=Arabidopsis thaliana GN=NADP-ME2 PE=1 SV=1
AT4G35830	Q42560	0,372	cytosol	0,022	Aconitate hydratase 1 OS=Arabidopsis thaliana GN=ACO1 PE=1 SV=2
AT3G01500	P27140	-0,584	plastid	0,037	Isoform 3 of Beta carbonic anhydrase 1, chloroplastic OS=Arabidopsis thaliana GN=BCA1
AT4G33580	Q94CE3	-0,597	plastid	0,05	Beta carbonic anhydrase 5, chloroplastic OS=Arabidopsis thaliana GN=BCA5 PE=2 SV=1
Tetrapyrrole synthesis					
AT4G27440	P21218	1,457	plastid	0	Protochlorophyllide reductase B, chloroplastic OS=Arabidopsis thaliana GN=PORB PE=1 SV=3
AT1G03630	O48741;P21218	1,419	plastid	0,006	Protochlorophyllide reductase C, chloroplastic OS=Arabidopsis thaliana GN=PORC PE=1 SV=1
AT3G56940	Q9M591	0,606	plastid	0	Magnesium-protoporphyrin IX monomethyl ester [oxidative] cyclase, chloroplastic OS=Arabidopsis thaliana GN=CRD1 PE=1 SV=2
AT5G13630	Q9FNB0	0,545	plastid	0,001	Magnesium-chelatase subunit ChlH, chloroplastic OS=Arabidopsis thaliana GN=CHLH PE=1 SV=1
AT1G69740	Q9SFH9	0,47	plastid	0,002	Delta-aminolevulinic acid dehydratase 1, chloroplastic OS=Arabidopsis thaliana GN=HEMB1 PE=2 SV=1
AT3G59400	Q9LX31	0,441	plastid	0,048	Tetrapyrrole-binding protein, chloroplastic OS=Arabidopsis thaliana GN=GUN4 PE=1 SV=1
AT4G18480	P16127	0,42	plastid	0,011	Magnesium-chelatase subunit ChlI-1, chloroplastic OS=Arabidopsis thaliana GN=CHLI1 PE=1 SV=1
AT4G25080	Q9SW18	0,391	plastid	0,014	Magnesium protoporphyrin IX methyltransferase, chloroplastic OS=Arabidopsis thaliana GN=CHLM PE=1 SV=1
AT5G63570	P42799;Q42522	0,38	plastid	0,021	Glutamate-1-semialdehyde 2,1-aminomutase 1, chloroplastic OS=Arabidopsis thaliana GN=GSA1 PE=1 SV=1
AT3G48730	Q42522	0,373	plastid	0,035	Glutamate-1-semialdehyde 2,1-aminomutase 2, chloroplastic OS=Arabidopsis thaliana GN=GSA2 PE=2 SV=2
AT5G08280	Q43316	0,341	plastid	0,026	Porphobilinogen deaminase, chloroplastic OS=Arabidopsis thaliana GN=HEMC PE=1 SV=1
Transport					
AT1G15990	Q9S9N5	1,561	plasma membrane	0,004	Putative cyclic nucleotide-gated ion channel 7 OS=Arabidopsis thaliana GN=CNGC7 PE=3 SV=1
AT1G20260	Q8W4E2	-0,409	vacuole	0,032	V-type proton ATPase subunit B3 OS=Arabidopsis thaliana GN=VHA-B3 PE=2 SV=1
AT4G31390	Q8RWG1	-0,527	plastid	0,026	Uncharacterized aarF domain-containing protein kinase At4g31390, chloroplastic OS=Arabidopsis thaliana GN=At4g31390 PE=2 SV=1
AT5G40890	P92941	-0,578	vacuole	0,045	Chloride channel protein CLC-a OS=Arabidopsis thaliana GN=CLC-A PE=1 SV=2
AT4G35100	P93004	-0,597	plasma membrane	0,003	Aquaporin PIP2-7 OS=Arabidopsis thaliana GN=PIP2-7 PE=1 SV=2
AT1G79600	Q9MA15	-0,603	plastid	0,001	Uncharacterized aarF domain-containing protein kinase At1g79600, chloroplastic OS=Arabidopsis thaliana GN=At1g79600 PE=2 SV=1
AT2G45960	Q06611	-0,65	plasma membrane	0,001	Aquaporin PIP1-2 OS=Arabidopsis thaliana GN=PIP1-2 PE=1 SV=1
AT2G36830	P25818	-0,689	vacuole	0,015	Aquaporin TIP1-1 OS=Arabidopsis thaliana GN=TIP1-1 PE=1 SV=1
AT3G16240	Q41951	-0,693	vacuole	0,008	Aquaporin TIP2-1 OS=Arabidopsis thaliana GN=TIP2-1 PE=1 SV=2
AT4G17340	Q41975	-0,704	vacuole	0,032	Probable aquaporin TIP2-2 OS=Arabidopsis thaliana GN=TIP2-2 PE=1 SV=2
AT3G26520	Q41963	-0,802	vacuole	0,008	Aquaporin TIP1-2 OS=Arabidopsis thaliana GN=TIP1-2 PE=1 SV=2
AT1G22530	Q56ZI2	-0,806	cytosol	0,001	Patellin-2 OS=Arabidopsis thaliana GN=PATL2 PE=1 SV=2
AT2G37170	P43287	-0,876	plasma membrane	0	Aquaporin PIP2-2 OS=Arabidopsis thaliana GN=PIP2-2 PE=1 SV=2
AT3G61430	P61837;Q06611;Q08733	-0,893	plasma membrane	0,006	Aquaporin PIP1-1 OS=Arabidopsis thaliana GN=PIP1-1 PE=1 SV=1
AT3G53420	P43286;P43287	-0,984	plasma membrane	0,002	Aquaporin PIP2-1 OS=Arabidopsis thaliana GN=PIP2-1 PE=1 SV=1
AT1G58340	Q9SLV0	-1,062	plasma membrane	0,022	Protein DETOXIFICATION 48 OS=Arabidopsis thaliana GN=DTX48 PE=2 SV=1
AT1G72150	Q56WK6;Q56ZI2	-1,268	plasma membrane	0,001	Patellin-1 OS=Arabidopsis thaliana GN=PATL1 PE=1 SV=2
AT1G11260	P23586	-1,403	plasma membrane	0	Sugar transport protein 1 OS=Arabidopsis thaliana GN=STP1 PE=1 SV=2

Accession number	Protein ID	Fold change (log2)	Subcellular location	qvalue (FDR)	Description
Not assigned					
AT5G06540	Q9FG16	1,378	mitochondrion	0,008	Pentatricopeptide repeat-containing protein At5g06540 OS=Arabidopsis thaliana GN=PCMP-H88 PE=3 SV=1
AT5G52780	Q9LTD9	0,969	plastid	0,032	Uncharacterized protein PAM68-like OS=Arabidopsis thaliana GN=At5g52780 PE=2 SV=1
AT4G28080	F4HTP2	0,964	nucleus	0,042	DNA polymerase alpha subunit B OS=Arabidopsis thaliana GN=POLA2 PE=3 SV=1
AT3G54600	Q9M1G8	0,961	plasma membrane	0,001	DJ-1 protein homolog F OS=Arabidopsis thaliana GN=DJ1F PE=1 SV=1
AT5G22580	Q9FK81	0,943	vacuole	0,001	Stress-response A/B barrel domain-containing protein At5g22580 OS=Arabidopsis thaliana GN=At5g22580 PE=1 SV=1
AT3G62530	Q94K48	0,857	mitochondrion	0,001	ARM repeat superfamily protein OS=Arabidopsis thaliana GN=At3g62530 PE=2 SV=1
AT5G11710	Q8VY07	0,846	golgi;vacuole	0,047	Clathrin interactor EPSIN 1 OS=Arabidopsis thaliana GN=EPSIN1 PE=1 SV=1
AT5G25100	Q9C5N2	0,835	golgi	0,009	Transmembrane 9 superfamily member 9 OS=Arabidopsis thaliana GN=TMN9 PE=2 SV=1
AT5G64130	A8MS32	0,747	endoplasmic reticu	0,003	AT5G64130 protein OS=Arabidopsis thaliana GN=At5g64130 PE=1 SV=1
AT2G43090	Q9ZW85	0,679	nucleus	0,002	3-isopropylmalate dehydratase small subunit 3 OS=Arabidopsis thaliana GN=At2g43090 PE=1 SV=1
AT1G62780	Q8VY70	0,659	plastid	0	Putative uncharacterized protein At1g62780 OS=Arabidopsis thaliana GN=At1g62780 PE=2 SV=1
AT1G09310	Q9ZPZ4	0,649	plastid	0	Putative uncharacterized protein OS=Arabidopsis thaliana GN=T31J12.3 PE=1 SV=1
AT4G16390	Q8GWE0	0,646	cytosol	0,021	Pentatricopeptide repeat-containing protein At4g16390, chloroplastic OS=Arabidopsis thaliana GN=P67 PE=1 SV=3
AT1G01320	F4HS99;F4JKH6	0,641	plastid	0,007	Tetratricopeptide repeat-containing protein OS=Arabidopsis thaliana GN=At1g01320 PE=1 SV=1
AT1G27030	Q9LFY3	0,617	nucleus	0,01	At1g27030/T7N9_9 OS=Arabidopsis thaliana GN=At1g27030 PE=2 SV=1
AT3G20250	Q9LJX4	0,614	cytosol	0,027	Pumilio homolog 5 OS=Arabidopsis thaliana GN=APUM5 PE=1 SV=2
AT4G12650	F4JRE0;Q9FYQ8	0,589	cytosol	0,041	Transmembrane 9 superfamily member 12 OS=Arabidopsis thaliana GN=TMN12 PE=2 SV=1
AT4G34830	Q0WLC6	0,583	golgi	0,016	Pentatricopeptide repeat-containing protein MRL1, chloroplastic OS=Arabidopsis thaliana GN=MRL1 PE=1 SV=2
AT5G58250	Q9LVM3	0,573	plastid	0,001	EMB3143 OS=Arabidopsis thaliana GN=At5g58250 PE=4 SV=1
AT4G21210	O49562	0,566	plastid	0,001	Pyruvate, phosphate dikinase regulatory protein 1, chloroplastic OS=Arabidopsis thaliana GN=RP1 PE=1 SV=1
AT2G01970	Q9ZPS7	0,491	plastid	0,007	Transmembrane 9 superfamily member 3 OS=Arabidopsis thaliana GN=TMN3 PE=2 SV=1
AT1G70770	Q9S791	0,447	plastid	0,018	AT1G70770 protein OS=Arabidopsis thaliana GN=F5A18.5 PE=1 SV=1
AT1G50900	Q8VY88	0,447	peroxisome	0,024	Protein LHCP TRANSLOCATION DEFECT OS=Arabidopsis thaliana GN=LTD PE=1 SV=1
AT5G51110	Q9LU63	0,445	golgi	0,026	AT5g51110/MWD22_5 OS=Arabidopsis thaliana GN=pdl1 PE=2 SV=1
AT5G24690	Q93W02	0,421	plastid	0,03	AT5g24690/MXC17_8 OS=Arabidopsis thaliana GN=At5g24690 PE=2 SV=1
AT5G11950	Q84MC2	0,421	endoplasmic reticu	0,038	Cytokinin riboside 5'-monophosphate phosphoribohydrolase LOG8 OS=Arabidopsis thaliana GN=LOG8 PE=1 SV=1
AT1G53280	Q9MAH3	0,416	plastid	0,031	Protein DJ-1 homolog B OS=Arabidopsis thaliana GN=DJ1B PE=1 SV=1
AT3G48420	Q94K71	-0,319	cytosol	0,049	Haloacid dehalogenase-like hydrolase domain-containing protein At3g48420 OS=Arabidopsis thaliana GN=At3g48420 PE=1 SV=1
AT1G16080	Q9S9M7	-0,328	plastid	0,036	Putative uncharacterized protein At1g16080 OS=Arabidopsis thaliana GN=T24D18.18 PE=1 SV=1
AT4G01150	O04616	-0,336	plastid	0,045	Protein CURVATURE THYLAKOID 1A, chloroplastic OS=Arabidopsis thaliana GN=CURT1A PE=1 SV=1
AT2G44920	O22160	-0,375	mitochondrion	0,03	Thylakoid lumenal 15 kDa protein 1, chloroplastic OS=Arabidopsis thaliana GN=At2g44920 PE=1 SV=2
AT3G58010	Q9M2P7	-0,384	plastid	0,024	Probable plastid-lipid-associated protein 9, chloroplastic OS=Arabidopsis thaliana GN=PAP9 PE=2 SV=1
AT3G05900	F4J9K9	-0,385	plastid	0,045	Neurofilament protein-like protein OS=Arabidopsis thaliana GN=At3g05900 PE=1 SV=1
AT2G34460	Q8H124	-0,387	plastid	0,028	Uncharacterized protein At2g34460, chloroplastic OS=Arabidopsis thaliana GN=At2g34460 PE=2 SV=1
AT1G18270	F4IAP5	-0,393	plastid	0,028	Ketose-bisphosphate aldolase class-II family protein OS=Arabidopsis thaliana GN=At1g18270 PE=4 SV=1
AT4G15545	Q93W28	-0,476	plastid	0,004	Uncharacterized protein At4g15545 OS=Arabidopsis thaliana GN=At4g15545 PE=1 SV=1
AT5G53490	P81760	-0,495	nucleus	0,003	Thylakoid lumenal 17.4 kDa protein, chloroplastic OS=Arabidopsis thaliana GN=TL17 PE=1 SV=2

Accession number	Protein ID	Fold change (log2)	Subcellular location	qvalue (FDR)	Description
AT5G48540	Q9LV60	-0,518	plastid	0,036	Cysteine-rich repeat secretory protein 55 OS=Arabidopsis thaliana GN=CRRSP55 PE=2 SV=1
AT2G30930	O80858	-0,522	cytosol	0,001	Expressed protein OS=Arabidopsis thaliana GN=At2g30930 PE=1 SV=1
AT4G24350	Q94K59	-0,538	plastid	0,014	Phosphorylase family protein OS=Arabidopsis thaliana GN=At4g24350 PE=2 SV=1
AT4G13500	Q9T0H1	-0,545	plastid	0,012	At4g13500 OS=Arabidopsis thaliana GN=T6G15.50 PE=2 SV=1
AT1G21670	Q9XI11	-0,568	nucleus	0,004	F8K7.9 OS=Arabidopsis thaliana GN=F8K7.9 PE=2 SV=1
AT3G44100	Q9LXQ2	-0,585	plastid	0,037	At3g44100 OS=Arabidopsis thaliana GN=F26G5_50 PE=2 SV=1
AT1G21500	Q9LPK9	-0,627	plastid	0,001	F24I8.11 protein OS=Arabidopsis thaliana GN=F24I8.11 PE=2 SV=1
AT4G15840	F4JKX0	-0,628	extracellular	0,043	BTB/POZ domain-containing protein OS=Arabidopsis thaliana GN=At4g15840 PE=4 SV=1
AT5G62140	Q9FIS4	-0,64	plasma membrane	0,009	At5g62140 OS=Arabidopsis thaliana GN=At5g62140 PE=2 SV=1
AT4G01870	Q9SYI5	-0,675	extracellular	0,004	Putative uncharacterized protein AT4g01870 OS=Arabidopsis thaliana GN=T7B11.13 PE=2 SV=1
AT1G32220	Q9FVR6	-0,719	plastid	0,001	Uncharacterized protein At1g32220, chloroplastic OS=Arabidopsis thaliana GN=At1g32220 PE=2 SV=1
AT1G07040	Q9LMI7	-0,726	extracellular	0,001	At1g07040 OS=Arabidopsis thaliana GN=F10K1.25 PE=2 SV=1
AT5G47860	Q9FIJ5	-0,753	extracellular	0	AT5g47860/MCA23_20 OS=Arabidopsis thaliana GN=At5g47860 PE=2 SV=1
AT5G05200	Q9ASX5	-0,804	plastid	0,002	Uncharacterized aarF domain-containing protein kinase At5g05200, chloroplastic OS=Arabidopsis thaliana GN=At5g05200 PE=2 SV=1
AT2G05540	Q9SL13	-0,89	cytosol	0,043	At2g05540/T20G20.11 OS=Arabidopsis thaliana GN=At2g05540 PE=2 SV=1
AT2G34400	O64705	-0,926	plastid	0,041	Pentatricopeptide repeat-containing protein At2g34400 OS=Arabidopsis thaliana GN=PCMP-E23 PE=3 SV=2
AT5G28750	Q9LKU2	-0,946	cytosol	0,049	Sec-independent protein translocase protein TATA, chloroplastic OS=Arabidopsis thaliana GN=TATA PE=1 SV=1
AT1G53705	F4HTB0	-1,02	plastid	0,003	Aminoacyl-tRNA synthetase, class II-like domain containing protein OS=Arabidopsis thaliana GN=At1g53705 PE=4 SV=1
AT5G66930	F4K265	-1,121	plastid	0,039	Autophagy-related protein 101 OS=Arabidopsis thaliana GN=ATG101 PE=1 SV=1
AT4G13220	Q6NLB6	-1,226	plastid	0,028	At4g13220 OS=Arabidopsis thaliana GN=At4g13220 PE=2 SV=1
AT5G63500	Q9FMV2	-1,381	plastid	0,015	At5g63500 OS=Arabidopsis thaliana GN=At5g63500 PE=2 SV=1
AT4G09660	Q9SZ82	-1,459	extracellular	0,012	Putative uncharacterized protein AT4g09660 OS=Arabidopsis thaliana GN=F17A8.10 PE=4 SV=1
AT2G05380	Q9ZSJ6	-1,603	cytosol	0,001	Glycine-rich protein 3 short isoform OS=Arabidopsis thaliana GN=GRP3S PE=1 SV=2
AT4G15610	Q9FEZ9	-2,272	plastid	0,001	CASP-like protein 1D1 OS=Arabidopsis thaliana GN=At4g15610 PE=2 SV=1
AT4G31340	Q8GUN1	0,747	cytosol	0,015	AT4G31340 protein OS=Arabidopsis thaliana GN=At4g31340 PE=2 SV=1
AT5G19940	Q941D3	0,516	cytosol	0,002	Probable plastid-lipid-associated protein 8, chloroplastic OS=Arabidopsis thaliana GN=PAP8 PE=1 SV=1
AT1G35720	Q9SYT0	0,5	plastid	0,001	Annexin D1 OS=Arabidopsis thaliana GN=ANN1 PE=1 SV=1
AT1G22450	Q9S7L9	0,374	plastid	0,029	Cytochrome c oxidase subunit 6b-1 OS=Arabidopsis thaliana GN=COX6B-1 PE=1 SV=1
AT2G46910	Q8W4F1	-0,421	extracellular	0,029	Probable plastid-lipid-associated protein 10, chloroplastic OS=Arabidopsis thaliana GN=PAP10 PE=2 SV=1
AT2G35490	O82291	-0,432	nucleus	0,007	Probable plastid-lipid-associated protein 3, chloroplastic OS=Arabidopsis thaliana GN=PAP3 PE=2 SV=1
AT3G23400	Q9LW57	-0,492	extracellular	0,001	Probable plastid-lipid-associated protein 6, chloroplastic OS=Arabidopsis thaliana GN=PAP6 PE=1 SV=1
AT4G04020	O81439	-1,19	plastid	0,03	Probable plastid-lipid-associated protein 1, chloroplastic OS=Arabidopsis thaliana GN=PAP1 PE=1 SV=1
AT4G22240	Q49629;Q81439	-1,815	plasma membrane	0	Probable plastid-lipid-associated protein 2, chloroplastic OS=Arabidopsis thaliana GN=PAP2 PE=2 SV=1

Table S2: List of proteins differentiallyexpressed in the comparative proteomic study between leaves of WT (Ws-2) and *gpt2-1* plants cultured in the presence of small fungal VCs.

Description	log2_fold_change	pvalue	evalue	qvalue (FDR)
AT5g37380/MNJ8_170 OS=Arabidopsis thaliana GN=At5g37380 PE=2 SV=1	6,638	9,9999E-06	0,04	0,02
reversed DNA topoisomerase, type IA, core OS=Arabidopsis thaliana GN=At4g31210 PE=3 SV=1	2,406	1,99998E-05	0,08	0,027
Putative uncharacterized protein AT4g09660 OS=Arabidopsis thaliana GN=F17A8.10 PE=4 SV=1	2,307	3,99996E-05	0,16	0,04
Probable apyrase 3 OS=Arabidopsis thaliana GN=APY3 PE=2 SV=1	1,378	9,9999E-06	0,04	0,04
reversed ADP-ribosylation factor-like protein 8c OS=Arabidopsis thaliana GN=ARL8C PE=2 SV=1	-1,974	7,99992E-05	0,32	0,045
reversed Putative cyclic nucleotide-gated ion channel 7 OS=Arabidopsis thaliana GN=CNGC7 PE=3 SV=1	-2,099	5,99994E-05	0,24	0,048

Table S3: List of differentially expressed proteins (DEPs) identified in the comparative proteomic study between leaves of WT (Ws-2) and *pgi1-2* plants cultured in the presence of small fungal VCs with a "confident" statistical significance level (*pgi1-2* vs. Ws-2). DEPs are classified according to their functions. DEPs that are discussed in the main text are highlighted in orange.

Accesión number	Protein ID	Fold change (log2)	qValue (FDR)	Subcellular location	Description
Amino acid metabolism					
AT3G45300	Q9SWG0	0,701	0,012	Mitochondrion	Isovaleryl-CoA dehydrogenase, mitochondrial OS=Arabidopsis thaliana GN=IVD PE=1 SV=2
AT1G22410	Q9SK84	0,555	0,018	Plastid	Phospho-2-dehydro-3-deoxyheptonate aldolase OS=Arabidopsis thaliana GN=F12K8.24 PE=3 SV=1
Biodegradation of Xenobiotics					
AT1G53580	Q9C8L4	0,42	0,034	mitochondrion	Persulfide dioxygenase ETHE1 homolog, mitochondrial OS=Arabidopsis thaliana GN=GLY3 PE=1 SV=3
Cell wall					
AT4G30270	P24806;Q388	0,909	0,03	Golgi	Xyloglucan endotransglucosylase/hydrolase protein 24 OS=Arabidopsis thaliana GN=XTH24 PE=1 SV=2
AT5G49360	Q9FGY1	0,631	0,003	Plastid	Beta-D-xylosidase 1 OS=Arabidopsis thaliana GN=BXL1 PE=1 SV=1
Fermentation					
AT1G54100	Q9SYG7	0,418	0,011	Plastid	Aldehyde dehydrogenase family 7 member B4 OS=Arabidopsis thaliana GN=ALDH7B4 PE=2 SV=3
Glycolysis					
AT4G24620	Q8H103	-1,138	0,003	Plastid	Glucose-6-phosphate isomerase 1, chloroplastic OS=Arabidopsis thaliana GN=PGI1 PE=1 SV=1
Glyoxylate cycle					
AT4G15530	O23404	0,503	0,018	Plastid	Pyruvate, phosphate dikinase 1, chloroplastic OS=Arabidopsis thaliana GN=PPDK PE=1 SV=2
Hormone metabolism					
AT3G44300	P32962	1,235	0,002	Cytosol	NIT2 Nitrilase 2 OS=Arabidopsis thaliana GN=NIT2 PE=1 SV=1
Lipid metabolism					
AT4G16760	O65202	0,358	0,038	Peroxisome	Peroxisomal acyl-coenzyme A oxidase 1 OS=Arabidopsis thaliana GN=ACX1 PE=1 SV=1
Major CHO metabolism					
AT1G69830	Q94A41	-0,635	0,003	Plastid	AMY3 Alpha-amylase 3, chloroplastic OS=Arabidopsis thaliana GN=AMY3 PE=2 SV=1
AT1G32900	Q9MAQ0	-0,684	0,003	Plastid	GBSS Granule-bound starch synthase 1, chloroplastic/amyloplastic OS=Arabidopsis thaliana GN=GBSS1 PE=1 SV=1
Minor CHO metabolism					
AT5G57655	Q9FKK7	0,497	0,002	ER	Xylose isomerase OS=Arabidopsis thaliana GN=XYLA PE=2 SV=2
AT5G20250	Q8RX87	0,407	0,02	Plastid	Probable galactinol--sucrose galactosyltransferase 6 OS=Arabidopsis thaliana GN=RFS6 PE=2 SV=2
Metal handling					
AT3G56240	A0A1I9LNC0	-0,34	0,046	Peroxisome	Copper chaperone OS=Arabidopsis thaliana GN=CCH PE=4 SV=1

Accesión number	Protein ID	Fold change (log2)	qValue (FDR)	Subcellular location	Description
Miscellaneous enzyme family					
AT1G02930	P42760;Q9SF	1,039	0,002	Cytosol	Glutathione S-transferase F6 OS=Arabidopsis thaliana GN=GSTF6 PE=2 SV=2
AT2G44790	O80517	0,864	0,032	Plasma membrane	Uclacyanin-2 OS=Arabidopsis thaliana GN=At2g44790 PE=1 SV=1
AT4G08770	Q9LDN9;Q9S	0,8	0,044	Cytosol	Peroxidase 37 OS=Arabidopsis thaliana GN=PER37 PE=2 SV=1
AT4G02520	P46422	0,755	0,036	Extracellular	GSTF2 Glutathione S-transferase F2 OS=Arabidopsis thaliana GN=GSTF2 PE=1 SV=3
AT5G56870	Q9SCV8	0,736	0,002	Extracellular	Beta-galactosidase 4 OS=Arabidopsis thaliana GN=BGAL4 PE=1 SV=1
AT1G02920	Q9SRY5	0,695	0,006	Cytosol	GSTF7 Glutathione S-transferase F7 OS=Arabidopsis thaliana GN=GSTF7 PE=2 SV=3
AT4G16260	Q8VZJ2	0,694	0,004	Extracellular	Probable glucan endo-1,3-beta-glucosidase At4g16260 OS=Arabidopsis thaliana GN=At4g16260 PE=1 SV=1
AT3G49120	Q9SMU8	0,55	0,007	Extracellular	Peroxidase 34 OS=Arabidopsis thaliana GN=PER34 PE=1 SV=1
AT1G30720	Q9SA87	0,535	0,022	Extracellular	Berberine bridge enzyme-like 10 OS=Arabidopsis thaliana GN=At1g30720 PE=2 SV=1
AT4G20830	Q9SVG4	0,356	0,043	Extracellular	Berberine bridge enzyme-like 19 OS=Arabidopsis thaliana GN=At4g20830 PE=1 SV=2
AT1G78370	Q8L7C9	-0,326	0,034	Peroxisome	Glutathione S-transferase U20 OS=Arabidopsis thaliana GN=GSTU20 PE=1 SV=1
Nucleotide metabolism					
AT1G14240	Q9XI62	1,128	0,004	Plasma membrane	Probable apyrase 3 OS=Arabidopsis thaliana GN=APY3 PE=2 SV=1
N-metabolism					
AT5G07440	Q38946	0,555	0,005	Mitochondrion	gdh2 Glutamate dehydrogenase 2 OS=Arabidopsis thaliana GN=GDH2 PE=1 SV=1
Photosynthesis					
ATCG00280	P56778	-0,32	0,019	Plastid	Photosystem II CP43 reaction center protein OS=Arabidopsis thaliana GN=psbC PE=1 SV=3
AT1G06680	Q42029	-0,332	0,031	Plastid	Oxygen-evolving enhancer protein 2-1, chloroplastic OS=Arabidopsis thaliana GN=PSBP1 PE=1 SV=2
AT3G12780	Q9LD57	-0,337	0,01	Plastid	Phosphoglycerate kinase 1, chloroplastic OS=Arabidopsis thaliana GN=PGK1 PE=1 SV=1
AT4G21280	Q9XFT3-2	-0,359	0,009	Plastid	Isoform 2 of Oxygen-evolving enhancer protein 3-1, chloroplastic OS=Arabidopsis thaliana GN=PSBQ1
AT5G66570	P23321	-0,362	0,01	Plastid	Oxygen-evolving enhancer protein 1-1, chloroplastic OS=Arabidopsis thaliana GN=PSBO1 PE=1 SV=2
AT4G03280	Q9ZR03	-0,372	0,031	Plastid	Cytochrome b6-f complex iron-sulfur subunit, chloroplastic OS=Arabidopsis thaliana GN=petC PE=1 SV=1
AT1G56190	P50318;Q9LF	-0,374	0,008	Plastid	Phosphoglycerate kinase 2, chloroplastic OS=Arabidopsis thaliana GN=At1g56190/PGK2 PE=1 SV=3
AT4G05180	Q41932	-0,415	0,002	Plastid	Oxygen-evolving enhancer protein 3-2, chloroplastic OS=Arabidopsis thaliana GN=PSBQ2 PE=1 SV=2
AT3G01500	A0A1I9LQB3;	-0,471	0,009	Plastid	Carbonic anhydrase 1 OS=Arabidopsis thaliana GN=CA1 PE=4 SV=1
AT3G62410	Q9LZP9	-0,81	0,038	Plastid	Calvin cycle protein CP12-2, chloroplastic OS=Arabidopsis thaliana GN=CP12-2 PE=1 SV=1
Protein					
AT4G02930	Q9ZT91	0,952	0,017	Mitochondrion	reversed Elongation factor Tu, mitochondrial OS=Arabidopsis thaliana GN=TUFA PE=1 SV=1
AT5G37680	Q8W4C8	-2,076	0,004	Plasma membrane	reversed ADP-ribosylation factor-like protein 8c OS=Arabidopsis thaliana GN=ARL8C PE=2 SV=1
AT5G22610	Q9FNK0	-1,6	0,01	Cytosol	reversed Putative F-box/FBD/LRR-repeat protein At5g22610 OS=Arabidopsis thaliana GN=At5g22610 PE=4 SV=1
AT4G21650	Q8GUK4	-0,422	0,037	Extracellular	Subtilisin-like protease SBT3.13 OS=Arabidopsis thaliana GN=SBT3.13 PE=2 SV=1
AT5G43010	Q95EI3	-1,035	0,021	Cytosol	26S protease regulatory subunit 10B homolog A OS=Arabidopsis thaliana GN=RPT4A PE=1 SV=1

Accesión number	Protein ID	Fold change (log2)	qValue (FDR)	Subcellular location	Description
Redox regulation					
AT1G20620	Q42547	0,555	0,007	Peroxisome	CAT3 Catalase-3 OS=Arabidopsis thaliana GN=CAT3 PE=1 SV=3
AT1G45145	Q39241	0,554	0,017	Cytosol	Thioredoxin H5 OS=Arabidopsis thaliana GN=TRX5 PE=1 SV=1
RNA					
AT3G04500	Q9M837	1,758	0,01	Nucleus	Putative RRM-containing protein OS=Arabidopsis thaliana GN=At3g04500 PE=2 SV=1
AT5G26742	Q8L7S8	0,303	0,042	plastid	DEAD-box ATP-dependent RNA helicase 3, chloroplastic OS=Arabidopsis thaliana GN=RH3 PE=1 SV=2
Secondary metabolism					
AT5G26000	P37702	-0,736	0,002	Peroxisome	Myrosinase 1 OS=Arabidopsis thaliana GN=TGG1 PE=1 SV=1
AT5G23020	Q9FN52	-1,021	0,003	Plastid	Methylthioalkylmalate synthase 3, chloroplastic OS=Arabidopsis thaliana GN=MAM3 PE=1 SV=1
Signalling					
AT5G09440	Q9FY71	0,595	0,028	Extracellular	Protein EXORDIUM-like 4 OS=Arabidopsis thaliana GN=EXL4 PE=2 SV=1
AT3G22060	Q9LRJ9	0,627	0,011	Extracellular	Cysteine-rich repeat secretory protein 38 OS=Arabidopsis thaliana GN=CRRSP38 PE=2 SV=1
Stress					
AT5G37380	Q9FHS7	1,841	0,005	Nucleus	AT5g37380/MNJ8_170 OS=Arabidopsis thaliana GN=At5g37380 PE=2 SV=1
AT1G75040	P28493	1,072	0,003	Extracellular	Pathogenesis-related protein 5 OS=Arabidopsis thaliana GN=At1g75040 PE=1 SV=1
AT2G14610	P33154	1,746	0,002	Extracellular	Pathogenesis-related protein 1 OS=Arabidopsis thaliana GN=At2g14610 PE=1 SV=1
AT1G73260	Q8RXD5	0,751	0,002	Extracellular	Kunitz trypsin inhibitor 1 OS=Arabidopsis thaliana GN=KTI1 PE=2 SV=1
AT2G43620	O22841	0,508	0,019	Extracellular	Endochitinase At2g43620 OS=Arabidopsis thaliana GN=At2g43620 PE=3 SV=1
AT4G23670	Q9SUR0	-0,541	0,002	Cytosol	AT4G23670 protein OS=Arabidopsis thaliana GN=F9D16.140 PE=2 SV=1
Transport					
AT1G15990	Q9S9N5	-2,634	0,004	Plasma membrane	reversed Putative cyclic nucleotide-gated ion channel 7 OS=Arabidopsis thaliana GN=CNGC7 PE=3 SV=1
not assigned					
AT4G15610	Q9FE29	1,95	0,008	plasma membrane	CASP-like protein 1D1 OS=Arabidopsis thaliana GN=At4g15610 PE=2 SV=1
AT4G09660	Q9SZ82	1,69	0,017	Nucleus	Putative uncharacterized protein AT4g09660 OS=Arabidopsis thaliana GN=F17A8.10 PE=4 SV=1
AT3G20250	Q9LJX4	-1,106	0,006	Nucleus	Pumilio homolog 5 OS=Arabidopsis thaliana GN=APUM5 PE=1 SV=2
AT3G47070	Q9SD66	-0,38	0,006	Plastid	Putative uncharacterized protein OS=Arabidopsis thaliana GN=F13I12.120 PE=1 SV=1
AT1G09340	Q9SA52	-0,308	0,027	Plastid	Chloroplast stem-loop binding protein of 41 kDa b, chloroplastic OS=Arabidopsis thaliana GN=CSP41B PE=1 SV=1

Table S4: List of differentially expressed proteins (DEPs) identified in the comparative proteomic study between leaves of WT (Ws-2) and *pgi1-2gpt2-1* plants cultured in the presence of small fungal VCs with a "confident" statistical significance level (*pgi1-2gpt2-1* vs. Ws-2). DEPs are classified according to their functions. DEPs that are discussed in the main text are highlighted in orange.

Accesión number	Protein ID	Fold change (log2)	qValue (FDR)	Subcellular location	Description
Amino acid metabolism					
AT3G45300	Q9SWG0	0,856	0,009	Mitochondrion	Isovaleryl-CoA dehydrogenase, mitochondrial OS=Arabidopsis thaliana GN=IVD PE=1 SV=2
AT4G33150	Q9SMZ4	0,737	0,034	Cytosol	Alpha-aminoadipic semialdehyde synthase OS=Arabidopsis thaliana GN=LKR/SDH PE=1 SV=1
AT3G47340	P49078	0,647	0,013	Cytosol	Asparagine synthetase [glutamine-hydrolyzing] 1 OS=Arabidopsis thaliana GN=ASN1 PE=2 SV=2
AT1G03090	Q42523	0,5	0,004	Mitochondrion	Methylcrotonoyl-CoA carboxylase subunit alpha, mitochondrial OS=Arabidopsis thaliana GN=MCCA PE=1 SV=2
AT5G48880	Q570C8	0,405	0,037	Peroxisome	3-ketoacyl-CoA thiolase 5, peroxisomal OS=Arabidopsis thaliana GN=KAT5 PE=2 SV=2
AT2G14170	Q0WM29	0,354	0,031	Mitochondrion	Methylmalonate-semialdehyde dehydrogenase [acylating], mitochondrial OS=Arabidopsis thaliana GN=ALDH6B2 PE=2 SV=2
Cell wall					
AT5G49360	Q9FGY1	0,625	0,002	Extracellular	Beta-D-xylosidase 1 OS=Arabidopsis thaliana GN=BXL1 PE=1 SV=1
Co-factor and vitamine metabolism					
AT2G38230	O80448	0,322	0,032	Cytosol	Pyridoxal 5'-phosphate synthase subunit PDX1.1 OS=Arabidopsis thaliana GN=PDX11 PE=1 SV=1
C1-metabolism					
AT4G37930	Q9SZJ5	-0,288	0,012	Mitochondrion	Serine hydroxymethyltransferase 1, mitochondrial OS=Arabidopsis thaliana GN=SHM1 PE=1 SV=1
Fermentation					
AT1G54100	Q9SYG7	0,369	0,013	Cytosol	Aldehyde dehydrogenase family 7 member B4 OS=Arabidopsis thaliana GN=ALDH7B4 PE=2 SV=3
Glycolysis					
AT3G22960	Q9LIK0	0,34	0,012	Plastid	Plastidial pyruvate kinase 1, chloroplastic OS=Arabidopsis thaliana GN=PKP1 PE=1 SV=1
AT4G24620	Q8H103	-1,056	0,003	Plastid	Glucose-6-phosphate isomerase 1, chloroplastic OS=Arabidopsis thaliana GN=PGI1 PE=1 SV=1
Glyoxylate cycle					
AT4G15530	O23404	0,565	0,012	Plastid	Pyruvate, phosphate dikinase 1, chloroplastic OS=Arabidopsis thaliana GN=PPDK PE=1 SV=2
Hormone metabolism					
AT3G63210	Q8LGS1	1,362	0,031	Mitochondrion	reversed Protein MARD1 OS=Arabidopsis thaliana GN=MARD1 PE=2 SV=2
AT3G44300	P32962	0,727	0,003	Cytosol	NIT2 Nitrilase 2 OS=Arabidopsis thaliana GN=NIT2 PE=1 SV=1
AT5G48180	Q93XW5	0,467	0,038	Cytosol	nsp5 Nitrile-specifier protein 5 OS=Arabidopsis thaliana GN=NSP5 PE=2 SV=1
Major CHO metabolism					
AT1G32900	Q9MAQ0	-0,895	0,004	Plastid	GBSS Granule-bound starch synthase 1, chloroplastic/amyloplastic OS=Arabidopsis thaliana GN=GBSS1 PE=1 SV=1
AT1G69830	Q94A41	-0,918	0,007	Plastid	AMY3 Alpha-amylase 3, chloroplastic OS=Arabidopsis thaliana GN=AMY3 PE=2 SV=1

Accesión number	Protein ID	Fold change (log2)	qValue (FDR)	Subcellular location	Description
Metal handling					
AT3G56240	A0A19LNC0	-0,311	0,046	Peroxisome	Copper chaperone OS=Arabidopsis thaliana GN=CCH PE=4 SV=1
Minor CHO metabolism					
AT5G57655	Q9FKK7	0,47	0,002	ER	Xylose isomerase OS=Arabidopsis thaliana GN=XYLA PE=2 SV=2
AT5G20250	Q8RX87	0,442	0,008	Plastid	Probable galactinol--sucrose galactosyltransferase 6 OS=Arabidopsis thaliana GN=RFS6 PE=2 SV=2
Miscellaneous enzyme family					
AT5G56870	Q9SCV8	0,65	0,002	Extracellular	Beta-galactosidase 4 OS=Arabidopsis thaliana GN=BGAL4 PE=1 SV=1
AT1G30720	Q9SA87	0,465	0,049	Extracellular	Berberine bridge enzyme-like 10 OS=Arabidopsis thaliana GN=At1g30720 PE=2 SV=1
AT3G16530	Q9LK72	-0,313	0,043	Extracellular	Lectin-like protein At3g16530 OS=Arabidopsis thaliana GN=At3g16530 PE=1 SV=1
N-metabolism					
AT5G07440	Q38946	0,549	0,004	Mitochondrion	gdh2 Glutamate dehydrogenase 2 OS=Arabidopsis thaliana GN=GDH2 PE=1 SV=1
AT5G35630	Q43127	-0,282	0,013	Plastid	Glutamine synthetase, chloroplastic/mitochondrial OS=Arabidopsis thaliana GN=GLN2 PE=1 SV=1
OPPP					
AT1G12230	F4IC59	0,313	0,037	Plastid	Transaldolase-like protein OS=Arabidopsis thaliana GN=At1g12230 PE=4 SV=1
Photosynthesis					
ATCG00540	P56771	-0,242	0,05	Plastid	Cytochrome f OS=Arabidopsis thaliana GN=petA PE=3 SV=1
AT1G20020	Q8W493	-0,262	0,036	Plastid	Ferredoxin--NADP reductase, leaf isozyme 2, chloroplastic OS=Arabidopsis thaliana GN=LFNR2 PE=1 SV=1
AT5G66190	Q9FKW6	-0,269	0,031	Plastid	Ferredoxin--NADP reductase, leaf isozyme 1, chloroplastic OS=Arabidopsis thaliana GN=LFNR1 PE=1 SV=1
AT4G02770	Q9S7H1;Q9S	-0,29	0,028	Plastid	Photosystem I reaction center subunit II-1, chloroplastic OS=Arabidopsis thaliana GN=psaD1 PE=1 SV=1
ATCG00680	P83755	-0,307	0,035	Plastid	Photosystem II protein D1 OS=Arabidopsis thaliana GN=psbA PE=1 SV=2
AT1G61520	Q9SY97	-0,31	0,032	Plastid	Photosystem I chlorophyll a/b-binding protein 3-1, chloroplastic OS=Arabidopsis thaliana GN=LHCA3 PE=1 SV=1
AT5G64040	P49107	-0,313	0,05	Plastid	PSAN Photosystem I reaction center subunit N, chloroplastic OS=Arabidopsis thaliana GN=PSAN PE=1 SV=2
AT3G08940	Q9XF88	-0,321	0,043	Plastid	lhcb4 Chlorophyll a-b binding protein CP29.2, chloroplastic OS=Arabidopsis thaliana GN=LHCB4.2 PE=1 SV=1
AT4G32260	Q42139	-0,325	0,011	Plastid	AT4g32260/F10M6_100 OS=Arabidopsis thaliana GN=F10M6.100 PE=1 SV=2
AT1G03600	Q9LR64	-0,352	0,032	Plastid	Photosystem II repair protein PSB27-H1, chloroplastic OS=Arabidopsis thaliana GN=PSB27-1 PE=1 SV=1
AT3G54890	Q01667	-0,356	0,041	Plastid	Chlorophyll a-b binding protein 6, chloroplastic OS=Arabidopsis thaliana GN=LHCA1 PE=1 SV=1
ATCG00020	P56777	-0,36	0,035	Plastid	Photosystem II CP47 reaction center protein OS=Arabidopsis thaliana GN=psbB PE=1 SV=1
ATCG00270	P56761	-0,361	0,005	Plastid	Photosystem II D2 protein OS=Arabidopsis thaliana GN=psbD PE=1 SV=3
AT3G50820	Q95841	-0,361	0,008	Plastid	Oxygen-evolving enhancer protein 1-2, chloroplastic OS=Arabidopsis thaliana GN=PSBO2 PE=1 SV=1
AT3G12780	Q9LD57	-0,367	0,002	Plastid	Phosphoglycerate kinase 1, chloroplastic OS=Arabidopsis thaliana GN=PGK1 PE=1 SV=1
AT5G38410	B3H552	-0,38	0,013	Plastid	Ribulose bisphosphate carboxylase small chain OS=Arabidopsis thaliana GN=At5g38410 PE=3 SV=1
AT3G61470	Q9SYW8	-0,39	0,031	Plastid	Photosystem I chlorophyll a/b-binding protein 2, chloroplastic OS=Arabidopsis thaliana GN=LHCA2 PE=1 SV=1
AT5G38430	P10796	-0,402	0,05	Plastid	Ribulose bisphosphate carboxylase small chain 1B, chloroplastic OS=Arabidopsis thaliana GN=RBCS-1B PE=1 SV=1
ATCG00580	P56779	-0,404	0,048	Plastid	Cytochrome b559 subunit alpha OS=Arabidopsis thaliana GN=psbE PE=1 SV=4
AT1G06680	Q42029	-0,414	0,004	Plastid	Oxygen-evolving enhancer protein 2-1, chloroplastic OS=Arabidopsis thaliana GN=PSBP1 PE=1 SV=2
AT1G56190	P50318;Q9LI	-0,424	0,002	Plastid	Phosphoglycerate kinase 2, chloroplastic OS=Arabidopsis thaliana GN=At1g56190/PGK2 PE=1 SV=3
AT4G21280	Q9XFT3-2	-0,424	0,005	Plastid	Isoform 2 of Oxygen-evolving enhancer protein 3-1, chloroplastic OS=Arabidopsis thaliana GN=PSBQ1
ATCG00280	P56778	-0,43	0,002	Plastid	Photosystem II CP43 reaction center protein OS=Arabidopsis thaliana GN=psbC PE=1 SV=3
AT4G03280	Q9ZR03	-0,436	0,006	Plastid	Cytochrome b6-f complex iron-sulfur subunit, chloroplastic OS=Arabidopsis thaliana GN=petC PE=1 SV=1
ATCG66570	P23321;Q9S	-0,471	0,001	Plastid	Oxygen-evolving enhancer protein 1-1, chloroplastic OS=Arabidopsis thaliana GN=PSBO1 PE=1 SV=2
AT4G05180	Q41932	-0,515	0,002	Plastid	Oxygen-evolving enhancer protein 3-2, chloroplastic OS=Arabidopsis thaliana GN=PSBQ2 PE=1 SV=2
AT3G01500	A0A19LQB3,	-0,531	0,002	Plastid	Carbonic anhydrase 1 OS=Arabidopsis thaliana GN=CA1 PE=4 SV=1
AT1G79040	P27202	-0,556	0,004	Plastid	Photosystem II 10 kDa polypeptide, chloroplastic OS=Arabidopsis thaliana GN=PSBR PE=1 SV=1
AT3G62410	Q9LZP9	-0,625	0,048	plastid	Calvin cycle protein CP12-2, chloroplastic OS=Arabidopsis thaliana GN=CP12-2 PE=1 SV=1

Accesión number	Protein ID	Fold change (log2)	qValue (FDR)	Subcellular location	Description
Protein					
AT5G43010	Q9SEI3	-0,952	0,036	Cytosol	26S protease regulatory subunit 10B homolog A OS=Arabidopsis thaliana GN=RPT4A PE=1 SV=1
AT5G37680	Q8W4C8	-2,022	0,007	Plasma membrane	reversed ADP-ribosylation factor-like protein 8c OS=Arabidopsis thaliana GN=ARL8C PE=2 SV=1
AT5G22610	Q9FNK0	-2,2	0,004	Cytosol	reversed Putative F-box/FBD/LRR-repeat protein At5g22610 OS=Arabidopsis thaliana GN=At5g22610 PE=4 SV=1
Redox regulation					
AT1G20620	Q42547	0,272	0,035	Peroxisome	CAT3 Catalase-3 OS=Arabidopsis thaliana GN=CAT3 PE=1 SV=3
AT4G21860	Q9C5C8-2	-1,981	0,012	Plastid	reversed Isoform 2 of Peptide methionine sulfoxide reductase B2, chloroplastic OS=Arabidopsis thaliana GN=MSRB2
RNA					
AT3G04500	Q9VM837	1,966	0,013	Nucleus	Putative RRM-containing protein OS=Arabidopsis thaliana GN=At3g04500 PE=2 SV=1
AT5G26742	Q8L758	0,375	0,003	Plastid	DEAD-box ATP-dependent RNA helicase 3, chloroplastic OS=Arabidopsis thaliana GN=RH3 PE=1 SV=2
AT3G63140	Q9LYA9	-0,289	0,012	Plastid	Chloroplast stem-loop binding protein of 41 kDa a, chloroplastic OS=Arabidopsis thaliana GN=CSP41A PE=1 SV=1
Secondary metabolism					
AT5G26000	P37702	-0,706	0,006	Peroxisome	Myrosinase 1 OS=Arabidopsis thaliana GN=TGG1 PE=1 SV=1
AT5G23020	Q9FN52	-0,746	0,003	Plastid	Methylthioalkylmalate synthase 3, chloroplastic OS=Arabidopsis thaliana GN=MAM3 PE=1 SV=1
Signalling					
AT1G62480	Q9SXE9	0,549	0,048	Cytosol	At1g62480/T3P18_4 OS=Arabidopsis thaliana GN=At1g62480 PE=1 SV=1
Stress					
AT5G37380	Q9FHS7	4,764	0,001	Nucleus	AT5g37380/MNJ8_170 OS=Arabidopsis thaliana GN=At5g37380 PE=2 SV=1
AT4G23680	Q9SUQ9;Q9Z	-0,768	0,05	Cytosol	AT4g23680/F9D16_150 OS=Arabidopsis thaliana GN=F9D16.150 PE=2 SV=1
Tetrapyrrole synthesis					
AT4G27440	P21218	-0,278	0,05	Plastid	PORB Protochlorophyllide reductase B, chloroplastic OS=Arabidopsis thaliana GN=PORB PE=1 SV=3
Transport					
AT1G15990	Q9SN75	-2,508	0,002	Plasma membrane	reversed Putative cyclic nucleotide-gated ion channel 7 OS=Arabidopsis thaliana GN=CNGC7 PE=3 SV=1
not assigned					
AT4G09660	Q9SZ82	1,487	0,035	Nucleus	Putative uncharacterized protein AT4g09660 OS=Arabidopsis thaliana GN=F17A8.10 PE=4 SV=1
AT1G18270	F4IAP5	0,357	0,037	Cytosol	Ketose-bisphosphate aldolase class-II family protein OS=Arabidopsis thaliana GN=At1g18270 PE=4 SV=1
AT1G09340	Q9SAS2	-0,325	0,007	Plastid	Chloroplast stem-loop binding protein of 41 kDa b, chloroplastic OS=Arabidopsis thaliana GN=CSP41B PE=1 SV=1
AT5G11420	Q9LYE7	-0,385	0,024	Extracellular	Putative uncharacterized protein At5g11420 OS=Arabidopsis thaliana GN=F15N18_10 PE=1 SV=1
AT1G21500	Q9LPK9	-0,398	0,035	Plastid	F24J8.11 protein OS=Arabidopsis thaliana GN=F24J8.11 PE=2 SV=1
AT1G49750	Q9FXA1	-0,46	0,011	Extracellular	AT1G49750 protein OS=Arabidopsis thaliana GN=F14J22.4 PE=2 SV=1
AT3G47070	Q9SD66	-0,472	0,003	Plastid	Putative uncharacterized protein OS=Arabidopsis thaliana GN=F13I12.120 PE=1 SV=1
AT3G20250	Q9LJX4	-1,242	0,003	Nucleus	Pumilio homolog 5 OS=Arabidopsis thaliana GN=APUM5 PE=1 SV=2

Table S5: List of differentially expressed proteins (DEPs) identified in the comparative proteomic study between leaves of WT (Ws-2) and *pgi1-2gpt2-1* plants cultured in the absence of small fungal VCs with a "confident" statistical significance level (*pgi1-2gpt2-1* vs. Ws-2). DEPs are classified according to their functions. DEPs that are discussed in the main text are highlighted in orange. DEPs identified in the comparative proteomic study between leaves of small VC-exposed *pgi1-2gpt2-2* and Ws-2 plants (cf. Table S6) are highlighted in yellow.

Accesión number	Protein ID	Fold change (log2)	qValue (FDR)	Subcellular localization	Description
Glycolysis					
AT4G24620	Q8H103	-1,215	0,012	plastid	Glucose-6-phosphate isomerase 1, chloroplastic OS=Arabidopsis thaliana GN=PGI1 PE=1 SV=1
Gluconeogenesis					
AT4G15530	O23404	0,383	0,009	plastid	Pyruvate, phosphate dikinase 1, chloroplastic OS=Arabidopsis thaliana GN=PPDK PE=1 SV=2
Hormone metabolism					
AT3G44300	P32962	0,545	0,014	cytosol	Nitrilase 2 OS=Arabidopsis thaliana GN=NIT2 PE=1 SV=1
AT4G19170	O49675	-0,346	0,049	plastid	Probable carotenoid cleavage dioxygenase 4, chloroplastic OS=Arabidopsis thaliana GN=CCD4/NCED4 PE=1 SV=1
Major CHO metabolism					
AT1G32900	Q9MAQ0	-0,354	0,048	plastid	Granule-bound starch synthase 1, chloroplastic/amyloplastic OS=Arabidopsis thaliana GN=GBSS1 PE=1 SV=1
AT1G69830	Q94A41	-0,423	0,022	plastid	Alpha-amylase 3, chloroplastic OS=Arabidopsis thaliana GN=AMY3 PE=2 SV=1
Miscellaneous enzyme family					
AT5G20230	Q07488	0,045	1,8	plasma membrane	Blue copper protein OS=Arabidopsis thaliana GN=BCB PE=1 SV=2
AT1G02930	P42760;Q9SRY5	0,479	0,007	cytosol	Glutathione S-transferase F6 OS=Arabidopsis thaliana GN=GSTF6 PE=2 SV=2
AT1G02920	Q9SRY5	0,438	0,025	cytosol	Glutathione S-transferase F7 OS=Arabidopsis thaliana GN=GSTF7 PE=2 SV=3
Mitochondrial electron transport					
AT1G22450	Q9S7L9	0,358	0,048	mitochondrion	Cytochrome c oxidase subunit 6b-1 OS=Arabidopsis thaliana GN=COX6B-1 PE=1 SV=1
N-metabolism					
AT5G07440	Q38946	0,419	0,009	mitochondrion	Glutamate dehydrogenase 2 OS=Arabidopsis thaliana GN=GDH2 PE=1 SV=1
Photosynthesis					
AT1G56190	P50318;Q9LD57	-0,285	0,045	plastid	Phosphoglycerate kinase 2, chloroplastic OS=Arabidopsis thaliana GN=At1g56190/PGK2 PE=1 SV=3
AT3G47470	P27521	-0,295	0,044	plastid	Chlorophyll a-b binding protein 4, chloroplastic OS=Arabidopsis thaliana GN=LHCA4 PE=1 SV=1
ATCG00350	P56766	-0,305	0,049	plastid	Photosystem I P700 chlorophyll a apoprotein A1 OS=Arabidopsis thaliana GN=psaA PE=2 SV=1
AT1G61520	Q9SY97	-0,317	0,042	plastid	Photosystem I chlorophyll a/b-binding protein 3-1, chloroplastic OS=Arabidopsis thaliana GN=LHCA3 PE=1 SV=1
AT4G03280	Q9ZR03	-0,322	0,049	plastid	Cytochrome b6-f complex iron-sulfur subunit, chloroplastic OS=Arabidopsis thaliana GN=petC PE=1 SV=1
AT4G12800	Q9SUI4	-0,326	0,043	plastid	Photosystem I reaction center subunit XI, chloroplastic OS=Arabidopsis thaliana GN=PSAL PE=1 SV=2
AT3G61470	Q9SYW8	-0,327	0,045	plastid	Photosystem I chlorophyll a/b-binding protein 2, chloroplastic OS=Arabidopsis thaliana GN=LHCA2 PE=1 SV=1
AT1G03600	Q9LR64	-0,339	0,041	plastid	Photosystem II repair protein PSB27-H1, chloroplastic OS=Arabidopsis thaliana GN=PSB27-1 PE=1 SV=1
AT4G10340	Q9XF89	-0,34	0,014	plastid	Chlorophyll a-b binding protein CP26, chloroplastic OS=Arabidopsis thaliana GN=LHCB5 PE=1 SV=1
ATCG00680	P56777	-0,348	0,013	plastid	Photosystem II CP47 reaction center protein OS=Arabidopsis thaliana GN=psbB PE=1 SV=1
AT3G50820	Q9S841	-0,35	0,019	plastid	Oxygen-evolving enhancer protein 1-2, chloroplastic OS=Arabidopsis thaliana GN=PSBO2 PE=1 SV=1
AT3G01500	A0A1I9LQB3;P27140-3	-0,353	0,023	plastid	Carbonic anhydrase 1 OS=Arabidopsis thaliana GN=CA1 PE=4 SV=1

Accesión number	Protein ID	Fold change (log2)	qValue (FDR)	Subcellular localization	Description
AT1G31330	Q9SHE8	-0,354	0,024	plastid	Photosystem I reaction center subunit III, chloroplastic OS=Arabidopsis thaliana GN=PSAF PE=1 SV=1
AT2G05070	Q9S7I7;Q9XF87	-0,355	0,044	plastid	Chlorophyll a-b binding protein 2.2, chloroplastic OS=Arabidopsis thaliana GN=LHCB2.2 PE=1 SV=1
AT4G02770	Q9S7H1;Q9SA56	-0,366	0,009	plastid	Photosystem I reaction center subunit II-1, chloroplastic OS=Arabidopsis thaliana GN=psaD1 PE=1 SV=1
AT3G54890	Q01667	-0,367	0,042	plastid	Chlorophyll a-b binding protein 6, chloroplastic OS=Arabidopsis thaliana GN=LHCA1 PE=1 SV=1
ATCG00280	P56778	-0,368	0,008	plastid	Photosystem II CP43 reaction center protein OS=Arabidopsis thaliana GN=psbC PE=1 SV=3
ATCG00020	P83755	-0,369	0,022	plastid	Photosystem II protein D1 OS=Arabidopsis thaliana GN=psbA PE=1 SV=2
AT5G64040	P49107	-0,385	0,02	plastid	Photosystem I reaction center subunit N, chloroplastic OS=Arabidopsis thaliana GN=PSAN PE=1 SV=2
ATCG00270	P56761	-0,401	0,008	plastid	Photosystem II D2 protein OS=Arabidopsis thaliana GN=psbD PE=1 SV=3
AT4G21280	Q9XFT3-2	-0,407	0,017	plastid	Isoform 2 of Oxygen-evolving enhancer protein 3-1, chloroplastic OS=Arabidopsis thaliana GN=PSBQ1
AT5G66570	P23321;Q9S841	-0,408	0,009	plastid	Oxygen-evolving enhancer protein 1-1, chloroplastic OS=Arabidopsis thaliana GN=PSBO1 PE=1 SV=2
AT1G06680	Q42029	-0,432	0,009	plastid	Oxygen-evolving enhancer protein 2-1, chloroplastic OS=Arabidopsis thaliana GN=PSBP1 PE=1 SV=2
ATCG00580	P56779	-0,432	0,035	plastid	Cytochrome b559 subunit alpha OS=Arabidopsis thaliana GN=psbE PE=1 SV=4
AT3G08940	Q9XF88	-0,443	0,01	plastid	Chlorophyll a-b binding protein CP29.2, chloroplastic OS=Arabidopsis thaliana GN=LHCB4.2 PE=1 SV=1
AT2G20260	Q9S714;Q9S831	-0,459	0,044	plastid	Photosystem I reaction center subunit IV B, chloroplastic OS=Arabidopsis thaliana GN=PSAE2 PE=2 SV=1
AT1G79040	P27202	-0,542	0,006	plastid	Photosystem II 10 kDa polypeptide, chloroplastic OS=Arabidopsis thaliana GN=PSBR PE=1 SV=1
AT4G05180	Q41932	-0,646	0,035	plastid	Oxygen-evolving enhancer protein 3-2, chloroplastic OS=Arabidopsis thaliana GN=PSBQ2 PE=1 SV=2
Redox regulation					
AT4G21860	Q9C5C8-2	-0,904	0,049	plastid	reversed Isoform 2 of Peptide methionine sulfoxide reductase B2, chloroplastic OS=Arabidopsis thaliana GN=MSRB2
RNA					
AT5G52470	Q9FEF8	0,368	0,049	nucleus	Probable mediator of RNA polymerase II transcription subunit 36b OS=Arabidopsis thaliana GN=MED36B PE=1 SV=1
Secondary metabolism					
AT5G26000	P37702	-0,349	0,012	peroxisome	Myrosinase 1 OS=Arabidopsis thaliana GN=TGG1 PE=1 SV=1
Signalling					
AT1G48630	Q9C426;Q9LV28	0,523	0,012	cytosol	Receptor for activated C kinase 1B OS=Arabidopsis thaliana GN=RACK1B PE=1 SV=1
Stress					
AT5G37380	Q9FHS7	4,748	0,07	nucleus	AT5g37380/MNI8_170 OS=Arabidopsis thaliana GN=At5g37380 PE=2 SV=1
AT1G73260	Q8RXD5	0,482	0,035	extracellular	Kunitz trypsin inhibitor 1 OS=Arabidopsis thaliana GN=KTI1 PE=2 SV=1
AT1G24020	Q93VR4	0,592	0,009	golgi	MLP-like protein 423 OS=Arabidopsis thaliana GN=MLP423 PE=2 SV=1
Transport					
AT1G72150	Q56WK6	-0,33	0,02	plasma membrane	Patellin-1 OS=Arabidopsis thaliana GN=PATL1 PE=1 SV=2
Not assigned					
AT2G45070	P38389	1,082	0,048	endoplasmic reticulum	Protein transport protein Sec61 subunit beta OS=Arabidopsis thaliana GN=At2g45070 PE=1 SV=1
AT1G30720	Q9SA87	0,654	0,008	extracellular	Berberine bridge enzyme-like 10 OS=Arabidopsis thaliana GN=At1g30720 PE=2 SV=1
AT3G53460	Q43349	0,483	0,013	plastid	29 kDa ribonucleoprotein, chloroplastic OS=Arabidopsis thaliana GN=CP29A PE=2 SV=2
AT5G48480	Q9LV66	0,418	0,015	cytosol	Uncharacterized protein At5g48480 OS=Arabidopsis thaliana GN=At5g48480 PE=1 SV=1
AT3G47070	Q9SD66	-0,403	0,007	plastid	Putative uncharacterized protein OS=Arabidopsis thaliana GN=F13I12.120 PE=1 SV=1
AT2G05380	Q92SI6	-0,636	0,023	extracellular	Glycine-rich protein 3 short isoform OS=Arabidopsis thaliana GN=GRP3S PE=1 SV=2
AT5G22610	Q9FNK0	-1,535	0,015	cytosol	reversed Putative F-box/FBD/LRR-repeat protein At5g22610 OS=Arabidopsis thaliana GN=At5g22610 PE=4 SV=1

Table S6: Primers used for PCR amplification of *PGI1* and *GPT2* cDNAs, *GUS* and the *Athspr* and *GPT2* promoters. Primer sequences for attB sites (see **Supplemental Figure 5**) are indicated in bold.

Primer	Sequence
PGI1	
attB1 *PGI1*	5'-**ggggacaagtttgtacaaaaaagcaggctta**atggcctctctctcaggc -3'
attB2 *PGI1*	5'-**ggggaccactttgtacaagaaagctgggta**ttatgcgtacaggtcatccac-3'
GPT2	
attB1 *GPT2*	5'**ggggacaagtttgtacaaaaaagcaggctta**atgctttcttcaatcaaaccatc-3'
attB2 *GPT2*	5'-**ggggaccactttgtacaagaaagctgggta**tcactgcttcgcctgtgag-3'
promAthspr	
attB4 *ATHSPR* promoter	5'-**ggggacaactttgtatagaaaagttgct**cgctctttgagttctgtagttc-3'
attB1 *ATHSPR* promoter	5'-**ggggactgcttttttgtacaaacttgc**cacaaaaccacccaccttaaatc-3'
promGPT2	
attB4 *GPT2* promoter	5'-**ggggacaactttgtatagaaaagttgct**gccattactttggaaaaggtcc-3'
attB1 *GPT2* promoter	5'-**ggggactgcttttttgtacaaacttgc**gtgctttttatggctaattgatg-3'
GUS	
attB1 *GUS*	5'-**ggggacaagtttgtacaaaaaagcaggctta**atgttacgtcctgtagaaaccc-3'
attB2 *GUS*	5'-**ggggaccactttgtacaagaaagctgggta**tcattgtttgcctccctgctg-3'

Table S7: Primers used in qRT-PCR.

Gene		Sequence
EF-1 alfa	Forward	TTCGTCTCCCACTTCAGGAT
At1g07940	Reverse	GGAGCAAAGGTCACAACCAT
GPT2	Forward	TTAGACCAGATTTCGCCGTTA
At1g61800	Reverse	GTTGAATCGGGGTATGGAAA
GUS	Forward	GTAATTATGCGGGCAACGTC
	Reverse	TAATGAGTGACCGCATCGAA

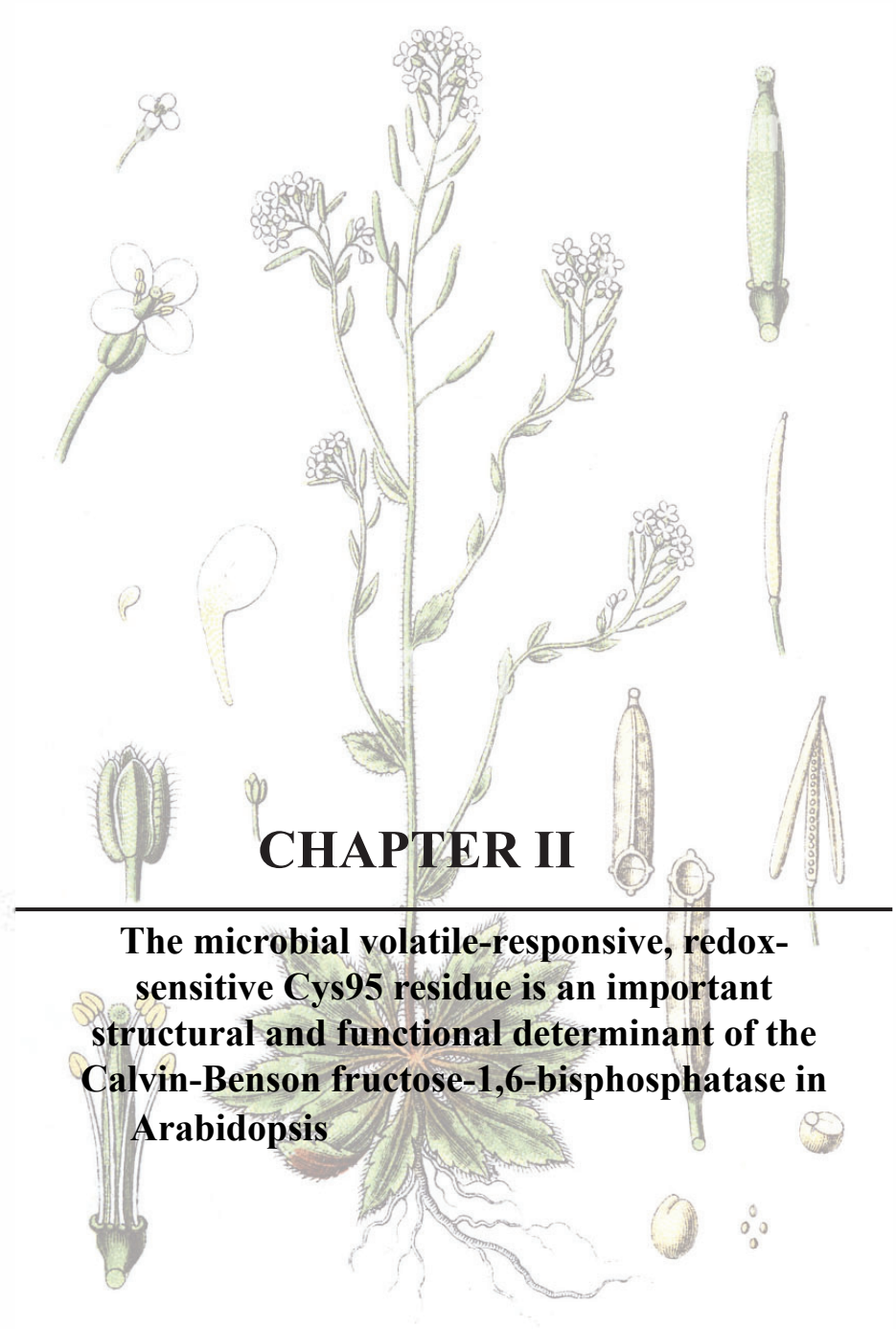

CHAPTER II

The microbial volatile-responsive, redox-sensitive Cys95 residue is an important structural and functional determinant of the Calvin-Benson fructose-1,6-bisphosphatase in Arabidopsis

INTRODUCTION

Microorganisms can emit complex mixtures of volatile compounds (VCs) of less than 300 Da that promote plant growth and photosynthesis as well as drastic changes in the hormonome, transcriptome, proteome and metabolome (Ryu et al., 2003; Zhang et al., 2009; Bitas et al., 2015; Sánchez-López et al., 2016a,b; Cordovez et al., 2017; Li et al., 2018b; Ameztoy et al., 2021; Gámez-Arcas et al., 2022b). Although growth and developmental changes promoted by microbial VCs have frequently been associated with organic VCs with molecular masses ranging between ca. 45 Da and 300 Da, recent studies showed that microbial VCs of less than 45 Da (hereafter designated as "small VCs") are major determinants of plant responses to microbial volatile emissions (García-Gómez et al., 2019; Gámez-Arcas et al., 2022a). Some of these small VCs (e.g. nitric oxide, nitrogen dioxide, nitrous oxide, carbon monoxide, hydrogen sulfide, ethylene and methanol) play important roles in plant-microbe interactions, are very reactive with proteins and/or act as signaling molecules that promote photosynthesis, growth and developmental changes when exogenously applied in a discrete form and/or in low concentrations (Gámez-Arcas et al., 2022a). However, their mechanisms of action from perception to the processes that enhance photosynthesis and growth are still poorly understood.

Reversible reduction-oxidation (redox) thiol modifications of Cys residues of proteins provide fundamental post-translational "switches" that play important roles in the regulatory mechanisms of metabolism, growth and development that allow plants to adjust to continuously changing environmental constraints (Couturier et al., 2013). Therefore, identification of reactive cysteine residues is crucial not only for understanding protein functions but also for obtaining insights into the mechanisms involved in plants´ responses to environmental changes. Recent OxiTRAQ-based quantitative and site-specific redox-proteomic analyses revealed that small microbial VCs induced global thiol redox proteome changes (Ameztoy et al., 2019). These changes included the reduction of highly conserved Cys residues in proteins involved in photochemical reactions and Calvin-Benson cycle (CBC) enzymes including phosphoribulokinase, sedoheptulose-1,7-bisphosphatase and one of the two isoforms of plastid-localized fructose-1,6-bisphosphatase (cFBP1) (Ameztoy et al., 2019). The same studies showed that NADPH-dependent thioredoxin (Trx) reductase C (NTRC), an especial type of Trx that participates in the regulation of the redox status and activity

of photosynthesis-related enzymes, is an important mediator of plant responses to microbial VCs (Ameztoy et al., 2019). It thus appears that the response of plants to microbial VCs is due, at least partly, to redox switching mechanisms that involve rapid thiol redox activation of the photosynthetic machinery. In support of this hypothesis, we recently showed that small microbial VCs did not stimulate growth and did not promote metabolic and proteomic changes in cFBP1-lacking *cfbp1* plants (Ameztoy et al., 2021).

cFBP1 is a homotetrameric metal (Mg^{2+})-requiring enzyme of the CBC that catalyses the hydrolytic breakdown of fructose-1-6-bisphosphate (FBP) to fructose-6-phosphate and Pi (Villeret et al., 1995; Jacquot et al., 1995; Chiadmi et al., 1999; Serrato et al., 2009). Unlike other CBC enzymes which are close to limiting carbon fixation through the CBC (Harrison et al., 1998; Henkes et al., 2001), cFBP1 is considered an "excess" enzyme of the CBC (Kossmann et al., 1994). In Arabidopsis, the total absence of cFBP1 causes dwarfism and reduced photosynthetic activity (Rojas-González et al., 2015). cFBP1 is regulated by light through mechanisms involving reduction of disulfide groups of Cys residues via the ferredoxin (Fdx)/Trx and NTRC systems (Thormählen et al., 2015; Yoshida et al., 2015; Nikkanen et al., 2016; Pérez-Ruiz et al., 2017). In addition, cFBP1 can be inactivated by S-nitrosylation of Cys residues subjected to Fdx/Trx redox modifications (Serrato et al., 2018). In the ca. 40 kDa constituent monomer of the Arabidopsis mature cFBP1, the residues which define the binding domain of the catalytic cofactor Mg^{2+} are Glu108, Asp129 and Asp132 (**Supplemental Figure S1**), as deduced from crystallographic and site-directed mutagenesis studies of pig fructose-1,6-bisphosphatase (FBPase) (Chen et al., 1993; Nelson et al., 2004) and plant cFBP1 (Villeret et al., 1995; Chiadmi et al., 1999). From the same studies, it can be inferred that the residues which define the active FBP binding site of Arabidopsis mature cFBP1 monomer are Asp132, Gly133, Asn238, Arg269, Tyr270, Tyr290, Lys300 and Arg302. The active sites are located in the FBP domain near the interface between two monomers (**Supplemental Figure S1**). Plant cFBP1 monomers contain seven highly conserved Cys residues, which in Arabidopsis are located at positions 52, 95, 156, 174, 179, 191, 307 (**Supplemental Figure S1**) (Villeret et al., 1995; Rodríguez-Suárez et al., 1997). Most of these residues are not present in the cytosolic isoform of plant FBPase (CyFBP) (**Supplemental Figure S1**), which would indicate that Cys residues in cFBP1 play important roles in regulation of FBPase activity in the chloroplastic compartment. Data obtained from studies using

site-directed mutated variants of rapeseed (*Brassica napus*) cFBP1 provided evidence that (i) none of these Cys residues are important determinants of the catalytic activity of the enzyme and (ii) Cys52 (Cys53 in rapeseed) and Cys191 are important for cFBP1 stability (Rodríguez-Suárez et al., 1997). Furthermore, studies using site-directed mutated pea and rapeseed cFBP1 variants showed that residues Cys156 (Cys157 in rapeseed), Cys174 and Cys179 mediate the redox regulation of cFBP1 by the Fdx/Trx system (Jacquot et al., 1997; Rodríguez-Suárez et al., 1997; Serrato et al., 2018). Given that mutation at Cys95 (Cys96 in rapeseed) neither destabilizes nor affects the reductive modulation of cFBP1 (Rodríguez-Suárez et al., 1997), its function and the reasons for its absolute conservation throughout plant evolution still remain unknown.

We recently showed that small fungal VCs promote the reduction of Cys95 of cFBP1 in Arabidopsis (Ameztoy et al., 2019). Although this residue is not located in the proposed regulatory Trx redox or catalytic domains of cFBP1 inferred from the rapeseed and pea cFBP1 studies, we still hypothesized that the redox state of Cys95 of cFBP1 could play roles in the structural and functional properties of cFBP1 (Ameztoy et al., 2019). To test this hypothesis, in this work we produced in *Escherichia coli* mature wild type (WT) cFBP1 and a mutated form of cFBP1 (C95S) in which the Cys95 residue has been replaced by serine, and compared their structural and functional properties. We also produced and characterized cFBP1-lacking *cfbp1* plants ectopically expressing the WT and the C95S forms of cFBP1. Results presented in this work provide strong evidence that the Cys95 residue of cFBP1 is an important determinant of cFBP1 and photosynthetic activities in Arabidopsis.

RESULTS

Mutation of the Cys95 residue alters the structure of cFBP1

To investigate the possible dependence of cFBP1 structure on Cys95, we assayed mobilities in SDS-PAGE of recombinant mature WT and C95S cFBP1 forms in the presence or absence of different concentrations (0, 5, 10 and 100 mM) of the reducing agent DTT. Western blot analyses revealed that, in the absence of DTT, the monomeric WT and C95S forms of cFBP1 were fully oxidized and present as two polypeptide species (ox1 and ox2 in **Figure 1**). In addition, the C95S cFBP1 preparations presented an additional oxidized polypeptide species (ox3 in **Figure 1**). With 10 mM DTT, most C95S cFBP1 was present in oxidized state, whereas nearly half of the WT was present

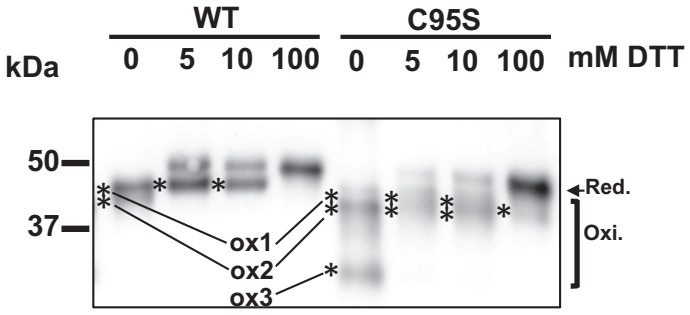

Figure 1: Western blot analysis of recombinant mature WT and C95S cFBP1 incubated with different concentrations of DTT. Gels were loaded with 90 ng of protein per lane. Asterisks indicate the positions of different oxidized polypeptide species of the monomeric WT and C95S cFBP1 forms.

in reduced state. In the presence of 100 mM DTT, the WT and C95S cFBP1 forms were fully reduced and exhibited the same electrophoretic mobilities (**Figure 1**).

Mutation of the Cys95 residue reduces the activity and Mg^{2+} cooperativity of cFBP1

Whether Cys95 plays an important role in cFBP1 function was investigated by characterizing the kinetic properties of recombinant mature WT and C95S cFBP1 forms using different concentrations of FBP and Mg^{2+} in the presence or absence of 100 mM DTT. In the absence of DTT, the specific activity of C95S cFBP1 was ca. 20-fold lower than that of the WT cFBP1 at saturating FBP and Mg^{2+} concentrations (**Figure 2**). DTT strongly stimulated the WT and C95S cFBP1, but the specific activity of the C95S variant was still ca. 4-fold lower than that of WT at saturating FBP and Mg^{2+} concentrations (**Figure 2**). With 100 mM DTT, Kcat of the C95S cFBP1 (2.2 ± 0.2 s^{-1}) was substantially lower than that of WT (13.2 ± 1.0 s^{-1}) (**Table 1**). Under these conditions, WT and C95S cFBP1 exhibited a Michaelis Menten kinetics with

Table 1: Kinetic constants of recombinant mature WT and C95S cFBP1 in the presence of 100mM DTT. Values represent catalytic activity (K_{cat}), F6P and Mg^{2+} specificity (Km) and Mg^{2+} cooperativity (Hill coefficient and $K_{0.5}$) of three independent experiments.

FBPase	K_{cat} (s^{-1})	*K*m (mM) FBP	*K*s (mM) FBP	Hill coefficient Mg^{+2}	$K_{0.5}$(mM) Mg^{+2}	*K*m (mM) Mg^{+2}
WT	13.2±1.0	0.20±0.09	19.7±10.1	1.8±0.1	1.3±0.1	-
C95S	2.2±0.2	0.17±0.02	not inhibited	not allosteric	-	4.7±2.3

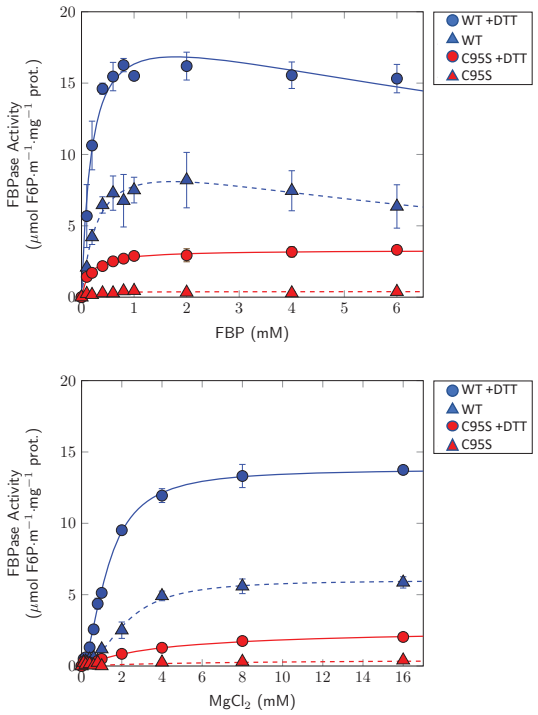

Figure 2: Dependence on substrate concentration and effect of Mg^{2+} on the activity of recombinant mature WT and C95S cFBP1 incubated with or without DTT. The graphs represent the FBPase activity curves with respect to (A) FBP and (B) Mg^{2+} concentrations. In the presence of DTT, FBP and Mg^{2+} ranged concentrations appropriate for enzymatic parameter determinations. Means of three independent experiments are indicated in **Table 1**.

respect to FBP, with *Km* values of 0.20 ± 0.09 mM and 0.17 ± 0.02 mM, respectively (**Table 1**). Mg^{2+} cooperatively activated WT cFBP1, which is consistent with previous reports on kinetic properties of plant cFBP1s (Charles and Halliwell, 1980; Serrato et al., 2009) and mammalian FBPases (Chen et al., 1993; Nelson et al., 2004); $K_{0.5}$ and Hill coefficient values for Mg^{2+} were 1.3 ± 0.1 mM and 1.8 ± 0.1, respectively (**Table 1**). In contrast, the C95S cFBP1 variant exhibited no cooperativity with respect to Mg^{2+}, but a Michaelis Menten kinetics with *Km* values for Mg^{2+} of 4.7 ± 2.3 mM.

The ectopic expression of C95S cFBP1 only partially reverted to WT the reduced total FBPase and photosynthetic activities of *cfbp1* plants

Whether Cys95 determines cFBP1 activity was further investigated by comparing the

total FBPase and photosynthetic activities of WT, *cfbp1* and *cfbp1* plants transformed with *promcFBP1:cFBP1* and *promcFBP1:cFBP1mut*, which expressed the WT and C95S cFBP1 forms under the control of the 1,094 bp *promcFBP1* region immediately upstream the translation start codon of cFBP1, respectively. The rationale behind this experimental approach was that, if Cys95 mediates cFBP1 activity, the total FBPase activities and net rates of CO_2 assimilation (A_n) of WT plants and *cfbp1* plants expressing the WT form of cFBP1 should be higher than those of *cfbp1* plants expressing the C95S cFBP1 variant. Conversely, if Cys95 is not a major determinant of cFBP1 activity, C95S cFBP1-expressing *cfbp1* plants should have WT total FBPase activity and A_n values.

We characterized three independent lines each of WT and C95S cFBP1-expressing *cfbp1* plants. As shown in **Figure 3A, B,** expression of the recombinant proteins was confirmed by both reducing and non-reducing western blot analyses. Notably, the ratio of reduced cFBP1 vs. oxidized cFBP1 in leaves of *cfbp1* plants ectopically expressing C95S cFBP1 was substantially lower than in leaves of WT plants and *cfbp1* plants expressing WT cFBP1 (**Figure 3B, C**). In keeping with Rojas-González et al. (2015), *cfbp1* leaves had reduced total FBPase activity and A_n (45% and 60% of WT levels, respectively) (**Figure 3D, E**). As expected, the ectopic expression of WT cFBP1 countered the reduced FBPase activity and A_n values of *cfbp1* plants, reverting them to the WT (**Figure 3D, E**). In contrast, the ectopic expression of C95S cFBP1 only slightly reverted to WT the total FBPase and photosynthetic activities of *cfbp1* plants, as maximum total FBPase activity and A_n values in *cfbp1* leaves transformed with *promcFBP1:cFBP1mut* were ca. 65% and 75% of those of WT leaves, respectively (**Figure 3D, E**).

The ectopic expression of C95S cFBP1 is sufficient to revert the dwarf growth phenotype of *cfpb1* plants back to that of WT

We compared growth rates of WT and *cfbp1* plants and *cfbp1* plants ectopically expressing WT and C95S cFBP1. In keeping with Rojas-González et al. (2015),

Figure 3: The ectopic expression of C95S cFBP1 only partially reverts to WT the reduced cFBP and photosynthetic activities of *cfbp1* plants (A) Reducing and (B) non-reducing western blots of cFBP1, (C) FBPase activities and (D) net CO_2 assimilation rates (A_n) in leaves of WT and *cfbp1* plants and three independent lines each of WT and C95S cFBP1-expressing *cfbp1* plants. In (A) and "B", gels were loaded with 60 μg of protein per lane. In (C) and (D), lowercase letters indicate significant differences, according to Student´s t-test ($P<0.05$), between: "a" WT and mutant plants, "b" *cfbp1* plants and both WT and WT and C95S cFBP1-expressing *cfbp1* plants

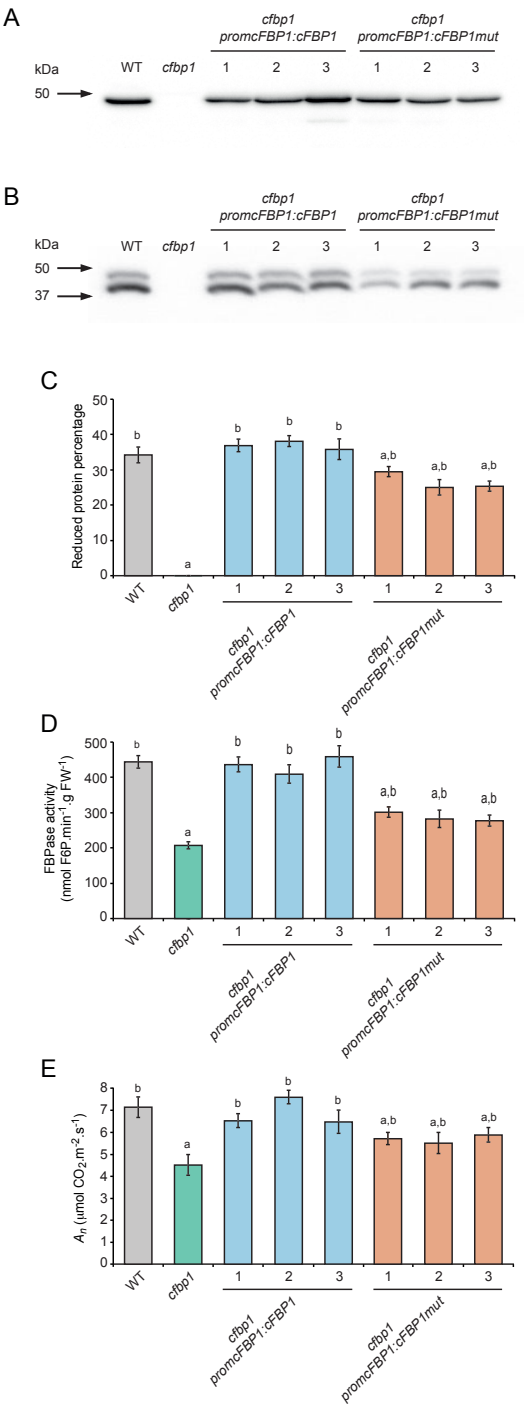

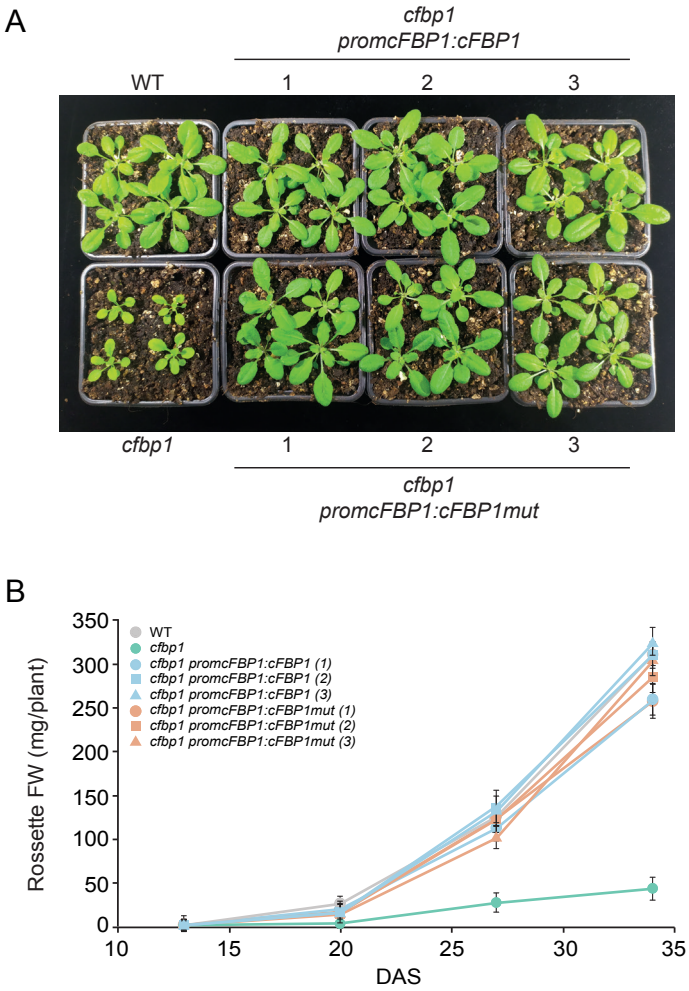

Figure 4: The ectopic expression of C95S cFBP1 is sufficient to revert the dwarf growth phenotype of *cfpb1* plants back to that of WT. (A) External phenotype and (B) time-series for fresh weight (FW) of rosettes of WT, *cfbp1* plants and three independent lines each of WT and C95S cFBP1-expressing *cfbp1* plants. Days after sowing (DAS).

cfbp1 plants showed a slow growth phenotype when compared with that of WT plants (**Figure 4**). As shown in **Figure 4**, not only the ectopic expression of WT cFBP1, but also that of C95S cFBP1 reverted to WT the dwarf phenotype of *cfbp1* plants.

The ectopic expression of C95S cFBP1 restores to WT the poor growth response of *cfbp1* plants to small microbial VCs

Small microbial VC-promoted growth is associated with global reduction of the thiol redox proteome. Whether the Cys95 residue of cFBP1 can individually determine the response of plants to small microbial VCs was investigated by comparing the growth responses of WT and *cfbp1* plants, and *cfbp1* plants ectopically expressing WT or C95S cFBP1 cultured in the absence or presence of small VCs emitted by *Alternaria alternata*. In keeping with Ameztoy et al. (2021), small VCs did not stimulate growth in *cfbp1* (**Figure 5**). Furthermore, VCs promoted similar to WT increases in growth (**Figure 5**).

DISCUSSION

Cys95 is an important structural and functional determinant of cFBP1

A previous study on the structural and functional roles of the seven highly conserved Cys residues of cFBP1 showed that Cys96 of rapeseed cFBP1 (Cys95 in Arabidopsis) is not important for the catalytic activity, the stability and redox regulation of the enzyme (Rodríguez-Suárez et al., 1997). However, results presented here provided strong evidence that Cys95 is an important determinant of the structure, activity, regulatory properties and redox state of Arabidopsis cFBP1. First, the electrophoretic mobilities of recombinant WT cFBP1 and C95S cFBP1 were different under varying DTT concentration conditions, the state of C95S cFBP1 being more oxidized than that of WT cFBP1 at any DTT concentration (**Figure 1**). Second, mutation of the Cys95 residue strongly reduced the activity and Mg^{2+} binding affinity and cooperativity of recombinant cFBP1 even in fully reduced state conditions (**Table 1, Figure 2**). Similar responses have been reported when mutating the metal binding sites of the porcine FBPases (Chen et al., 1993). This would strongly indicate that Cys95 is important for metal binding and that this site may be in some way associated with subunit-subunit interactions, or alternatively, with metal site-metal site interaction within a single subunit. Third, the ratio of reduced cFBP1 vs. oxidized cFBP1 in

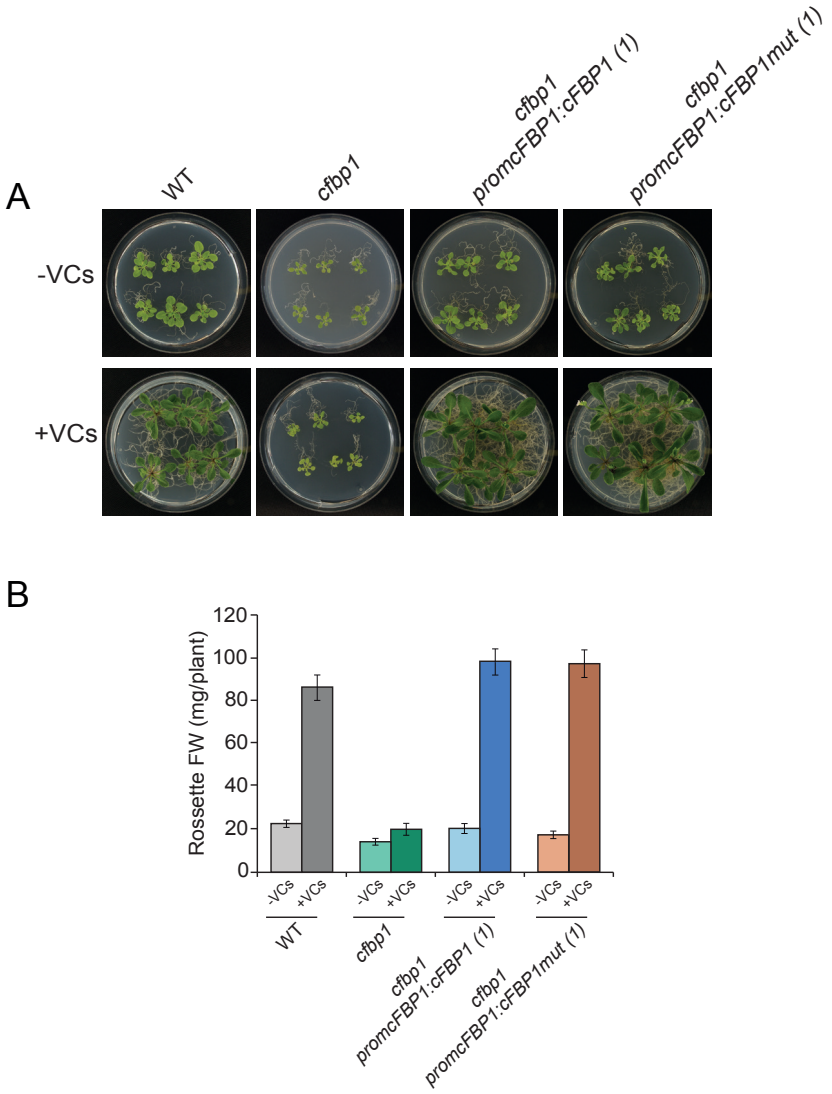

Figure 5: The ectopic expression of C95S cFBP1 restores to WT the response of *cfbp1* plants to small microbial VCs. (A) External phenotype and (B) rosette fresh weight (FW) of WT and *cfbp1* plants and WT and C95S cFBP1-expressing *cfbp1* plants cultured in the absence or continuous presence of small fungal VCs for one week. Values in panel (B) are means ± SE for three biological replicates (each a pool of 12 plants) obtained from four independent experiments.

leaves of *cfbp1* plants ectopically expressing C95S was substantially lower than in leaves of WT plants and *cfbp1* plants expressing WT cFBP1 (**Figure 3B, C**). Fourth, the ectopic expression of C95S cFBP1 only partially reverted to WT the reduced total FBPase activity of *cfbp1* plants (**Figure 3D**). That *Km* values of WT cFBP1 and C95S cFBP1 for FBP1were comparable, and that DTT increased the activity of cFBP1mut (**Table 1**) strongly indicated that Cys95 is not an important determinant of substrate affinity and does not mediate DTT reactivity with cFBP1.

Cys156, Cys174 and Cys179 are the main Fdx/Trx system-mediated redox regulatory cysteines of Arabidopsis cFBP1 (Jacquot et al., 1997; Rodríguez-Suárez et al., 1997; Serrato et al., 2018). In Arabidopsis, much of the cFBP1 is present in oxidized state in illuminated leaves (Thormählen et al., 2015; Yoshida et al., 2015; Nikkanen et al., 2016; Pérez-Ruiz et al., 2017). This would indicate that mechanisms other than light-dependent, Fdx/Trx-mediated cFBP1 reduction may influence in the redox state and activity of the enzyme. In line with this presumption, Serrato et al. (2018) showed that, *in vitro*, some oxidizing agents promoted the formation of different oxidized polypeptide species in recombinant pea cFBP1 forms in which the Cys153, Cys173 and Cys178 residues were replaced by serine. Furthermore, here we found that recombinant WT cFBP1 and C95S cFBP1 exhibited different redox states under varying DTT concentrations conditions (**Figure 1**).

Previous crystallographic studies of cFBP1 showed that the contours of the active site of oxidized cFBP1 are not compatible with the binding of Mg^{2+} to the enzyme (Chiadmi et al., 1999). Because mutation at Cys95 promotes cFBP1 oxidation (**Figure 1, Figure 3B, C**), it is conceivable that the reduced activity of C95S cFBP1 is due, at least partly, to reduced accessibility of Mg^{2+} to the enzyme, as strongly suggested by the kinetic properties of C95S cFBP1 (**Table 1, Figure 2**). However, three-dimensional structural studies of crystallized spinach cFBP1 strongly indicated that Cys95 cannot form disulfide bridges with other Cys residues within the monomer, as no Cys residues are present in its close neighborhood (Villeret et al., 1995). Therefore, further crystallographic studies of C95S cFBP1 will be required to understand how the C95S mutation affects the conformational and redox status of cFBP1.

Cys95 of the "excess" enzyme cFBP1 can potentially act as an important determinant of photosynthesis, but not of growth in Arabidopsis

Maximum total FBPase activities in leaves of *cfbp1* plants and *cfbp1* plants transformed with *promcFBP1:cFBP1mut* were ca. 45% and 60% of those of WT leaves, respectively (**Figure 3D**), which indicated that chloroplastic FBPase activity due to C95S cFBP1 expression in *promcFBP1:cFBP1* leaves is ca. 15% of that of WT leaves. In addition, A_n values in leaves of *cfbp1* plants and *cfbp1* plants transformed with *promcFBP1:cFBP1mut* were ca. 65% and 75% of those of WT leaves, respectively (**Figure 3E**). Furthermore, the ratio of reduced cFBP1 vs. oxidized cFBP1 in leaves of *cfbp1* plants ectopically expressing C95S cFBP1 was substantially lower than in leaves of WT plants (**Figure 3C**). It is thus conceivable that the Cys95 residue of cFBP1 can regulate photosynthesis through changes in its redox status.

Previous studies using antisense potato plants showed that 60% reduction of cFBP1 activity promoted a discrete (10-15%) reduction of photosynthetic activity, but null growth retardation (Kossmann et al., 1994). This strongly indicated that, in potato, cFBP1 is an excess enzyme which has reduced flux-control over CO_2 assimilation and growth. Here we showed that, despite having lower than WT plastidial cFBP1 and photosynthetic activities, C95S cFBP1 expressing *cfbp1* Arabidopsis plants did not exhibit growth retardation under both soil culture and *in vitro* culture conditions (**Figures 4 and 5**). This indicates that the maximal photosynthetic activity in these plants is greater than that required for full growth and, like in potato, cFBP1 is present in excess in Arabidopsis. Furthermore, the microbial VC treatment promoted similar to WT growth increase in C95S cFBP1 expressing *cfbp1* plants (**Figure 5**). The latter findings strongly indicate that (i) individually, changes in the redox state of the Cys95 residue of cFBP1 exert a minor control, if any, on plant growth and (ii) factors other than Cys95 reduction are important for microbial VC-promoted growth. This agrees with current ideas arguing against photosynthesis being the main rate-controlling factor for plant growth (Körner, 2015; Gámez-Arcas et al., 2022b). In this respect, we must emphasize that microbial VCs promoted global reduction of the thiol redox proteome (Ameztoy et al., 2019), which probably results in the stimulation of growth-related processes. In addition, microbial VCs enhanced the expression of proteins of growth-related metabolic pathways such as shikimate and cytosolic glycolytic enzymes, proteins involved in the synthesis of photosynthetic pigments, ribosomal proteins, chaperones and

enzymes of the plastid-localized 2-C-methyl-D-erythritol 4-P pathway involved in the production of compounds necessary for the synthesis of isoprenoid-derived hormones.

MATERIALS AND METHODS

Plants

The work was carried out using *Arabidopsis thaliana L*. (Heynh) WT plants (ecotype Columbia Col-0), the *cfbp1* knockout mutant, line GK-472G06 (Rojas-González et al., 2015) and *cfbp1* plants transformed with either *promcFBP1:cFBP1* or *promcFBP1:cFBP1mut*, which express *cFBP1* and *cFBP1mut* under the control of the 1,094 bp *promcFBP1* immediately upstream the translation start codon of cFBP1 (**Supplemental Figure S2**). Briefly, a complete cDNA corresponding to the WT *cFBP1* gene (At3g54050) was obtained from the RIKEN Arabidopsis cDNA collection (pda00367) (Seki et al., 1998, 2002), amplified by PCR using specific primers "attB1 *cFBP1*" and "attB2 *cFBP1*" (**Supplemental Table S1**) and cloned into the pDONR/Zeo plasmid using BP clonase (Invitrogen). The *cFBP1mut* cDNA was generated by site-directed mutagenesis using as template the plasmid pDONR-cFBP1, the primers 5´-ctaatgaggtgttttccaactctttgagatcaagtggaagaac-3´ and 5´- gttcttccacttgatctcaaagagttggaaaacacctcattag-3´, and the QuickChange site-directed mutagenesis kit (Stratagene) to replace the codon initially encoding Cys95 by a codon encoding Ser95. To construct *promcFBP1:cFBP1* and *promcFBP1:cFBP1mut* plasmids, pDONR-cFBP1 and pDONR-cFBP1mut entry clones were subjected to LR recombination using the R4pGWB501 destination vector, respectively. All plasmid constructs were electroporated and propagated in *E. coli* TOP 10. All final destination vectors were confirmed by sequencing (**Supplemental Figure S3**) and were transferred to *Agrobacterium tumefaciens* EHA105 cells by electroporation and utilized to transform Arabidopsis plants as described by Clough and Bent (1998). Transgenic plants were selected on hygromycin-containing medium.

Production of recombinant WT and C95S cFBP1 mature forms in *Eschericia coli* and purification

Escherichia coli TOP 10 was used for gene cloning, and BL21(DE3) was employed for recombinant WT and C95S cFBP1 expression. pDEST17-cFBP1 and pDEST17-cFBP1mut plasmids used to express mature forms of WT and C95S cFBP1 were

produced using the Gateway technology as shown in **Supplemental Figure S2** and confirmed by sequencing (**Supplemental Figure S3**). Briefly, a cDNA from *cFBP1* and *cFBP1mut* were obtained by PCR using as template pDONR-cFBP1 and pDONR -cFBP1mut, respectively, and the specific primers "attB1 *cFBP1**" and "attB2 *cFBP1*" (**Supplemental Table S1**) and cloned into the pDONR/Zeo plasmid using BP clonase (Invitrogen). To produce pDEST17-cFBP1 and pDEST17-cFBP1mut , pDONR-cFBP1 and pDONR-cFBP1mut entry clones were subjected to LR recombination using the pDEST17 destination vector, respectively. All final destination vectors were confirmed by sequencing (**Supplemental Figure S3**). BL21(DE3) cells transformed with pDEST17-cFBP1 and pDEST17-cFBP1mut were grown at 37 ^{o}C in one liter of LB medium supplemented with 50 μg ml^{-1} carbenicillin to an attenuance at 600 nm of 0.6, and then 0.4 mM isopropyl-β-D-thiogalactopyranoside was added to the culture medium. After 3 h, the bacterial culture was centrifuged at 6,000 x g for 10 min. The pelleted bacteria were resuspended in 6 ml of HiTrap-TALON crude binding buffer (GE Healthcare Life Sciences, Marlborough, MA, USA), sonicated and centrifuged at 10,000 x g for 10 min. The supernatant thus obtained was subjected to Co^{2+} affinity chromatography according to the manufacturer's instructions (GE Healthcare Life Sciences, Marlborough, MA, USA).

Growth conditions and sampling

Plants were cultured on soil or in Petri dishes (92 x 16 mm, Sarstedt, Ref. 82.1472.001) containing half-strength agar solidified Murashige and Skoog (MS) (Phytotechlab M519) medium in growth chambers with a 16 h light (22^{o}C, 90 μmol photons sec^{-1} m^{-2})/8 h dark (18^{o}C) cycles. To investigate effects of small fungal VCs on plants we used the "plasticized PVC wrap and charcoal filter-based box-in-box" co-cultivation system in which plants were grown in the vicinity of *A. alternata* cultures covered with charcoal filters that adsorb VCs of molecular masses higher than ca. 45 Da (García-Gómez et al., 2019; Gámez-Arcas et al., 2022a). *A. alternata* was cultured in Petri dishes containing agar solidified MS medium supplemented with 90 mM sucrose.

Determination of FBPase activity

We used the spectrophotometric assay method described in Sahrawy et al. (2022). The assay was conducted using microtiter plates in a final volume of 200 μl. The

reaction mixture contained 100 mM Tris–HCl pH 8.0, 10 mM $MgCl_2$ (or a variable concentration for *Km* determination), 0.3 mM NAD, 2 mM FBP (or a variable concentration for *Km* determination), 0.7 U of glucose-6-P dehydrogenase (G8404 SIGMA) and 0.3 U of phosphoglucose isomerase (P5381 SIGMA). For redox activation assays, cFBP1 was incubated for 30 min at 22 ºC with DTT (concentration depending on the assay). The increase of absorbance at 340 nm (NADPH formation) versus time was read with a microplate reader (Tecan Sunrise™ (Tecan Trading AG, Männedorf, Switzerland). Incubations and activity assays were performed at room temperature (22–24 °C). A plot of velocity versus substrate concentration was used in the Km determination. Curve fitting and determination of enzyme parameters were performed using R software (RStudio Team (2020). RStudio: Integrated Development for R. RStudio, PBC, Boston, MA. Available online: http://www.rstudio.com/).

Western blot analyses

For immunoblot analyses, protein samples were separated on 10% SDS-PAGE under reducing or non-reducing conditions as described in Sahrawy et al. (2022), transferred to PVDF, and immunodecorated by using the antisera raised against cFBP1 from pea (Rojas-González et al., 2015) and a goat anti-rabbit IgG horseradish peroxidase conjugate as secondary antibody (Sigma).

Determination of gas exchange rates and photosynthetic parameters

Gas exchange rates were determined as described by Sánchez-López et al. (2016b) using a LI-COR 6400 gas exchange portable photosynthesis system (LI-COR, Lincoln, NE, USA). An was calculated as described by von Caemmerer and Farquhar (1981).

Statistical analysis

Unless otherwise indicated, presented data are means (± SE) obtained from 3-4 independent experiments, with 3 replicates for each experiment. The significance of differences between plants was statistically evaluated with Student´s t-test using SPSS software. Differences were considered significant if $P<0.05$.

SUPPLEMENTAL MATERIAL

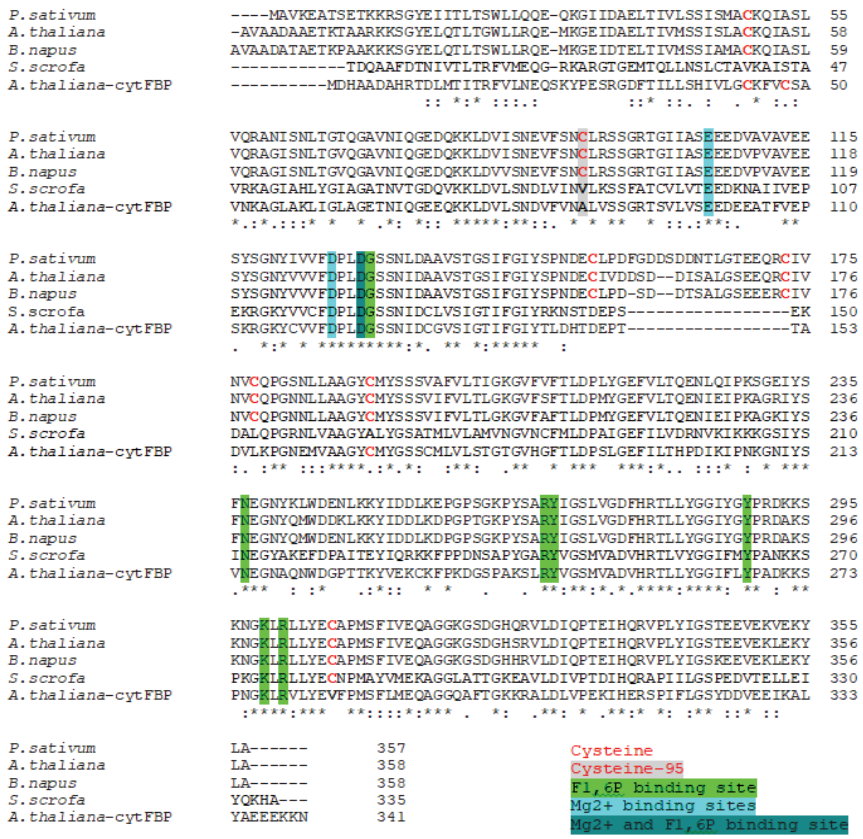

Supplemental Figure S1: Sequence comparisons of pig fructose-1,6-bisphosphatase (FBPase), cytosolic FBPase (cyFBPase) of Arabidopsis and cFBP1 from pea, rapeseed and Arabidopsis.

Supplemental Figure S2: Stages in the construction of the *promcFBP1:cFBP1*, *promcFBP1:cFBP1mut*, *pDEST17-cFBP1* and *pDEST17-cFBP1mut* plasmids. Plasmid constructs were produced using Gateway technology and confirmed by sequencing. Primers used for PCR amplification of complete a cFBP1 cDNA obtained from the RIKEN Arabidopsis cDNA collection (Seki et al., 1998, 2002) are listed in **Supplemental Table S1**.

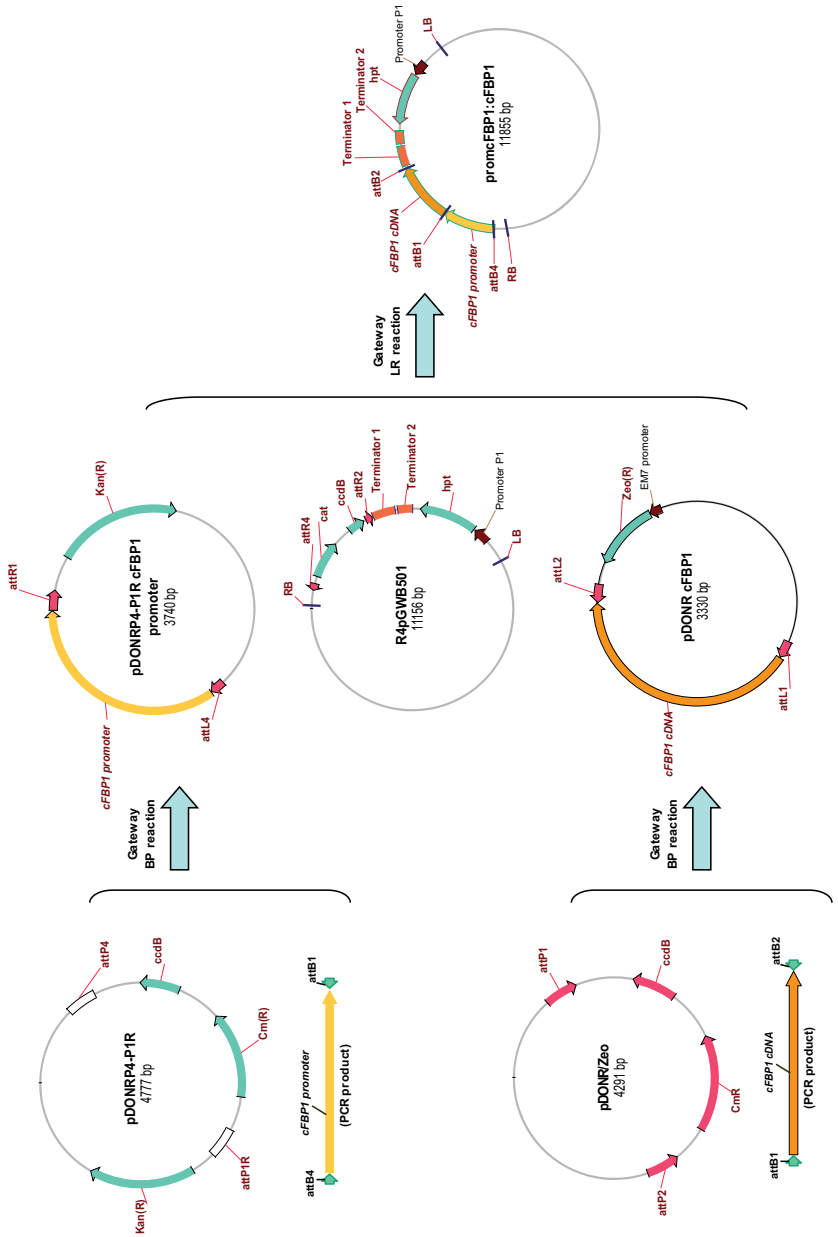

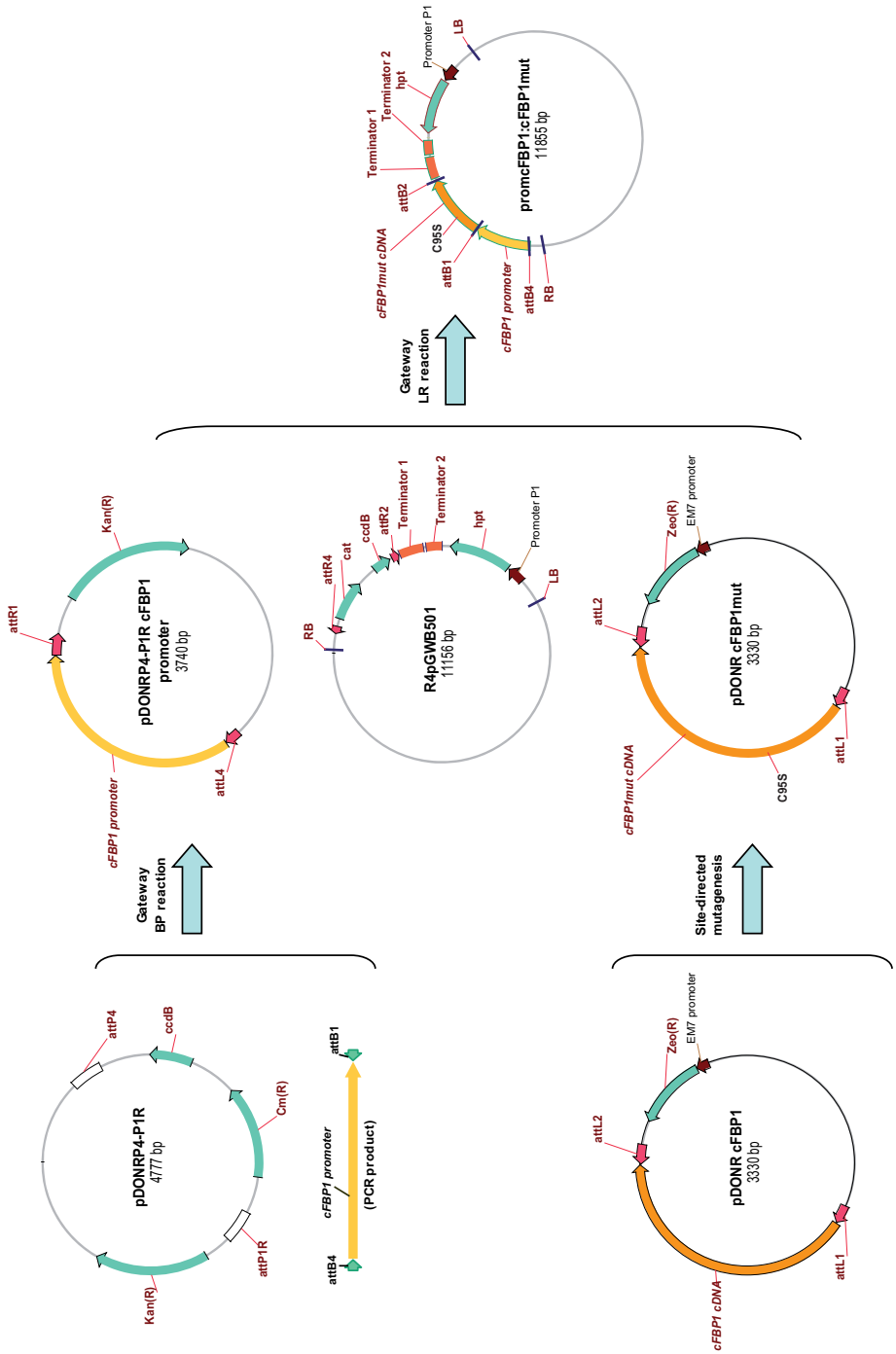

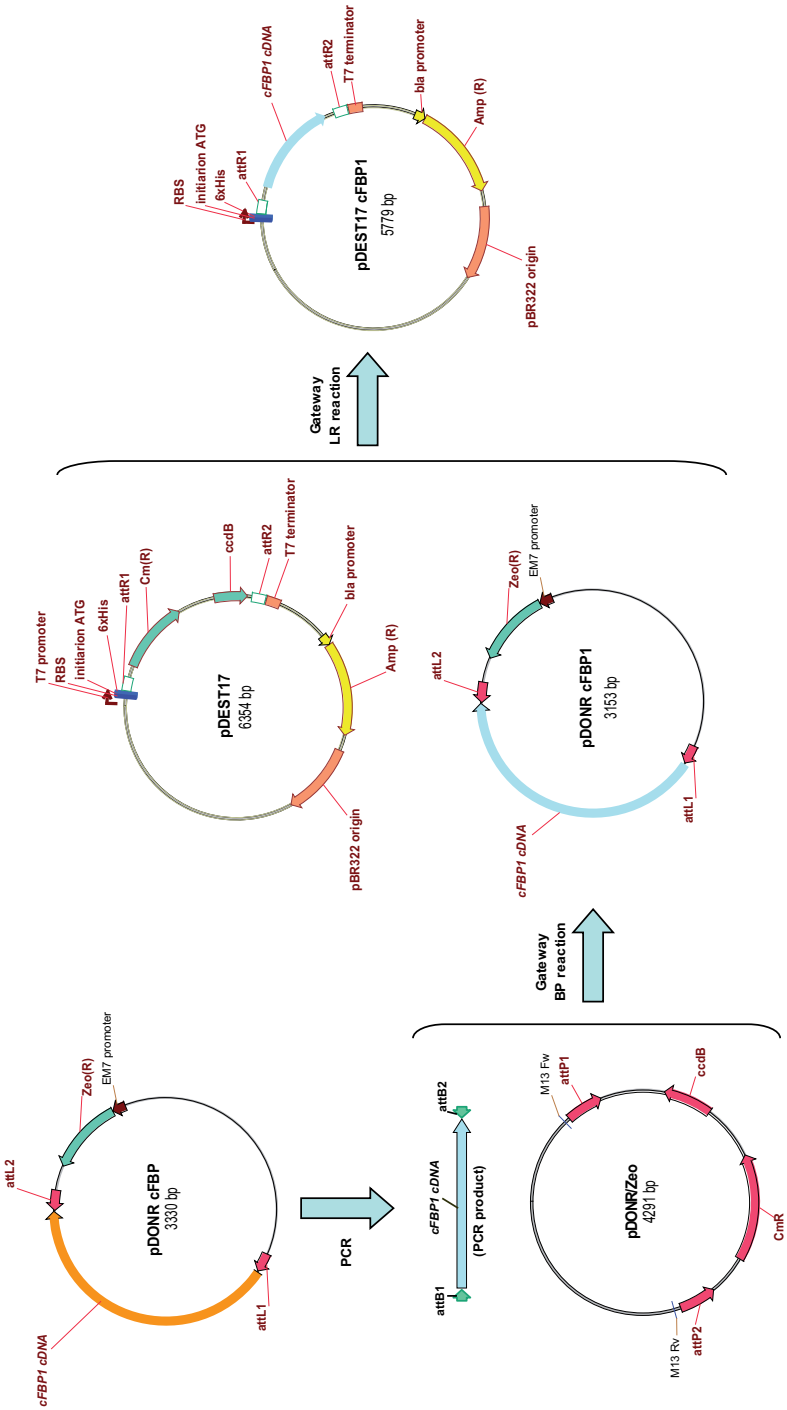

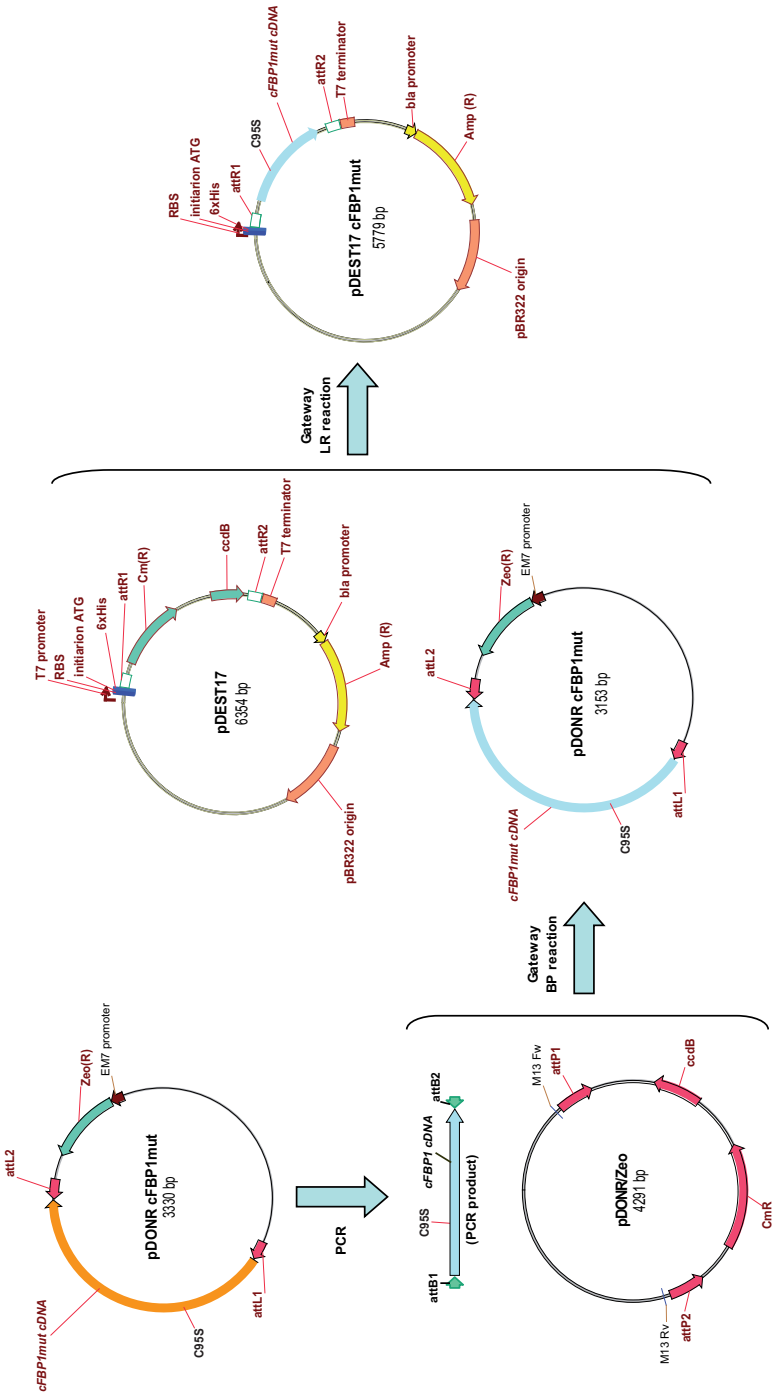

Supplemental Figure S3: Comparison between the encoding sequence of At3g54050 (https://www.ncbi.nlm.nih.gov/nuccore/AY039934.1/) and *cFBP1* sequences at pDEST17-cFBP1, pDEST17-cFBP1mut, promcFBP1:cFBP1 and promcFBP1:cFBP1mut plasmids. Highlighted in red are the nucleotide change to produce cFBPmut

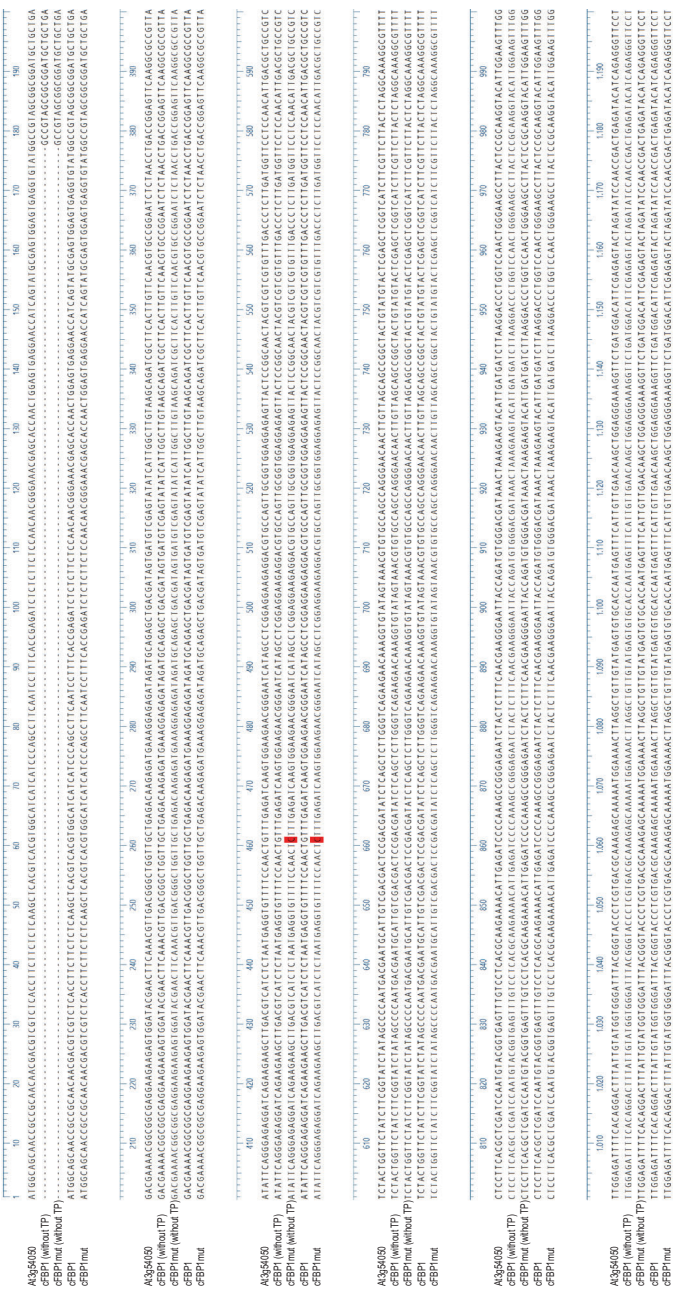

Table S1: Primers used for PCR amplification of *cFBP1*, *cFBP1mut* and *cFBP1* promoter to produce the pDEST17-cFBP1, pDEST17-cFBP1mut, promcFBP1:cFBP1 and promcFBP1:cFBP1mut plasmids. Primer sequences for attB sites (are indicated in bold) see **Supplemental Figure S2**)

Primer	Sequence
***cFBP1* for promcFBP1:cFBP1 and promcFBP1:mut**	
attB1 *cFBP1*	5'-**ggggacaagtttgtacaaaaaagcaggctta**atggcagcaaccgccgcaac-3'
attB2 *cFBP1*	5'-**ggggaccactttgtacaagaaagctgggta**tcaagccaagtacttctccagc-3'
***promcFBP1* for promcFBP1:cFBP1 and promcFBP1:mut**	
attB4 *cFBP1* promoter	5'-**ggggacaactttgtatagaaaagttgct**ggttaatcaacgattcaatgaactag-3'
attB1 *cFBP1* promoter	5'-**ggggactgctttttttgtacaaacttgc**tttttctgtgttgttttgaaaaaaac-3'
***cFBP1** for pDEST17-cFBP1 and pDEST17-cFBP1mut**	
attB1 *cFBP1**	5'-**ggggacaagtttgtacaaaaaagcaggctta**gccgtagcggcggatgctg-3'
attB2 *cFBP1*	5'-**ggggaccactttgtacaagaaagctgggta**tcaagccaagtacttctccagc-3'

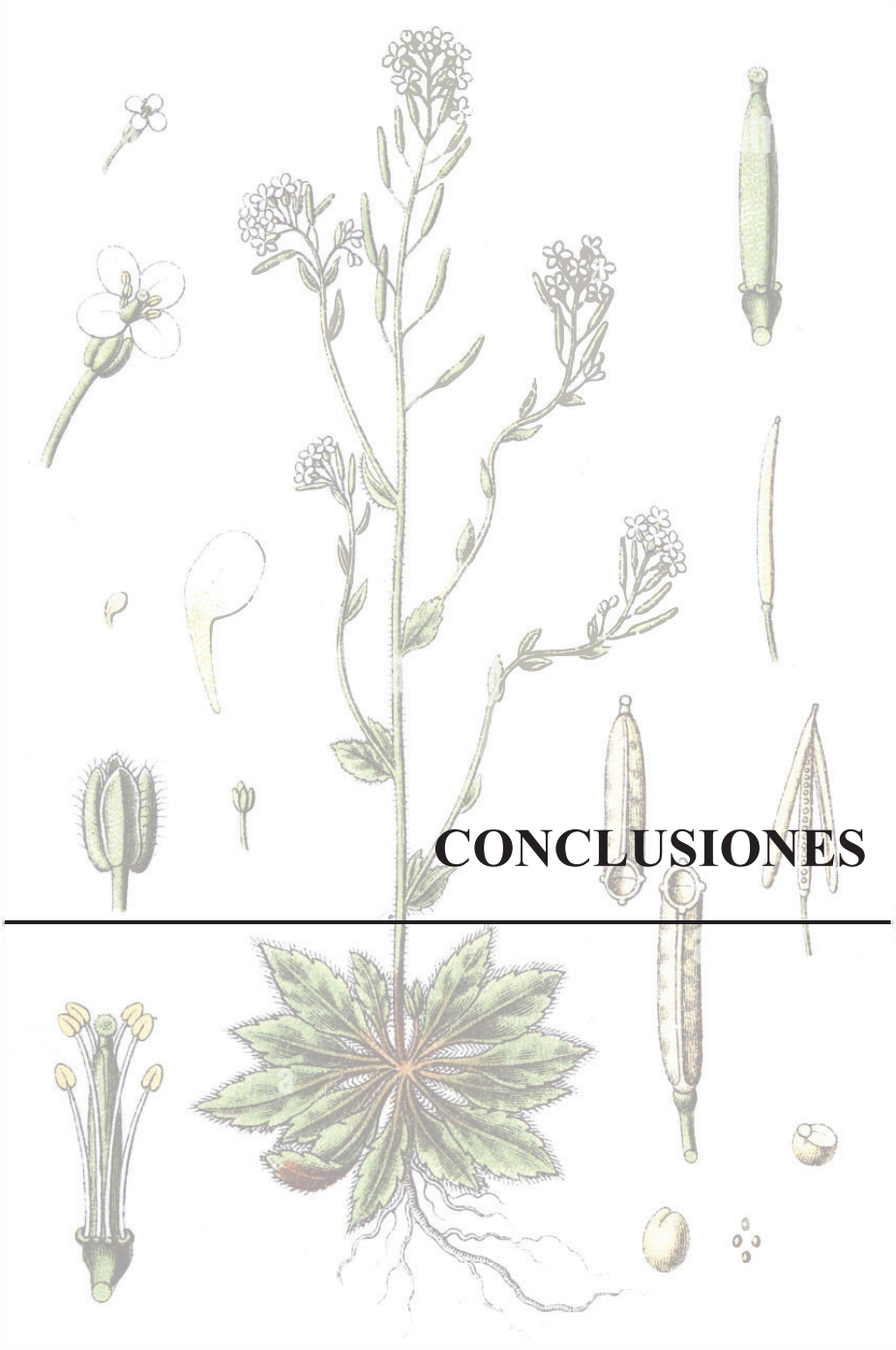

CONCLUSIONES

1. *GPT2* juega un papel importante en la respuesta de plantas *pgi1-2* a VCs fúngicos.

2. Comparada con la respuesta de plantas *pgi1-2*, la respuesta de plantas *pgi1-2gpt2-1* a VCs es reducida. Ello puede atribuirse, al menos en parte, a la reducida expresión de proteínas relacionadas con la fotosíntesis.

3. La sobre-acumulación de almidón en el mesófilo de hojas de plantas *pgi1-2* inducida por VCs fúngicos no es debida a una estimulación de la incorporación de G6P citosólica a través de GPT2.

4. La expresión de PGI1 y GPT2 en las puntas de las raíces y en las células vasculares, juega un papel clave en la respuesta de las plantas a VCs a través de mecanismos implicados en la regulación del crecimiento, la fotosíntesis y el metabolismo de la planta.

5. La expresión de GPT2 está sujeta a complejos mecanismos de regulación mediados por elementos ubicados a ambos lados del codon ATG de inicio de la transcripción de GPT2 y/o a ambos lados del codon AUG de inicio de la traducción de transcritos de GPT2.

6. El residuo Cys95 de la cFBP1 madura es un determinante importante de la estructura, el estado redox y la actividad de cFBP1 en Arabidopsis.

7. Potencialmente, el residuo Cys95 de la cFBP1 puede actuar como un importante determinante de la fotosíntesis, pero no del crecimiento en plantas de Arabidopsis.

8. Individualmente, la reducción del residuo de Cys95 de Arabidopsis no es un determinante del crecimiento de Arabidopsis en respuesta a VCs fúngicos.

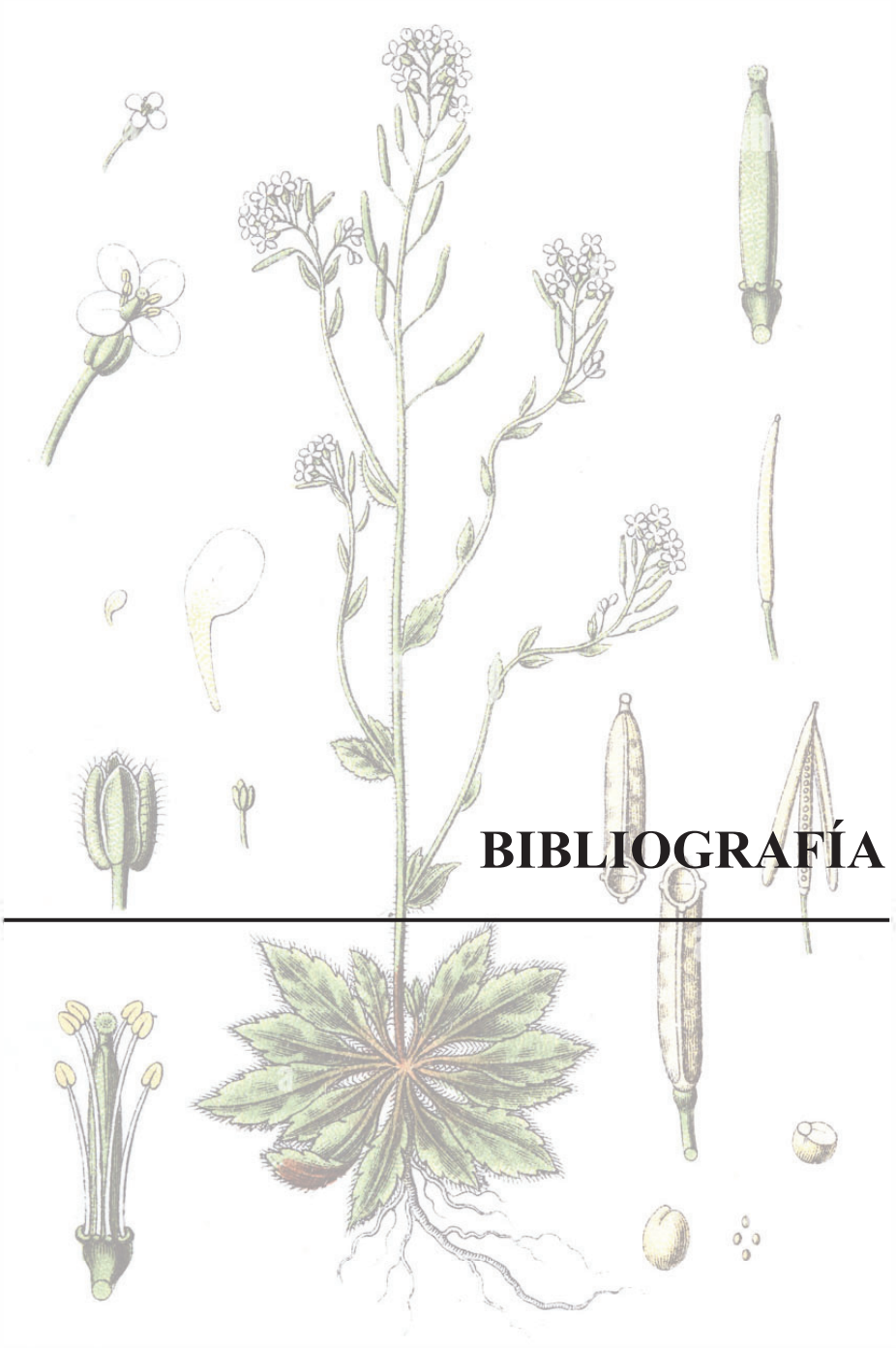

BIBLIOGRAFÍA

Ainsworth EA, Rogers A (2007) The response of photosynthesis and stomatal conductance to rising [CO_2]: Mechanisms and environmental interactions. Plant Cell Environ. 30: 258-270.

Aliverti A, Piubelli L, Zanetti G, Curti B, Lübberstedt T, Herrmann RG (1993) The role of cysteine residues of spinach ferredoxin-NADP+ reductase as assessed by site-directed mutagenesis. Biochem. 32: 6374-6380.

Aloni R, Langhans M, Aloni E, Dreieicher E, Ullrich CI (2005) Root-synthesized cytokinin in Arabidopsis is distributed in the shoot by the transpiration stream. J. Exp. Bot. 56: 1535-1544.

Alonso C, Ramos-Cruz D, Becker C (2019) The role of plant epigenetics in biotic interactions. New Phytol. 221:731-737.

Ameztoy K, Baslam M, Sánchez-López ÁM, Muñoz FJ, Bahaji A, Almagro G, García-Gómez P, Baroja-Fernández E, De Diego N, Humplík JF, Ugena L, Spíchal K, Doležal K, Kaneko T, Mitsui F, Cejudo J, Pozueta-Romero J (2019) Plant responses to fungal volatiles involve global post-translational thiol redox proteome changes that affect photosynthesis. Plant Cell Environ. 42: 2627-2644.

Ameztoy K, Sánchez-López ÁM, Muñoz FJ, Bahaji A, Almagro G, Baroja-Fernández E, Gámez-Arcas S, De Diego N, Doležal K, Novák O, Pěnčík A, Alpízar A, Rodríguez-Concepción M, Pozueta-Romero J (2021) Proteostatic regulation of MEP and shikimate pathways by redox-activated photosynthesis signaling in plants exposed to small fungal volatiles. Front. Plant Sci. doi: 10.3389/fpls.2021.637976.

Arenas-Alfonseca L, Gotor C, Romero LC, García I (2018) β-cyanoalanine synthase action in root hair elongation is exerted at early steps of the root hair elongation pathway and is independent of direct cyanide inactivation of NADPH oxidase. Plant Cell Physiol. 59: 1072-1083.

Arribas-Hernández L, Brodersen P (2020) Occurrence and functions of m^6A and other covalent modifications in plant mRNA. Plant Physiol. 182: 79-96.

Athanasiou K, Dyson BC, Webster RE, Johnson GN (2010) Dynamic acclimation of photosynthesis increases plant fitness in changing environments. Plant Physiol. 152: 366-373.

Backer R, Rokem JS, Ilangumaran G, Lamont J, Praslickova D, Ricci E, Subramanian S, Smith DL (2018) Plant growth-promoting rhizobacteria: Context, mechanisms of action, and roadmap to commercialization of biostimulants for sustainable agriculture. Front. Plant Sci. 871: 371-387

Backhausen JE, Jöstingmeyer P, Scheibe R (1997) Competitive inhibition of spinach leaf phosphoglucose isomerase isoenzymes by erythrose 4-phosphate. Plant Sci. 130: 121-131.

Bahaji A, Almagro G, Ezquer I, Gámez-Arcas S, Sánchez-López ÁM, Muñoz FJ, Barrio RJ, Sampedro MC, De Diego N, Spíchal L, Doležal K, Tarkowská D, Caporali E, Mendes MA, Baroja-Fernández E, Pozueta-Romero J (2018) Plastidial phosphoglucose isomerase is an important determinant of seed yield through its involvement in gibberellin-mediated reproductive development and storage reserve biosynthesis in Arabidopsis. Plant Cell. 30: 2082-2098.

Bahaji A, Li J, Ovecka M, Ezquer I, Muñoz FJ, Baroja-Fernández E, Romero JM, Almagro G, Montero M, Hidalgo M, Sesma MT, Pozueta-Romero J (2011) *Arabidopsis thaliana* mutants lacking ADP-glucose pyrophosphorylase accumulate starch and wild-type ADP-glucose content: further evidence for the occurrence of important sources, other than ADP-glucose pyrophosphorylase, of ADP-glucose linked to leaf starch biosynthesis. Plant Cell Physiol. 52: 1162-1176.

Bahaji A, Li J, Sánchez-López ÁM, Baroja-Fernández E, Muñoz FJ, Ovecka M, Almagro G, Montero M, Ezquer I, Etxeberria E, Pozueta-Romero J (2014) Starch biosynthesis, its regulation and biotechnological approaches to improve crop yields. Biotechnol. Adv. 32: 87-106.

Bahaji A, Sánchez-López ÁM, De Diego N, Muñoz FJ, Baroja-Fernández E, Li J, Ricarte-Bermejo A, Baslam M, Aranjuelo I, Almagro G, Humplík JF, Novák O, Spíchal L, Doležal K, Pozueta-Romero J (2015) Plastidic phosphoglucose isomerase is an important determinant of starch accumulation in mesophyll cells, growth, photosynthetic capacity, and biosynthesis of plastidic cytokinins in Arabidopsis. PLoS One.10: e0119641.

Ballester AR, González-Candelas L (2020) EFE-mediated ethylene synthesis is the major pathway in the citrus postharvest pathogen *Penicillium digitatum* during fruit infection. J. Fungi. 6:175. doi: 10.3390/jof6030175.

Banerjee A, Wu Y, Banerjee R, Li Y, Yan H, Sharkey TD (2013) Feedback inhibition of deoxy-D-xylulose-5-phosphate synthase regulates the methylerythritol 4-phosphate pathway. J. Biol. Chem. 288: 16926-16936.

Baroja-Fernández E, Almagro G, Sánchez-López ÁM, Bahaji A, Gámez-Arcas S, De Diego N, Dolezal K, Muñoz FJ, Climent Sanz E, Pozueta-Romero J (2021) Enhanced yield of pepper plants promoted by soil application of volatiles from cell-free fungal culture filtrates is associated with activation of the beneficial soil microbiota. Front. Plant Sci. doi: 10.3389/fpls.2021.752653.

Baroja-Fernández E, Muñoz FJ, Li J, Bahaji A, Almagro G, Montero M, Etxeberria E, Hidalgo M, Sesma MT, Pozueta-Romero J (2012) Sucrose synthase activity in the *sus1/sus2/sus3/sus4* Arabidopsis mutant is sufficient to support normal cellulose and starch production. Proc. Natl. Acad. Sci. USA. 109: 321-326.

Baune M-C, Lansing H, Fischer K, Meyer T, Charton L, Linka N, von Schaewen A (2020) The Arabidopsis plastidial glucose-6-phosphate transporter GPT1 is dually targeted to peroxisomes via the endoplasmic reticulum. Plant Cell. 32: 1703-1726.

Behnam B, Iuchi S, Fujita M, Fujita Y, Takasaki H, Osakabe Y, Yamaguchi-Shinozaki K, Kobayashi M, Shinozaki K (2013) Characterization of the promoter region of an Arabidopsis gene for 9-cis-epoxycarotenoid dioxygenase involved in dehydration-inducible transcription. DNA Res. 20: 315-324.

Berkowitz O, Xu Y, Liew LC, Wang Y, Zhu Y, Hurgobin B, Lewsey MG, Whelan J (2021) RNA-seq analysis of laser microdissected *Arabidopsis thaliana* leaf epidermis, mesophyll and vasculature defines tissue-specific transcriptional responses to multiple stress treatments. Plant J. 107: 938-955.

Bitas V, McCartney N, Li N, Demers J, Kim JE, Kim HS, Brown KM, Kang S (2015) *Fusarium oxysporum* volatiles enhance plant growth via affecting auxin transport and signaling. Front. Microbiol. doi:10.3389/fmicb.2015.01248.

Blom D, Fabbri C, Eberl L, Weisskopf L (2011) Volatile-mediated killing of *Arabidopsis thaliana* by bacteria is mainly due to hydrogen cyanide. Appl. Environ. Microbiol. 77: 1000-1008.

Bodi Z, Zhong S, Mehra S, Song J, Graham N, Li H, May S, Fray RG (2012) Adenosine methylation in Arabidopsis mRNA is associated with the 3′ end and reduced levels cause developmental defects. Front. Plant Sci. doi: 10.3389/fpls.2012.00048.

Boonman A, Prinsen E, Gilmer F, Schurr U, Peeters AJM, Voesenek LACJ, Pons TL (2007) Cytokinin import rate as a signal for photosynthetic acclimation to canopy light gradients. Plant Physiol. 143: 1841-1852.

Bouguyon E, Perrine-Walker F, Pervent M, Rochette J, Cuesta C, Benkova E, Martinière A, Bach L, Krouk G, Gojon A, Nacry P (2016) Nitrate controls root development through post-transcriptional regulation of the NRT1.1/NPF6.3 transporter/sensor. Plant Physiol. 172: 1237-1248.

Bürkle L, Cedzich A, Döpke C, Stransky H, Okumoto S, Gillissen B, Kühn C, Frommer WB (2003) Transport of cytokinins mediated by purine transporters of the PUP family expressed in phloem, hydathodes, and pollen of Arabidopsis. Plant J. 34: 13-26.

Camarena-Pozos DA, Flores-Núñez VM, López MG, López-Bucio J, Partida-Martínez LP (2019) Smells from the desert: microbial volatiles that affect plant growth and development of native and non-native plant species. Plant Cell Environ. 42: 1368-1380.

Cao ZY, Xuan W, Liu ZY, Li XN, Zhao N, Xu P, Wang Z, Guan RZ, Shen WB (2007) Carbon monoxide promotes lateral root formation in rapeseed. J. Integr. Plant Biol. 49: 1070-1079.

Casarrubia S, Sapienza S, Fritz H, Daghino S, Rosenkranz M, Schnitzler JP, Martin F, Perotto S, Martino E (2016) Ecologically different fungi affect Arabidopsis development: contribution of soluble and volatile compounds. PLoS OnE. 11: e0168236. doi:10.1371/journal.pone.0168236.

Carretero-Paulet L, Ahumada I, Cunillera N, Rodríguez-Concepción M, Ferrer A, Boronat A, Campos N (2002) Expression and molecular analysis of the Arabidopsis DXR gene encoding 1-deoxy-D-xylulose 5-phosphate reductoisomerase, the first committed enzyme of the 2-C-methyl-D-erythritol 4-phosphate pathway. Plant Physiol. 129: 1581-1591.

Ceccarelli EA, Arakaki AK, Cortez N, Carrillo N (2004) Functional plasticity and catalytic efficiency in plant and bacterial ferredoxin-NADP(H) reductases. Biochim. Biophys. Acta. 1698: 155-165.

Charles, S.A., Halliwell, B (1980) Properties of freshly purified and thiol-treated spinach chloroplast fructose bisphosphatase. Biochem. J. 185: 689-693.

Chan KX, Phua SY, Crisp P, McQuinn R, Pogson BJ (2016) Learning the languages of the chloroplast: Retrograde signaling and beyond. Annu. Rev. Plant Biol. 67: 25-53.

Chaput M, Claes V, Portetelle D, Cludts I, Cravador A, Burny A, Gras, H, Tartar A (1988) The neurotrophic factor neuroleukin is 90% homologous with phosphohexose isomerase. Nature. 332: 454-455.

Chen J, Wu FH, Wang WH, Zheng CJ, Lin GH, Dong XJ, He JX, Pei ZM, Zheng HL (2011) Hydrogen sulphide enhances photosynthesis through promoting chloroplast biogenesis, photosynthetic enzyme expression, and thiol redox modification in *Spinacia oleracea* seedlings. J. Exp. Bot. 62: 4481-4493.

Chen L, Hegde R, Chen M, Fromm HJ (1993) Site-specific mutagenesis of the metal binding sites of porcine fructose-16,-bisphosphatase. Arch. Biochem. Biophys. 307: 350-354.

Chiadmi M, Navaza A, Miginiac-Maslow M, Jacquot JP, Cherfils J (1999) Redox signaling in the chloroplast: structure of oxidized pea fructose-1,6-bisphosphate phosphatase. EMBO J. 18: 6809-6815.

Cho SM, Kang BR, Han SH, Anderson AJ, Park JY, Lee YH, Cho BH, Yang KY, Ryu CM, Kim YC (2008) 2R,3R-butanediol, a bacterial volatile produced by *Pseudomonas chlororaphis* O6, is involved in induction of systemic tolerance to drought in *Arabidopsis thaliana*. Mol. Plant Microbe Interact. 21: 1067-1075.

Cho MH, Lim H, Shin DH, Jeon JS, Bhoo SH, Park Y Il, Hahn TR (2011) Role of the plastidic glucose translocator in the export of starch degradation products from the chloroplasts in *Arabidopsis thaliana*. New Phytol. 190: 101-112.

Clough SJ, Bent AF (1998) Floral dip: A simplified method for Agrobacterium-mediated transformation of *Arabidopsis thaliana*. Plant J. 16: 735-743.

Conrath U, Amoroso G, Köhle H, Sültemeyer DF (2004) Non-invasive online detection of nitric oxide from plants and some other organisms by mass spectrometry. Plant J. 38: 1015-1022.

Córdoba E, Salmi M, León P (2009) Unravelling the regulatory mechanisms that modulate the MEP pathway in higher plants. J. Exp. Bot. 60: 2933-2943.

Cordovez V, Mommer L, Moisan K, Lucas-Barbosa D, Pierik R, Mumm R, Carrion VJ, Raaijmakers JM (2017) Plant phenotypic and transcriptional changes induced by volatiles from the fungal root pathogen *Rhizoctonia solani*. Front. Plant Sci. 8:1262. doi: 10.3389/fpls.2017.01262.

Cortleven A, Schmülling T (2015) Regulation of chloroplast development and function by cytokinin. J. Exp. Bot. 66: 4999-5013.

Cortleven A, Valcke R (2012) Evaluation of the photosynthetic activity in transgenic tobacco plants with altered endogenous cytokinin content: lessons from cytokinin. Physiol. Plant.144: 394-408.

Couturier J, Chibani K, Jacquot JP, Rouhier N (2013) Cysteine-based redox regulation and signaling in plants. Front. Plant Sci. 4: 105. doi: 10.3389/fpls.2013.00105.

Crisp PA, Ganguly DR, Smith AB, Murray KD, Estavillo GM, Searle I, Ford E, Bogdanović O, Lister R, Borevitz JO, Eichten SR, Pogson BJ (2017) Rapid recovery gene downregulation during excess-light stress and recovery in Arabidopsis. Plant Cell. 29: 1836-1863.

Da Q, Wang P, Wang M, Sun T, Jin H, Liu B, Wang J, Grimm B, Wang H Bin (2017)

Thioredoxin and NADPH-dependent thioredoxin reductase C regulation of tetrapyrrole biosynthesis. Plant Physiol. 175: 652-666.

De-la-Peña C, Loyola-Vargas VM (2014) Biotic interactions in the rhizosphere: a diverse cooperative enterprise for plant productivity. Plant Physiol. 166: 701-709.

Delgado-Baquerizo M, Maestre FT, Reich PB, Jeffries TC, Gaitan JJ, Encinar D, Berdugo M, Campbell CD, Singh BK (2016) Microbial diversity drives multifunctionality in terrestrial ecosystems. Nat. Commun. 7:10541. doi: 10.1038/ncomms10541.

Denison FC, Paul AL, Zupanska AK, Ferl RJ (2011) 14-3-3 proteins in plant physiology. Semin. Cell Dev. Biol. 22: 720-727.

Dietz KJ (1985) A possible rate-limiting function of chloroplast hexosemonophosphate isomerase in starch synthesis of leaves. Biochim. Biophys. Acta - Gen. Subj. 839: 240-248.

Ditengou FA, Müller A, Rosenkranz M, Felten J, Lasok H, Van Doorn MM, Legué V, Palme K, Schnitzler JP, Polle A (2015) Volatile signalling by sesquiterpenes from ectomycorrhizal fungi reprogrammes root architecture. Nat. Commun. 6. doi: 10.1038/ncomms7279.

Dong Z, Wu L, Kettlewell B, Caldwell CD, Layzell DB (2003) Hydrogen fertilization of soils - Is this a benefit of legumes in rotation? Plant Cell Environ. 26: 1875-1879.

Donnelly MI, Dagley S (1980) Production of methanol from aromatic acids by Pseudomonas putida. Journal of Bacteriology 142: 916-924.

Dooley FD, Nair SP, Ward PD (2013) Increased growth and germination success in plants following hydrogen sulfide administration. PLoS ONE 8: e62048.

Du SY, Zhang XF, Lu Z, Xin Q, Wu Z, Jiang T, Lu Y, Wang XF, Zhang DP (2012) Roles of the different components of magnesium chelatase in abscisic acid signal transduction. Plant Mol. Biol. 80: 519-537.

Dyson BC, Allwood JW, Feil R, Xu Y, Miller M, Bowsher CG, Goodacre R, Lunn JE, Johnson GN (2015) Acclimation of metabolism to light in *Arabidopsis thaliana*: The glucose 6-phosphate/phosphate translocator GPT2 directs metabolic acclimation. Plant Cell Environ. 38: 1404-1417.

Dyson BC, Webster RE, Johnson GN (2014) GPT2: A glucose 6-phosphate/phosphate translocator with a novel role in the regulation of sugar signalling during seedling development. Ann. Bot 113: 643-652.

Engel RR, Matsen JM, Chapman SS, Schwartz S (1972) Carbon monoxide production from heme compounds by bacteria. J. Bacteriol. 112: 1310-1315.

Entus R, Poling M, Herrmann KM (2002) Redox regulation of Arabidopsis 3-deoxy-D-arabino-heptulosonate 7-phosphate synthase. Plant Physiol. 129: 1866-1871.

Estavillo GM, Crisp PA, Pornsiriwong W, Wirtz M, Collinge D, Carrie C, Giraud E, Whelan J, David P, Javot H, Brearley C, Hell R, Marin E, Pogson BJ (2011) Evidence for a SAL1-PAP chloroplast retrograde pathway that functions in drought and high light signaling in Arabidopsis. Plant Cell 23: 3992-4012.

Ezquer I, Li J, Ovecka M, Baroja-Fernández E, Muñoz FJ, Montero M, Díaz de Cerio J, Hidalgo M, Sesma MT, Bahaji A, Etxeberria E, Pozueta-Romero J (2010) Microbial volatile emissions promote accumulation of exceptionally high levels of starch in leaves in mono- and dicotyledonous plants. Plant Cell Physiol. 51: 1674-1693.

Ferreira FJ, Kieber JJ (2005) Cytokinin signaling. Curr. Opin. Plant Biol. 145: 1-8.

Fincheira P, Quiroz A (2018) Microbial volatiles as plant growth inducers. Microbiol. Res. 208: 63-75.

Foreman J, Demidchik V, Bothwell JH, Mylona P, Miedema H, Torres MA, Linstead P, Costa S, Brownlee C, Jones JD, Davies JM, Dolan L (2003) Reactive oxygen species produced by NADPH oxidase regulate plant cell growth. Nature 422: 442-446.

Flütsch S, Horrer D, Santelia D (2022) Starch biosynthesis in guard cells has features of both autotrophic and heterotrophic tissues. Plant Physiol. 189: 541-556.

Fünfgeld MMFF, Wang W, Ishihara H, Arrivault S, Feil R, Smith AM, Stitt M, Lunn JE, Niittylä T (2022) Sucrose synthases are not involved in starch synthesis in Arabidopsis leaves. Nat. Plants. doi: 10.1038/s41477-022-01140-y.

Gansel X, Muños S, Tillard P, Gojon A (2001) Differential regulation of the NO_3^- and NH_4^+ transporter genes AtNrt2.1 and AtAmt1.1 in Arabidopsis: relation with long-distance and local controls by N status of the plant. Plant J. 26: 143-155.

Gámez-Arcas S, Baroja-Fernández E, García-Gómez P, Muñoz FJ, Almagro G, Bahaji A, Sánchez-López ÁM, Pozueta-Romero J (2022a) Action mechanisms of small microbial volatile compounds in plants. J. Exp. Bot. 73: 498-510.

Gámez-Arcas S, Muñoz FJ, Ricarte-Bermejo A, Sánchez-López ÁM, Baslam M, Baroja-Fernández E, Bahaji A, Almagro G, De Diego N, Dolezal K, Novák O,

Leal-López J, Morcillo RJL, Castillo AG, Pozueta-Romero J (2022b) Glucose-6-P/phosphate translocator2 mediates the phosphoglucose-isomerase-1 independent response to microbial volatiles. Plant Physiol. doi: 10.1093/plphys/kiac433.

García-Gómez P, Almagro G, Sánchez-López ÁM, Bahaji A, Ameztoy K, Ricarte-Bermejo A, Baslam M, Antolín MC, Urdiain A, López-Belchi MD, López-Gómez P, Morán JF, Garrido J, Muñoz FJ, Baroja-Fernández E, Pozueta-Romero J (2019) Volatile compounds other than CO_2 emitted by different microorganisms promote distinct posttranscriptionally regulated responses in plants. Plant Cell Environ. 42: 1729-1746.

García-Gómez P, Bahaji A, Gámez-Arcas S, Muñoz FJ, Sánchez-lópez ÁM, Almagro G, Baroja-Fernández E, Ameztoy K, De Diego N, Ugena L, Spíchal L, Doležal K, Hajirezaei MR, Romero LC, García I, Pozueta-Romero J (2020) Volatiles from the fungal phytopathogen *Penicillium aurantiogriseum* modulate root metabolism and architecture through proteome resetting. Plant Cell Environ. 43: 2551-2570.

Garcia-Molina A, Kleine T, Schneider K, Mühlhaus T, Lehmann M, Leister D (2020) Translational components contribute to acclimation responses to high light, heat, and cold in Arabidopsis. iScience. doi: 10.1016/j.isci.2020.101331.

García I, Castellano JM, Vioque B, Solano R, Gotor C, Romero LC (2010) Mitochondrial β-cyanoalanine synthase is essential for root hair formation in *Arabidopsis thaliana*. Plant Cell 22: 3268-3279.

Garnica-Vergara A, Barrera-Ortiz S, Muñoz-Parra E, Raya-González J, Méndez-Bravo A, Macías-Rodríguez L, Ruiz-Herrera LF, López-Bucio J (2016) The volatile 6-pentyl-2H-pyran-2-one from *Trichoderma atroviride* regulates *Arabidopsis thaliana* root morphogenesis via auxin signaling and ETHYLENE INSENSITIVE 2 functioning. New Phytol. 209: 1496-1512.

Gautam H, Sehar Z, Rehman MT, Hussain A, AlAjmi MF, Khan NA (2021) Nitric oxide enhances photosynthetic nitrogen and sulfur-use efficiency and activity of ascorbate-glutathione cycle to reduce high temperature stress-induced oxidative stress in rice (*Oryza sativa* L.) plants. Biomolecules 11: 305.

Ghirardo A, Wright LP, Bi Z, Rosenkranz M, Pulido P, Rodríguez-Concepción M, Niinemets Ü, Brüggemann N, Gershenzon J, Schnitzler JP (2014) Metabolic flux analysis of plastidic isoprenoid biosynthesis in poplar leaves emitting and nonemitting isoprene. Plant Physiol. 165: 37-51.

Ghirardo A, Zimmer I, Brüggemann N, Schnitzler JP (2010) Analysis of 1-deoxy-d-xylulose 5-phosphate synthase activity in Grey poplar leaves using isotope ratio mass spectrometry. Phytochemistry 71: 918-922.

Giese JO, Herbers K, Hoffmann M, Klösgen RB, Sonnewald U (2005) Isolation and functional characterization of a novel plastidic hexokinase from *Nicotiana tabacum*. FEBS Lett. 579: 827-831.

Gjindali A, Herrmann HA, Schwartz JM, Johnson GN, Calzadilla PI (2021) A holistic approach to study photosynthetic acclimation responses of plants to fluctuating light. Front. Plant Sci. doi: 10.3389/fpls.2021.668512.

Gonzali S, Loreti E, Solfanelli C, Novi G, Alpi A, Perata P (2006) Identification of sugar-modulated genes and evidence for in vivo sugar sensing in Arabidopsis. J. Plant Res. 119: 115-123.

Groenhagen U, Baumgartner R, Bailly A, Gardiner A, Eberl L, Schulz S, Weisskopf L (2013) Production of bioactive volatiles by different *Burkholderia ambifaria* strains. J. Chem. Ecol. 39: 892-906.

Guo K, Kong WW, Yang ZM (2009) Carbon monoxide promotes root hair development in tomato. Plant Cell Environ. 32: 1033-1045.

Guo K, Xia K, Yang ZM (2008). Regulation of tomato lateral root development by carbon monoxide and involvement in auxin and nitric oxide. J. Exp. Bot. 59: 3443-3452.

Gutiérrez-Luna FM, López-Bucio J, Altamirano-Hernández J, Valencia-Cantero E, Reyes de La Cruz H, Macías-Rodríguez L (2010) Plant growth-promoting rhizobacteria modulate root-system architecture in *Arabidopsis thaliana* through volatile organic compound emission. Symbiosis 51: 75-83.

Han B, Yang Z, Xie Y, Nie L, Cui J, Shen W (2014) Arabidopsis HY1 confers cadmium tolerance by decreasing nitric oxide production and improving iron homeostasis. Mol. Plant 7: 388-403.

Hammond JP, Bennett MJ, Bowen HC, Broadley MR, Eastwood DC, May ST, Rahn C, Swarup R, Woolaway KE, White PJ (2003) Changes in gene expression in Arabidopsis shoots during phosphate starvation and the potential for developing smart plants. Plant Physiol. 132: 578-596.

Harrison EP, Willingham NM, Lloyd JC, Raines CA (1998) Reduced sedoheptulose-1,7-bisphosphatase levels in transgenic tobacco lead to decreased photosynthetic capacity and altered carbohydrate accumulation. Planta 204: 27-36.

He Y, Tang RH, Hao Y, Stevens RD, Cook CW, Ahn SM, Jing L, Yang Z, Chen L, Guo F, Fiorani F, Jackson RB, Crawford NM, Pei ZM (2004) Nitric oxide represses the Arabidopsis floral transition. Science 305: 1968-1971.

Hebelstrup KH, Jensen EØ (2008) Expression of NO scavenging hemoglobin is involved in the timing of bolting in *Arabidopsis thaliana*. Planta 227: 917-927.

Hebelstrup KH, Van Zanten M, Mandon J, Voesenek LACJ, Harren FJM, Cristescu SM, Møller IM, Mur LAJ (2012) Haemoglobin modulates NO emission and hyponasty under hypoxia-related stress in *Arabidopsis thaliana*. J. Exp. Bot. 63: 5581-5591.

Hendriks JHM, Kolbe A, Gibon Y, Stitt M, Geigenberger P (2003) ADP-glucose pyrophosphorylase is activated by posttranslational redox-modification in response to light and to sugars in leaves of Arabidopsis and other plant species. Plant Physiol. 133: 838-849.

Henkes S, Sonnewald U, Badur R, Flachmann R, Stitt M (2001) A small decrease of plastid transketolase activity in antisense tobacco transformants has dramatic effects on photosynthesis and phenylpropanoid metabolism. Plant Cell 13: 535-551.

Heuer B, Hansen MJ, Anderson LE (1982) Light modulation of phosphofructokinase in pea leaf chloroplasts. Plant Physiol. 69: 1404-1406.

Hill RD (2012) Non-symbiotic haemoglobins-What's happening beyond nitric oxide scavenging? AoB Plants doi: 10.1093/aobpla/pls004.

Ho CH, Lin SH, Hu HC, Tsay YF (2009) CHL1 functions as a nitrate sensor in plants. Cell 138: 1184-1194.

Hooper CM, Castleden IR, Tanz SK, Aryamanesh N, Millar AH (2017) SUBA4: The interactive data analysis centre for Arabidopsis subcellular protein locations. Nucleic Acids Res. doi: 10.1093/nar/gkw1041.

Huang AC, Jiang T, Liu YX, Bai YC, Reed J, Qu B, Goossens A, Nützmann HW, Bai Y, Osbourn A (2019) A specialized metabolic network selectively modulates Arabidopsis root microbiota. Science doi: 10.1126/science.aau6389.

Hunt PW, Klok EJ, Trevaskis B, Watts RA, Ellis MH, Peacock WJ, Dennis ES (2002) Increased level of hemoglobin 1 enhances survival of hypoxic stress and promotes early growth in *Arabidopsis thaliana*. Proc. Natl. Acad. Sci. USA 99: 17197-17202.

Jacquot JP, López-Jaramillo J, Chueca A, Cherfils J, Lemaire S, Chedozeau B, Miginiac-Mslow M, Decottignies P, Wolosiuk R, López-Gorge J (1995) High-level expression of recombinant pea chloroplast fructose-1,6-bisphosphatase and mutagenesis of its regulatory site. Eur. J. Biochem. 229: 675-681.

Jacquot JP, Lopez-Jaramillo J, Miginiac-Maslow M, Lemaire S, Cherfils J, Chueca A, López-Gorger J (1997) Cysteine-153 is required for redox regulation of pea chloroplast fructose-1,6-bisphosphatase. FEBS Lett. 401: 143-147.

Jefferson R, Kavanagh T, Bevan M (1987) GUS fusion: beta -glucuronidase as a sensitive and versatile gene fusion marker in higher plants. Embo J. 6: 3901-3907.

Jeffery C, Bahnson BJ, Chien W, Ringe D, Petsko, GA (2000) Crystal structure of rabbit phosphoglucose isomerase, a glycolytic enzyme that moonlights as neuroleukin, autocrine motility factor, and differentiation mediator. Biochemistry 39: 955-964.

Jin CW, Du ST, Zhang YS, Tang C, Lin X (2009) Atmospheric nitric oxide stimulates plant growth and improves the quality of spinach (*Spinacia oleracea*). Ann. Appl. Biol. 155: 113-120.

Jin Q, Zhu K, Cui W, Xie Y, Han B, Shen W (2013) Hydrogen gas acts as a novel bioactive molecule in enhancing plant tolerance to paraquat-induced oxidative stress via the modulation of heme oxygenase-1 signalling system. Plant Cell Environ. 155: 113-120.

Johnson GN (2005) Cyclic electron transport in C3 plants: Fact or artefact? J. Exp. Bot. 56: 407-416.

Johnson EG, Sparks JP, Dzikovski B, Crane BR, Gibson DM, Loria R (2008) Plant-pathogenic Streptomyces species produce nitric oxide synthase-derived nitric oxide in response to host signals. Chem. Biol. 15: 43-50.

Kai M, Piechulla B (2009) Plant growth promotion due to rhizobacterial volatiles - An effect of CO_2? FEBS Lett. 583: 3473-3477.

Kammerer B, Fischer K, Hilpert B, Schubert S, Gutensohn M, Weber A, Flugge UI (1998) Molecular characterization of a carbon transporter in plastids from heterotrophic tissues: The glucose 6-phosphate/phosphate antiporter. Plant Cell 10: 105-117.

Kanchiswamy CN, Malnoy M, Maffei ME (2015) Chemical diversity of microbial volatiles and their potential for plant growth and productivity. Front Plant Sci. 6: 151. doi: 10.3389/fpls.2015.00151.

Karim MF (2021) Acclimation of photosynthesis to changes in the environment results in decreases of oxidative stress in *Arabidopsis thaliana*. Front Plant Sci. doi: 10.3389/fpls.2021.683986.

Kiba T, Takebayashi Y, Kojima M, Sakakibara H (2019). Sugar-induced de novo

cytokinin biosynthesis contributes to Arabidopsis growth under elevated CO_2. Sci. Rep. 9:7765. doi: 10.1038/s41598-019-44185-4.

Kieber JJ, Schaller GE (2014) Cytokinins. Arabidopsis Book. doi: 10.1199/tab.0168.

Kirchsteiger K, Pulido P, González M, Cejudo FJ (2009) NADPH Thioredoxin reductase C controls the redox status of chloroplast 2-Cys peroxiredoxins in *Arabidopsis thaliana*. Mol. Plant 2: 298-307.

Ko D, Kang J, Kiba T, Park J, Kojima M, Do J, Kim KY, Kwon MM, Endler A, Song WY, Martinoia E, Sakakibara H, Lee Y (2014) Arabidopsis ABCG14 is essential for the root-to-shoot translocation of cytokinin. Proc. Natl. Acad. Sci. USA 111: 7150-7155.

Körner C (2015) Paradigm shift in plant growth control. Curr. Opin. Plant Biol. 25: 107-114.

Kossmann J, Sonnewald U, Willmitzer L (1994) Reduction of the chloroplastic fructose-1,6-bisphosphatase in transgenic potato plants impairs photosynthesis and plant growth. Plant J. 6: 637-650.

Kunz HH, Häusler RE, Fettke J, Herbst K, Niewiadomski P, Gierth M, Bell K, Steup M, Flügge UI, Schneider A (2010) The role of plastidial glucose-6-phosphate/ phosphate translocators in vegetative tissues of *Arabidopsis thaliana* mutants impaired in starch biosynthesis. Plant Biol. 12: 115-128.

Kuruthukulangarakoola GT, Zhang J, Albert A, Winkler B, Lang H, Buegger F, Gaupels F, Heller W, Michalke B, Sarioglu H, Schnitzler JP, Hebelstrup KH, Durner J, Lindermayr C (2017) Nitric oxide-fixation by non-symbiotic haemoglobin proteins in *Arabidopsis thaliana* under N-limited conditions. Plant Cell Environ. 40: 36-50.

Kushwah S, Laxmi A (2014) The interaction between glucose and cytokinin signal transduction pathway in *Arabidopsis thaliana*. Plant Cell Environ. 37: 235-253.

Kwon YS, Ryu CM, Lee S, Park HB, Han KS, Lee JH, Lee K, Chung WS, Jeong MJ Kim HK, Bae DW (2010) Proteome analysis of Arabidopsis seedlings exposed to bacterial volatiles. Planta 232: 1355-1370.

Lämke J, Bäurle I (2017) Epigenetic and chromatin-based mechanisms in environmental stress adaptation and stress memory in plants. Genome Biol. 18: 124. doi: 10.1186/ s13059-017-1263-6.

Lan P, Li W, Schmidt W (2012) Complementary proteome and transcriptome profiling in phosphate-deficient Arabidopsis roots reveals multiple levels of gene regulation.

Mol. Cell. Proteomics 11: 1156-1166.

Ledger T, Rojas S, Timmermann T, Pinedo I, Poupin MJ, Garrido T, Richter P, Tamayo J, Donoso R (2016) Volatile-mediated effects predominate in *Paraburkholderia phytofirmans* growth promotion and salt stress tolerance of *Arabidopsis thaliana*. Front. Microbiol. 7: 1-18.

Lei M, Liu Y, Zhang B, Zhao Y, Wang X, Zhou Y, Raghothama KG, Liu D (2011) Genetic and genomic evidence that sucrose is a global regulator of plant responses to phosphate starvation in Arabidopsis. Plant Physiol. 156: 1116-1130.

Lejay L, Wirth J, Pervent M, Cross JMF, Tillard P, Gojon A (2008) Oxidative pentose phosphate pathway-dependent sugar sensing as a mechanism for regulation of root ion transporters by photosynthesis. Plant Physiol. 146: 2036-2053.

Lemfack MC, Gohlke BO, Toguem SMT, Preissner S, Piechulla B, Preissner R (2018) mVOC 2.0: a database of microbial volatiles. Nucleic Acids Res 46: 1261-1265.

Lewis DR, Negi S, Sukumar P, Muday GK (2011) Ethylene inhibits lateral root development, increases IAA transport and expression of PIN3 and PIN7 auxin efflux carriers. Development 138: 3485-3495.

Li J, Chen S, Wang X, Shi C, Liu H, Yang J, Shi W, Guo J, Jia H (2018a) Hydrogen sulfide disturbs actin polymerization via S-sulfhydration resulting in stunted root hair growth. Plant Physiol. 178: 936-949.

Li J, Ezquer I, Bahaji A, Montero M, Ovecka M, Baroja-Fernández E, Muñoz FJ, Mérida Á, Almagro G, Hidalgo M, et al (2011) Microbial volatile-induced accumulation of exceptionally high levels of starch in Arabidopsis leaves is a process involving NTRC and starch synthase classes III and IV. Mol. Plant Microbe Interact. 24: 1165-1178.

Li N, Wang W, Bitas V, Subbarao K, Liu X, Kang S (2018b) Volatile compounds emitted by diverse Verticillium species enhance plant growth by manipulating auxin signaling. Mol. Plant Microbe Interact 31: 1021-1031.

Lin Y, Zhang W, Qi F, Cui W, Xie Y, Shen W (2014) Hydrogen-rich water regulates cucumber adventitious root development in a heme oxygenase-1/carbon monoxide-dependent manner. J. Plant Physiol. 171: 1-8.

Lichtenthaler HK (1987) Chlorophylls and carotenoids: Pigments of photosynthetic biomembranes. Methods Enzymol. 148: 350-382.

Lima JE, Kojima S, Takahashi H, Von Wiren N (2010) Ammonium triggers lateral root

branching in Arabidopsis in an AMMONIUM TRANSPORTER1;3-dependent manner. Plant Cell 22: 3621-3633.

Lisjak M, Teklic T, Wilson ID, Whiteman M, Hancock JT (2013) Hydrogen sulfide: environmental factor or signalling molecule? Plant Cell Environ 36: 1607-1616.

Lister R, O'Malley RC, Tonti-Filippini J, Gregory BD, Berry CC, Millar AH, Ecker JR (2008) Highly integrated single-base resolution maps of the epigenome in Arabidopsis. Cell 133: 523-536.

Liu P, Zhang H, Wang H, Xia Y (2014) Identification of redox-sensitive cysteines in the Arabidopsis proteome using OxiTRAQ, a quantitative redox proteomics method. Proteomics 14: 750-762.

Long SP, Bernacchi CJ (2003) Gas exchange measurements, what can they tell us about the underlying limitations to photosynthesis? Procedures and sources of error. J. Exp. Bot. 54: 2393-2401.

Llamas E, Pulido P, Rodriguez-Concepcion M (2017) Interference with plastome gene expression and Clp protease activity in Arabidopsis triggers a chloroplast unfolded protein response to restore protein homeostasis. PLoS Genet. doi.org/10.1371/journal.pgen.1007022.

Makino A, Tadahiko M, Mae T (1999) Photosynthesis and plant growth at elevated levels of CO_2. Plant Cell Physiol. 40: 999-1006.

Mangano S, Denita-Juarez SP, Choi HS, Marzol E, Hwang Y, Ranocha P, Velasquez SM, Borassi C, Barberini ML, Aptekmann AA, Muschietti JP, Nadra AD, Dunand C, Cho HT, Estevez JM (2017) Molecular link between auxin and ROS-mediated polar growth. Proc. Natl. Acad. Sci. USA 114: 5289-5294.

Martínez-Medina A, Van Wees SCM, Pieterse CMJ (2017) Airborne signals from Trichoderma fungi stimulate iron uptake responses in roots resulting in priming of jasmonic aciddependent defences in shoots of *Arabidopsis thaliana* and *Solanum lycopersicum*. Plant Cell Environ. 40: 2691-2705.

McWhite CD, Papoulas O, Drew K, Cox RM, June V, Dong OX, Kwon T, Wan C, Salmi ML, Roux SJ, Browning KS, Chen ZJ, Ronald PC, Marcotte EM (2020) A pan-plant protein complex map reveals deep conservation and novel assemblies. Cell 181: 460-474.

Mei Y, Chen H, Shen W, Shen W, Huang L (2017) Hydrogen peroxide is involved in hydrogen sulfide-induced lateral root formation in tomato seedlings. BMC Plant Biol. 17: 162. doi: 10.1186/s12870-017-1110-7.

Merchante C, Stepanova AN, Alonso JM (2017) Translation regulation in plants: an interesting past, an exciting present and a promising future. Plant J. 90: 628-653.

Miller MAE, O'Cualain R, Selley J, Knight D, Karim MF, Hubbard SJ, Johnson GN (2017) Dynamic acclimation to high light in *Arabidopsis thaliana* involves widespread reengineering of the leaf proteome. Front. Plant Sci. doi: 10.3389/fpls.2017.01239.

Mitchum MG, Yamaguchi S, Hanada A, Kuwahara A, Yoshioka Y, Kato T, Tabata S, Kamiya Y, Sun TP (2006) Distinct and overlapping roles of two gibberellin 3-oxidases in Arabidopsis development. Plant J. 45: 804-818.

Miyawaki K, Matsumoto-Kitano M, Kakimoto T (2004) Expression of cytokinin biosynthetic isopentenyltransferase genes in Arabidopsis: Tissue specificity and regulation by auxin, cytokinin, and nitrate. Plant J. 37: 128-138.

Molina-Favero C, Creus CM, Simontacchi M, Puntarulo S, Lamattina L (2008) Aerobic nitric oxide production by *Azospirillum brasilense* Sp245 and its influence on root architecture in tomato. Mol. Plant Microbe Interact. 21: 1001-1009.

Moore B, Zhou L, Rolland F, Hall Q, Cheng WH, Liu YX, Hwang I, Jones T, Sheen J (2003) Role of the Arabidopsis glucose sensor HXK1 in nutrient, light, and hormonal signaling. Science 300: 332-336.

Murakami R, Ifuku K, Takabayashi A, Shikanai T, Endo T, Sato F (2005) Functional dissection of two Arabidopsis PsbO proteins PsbO1 and PsbO2. FEBS J. 272: 2165-2175.

Nagawa S, Sawa S, Sato S, Kato T, Tabata S, Fukuda H (2006) Gene trapping in Arabidopsis reveals genes involved in vascular development. Plant Cell Physiol. 47: 1394-1405.

Nakaminami K, Matsui A, Nakagami H, Minami A, Nomura Y, Tanaka M, Morosawa T, Ishida J, Takahashi S, Uemura M, Shirasu K, Seki M (2014) Analysis of differential expression patterns of mRNA and protein during cold-acclimation and de-acclimation in Arabidopsis. Mol. Cell Proteomics 13: 3602-3611.

Nandi R, Sengupta S (1998) Microbial production of hydrogen: an overview. Crit. Rev. Microbiol 24: 61-84.

Naranjo B, Mignée C, Krieger-Liszkay A, Hornero-Méndez D, Gallardo-Guerrero L, Cejudo, FJ, Lindahl M (2016). The chloroplast NADPH thioredoxin reductase C, NTRC, controls non-photochemical quenching of light energy and photosynthetic electron transport in Arabidopsis. Plant Cell Environ. 39: 804-822.

Naznin HA, Kimura M, Miyazawa M, Hyakumachi M (2013) Analysis of volatile organic compounds emitted by plant growth-promoting fungus Phoma sp. GS8-3 for growth promotion effects on tobacco. Microbes Environ. 28: 42-49.

Negi S, Ivanchenko MG, Muday GK (2008) Ethylene regulates lateral root formation and auxin transport in *Arabidopsis thaliana*. Plant J. 55: 175-187.

Nelson SW, Honzatko RB, Fromm HJ (2004) Origin of cooperativity in the activation of fructose-1,6-bisphosphatase by Mg^{2+}. J. Biol. Chem. 279: 18481-18487.

Niewiadomski P, Knappe S, Geimer S, Fischer K, Schulz B, Unte US, Rosso MG, Ache P, Flügge UI, Schneider A (2005) The Arabidopsis plastidic glucose 6-phosphate/phosphate translocator GPT1 is essential for pollen maturation and embryo sac development. Plant Cell 17: 769-775.

Nikkanen L, Toivola J, Rintamäki E (2016) Crosstalk between chloroplast thioredoxin systems in regulation of photosynthesis. Plant Cell Environ. 39: 1691-1705.

Nishimura K, Asakura Y, Friso G, Kim J, Oh SH, Rutschow H, Ponnala L, van Wijk KJ (2013) ClpS1 is a conserved substrate selector for the chloroplast Clp protease system in Arabidopsis. Plant Cell 25: 2276-2301.

Niu Y, Jin C, Jin G, Zhou Q, Lin X, Tang C, Zhang YS (2011) Auxin modulates the enhanced development of root hairs in *Arabidopsis thaliana* (L.) Heynh. under elevated CO_2. Plant Cell Environ. 34: 1304-1317.

Nonomura AM, Benson AA (1992). The path of carbon in photosynthesis: Improved crop yields with methanol. Proc. Natl. Acad. Sci. USA 89: 9794-9798.

Novák O, Hauserová E, Amakorová P, Doležal K, Strnad M (2008) Cytokinin profiling in plant tissues using ultra-performance liquid chromatography-electrospray tandem mass spectrometry. Phytochemistry 69: 2214-2224.

Ojeda V, Pérez-Ruiz JM, González M, Nájera VA, Sahrawy M, Serrato AJ, Geigenberger P, Cejudo FJ (2017) NADPH thioredoxin reductase C and thioredoxins act concertedly in seedling development. Plant Physiol. 174: 1436-1448.

Park YS, Dutta S, Ann M, Raaijmakers JM, Park K (2015) Promotion of plant growth by *Pseudomonas fluorescens* strain SS101 via novel volatile organic compounds. Biochem. Biophys. Res. Commun. 461: 361-365.

Passardi F, Tognolli M, De Meyer M, Penel C, Dunand C (2006) Two cell wall associated peroxidases from Arabidopsis influence root elongation. Planta 223: 965-974.

Pérez-Ruiz JM (2006) Rice NTRC is a high-efficiency redox system for chloroplast protection against oxidative damage. Plant Cell 18: 2356-2368.

Pérez-Ruiz JM, Guinea M, Puerto-Galán L, Cejudo FJ (2014) NADPH thioredoxin reductase C is involved in redox regulation of the Mg-chelatase I subunit in *Arabidopsis thaliana* chloroplasts. Mol. Plant 7: 1252-1255.

Pérez-Ruiz JM, Naranjo B, Ojeda V, Guinea M, Cejudo FJ (2017) NTRC-dependent redox balance of 2-Cys peroxiredoxins is needed for optimal function of the photosynthetic apparatus. Proc. Natl. Acad. Sci. USA 114: 12069-12074.

Philippot L, Raaijmakers JM, Lemanceau P, van Der Putten WH (2013) Going back to the roots: The microbial ecology of the rhizosphere. Nat. Rev Microbiol. 11: 789-799.

Piechulla B, Lemfack MC, Kai M (2017) Effects of discrete bioactive microbial volatiles on plants and fungi. Plant Cell Environ. 40: 2042-2067.

Piechulla B, Schnitzler JP (2016) Circumvent CO_2 effects in volatile-based microbe-plant interactions. Trends Plant Sci. 21: 541-543.

Pokhilko A, Bou-Torrent J, Pulido P, Rodríguez-Concepción M, Ebenhöh O (2015) Mathematical modelling of the diurnal regulation of the MEP pathway in Arabidopsis. New Phytol 206: 1075-1085.

Pozueta-Romero J, Ardila F, Akazawa T (1991) ADP-Glucose transport by the chloroplast adenylate translocator is linked to starch biosynthesis. Plant Physiol. 97: 1565-72.

Puerto-Galán L, Pérez-Ruiz JM, Guinea M, Cejudo FJ (2015) The contribution of NADPH thioredoxin reductase C (NTRC) and sulfiredoxin to 2-Cys peroxiredoxin overoxidation in *Arabidopsis thaliana* chloroplasts. J. Exp. Bot. 66: 2957-2966.

Pulido P, Spínola MC, Kirchsteiger K, Guinea M, Pascual MB, Sahrawy M, Sandalio LM, Dietz KJ, González M, Cejudo FJ (2010) Functional analysis of the pathways for 2-Cys peroxiredoxin reduction in *Arabidopsis thaliana* chloroplasts. J. Exp. Bot. 61: 4043-4054.

Pulido P, Toledo-Ortiz G, Phillips MA, Wright LP, Rodríguez-Concepción M (2013) Arabidopsis J-Protein J20 delivers the first enzyme of the plastidial isoprenoid pathway to protein quality control. Plant Cell 25: 4183-4194.

Ramírez I, Dorta F, Espinoza V, Jiménez E, Mercado A, Peña-Cortés H (2006) Effects of foliar and root applications of methanol on the growth of Arabidopsis, tobacco,

and tomato plants. J. Plant Growth Regul. 25: 30-44.

Reiland S, Messerli G, Baerenfaller K, Gerrits B, Endler A, Grossmann J, Gruissem W, Baginsky S (2009) Large-scale Arabidopsis phosphoproteome profiling reveals novel chloroplast kinase substrates and phosphorylation networks. Plant Physiol. 150: 889-903.

Richter AS, Peter E, Rothbart M, Schlicke H, Toivola J, Rintamäki E, Grimm B (2013) Posttranslational influence of NADPH-dependent thioredoxin reductase C on enzymes in tetrapyrrole synthesis. Plant Physiol. 16: 63-73.

Rodríguez-Concepción M, D'Andrea L, Pulido P (2019) Control of plastidial metabolism by the Clp protease complex. J. Exp. Bot. 70: 2049-2058.

Rodríguez-Suárez RJ, Mora-García S, Wolosiuk RA (1997) Characterization of cysteine residues involved in the reductive activation and structural stability of rapeseed (*Brassica napus*) chloroplast fructose-1,6-bisphosphatase. Biochem. Biophys. Res. Commun. 232: 388-393.

Rojas-González JA, Soto-Súarez M, García-Díaz Á, Romero-Puertas MC, Sandalio LM, Mérida Á (2015) Disruption of both chloroplastic and cytosolic FBPase genes results in a dwarf phenotype and important starch and metabolite changes in *Arabidopsis thaliana*. J. Exp. Bot. 66: 2673-2689.

Rolland F, Baena-Gonzalez E, Sheen J (2006) Sugar sensing and signaling in plants: conserved and novel mechanisms. Annu. Rev. Plant Biol. 57: 675-709.

Ryu CM, Farag MA, Hu CH, Reddy MS, Wei HX, Pare PW, Kloepper JW (2003) Bacterial volatiles promote growth in Arabidopsis. Proc. Natl. Acad. Sci. USA 100: 4927-4932.

Sahrawy M, Fernández-Trijueque J, Vargas P, Serrato AJ (2022) Comprehensive expression analyses of plastidial thioredoxins of *Arabidopsis thaliana* indicate a main role of thioredoxin *m2* in roots. Antioxidants 11: 1365 doi:10.3390/antiox11071365.

Sánchez-López ÁM, Bahaji A, De Diego N, Baslam M, Li J, Muñoz FJ, Almagro G, García-Gómez P, Ameztoy K, Ricarte-Bermejo A, Novák O, Humplík JF, Spíchal L, Doležal K, Ciordia S, Mena MC, Navajas R, Baroja-Fernández E, Pozueta-Romero J (2016a) Arabidopsis responds to *Alternaria alternata* volatiles by triggering plastid phosphoglucose isomerase-independent mechanisms. Plant Physiol. 172: 1989-2001.

Sánchez-López ÁM, Baslam M, De Diego N, Muñoz FJ, Bahaji A, Almagro G, Ricarte-

Bermejo A, García-Gómez P, Li J, Humplík JF, Novák O, Spíchal L, Doležal K, Baroja-Fernández E, Pozueta-Romero J (2016b) Volatile compounds emitted by diverse phytopathogenic microorganisms promote plant growth and flowering through cytokinin action. Plant Cell Environ. 39: 2592-2608.

Schink B, Zeikus JG (1980) Microbial methanol formation: a major end product of pectin metabolism. Curr. Microbiol. 4: 387-389.

Schreiber F, Wunderlin P, Udert KM, Wells GF (2012) Nitric oxide and nitrous oxide turnover in natural and engineered microbial communities: biological pathways, chemical reactions, and novel technologies. Front. Microbiol. doi: 10.3389/fmicb.2012.00372.

Schwender J, König C, Klapperstück M, Heinzel N, Munz E, Hebbelmann I, Hay JO, Denolf P, De Bodt S, Redestig H, Caestecker E, Jakob PM, Borisjuk L, Rolletschek H (2014) Transcript abundance on its own cannot be used to infer fluxes in central metabolism. Front. Plant Sci. doi: 10.3389/fpls.2014.00668.

Seki M, Carninci P, Nishiyama Y, Hayashizaki Y, Shinozaki K (1998) High-efficiency cloning of Arabidopsis full-length cDNA by biotinylated CAP trapper. Plant J. 15: 707-720.

Seki M, Narusaka M, Kamiya A, Ishida J, Satou M, Sakurai T, Nakajima M, Enju A, Akiyama K, Oono Y, Muramatsu M, Hayashizaki Y, Kawai J, Carninci P, Itoh M, Ishii Y, Arakawa T, Shibata K, Shinagawa A, Shinozakie K (2002) Functional annotation of a full-length Arabidopsis cDNA collection. Science 296: 141-5.

Sergeeva LI, Keurentjes JJB, Bentsink L, Vonk J, van der Plas LHW, Koornneef M, Vreugdenhil D (2006) Vacuolar invertase regulates elongation of *Arabidopsis thaliana* roots as revealed by QTL and mutant analysis. Proc. Natl. Acad. Sci. USA. 103: 2994-2999.

Serrato AJ, Romero-Puertas MC, Lázaro-Payo A, Sahrawy M (2018) Regulation by S-nitrosylation of the Calvin-Benson cycle fructose-1,6-bisphosphatase in *Pisum sativum*. Redox Biol. 14: 409-416.

Serrato A.J, Yubero-Serrano E.M, Sandalio L.M, Muñoz-Blanco J, Chueca A, Caballero JL, Sahrawy M (2009) cpFBPaseII, a novel redox-independent chlroplastic isoform of fructose-1,6 bisphosphatase. Plant Cell Environ. 32: 811-827.

Sharifi R, Jeon JS, Ryu CM (2022) Belowground plant-microbe communications via volatile compounds. J. Exp. Bot. 73:463-486.

Shatalin K, Shatalina E, Mironov A, Nudler E (2011) H_2S: a universal defense against

antibiotics in bacteria. Science 334: 986-990.

Siegel SM, Siegel BZ (1987) Biogenesis of carbon monoxide: production by fungi and seed plants in the dark. Phytochemistry 26: 3117-3119.

Silverstone AL, Chang CW, Krol E, Sun TP (1997) Developmental regulation of the gibberellin biosynthetic gene *GA 1* in *Arabidopsis thaliana*. Plant J. 12: 9-19.

Song X, Kristie DN, Reekie EG (2009) Why does elevated CO_2 affect time of flowering? An exploratory study using the photoperiodic flowering mutants of *Arabidopsis thaliana*. New Phytol.181: 339-346.

Splivallo R, Fischer U, Göbel C, Feussner I, Karlovsky P (2009) Truffles regulate plant root morphogenesis via the production of auxin and ethylene. Plant Physiol. 150: 2018-2029.

Steyfkens F, Zhang Z, Van Zeebroeck G, Thevelein JM (2018) Multiple transceptors for macro- and micro-nutrients control diverse cellular properties through the PKA pathway in yeast: A paradigm for the rapidly expanding world of eukaryotic nutrient transceptors up to those in human cells. Front. Pharmcol. 9:191 doi: 10.3389/fphar.2018.00191.

Takahashi M, Furuhashi T, Ishikawa N, Horiguchi G, Sakamoto A, Tsukaya H, Morikawa H (2014) Nitrogen dioxide regulates organ growth by controlling cell proliferation and enlargement in Arabidopsis. New Phytol 201: 1304-1315.

Takahashi M, Sakamoto A, Ezura H, Morikawa H (2011) Prolonged exposure to atmospheric nitrogen dioxide increases fruit yield of tomato plants. Plant Biotechnol. 28: 485-487.

Thimm O, Bläsing O, Gibon Y, Nagel A, Meyer S, Krüger P, Selbig J, Müller LA, Rhee SY, Stitt M (2004) MAPMAN: A user-driven tool to display genomics data sets onto diagrams of metabolic pathways and other biological processes. Plant J. 37: 914-939.

Thormählen I, Meitzel T, Groysman J, Öchsner AB, von Roepenack-Lahaye E, Naranjo, B, Cejudo FJ, Geigenberger P (2015) Thioredoxin *f1* and NADPH-dependent thioredoxin reductase C have overlapping functions in regulating photosynthetic metabolism and plant growth in response to varying light conditions. Plant Physiol. 169: 1766-1786.

Tsukagoshi H, Busch W, Benfey PN (2010) Transcriptional regulation of ROS controls transition from proliferation to differentiation in the root. Cell 143: 606-616.

Tsuzuki T, Takahashi K, Inoue S, Okigaki Y, Tomiyama M, Hossain MA, Shimazaki K, Murata Y, Kinoshita T (2011) Mg-chelatase H subunit affects ABA signaling in stomatal guard cells, but is not an ABA receptor in *Arabidopsis thaliana*. J. Plant Res. 124: 527-538.

Tyagi S, Mulla SI, Lee KJ, Chae JC, Shukla P (2018) VOCs-mediated hormonal signaling and crosstalk with plant growth promoting microbes. Crit. Rev. Biotechnol. 8: 1277-1296.

Tzin V, Malitsky S, Zvi MM Ben, Bedair M, Sumner L, Aharoni A, Galili G (2012) Expression of a bacterial feedback-insensitive 3-deoxy-d-arabino-heptulosonate 7-phosphate synthase of the shikimate pathway in Arabidopsis elucidates potential metabolic bottlenecks between primary and secondary metabolism. New Phytol. 194: 430-439.

van Bockhaven J, Spíchal L, Novák O, Strnad M, Asano T, Kikuchi S, Höfte M, De Vleesschauwer D (2015) Silicon induces resistance to the brown spot fungus *Cochliobolus miyabeanus* by preventing the pathogen from hijacking the rice ethylene pathway. New Phytol. 206: 761-773.

van Dingenen J, de Milde L, Vermeersch M, Maleux K, de Rycke R, de Bruyne M, Storme V, Gonzalez N, Dhondt S, Inzé D (2016) Chloroplasts are central players in sugar-induced leaf growth. Plant Physiol. 171: 590-605.

Venneman J, Vandermeersch L, Walgraeve C, Audenaert K, Ameye M, Verwaeren J, Steppe K, Van Langenhove H, Haesaert G, Vereecke D (2020) Respiratory CO_2 combined with a blend of volatiles emitted by endophytic serendipita strains strongly stimulate growth of Arabidopsis implicating auxin and cytokinin signaling. Front. Plant Sci. doi: 10.3389/fpls.2020.544435.

Villeret V, Huang S, Zhang Y, Xue Y, Lipscomb WN (1995) Crystal structure of spinach chloroplast fructose-1,6-bisphosphatase at 2.8 Å resolution. Biochemistry 34: 4299-4306.

Vogel MO, Moore M, König K, Pecher P, Alsharafa K, Lee J, Dietz KJ (2014) Fast retrograde signaling in response to high light involves metabolite export, MITOGEN-ACTIVATED PROTEIN KINASE6, and AP2/ERF transcription factors in Arabidopsis. Plant Cell 26: 1151-1165.

Volpe V, Giovannetti M, Sun XG, Fiorilli V, Bonfante P (2016) The phosphate transporters LjPT4 and MtPT4 mediate early root responses to phosphate status in non mycorrhizal roots. Plant Cell Environ. 39: 660-671.

von Caemmerer S, Farquhar GD (1981) Some relationships between the biochemistry

of photosynthesis and the gas exchange of leaves. Planta 153: 376-387.

Vlot AC, Rosenkranz M (2022) Volatile compounds - the language of all kingdoms? J. Exp. Bot. 73: 445-448.

Wang M, Liao W (2016) Carbon monoxide as a signaling molecule in plants. Front. Plant Sci. doi: 10.3389/fpls.2016.00572.

Wang X, Bian Y, Cheng K, Gu LF, Ye M, Zou H, Sun SS, He JX (2013) A large-scale protein phosphorylation analysis reveals novel phosphorylation motifs and phosphoregulatory networks in Arabidopsis. J. Proteomics 14: 486-98.

Watanabe H, Takehana K, Date M, Shinozaki T, Raz A (1996) Tumor cell autocrine motility factor is the neuroleukin/phosphohexose isomerase polypeptide. Cancer Res. 56: 2960-2963.

Weber A, Servaites JC, Geiger DR, Kofler H, Hille D, Gröner F, Hebbeker U, Flügge UI (2000) Identification, purification, and molecular cloning of a putative plastidic glucose translocator. Plant Cell 12: 787-801.

Weingart H, Ullrich H, Geider K, Völksch B (2001) The role of ethylene production in virulence of *Pseudomonas syringae pvs. glycine*a and *phaseolicola*. Phytopathology 91: 511-518.

Weise SE, Liu T, Childs KL, Preiser AL, Katulski HM, Perrin-Porzondek C, Sharkey TD (2019) Transcriptional regulation of the glucose-6-phosphate/phosphate translocator 2 is related to carbon exchange across the chloroplast envelope. Front. Plant Sci. doi: 10.3389/fpls.2019.00827.

Weise T, Kai M, Piechulla B (2013) Bacterial ammonia causes significant plant growth inhibition. PLoS ONE 8: e63538.

Wharton DC, Weintraub ST (1980) Identification of nitric oxide and nitrous oxide as products of nitrite reduction by Pseudomonas cytochrome oxidase (nitrite reductase). Biochem. Biophys. Res Commun. 97: 236-242.

Xiao Y, Savchenko T, Baidoo EEK, Chehab WE, Hayden DM, Tolstikov V, Corwin JA, Kliebenstein DJ, Keasling JD, Dehesh K (2012) Retrograde signaling by the plastidial metabolite MEcPP regulates expression of nuclear stress-response genes. Cell 149: 1525-1535.

Xie Y, Ling T, Han Y, Liu K, Zheng Q, Huang L, Yuan X, He Z, Hu B, Fang L, Shen Z, Yang Q, Shen W (2008) Carbon monoxide enhances salt tolerance by nitric oxide-mediated maintenance of ion homeostasis and up-regulation of antioxidant

defence in wheat seedling roots. Plant Cell Environ. 31: 1864-1881.

Xie Y, Mao Y, Lai D, Zhang W, Shen W (2012) H_2 enhances Arabidopsis salt tolerance by manipulating ZAT10/12-mediated antioxidant defence and controlling sodium exclusion. PLoS ONE, 7: e49800. doi:10.1371/journal.pone.0049800.

Xuan W, Zhu FY, Xu S, Huang BK, Ling TF, Qi JY, Ye MB, Shen WB (2008) The heme oxygenase/carbon monoxide system is involved in the auxin-induced cucumber adventitious rooting process. Plant Physiol. 148: 881-893.

Yang L, Ji J, Wang H, Harris-Shultz KR, Abd_Allah EF, Luo Y, Guan Y, Hu X (2016) Carbon monoxide interacts with auxin and nitric oxide to cope with iron deficiency in Arabidopsis. Front. Plant Sci. doi: 10.3389/fpls.2016.00112.

Yang SY, Grønlund M, Jakobsen I, Grotemeyer MS, Rentsch D, Miyao A, Hirochika H, Kumar CS, Sundaresan V, Salamin N, Catausan S, Mattes N, Heuer S, Paszkowski U (2012) Nonredundant regulation of rice arbuscular mycorrhizal symbiosis by two members of the phosphate transporter1 gene family. Plant Cell 24: 4236-4251.

Yang T, Sun Y, Wang Y, Zhou L, Chen M, Bian Z, Lian Y, Xuan L, Yuan G, Wang X, Wang C (2020) *AtHSPR* is involved in GA- and light intensity-mediated control of flowering time and seed set in Arabidopsis. J. Exp. Bot. 71: 3543-3559.

Yin Z, Balmant K, Geng S, Zhu N, Zhang T, Dufresne C, Dai S, Chen S (2017) Bicarbonate induced redox proteome changes in Arabidopsis suspension cells. Front. Plant Sci. doi: 10.3389/fpls.2017.00058.

Yoshida K, Hara S, Hisabori T (2015) Thioredoxin selectivity for thiol-based redox regulation of target proteins in chloroplasts. J. Biol. Chem. 290: 14278-14288.

Yoshida K, Hisabori T (2016) Two distinct redox cascades cooperatively regulate chloroplast functions and sustain plant viability. Proc. Natl. Acad. Sci. USA. 113: 3967-3976.

Yu TS, Lue WL, Wang SM, Chen J (2000) Mutation of Arabidopsis plastid phosphoglucose isomerase affects leaf starch synthesis and floral initiation. Plant Physiol. 123: 319-326.

Žd'árská M, Zatloukalová P, Benítez M, Šedo O, Potěšil D, Novák O, Svačinová J, Pešek B, Malbeck J, Vašíčková J, Zdráhal Z, Hejátko J (2013) Proteome analysis in Arabidopsis reveals shoot- and root-specific targets of cytokinin action and differential regulation of hormonal homeostasis. Plant Physiol. 161: 918-930.

Zhang C, Zhang M, Yan Z, Wang F, Yuan X, Zhao S, Zhang L, Tian H, Ding Z (2021)

CO_2 is a key constituent of the plant growth-promoting volatiles generated by bacteria in a sealed system. Plant Cell Rep. 40, 59–68.

Zhang XF, Jiang T, Wu Z, Du SY, Yu YT, Jiang SC, Lu K, Feng XJ, Wang XF, Zhang DP (2013) Cochaperonin CPN20 negatively regulates abscisic acid signalilng in Arabidopsis. Plant Mol. Biol. 83: 205-218.

Zhang H, Kim MS, Krishnamachari V, Payton P, Sun Y, Grimson M, Farag MA, Ryu CM, Allen R, Melo IS, Paré PW (2007) Rhizobacterial volatile emissions regulate auxin homeostasis and cell expansion in Arabidopsis. Planta 226: 839-851.

Zhang P, Luo Q, Wang R, Xu J (2017) Hydrogen sulfide toxicity inhibits primary root growth through the ROS-NO pathway. Sci. Rep. 7: 868 doi: 10.1038/s41598-017-01046-2.

Zhang H, Murzello C, Sun Y, Kim MS, Xie X, Jeter RM, Zak JC, Dowd SE, Paré PW (2010) Choline and osmotic-stress tolerance induced in Arabidopsis by the soil microbe *Bacillus subtilis* (GB03). Mol. Plant Microbe Interact 23: 1097-1104.

Zhang B, Pasini R, Dan H, Joshi N, Zhao Y, Leustek T, Zheng ZL (2014). Aberrant gene expression in the Arabidopsis *SULTR1;2* mutants suggests a possible regulatory role for this sulfate transporter in response to sulfur nutrient status. Plant J. 77: 185-197.

Zhang H, Sun Y, Xie X, Kim MS, Dowd SE, Paré PW (2009) A soil bacterium regulates plant acquisition of iron via deficiency-inducible mechanisms. Plant J. 58: 568-577.

Zhang H, Xie X, Kim MS, Kornyeyev DA, Holaday S, Paré PW (2008) Soil bacteria augment Arabidopsis photosynthesis by decreasing glucose sensing and abscisic acid levels in planta. Plant J. 56: 264-273.

Zhang L, Yang T, Li X, Hao H, Xu S, Cheng W, Sun Y, Wang C (2014) Cloning and characterization of a novel *Athspr* promoter specifically active in vascular tissue. Plant Physiol. Biochem. 78: 88-96.

Zhu Y, Liao W, Wang M, Niu L, Xu Q, Jin X (2016) Nitric oxide is required for hydrogen gas-induced adventitious root formation in cucumber. J. Plant Physiol. 195: 50-58.

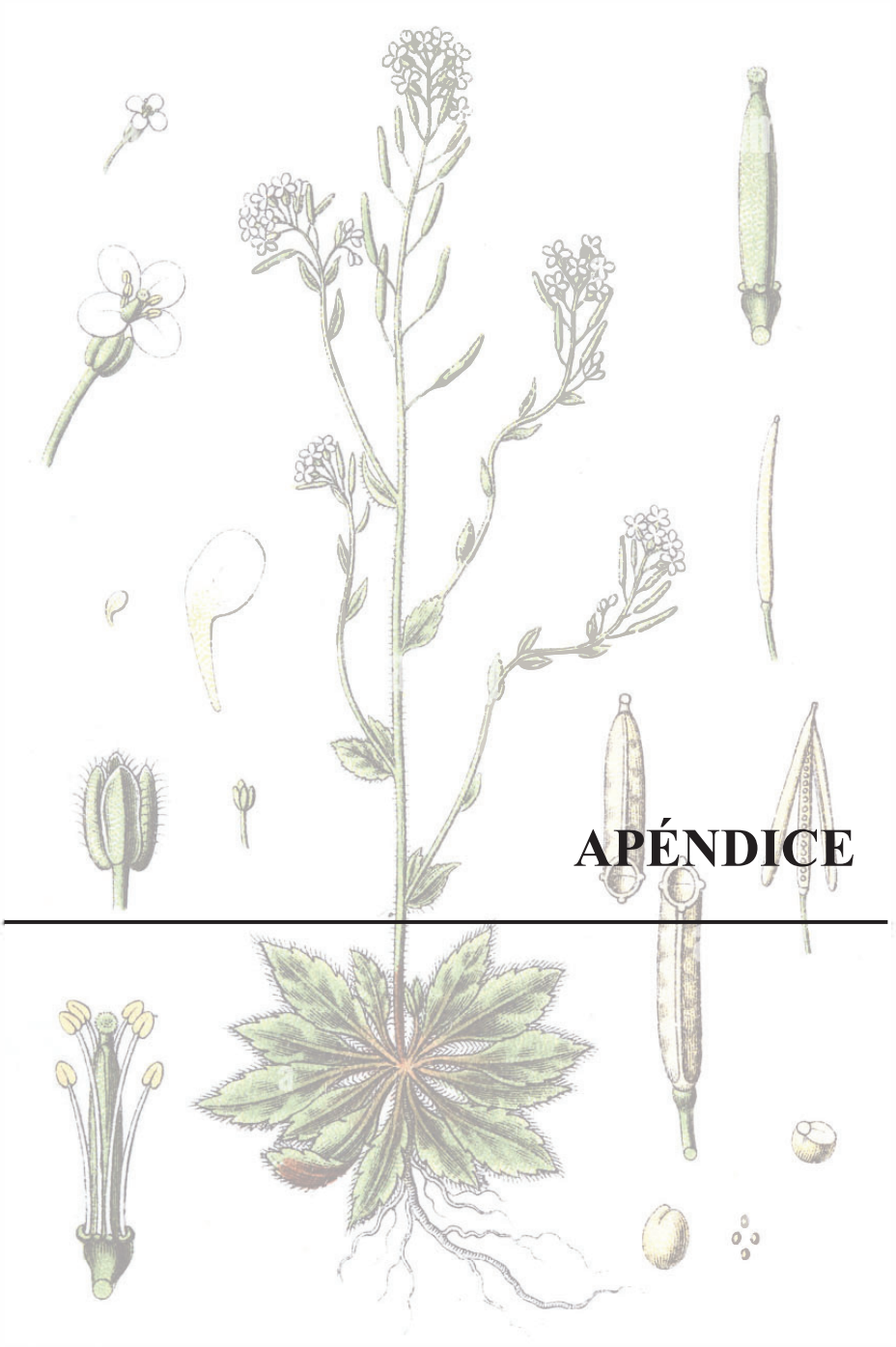

APÉNDICE

LISTA DE ABREVIATURAS

ABA	Abscisic acid
A_n	Net CO_2 assimilation rate CO_2
CBC	Calvin-Benson Cycle
cFBP1	plastidial fructose-1,6-bisphosphatase
CO	Carbon monoxide
CO_2	Carbon dioxide
CKs	Cytokinins
Clp	Caseinolithic protease
C_i	Intracellular CO_2 concentration
DEPs	Differentially expressed proteins
DXS	1-deoxy-D-xylulose-5-phosphate synthase
FBP	Fructose 1,6-biphosphate
FW	Fresh weight
F6P	Fructose 6-phosphate
GAP	Glyceraldeide-3-phosphate
GAs	Gibberellins
GPT2	Plastidial glucose-6-P/phosphate translocator
G6P	Glucose-6-P
H_2S	Hydrogen sulfide
HCN	Hydrogen cyanide
IRT1	Iron-regulated transporter 1
J_{max}	Maximum rate of electronic transport that contributes to the RuBP regeneration
K_{cat}	Catalytic activity
Km	Michaelis constans
Ks	Substrate dissociation constant
K_{05}	Substrate concentration at half maximum velocity
LR	Lateral root
MEP	Plastid-localized 2-C-methyl-D-erythritol 4-phosphate
MEcPP	2-C-methyl-D-erythritol-2,4-cyclopyrophosphate
m^6A	N^6-methylation of adenosine

NAD	Nicotinamide adenine dinucleotide
NADPH	Nicotinamide adenine dinucleotide phosphate
NO	Nitric oxide
NO_2	Nitrogen dioxide
NTRC	NADPH-dependent Trx reductase
PAP	3´-phosphoadenosine 5´-phosphate
PET	Photosynthetic electron transport
PGI1	Phosphoglucose isomerase 1
PQC	Protein quality control
PR	Primary root
PRXS	H_2O_2-detoxifying 2-Cys peroxiredoxins
PSI	Photosystem I
PVC	Plasticized polyvinyl chloride
RH	Root hair
ROS	Reactive oxygen species
RSA	Modulate root system architecture
RuBisCO	RuBP carboxylase oxygenase
RuBP	Ribulose 1,5-bisphosphate
Trx	Tioredoxine
tZ	Trans-zeatin
V_{cmax}	Rubisco maximum carboxylation rate
VCs	Volatile compounds
VOCs	Volatile organic compounds
WT	Wild-type

LISTA DE PUBLICACIONES

1. **Gámez-Arcas S**, Baroja-Fernández E, García-Gómez P, Muñoz FJ, Almagro G, Bahaji A, Sánchez-López ÁM, Pozueta-Romero J (2022a) Action mechanisms of small microbial volatile compounds in plants. J. Exp. Bot. 73: 498-510.

2. **Gámez-Arcas S**, Muñoz FJ, Ricarte-Bermejo A, Sánchez-López ÁM, Baslam M, Baroja-Fernández E, Bahaji A, Almagro G, De Diego N, Dolezal K, Novák O, Leal-López J, Morcillo RJL, Castillo AG, Pozueta-Romero J (2022b) Glucose-6-P/phosphate translocator2 mediates the phosphoglucose-isomerase-1 independent response to microbial volatiles. Plant Physiol. doi: 10.1093/plphys/kiac433.

3. **Gámez-Arcas S,** Muñoz FJ, Serrato AJ, Sánchez-López ÁM, Baroja-Fernández E, Bahaji A, Almagro G, López-Leal J, Morcillo-León JR, Pozueta-Romero J (2022) The Cys95 residue of the redox-regulated Calvin-Benson enzyme fructose-1,6-bisphosphatase, cFBP1, is an important determinant of photosynthetic activity in Arabidopsis (pendiente de publicacion).

4. Ameztoy K, Sánchez-López ÁM, Muñoz FJ, Bahaji A, Almagro G, Baroja-Fernández E, **Gámez-Arcas S**, De Diego N, Dolezal K, Novák O, Pencik A, Alpízar A, Rodríguez-Concepción M, Pozueta-Romero J (2021) Proteostatic regulation of MEP and shikimate pathways by redox-activated photosynthesis signaling in plants exposed to small fungal volatiles. Front. Plant Sci. doi: 10.3389/fpls.2021.637976.

5. Bahaji A, Almagro G, Ezquer I, **Gámez-Arcas S**, Sánchez-López ÁM, Muñoz FJ, Barrio RJ, Sampedro MC, De Diego N, Spíchal L, Dolezal K, Tarkowská D, Caporali E, Mendes MA, Baroja-Fernánez E, Pozueta-Romero J (2018) Plastidial phosphoglucose isomerase is an important determinant of seed yield through its involvement in gibberellin-mediated reproductive development and storage reserve biosynthesis in Arabidopsis. Plant Cell. 30: 2082-2098.

6. Baroja-Fernández E, Almagro G, Sánchez-López ÁM, Bahaji A, **Gámez-Arcas S**, De Diego N, Dolezal K, Muñoz FJ, Climent Sanz E, Pozueta-Romero J (2021) Enhanced yield of pepper plants promoted by soil application of volatiles from cell-free fungal culture filtrates is associated with activation of the beneficial soil microbiota. Front. Plant Sci. 12: doi: 10.3389/fpls.2021.752653.

7. García-Gómez P, Bahaji A, **Gámez-Arcas S**, Muñoz FJ, Sánchez-López ÁM, Almagro G, Baroja-Fernández E, Ameztoy K, De Diego N, Ugena L, Spíchal L, Dolezal K, Hajirezaei MR, Romero LC, García I, Pozueta-Romero J (2020) Volatiles from the fungal phytopathogen *Penicillium aurantiogriseum* modulate root metabolism and architecture through proteome resetting. Plant Cell Environ. 43: 2551-2570.

COMUNICACIONES CIENTÍFICAS

1. **Gámez-Arcas S**, Sánchez-López ÁM, Ricarte-Bermejo A, Baslam M, Baroja-Fernández E, García-Gómez P, Muñoz FJ, Bahaji A, Ugena L, Ameztoy K, et al., (2019) Arabidopsis plants lacking plastid phosphoglucose isomerase respond to microbial volatiles through GLUCOSE-6-P/PHOSPHATE TRANSLOCATOR2 action. XXIII Reunión Sociedad Española de Fisiología Vegetal y XVI Congreso Hispano-Luso de Fisiología Vegetal. Pamplona (España).

2. **Gámez-Arcas S**, Sánchez-López ÁM, Ricarte-Bermejo A, Baslam M, Baroja-Fernández E, García-Gómez P, Muñoz FJ, Bahaji A, Ugena L, Ameztoy K, et al., (2019) Arabidopsis plants lacking plastid phosphoglucose isomerase respond to microbial volatiles through GLUCOSE-6-P/PHOSPHATE TRANSLOCATOR2 action. XXIV Reunión Sociedad Española de Fisiología Vegetal y XVII Congreso Hispano-Luso de Fisiología Vegetal. Online-Málaga (España).

3. **Gámez-Arcas S**, Sánchez-López ÁM, Ricarte-Bermejo A, Baslam M, Baroja-Fernández E, García-Gómez P, Muñoz FJ, Bahaji A, Ugena L, Ameztoy K, et al., (2022) Arabidopsis plants lacking plastid phosphoglucose isomerase respond to microbial volatiles through GLUCOSE-6-P/PHOSPHATE TRANSLOCATOR2 action. XVI Reunión de Biología Molecular de Plantas (Sevilla).